

博士論文

**Improvement of Biocompatibility  
of the Diamond-like Carbon  
for Application to Medical Devices**

医療機器応用のためのダイヤモンドライクカーボンの  
生体適合性の向上に関する研究

岡本圭司

広島大学大学院先端物質科学研究科

2014年9月

# 目次

## 1. 主論文

Improvement of Biocompatibility of the Diamond-like Carbon for Application to Medical Devices

(医療機器応用のためのダイヤモンドライクカーボンの生体適合性の向上に関する研究)

岡本 圭司

## 2. 公表論文

(1) Differentiation Capability Evaluation of Osteoblast by Functionalized DLC Thin Films with Plasma Processing

Keishi Okamoto, Tatsuyuki Nakatani, Yuki Nitta, Seicho Makihira, Satoshi Iwata, Hiroki Nikawa, Takayuki Takahagi,

Journal of Photopolymer Science and Technology, 23 (2010) 591–594.

(2) Diamond-like carbon thin film with controlled zeta potential for medical material application

Yuki Nitta, Keishi Okamoto, Tatsuyuki Nakatani, Hideo Hoshi, Akihiko Homma, Eisuke Tatsumi, Yosiyuki Taenaka,

Diamond and Related Materials, 17 (2008) 1972–1976.

(3) Blood Compatibility of Gas Plasma treated Diamond-like Carbon Surface-Effect of Physicochemical Properties of DLC Surface on Blood Compatibility

Akira Mochizuki, Tatsuhisa Ogawa, Keishi Okamoto, Tatsuyuki Nakatani, Yuki Nitta,

Materials Science and Engineering, C31 (2011) 567–573.

## 3. 参考論文

(1) Surface Analysis of Carbon-Hydrogen Bonds in Diamondlike Carbon Films by X-ray Photoelectron Spectroscopy

Susumu Takabayashi, Keishi Okamoto, Tatsuyuki Nakatani, Hiroyuki Sakaue, Takayuki Takahagi,

Japanese Journal of Applied Physics, 48 (2009) 092304.

- (2) Development of surface-functionalized drug-eluting stent with diamond-like carbon nanocoated by using PECVD method  
Keishi Okamoto, Tatsuyuki Nakatani, Syuzo Yamashita, Susumu Takabayashi, Takayuki Takahagi,  
Surface and Coatings Technology, 202 (2008) 5750–5752.
- (3) Qualitative analysis of a diamondlike carbon film by angle-resolved x-ray photoelectron spectroscopy  
Susumu Takabayashi, Kunihiko Motomitsu, Takayuki Takahagi, Akira Terayama, Keishi Okamoto, and Tatsuyuki Nakatani,  
Journal of Applied Physics, 101 (2007) 103542.
- (4) Chemical Structural Analysis of Diamondlike Carbon Films with Different Electrical Resistivities by X-ray Photoelectron Spectroscopy  
Susumu Takabayashi, Keishi Okamoto, Kenya Shimada, Kunihiko Motomitsu, Hiroaki Motoyama, Tatsuyuki Nakatani, Hiroyuki Sakaue, Hitoshi Suzuki, and Takayuki Takahagi,  
Japanese Journal of Applied Physics, 47 (2008) 3376–3379.

# 主論文

# 目次

<b>Chapter 1. General Introduction</b> .....	1
1.1. Background to this study .....	1
1.2. Medical materials .....	2
1.2.1. Biocompatibility of medical material .....	2
1.2.2. Current situations and problems associated with materials for medical treatment .....	3
1.2.3. Status of research on medical materials .....	4
1.3. DLC .....	7
1.3.1. Outline of DLC .....	7
1.3.2. Manufacturing processes for DLC .....	8
1.3.3. Analysis of chemical structure of DLC .....	10
1.3.4. Application of DLC .....	12
1.4. Interaction between biological organisms and medical materials .....	15
1.5. Purpose of this study .....	17
1.6. References .....	18
<b>Chapter 2. Surface Analysis of Carbon–Hydrogen Bonds in Diamond-like Carbon by X-ray Photoelectron Spectroscopy</b> .....	23
2.1. Introduction .....	23
2.2. Methods and experimentation .....	27
2.3. Results and discussion .....	28
2.4. Conclusion .....	37
2.5. References .....	39
<b>Chapter 3. Chemical Structure and Physical Properties of Plasma-Treated Diamond-like Carbon Film Surface</b> .....	41
3.1. Introduction .....	41
3.2. Methods and experimentation .....	44

3.3. Result and discussion .....	46
3.3.1. Results of XPS spectrum measurement .....	46
3.3.2. Results of chemical modification XPS method .....	48
3.3.3. Results of contact angle measurement .....	52
3.3.4. Results of zeta potential measurement results .....	54
3.4. Conclusion .....	56
3.5. References .....	57

"This article was published in Copyright Elsevier (

#### **Chapter 4. Introduction of Carboxyl Groups onto Diamond-like Carbon Films**

<b>Doped with Silicon</b> .....	58
4.1. Introduction .....	58
4.2. Methods and experimentation .....	58
4.3. Results and discussion .....	59
4.4. Conclusion .....	62
4.5. References .....	63

#### **Chapter 5. Blood Compatibility of Plasma Surface Treated Diamond-like**

<b>Carbon <i>in-vitro</i></b> .....	64
5.1. Introduction .....	64
5.2. Methods and experimentation .....	64
5.3. Results and discussion .....	68
5.3.1. Surface chemical structure .....	68
5.3.2. Physicochemical property of surface .....	70
5.3.3. Evaluation of platelet adhesion of ID-DLC .....	71
5.3.4. Evaluation of blood coagulation of ID-DLC .....	74
5.3.5. Evaluation of kallikrein-like activity of ID-DLC .....	76
5.4. Conclusion .....	78
5.5. References .....	80

#### **Chapter 6. Bone Compatibility of Diamond-like Carbon *in-vitro*** ..... 81 |

6.1. Introduction .....	81
6.2. Methods and experimentation .....	81

6.3. Results and discussion .....	83
6.3.1. Surface structure .....	83
6.3.2. Differentiation capability evaluation in osteoblastic cells .....	85
6.4. Conclusion .....	86
6.5. References .....	88
<b>Chapter 7. Concluding Remarks .....</b>	<b>90</b>
<b>Acknowledgements .....</b>	<b>93</b>

### **Disseration copyright**

Chapter 2 was published in Japanese journal of Applied Physics, 48, 092304, Susumu Takabayashi, Keishi Okamoto, Tatsuyuki Nakatani, Hiroyuki Sakaue, Takayuki Takahagi, Surface Analysis of Carbon–Hydrogen Bonds in Diamondlike Carbon Films by X–ray Photoelectron Spectroscopy, Copyright The Japan Society of Applied Physics (2009).

Chapter 3 was published in Diamond and Related Materials, 17, 1972–1976, Yuki Nitta, Keishi Okamoto, Tatsuyuki Nakatani, Hideo Hoshi, Akihiko Homma, Eisuke Tatsumi, Yosiyuki Taenaka, Diamond–like carbon thin film with controlled zeta potential for medical material application, Copyright Elsevier (2008).

Chapter 4 was published in Surface and Coatings Technology, 202, 5750–5752, Keishi Okamoto, Tatsuyuki Nakatani, Syuzo Yamashita, Susumu Takabayashi, Takayuki Takahagi, Development of surface–functionalized drug–eluting stent with diamond–like carbon nanocoated by using PECVD method, Copyright Elsevier (2008).”

Chapter 5 was published in Materials Science and Engineering, C31, 567–573, Akira Mochizuki, Tatsuhisa Ogawa, Keishi Okamoto, Tatsuyuki Nakatani, Yuki Nitta, Blood Compatibility of Gas Plasma treated Diamond–like Carbon Surface–Effect of Physicochemical Properties of DLC Surface on Blood Compatibility, Copyright Elsevier (2011).”

Chapter 6 was published in Journal of Photopolymer Science and Technology, 23, 591–594. Keishi Okamoto, Tatsuyuki Nakatani, Yuki Nitta, Seicho Makihira, Satoshi Iwata, Hiroki Nikawa, Takayuki Takahagi, Differentiation Capability Evaluation of Osteoblast by Functionalized DLC Thin Films with Plasma Processing, Copyright The Conference of Photopolymer science and Technology (2010).”



# Chapter 1

## General Introduction

### 1.1. Background to this study

Living organisms continue to evolve and have acquired the anatomical features enabled them to adapt to a wide range of global environments. Moreover, organisms have acquired systems to defend themselves against foreign substances. Living organisms survive owing to their immune system and natural healing power. In addition, the human race has developed medical technology, which has extended the human life span.

The average life span of the men in Japan was 59.6 years in 1950–1952, which had increased to 71.7 years by 1975 and 79.6 years by 2010 [1]. Because of the high postwar economic growth rate, Japan became affluent, enabling the establishment of a universal healthcare system that covered a wide range of medical treatments available. The main reason for the increased average life span is the decrease in infant mortality rate. Medical technology developed during this era of high economic growth rate, which improved treatment contributed to the increased and average life span. The development of medical technology has been supported by advancements in medicine and medical devices. In particular, modern medical devices such as implants and diagnostic systems have rapidly developed.

It is now possible to treat by organ transplantation. However, the number of donors is greatly insufficient because transplantation is limited to between family members. There were 505 cases of living liver transplantation in 2006 [2], compared with 2200 patients per years requiring transplantation [3]. Therefore, it is presumed that many patients have died without receiving a transplant. Against this background, there is much expectation on regenerative medicine. Yamanaka's team first generated induced pluripotent stem (iPS) cells in 2006 [4]. These iPS cells are generated using the patient's own cells. There are no problems with ethical issues, in contrast to the case of embryonic stem cells, and there is no risk of rejection. Therefore, research on regenerative medicine using iPS cells is accelerating. Moreover, technology for establishing organized systems using cultured cells is being developed. Okano's team has developed the technique to collect a cell sheet without damaging it by applying a temperature-responsive polymer. This technique is being applied to the skin, cornea, and cardiac muscle [5–7]. However, considerable time will be necessary for realizing

the regeneration of complex internal organs.

## 1.2. Medical materials

### 1.2.1. Biocompatibility of medical material

The range of medical equipment is wide and includes tools, diagnostic equipment, therapeutic instruments, and devices that replace bodily functions. High biocompatibility is required for implant materials for long term use *in-vivo*.

Biocompatibility of a medical material is a characteristic reaction of a biological organ to a foreign substance. Reaction to a foreign substance reaction occurs even when the material is nontoxic. Therefore, a nontoxic material is not necessarily biocompatible. Figure 1 shows the types of biocompatibility based on the requirement for the medical material [8].

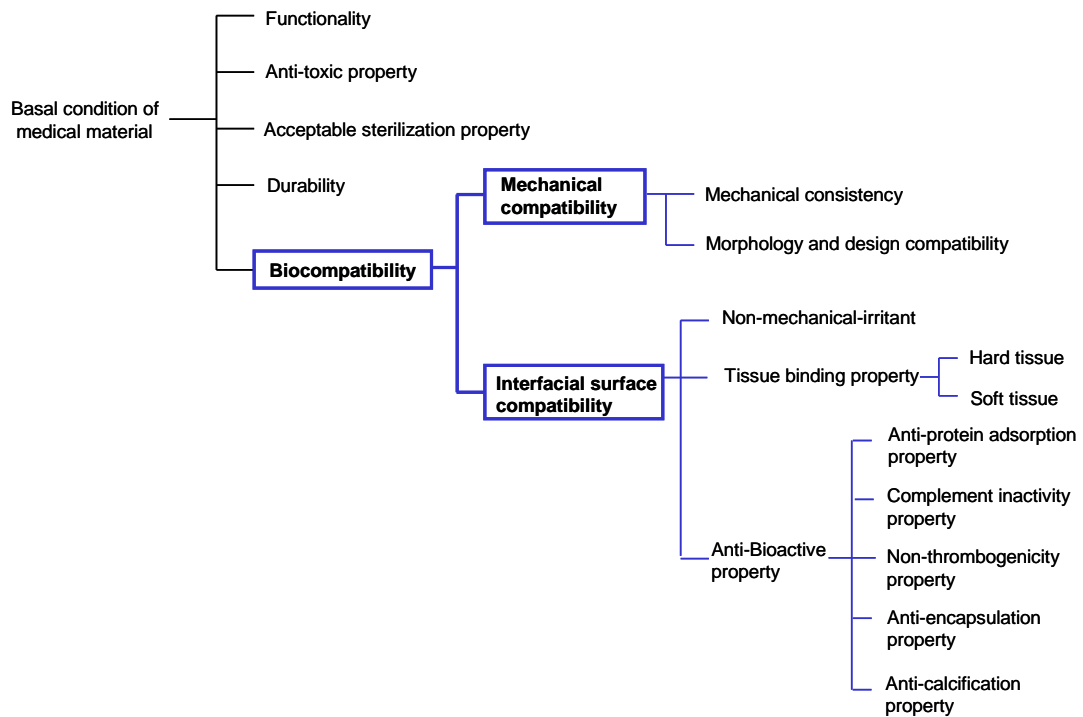


Figure 1. Types of biocompatibility based on requirement for medical material [8]

Biocompatibility characteristics are mainly divided into dynamic and interfacial characteristics, and the lack of either leads to failure in obtaining biocompatible materials. In addition, the material should attach to the biological tissue on the interface and be bioactive, that is, it does not react to foreign substances.

### 1.2.2. Current situations and problems associated with materials for medical treatment

A promising medical treatment of the change into the organ transplant is the use of implants made from artificial materials. For example, the treatment of ischemic heart disease was chiefly heart bypass surgery. However, percutaneous transluminal coronary angioplasty (PTCA) using a catheter and a stent have recently become popular. PTCA involves placement of a stent into the constricted portion of a coronary artery, thus reestablishing blood flow. That is, a stent is an artificial blood vessel that can expand similarly to a natural blood vessel. PTCA with a catheter through a thoracotomy incision is a minimally invasive technique and is necessary for heart bypass surgery. Moreover, because the duration of hospitalization for PTCA is shorted, treatment cost is reduced.

Regarding dental treatment, when teeth were lost, the use of artificial dentures or dental bridges was the basic treatment. However, mastication of hard food is difficult with artificial dentures, and dental bridges rub against the sides of teeth. For this reason, dental implant treatment has spread rapidly. Dental implants are fixed to the jawbone, similarly to the natural teeth. Therefore, the mastication function is recovered and dental implants aesthetically similar to natural teeth. Figure 2 shows dental implant bodies. It is used as a support to unite the jawbone and the upper implant structure.



Figure 2. Dental implant bodies.

Thus, implants made from artificial materials enable the recovery of specific functions and improve the quality of life. However, from the viewpoint of biocompatibility, artificial

materials cannot compare with biomaterials. Moreover, there are still many problems associated with artificial materials that remain unresolved.

### **1.2.3. Status of research on medical materials**

Here, I describe the status of research on medical materials. As for implants *in-vivo*, various materials such as metals, ceramics, and polymers are used. The material should satisfy biocompatibilities in terms of both interfacial and mechanical characteristics. There are various materials whose mechanical characteristics are much better than those of biomaterials. Materials with good interfacial characteristics are very limited. When inflammation, immune reactions, and blood clotting continue as the body's protective responses, the function of medical equipment cannot be maintained. Therefore, the surface chemical structure of a material is very important.

Metallic materials have high strength and flexibility, and excellent mechanical characteristics. It is necessary to prevent deterioration due to corrosion *in-vivo*. Therefore, stainless alloy, cobalt chrome alloy, titanium, and titanium alloy, for example, have been put to practical use owing to their high corrosion resistance. It is necessary to approximate the mechanical characteristic of an implant material to that of an alternative organ. Materials with appropriate mechanical properties are limited. As alternative materials for bone tissue for total hip replacement, Ti-6Al-4V alloy has been put to practical use. However, its Young's modulus is much higher (120 GPa) than that cortical bone (10-30 GPa). Stress shielding occurs because there is a difference in Young's modulus, and bone resorption and bone atrophy are concern [9]. Then, Niinomi et al. have developed a  $\beta$ -type titanium alloy with a low Young's modulus [10].

Ion elution is also a concern for metals. Vanadium shows cytotoxicity at concentrations used for titanium alloy [11]. Okazaki et al. reported that titanium alloy without vanadium has good mechanical properties and low cytotoxicity [12, 13]. On the other hand, it is necessary to refine used at ingot 1-10 tons for mass production. A powder metallurgy process for easy fabrication of a product of specific composition is expected. Kyogoku et al. developed a base material of titanium and titanium alloy by metal injection molding [14]. The cost of production by machining is low because metal injection molding using a near-net-shape process.

Ceramics consists chiefly of metallic oxide. For example, hydroxyapatite [HA:

$\text{Ca}_{10}(\text{PO}_4)_6(\text{OH})_2$  ], which is present in the bone and teeth, is used in artificial joints and dental implants. In dental implantation, first the implant body is surgically inserted into the jawbone. When the implant body has become integrated to the jawbone, the superstructure body is connected with the abutment.

In dental implantation, it is important that the new bone fills interspaces between the jawbone and the implant body. Moreover, the implant body must integrate strongly to the jawbone. HA coating is applied to improve bone compatibility. The methods of HA coating are HA dipping, flame spraying, and plasma spraying. Flaking off and HA loss through dissolution has been pointed out as problems associated with HA coating [15].

The linear coefficient of expansion of HA is higher than that of titanium. HA flaking off from a titanium based metal caused by temperature changes during sintering has been reported. HA flaking off is caused by residual distortion induced by sintering at high temperature with 850–1150 °C. The linear coefficient of expansion of HA ( $10\text{--}20 \times 10^{-6}/\text{K}$ ) is higher than that of titanium based materials ( $8.5 \times 10^{-6}/\text{K}$ ), because a mixture of glass and HA is shown to decrease the linear coefficient of expansion [16]. Hontsu et al. showed that a thin HA film (350 nm) prepared by laser ablation eases stress and improves adhesion [17].

Polymeric materials from organisms are used for prosthetic treatments. However, such materials have the risk of containing infectious agents, excluding those harvested from organs of patients. They are, however, still used because of their superior biocompatibility. For example, tissue valves harvested from a cow's pericardial sac is used in cardiac valve prostheses. The number of patients with mechanical valves is four times that with tissue valves, because calcification of tissue valves is a concern; for mechanical valves there is no concern deterioration and their durability is high [18]. However, patients with mechanical valves should continuously take anti coagulants, because mechanical valves have inferior blood compatibility.

Artificial polymers are used to treat various conditions. For preparing artificial blood vessels and sutures, drawing polytetrafluoroethylene (PTFE) is used. When blood comes in contact with minute cracks present in drawn PTFE, a thrombus film forms on the surface, resulting in the formation of a pseudointima [19]. Various artificial polymers with structures highly similar to those of biomolecules have been examined, as well. Nakabayashi et al. developed methacryloyloxyethylphosphorylcholine (MPC) with a structure highly similar that of the phosphorylcholine radical that composes the cell membrane [20–22].

Polymers are used as alternative materials for soft tissue, but their mechanical strength is generally inferior to that of metal. A balance between dynamics characteristics and interfacial characteristics can be archived by fixing a biocompatible polymer on the surface of a metallic base material. Composite materials fabricated using coating methods are expected. Drug-eluting stents (DESs) coated with drug-containing polymers are used to achieve an antithrombotic effect in PTCA [23, 24]. Figure 3 shows the result of scratching surface of DES with tweezers; the polymer coated on DES peeled easily [25]. There is a risk of a polymer peeling before DES reaches the affected part when DES comes in contact with a calcified intima of a vessel.

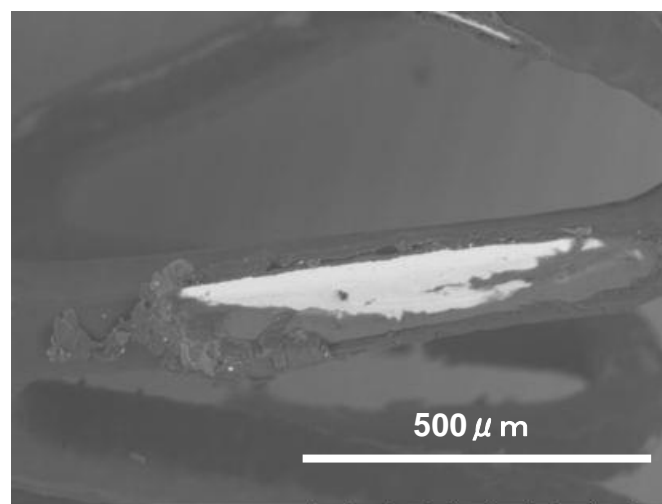


Figure 3 SEM image of surface of commercially available drug-eluting stent scratched with tweezers.

Research on specific materials has advanced, as shown above. However, available materials with mechanical compatibility and surface-interface compatibility are limited. Therefore, it aimed in this research to developed materials with mechanical compatibility and surface- interface compatibility, using coating methods.

Carbon was selected as a material in this research. The biocompatibility of carbon is also good. When one accidentally poked oneself with a pencil resulting in the graphite lead becoming embedded in the skin, it is known from experience that the lead is harmless in the skin. Pyrolytic carbon has been used for artificial heart valves over 30 years or more [26]. Carbon materials have save of many patients with valvular heart disease. In addition, among

carbon materials diamond-like carbon (DLC) has been focus of investigation, DLC is used as a coating material owing to its excellent mechanical property.

### 1.3. DLC

#### 1.3.1. Outline of DLC

Aisenberg and Chabot made prepared a film of carbon synthesized by the mass non separation ion beam method, which they named "diamondlike carbon" in 1971 [27]. DLC has not been clearly defined, but it generally refers to thin films containing on amorphous carbon-hydrogen structure. In general, DLC is composed of  $sp^3$  carbon,  $sp^2$  carbon, and hydrogen. Figure 4 shows a ternary phase diagram where the three corners correspond to  $sp^3$  carbon,  $sp^2$  carbon, and hydrogen [28, 29].

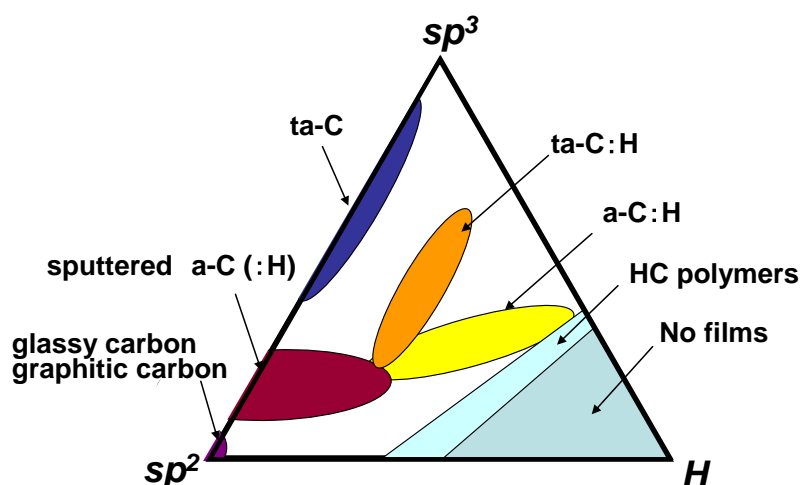


Figure 4. Ternary phase diagram of amorphous carbons. The three corners correspond to diamond ( $sp^3$ ), graphite ( $sp^2$ ), and hydrocarbons (H) [28,29].

Robertson defines ta-C as having the composition of  $sp^3$  carbon, not being 60% or higher, and hydrogen. Polymer-like a-C:H is defined as having the composition of 40–60% hydrogen and 70% or higher  $sp^3$  carbon. Polymer-like a-C:H has a low density because of hydrogen-terminated  $sp^3$  bonding. Diamond-like a-C:H is defined as having a composition of C-C  $sp^3$  bonding being more than polymer-like a-C:H and the hydrogen component being in the 20–40% range. ta-C:H is defined as having a hydrogen component being in the 20–40% range, and having the composition of C-C  $sp^3$  bonding. Moreover, the hydrogen components are lower than 20%, and the composition that contains many  $sp^2$  carbons is

defined as graphite-like a-C:H [30].

DLC with difficult composition ratios of  $sp^3$  carbon,  $sp^2$  carbon, and hydrogen show various characters. Table 1 shows the major properties of DLC [31]. For example, the hardness of DLC changes depending on hydrogen to  $sp^3$  composition ratio.

Table 1. Comparison of major properties of DLC with those of diamond, graphite, C<sub>60</sub>, and polyethylene as reference materials.<sup>[29]</sup>

	sp <sup>3</sup> (%)	H (%)	Density (g cm <sup>-3</sup> )	Gap (eV)	Hardness (Gpa)
Diamond	100	0	3.5	55	100
Graphite	0	0	2.3	0	
C <sub>60</sub>	0	0		1.6	
Glassy C	0	0	1.3-1.55	0.01	3
Evaporated C	0	0	1.9	0.4-0.7	3
Sputtered C	5	0	2.2	0.5	
ta-C	80-88	0	3.1	2.5	80
a-C:H hard	40	30-40	1.6-2.2	1.1-1.7	10-20
a-C:H soft	60	40-50	1.2-1.6	1.7-4.0	<10
ta-C:H	70	30	2.4	2.0-2.5	50
Polyethylene	100	67	0.9	6	0.01

### 1.3.2. Manufacturing processes for DLC

The manufacturing processes for DLC are roughly divided into chemical vapor deposition (CVD) using hydrocarbon gas and physical vapor deposition (PVD) using solid graphite.

A representative CVD process is plasma-enhanced CVD (PECVD). PECVD has three stages. (1) Hydrocarbon molecules are resolved with plasma, to generate radicals. (2) The radicals diffuse in the gas phase and are transported. At this point, the radical reaction progresses by molecular collision. (3) The radicals reach the surface of the base material and are deposited.

The DLC film prepared by the PECVD process contains hydrogen derived from the operation gas, and contains many hydrogen-terminated structures. For this reason, the hardness of the DLC film prepared by PECVD tends to be low. The PECVD methods includes the direct current glow discharge method, high-frequency discharge method typically using the 13.56 MHz band, electronic cyclotron resonance discharge method with magnetic fields, and ionized deposition method. [32–38].

On the other hand, PVD methods include the ion beam method, sputtering method, and



cathodic arc ion plating method. [39–42]. Because the DLC films prepared by PVD use solid graphite, the hydrogen content is lower than that of the films prepared by CVD. PVD can provide another element-doped DLC film using an evaporation source of another element together. For example, Dimigen et al. prepared metal-doped DLC by the sputtering method, which showed increased wear and abrasion resistance and decreased electric resistance [43]. The sputtering method has been described in detail by Kelly [44]. The principle of sputtering is as follows. The sputtering gas in the chamber is ionized with plasma. The evacuated chamber pressure is adjusted to operation pressure with sputtering gas. Ions are accelerated and impact onto the solid target. The ions penetrate into the target, and provide kinetic energy to the target atom by a phenomenon similar to the interaction of the billiard balls. When the kinetic energy exceeds the binding energy of the target material, a portion of target atoms flow out in the vapor phase. Because the target atom is secondarily driven, sputtering is inefficient compared with other PVD methods. Then, a magnetron sputtering method that utilizes the characteristic that magnetic field lines are orthogonal to electric current flows was designed. Electrons are trapped in the magnetic field when closed magnetic field lines are added to the surface of the target, these by increasing electron density, which increases sputter efficiency. However, the number of ions that reach the substrate does not increase markedly; thus electrons may concentrate on the target surface. Then, an unbalanced magnetron sputtering was designed, which expanded the plasma area in the direction of the substrate using open magnetic field lines [45]. Next, another type of unbalanced magnetron sputtering was designed, in magnetic field was closed between two or more targets [46, 47]. This design has high productivity because the target encloses the surrounding area of work and is suitable for the mass production of devices.

Kouznetsov et al. also designed a new magnetron sputtering method that used large currents and low-frequency pulses [48], which is called high-power impulse magnetron sputtering (HiPIMS). The ionization rate and deposition rate of HiPIMS are improve using an electric power of 1000W or higher. HiPIMS is extremely short with about 0.1% of the turning-on time of the electric power for HiPIMS. Therefore, overheating of the target and abnormal electrical discharges are controlled. Lattemann at el. uses HiPIMS together with the cathodic arc method, and obtains a high deposition rate and a smooth DLC surface [49].

The cathodic arc method has been described by Brown in detailed [50]. In this method, the cathode material, to which the energy of the arc discharge is applied, is sublimed and ionizes

in vacuum. Ions are attracted to the impressed voltage of the bias, collide with the substrate, and deposit as a film. The ionization rate and deposition rate are higher than those of other PVD methods. However, melted liquid droplets of the target material are discharged by the arc energy, and macroparticles of micro-meter size are generated [51]. Smoothness degrades when the macroparticles reaches the substrate and deposit the film. The filtered cathodic vacuum arc (FCVA) method is designed to exclude these macroparticles [50]. The feature of this method is that the inclination magnetic field filter is arranged only carbon ions can pass between the cathode and the substrate.

Aksenov et al. reported the fabrication of high-density and high-electrical-resistibility DLC films by the FCVA method [42]. The plasma duct with the magnetic field eliminates low-energy neutral atoms and increases the carbon ion current density.

Methods using plasma are effective, as shown above, for obtaining various types of DLC. In this research, DLC was prepared by the ionized deposition method with excellent mechanical and adhesion characteristics.

### 1.3.3. Analysis of chemical structure of DLC

DLC has an amorphous structure, and contains  $sp^2$  carbon,  $sp^3$  carbon, and hydrogen. For the analysis of chemical structures, infrared spectroscopy, Raman spectroscopy, and X-ray photoelectron spectroscopy (XPS) are used.

Infrared spectroscopy is also a good method for examining the bonding of functional groups in carbon materials. However, the analysis of  $sp^2$  carbon and  $sp^3$  carbon is difficult. Infrared spectroscopy suitable for surface analysis is multiple internal reflection infrared absorption (MIR-IR). Mizaikoff et al. analyzed element by MIR-IR in an electro bath with an attenuated total reflectance (ATR) prism coated with DLC of 100 nm thickness to protect ZnSe [52, 53]. It is important to understand the behavior of hydrocarbon during its preparation by CVD. Shinohara et al. analyzed by in situ MIR-IR the effects of the PECVD method on CH<sub>x</sub> species in the PLCH film. It is shown that the CH<sub>3</sub> species behavior is affected by substrate temperature and the rate of PLCH film deposition [54]. The structure changes when the PLCH film is exposed to hydrogen plasma, and the concentration of CH<sub>1-2</sub> species increases, whereas that of CH<sub>3</sub> species decreases [55].

Raman spectroscopy is commonly used for the analysis of DLC. Raman spectroscopy can provide information on the carbon atoms that compose DLC. However, Raman spectroscopy

can only provide information on atoms in the bulk material, not on the surface. DLC shows three peaks of G ( $1560\text{ cm}^{-1}$ ), D ( $1360\text{ cm}^{-1}$ ), and T ( $1060\text{ cm}^{-1}$ ) in Raman spectroscopy. The G peak originates from graphite, the D peak shows disorder, which does not exist in pure graphite [56, 57], and the T peak originates from diamond (tetrahedral  $sp^3$  carbon). However, because the excitation condition of visible excitation light such as  $\text{Ar}^+$  lasers does not enable the detection of the T band, information on  $sp^3$  carbon cannot be obtained. Because the energy of visible light corresponds to the  $\pi$ - $\pi^*$  orbital transition energy of the  $sp^2$  orbit of DLC, the resonance Raman effect is induced [58, 59]. Ferrari conducted Raman spectroscopy using the combination of visible light and ultraviolet light and was able to detect T band and examine the chemical structure of DLC. It is understood that the T peak is detected from ta-C and ta-C:H by the excitation of the ultraviolet light. The peak of ta-C of  $1060\text{ cm}^{-1}$  is assigned to the stretching vibration of  $sp^3$  carbon-  $sp^3$  carbon, and the peak of ta-C:H of  $980\text{ cm}^{-1}$  is assigned to the bending vibration of  $sp^3$  carbon-hydrogen, as determined by the theory calculation [60].

Ferrari also reported on the excitation light dependencies of the wavenumber of the G peak originating from a graphitized structure [61, 62]. The slope of wavenumber peak with the excitation light increases with increasing the  $sp^3$  element and has many amorphous structures. On the basis of these results, the dispersion of the wavenumber of the G peak can be evaluated qualitatively [61]. The  $sp^3$  element of DLC decreases when  $G\text{ disp.}$  is small and it increases when  $G\text{ disp.}$  is large. The qualitative analysis of DLC becomes easy by obtaining the Raman spectrum using different excitation lights. The DLC structure can be qualitatively evaluated by obtaining  $G\text{ disp.}$  from the Raman spectrum obtain using different excitation lights. However, other techniques are required for the analysis of the surface.

For DLC analysis, reports on XPS are few [64–68]. However, the depth of detection by XPS is shallow, which makes it most suitable for surface structure analysis. It is consistent that  $sp^3$  carbon is on the high-binding-energy side from  $sp^2$  carbon and the difference in the peak energy position is 0.9 eV. A different group is reporting on the XPS analysis of each DLC. This results shows that the increase of disorder elements induced by the  $sp^3$  carbon element increases the difference in energy level between two carbon orbits. Therefore, XPS analysis is possible although the distinction between  $sp^2$  carbon and  $sp^3$  carbon is difficult from the Raman spectrum.

Haerle et al. showed deconvolution of the C 1s spectrum of DLC deposited using a pulse

laser with XPS [66]. The energy axis was proofread using the Si 2p value (99.4 eV) of the bulk [64]. For deconvolution of  $sp^3$  carbon, the Gaussian function and the Lorentzian function are used, and because the deconvolution of  $sp^2$  carbon produces an asymmetric spectrum, the Doniach–Sunjic function used for graphitized materials is used for the deconvolution of the C 1s spectrum of  $sp^3$  carbon and  $sp^2$  carbon [67, 68]. On the other hand, Merel et al. showed the deconvolution of the C 1s spectrum of DLC deposited by a similar method. In their deconvolution method, they used the Gaussian function and the Lorentzian function, which is the symmetry function [66].

Analytical techniques for DLC have not been sufficiently. On the other hand, the structural analysis on the surface of DLC is indispensable for accurate biocompatibility assessment.

#### **1.3.4. Application of DLC**

DLC is widely used in machine parts and tools to improve durability because it is hard, and its coefficient of friction is low. For example, Mazda Motor Corporation is the first in the world to applied DLC in mass-produced engine parts. The rotary engine "RENESES RE" installed in "RX-8" was changed from the peripheral exhaust port to the side exhaust port. Because the overlap becomes unnecessary in this exhaust port layout, the emission can be decreased. However, lubrication shortage occurred because the corner seal was exposed to the opening of the exhaust port. High durability was however obtained with the mileage increased twofold as a result DLC application to the corner seal [69, 70]. In this case, a silicon-doped DLC film is used to realize heatproof and mechanical properties. This DLC film is a developed by Toyo Advanced Technologies Co., Ltd., to which I belong. Figure 5 shows the rotary engine and the DLC coating corner seal.

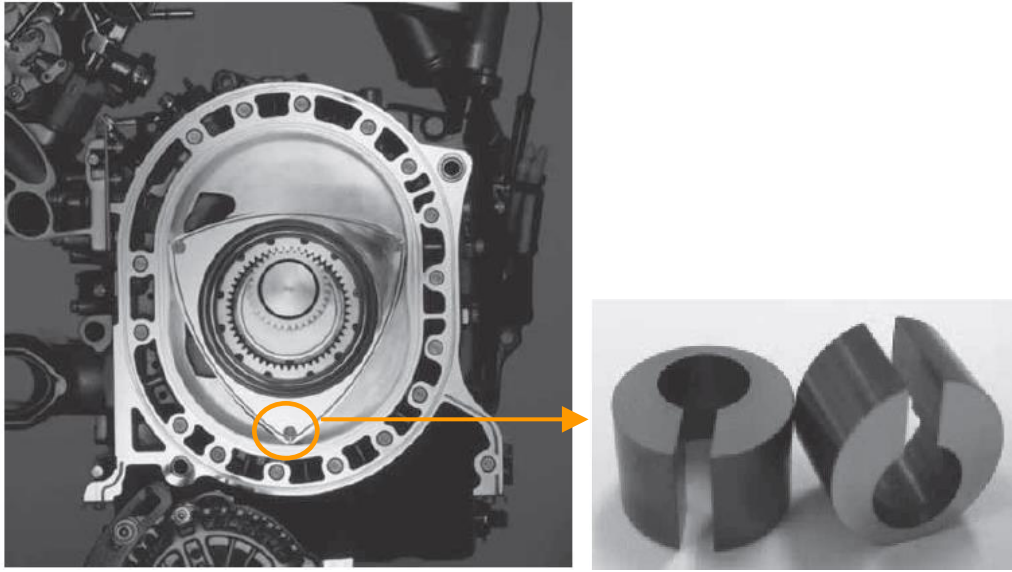


Figure 5. Cut model of rotary engine (left)  
and DLC-coated corner seal (right)

Afterwards, the advances in DLC application have also been adapted by other automotive makers. For example, Nissan Motor Co., Ltd. developed DLC that improves the absorbance of engine oil, which has been applied to valve lifters [71].

DLC is also widely applied to tools. The heat generated by friction of sliding parts causes plastic deformation that in turn causes adhesion of the of tools surface. This tendency is remarkable in low-melting-point metal, and adhesion occurs easily in tools for low-melting-point metalworking. However, the adhesion of metal does not occur easily in the DLC surface because it is nonmetal. Taking advantage of this characteristic, the DLC is applied to working tools of low-melting-point metal. For example, it is applied to the piercing tool for the IC lead frame [72].

The DLC film is used to protect of the head of the hard disk drive because it is smooth owing to its amorphous structure. The distance between the hard disk and the head is narrow (about 10 nm). Therefore, the accuracy of the head should be high, and the protective film should be extremely thin. Moreover, the adhesion of projecting macroparticles is not permitted. The suitable methods of DLC are the FCVA method, ion beam deposition method, and ECR plasma CVD method to obtain a smooth DLC film surface [73].

The gas barrier characteristic is also excellent. Recently, the material used for beverage

containers is polyethylene terephthalate (PET) to save resources and decrease cost. The oxidation of beverage was a problem because PET is slightly gas-permeable. Then, Kirin Brewery Co., Ltd. developed the technology that improved the gas barrier characteristic of PET bottles using the DLC film [74, 75]. In a 350 cc PET bottle/day, the amount of oxygen penetrating was 0.2 cc/ bottle/ day, but in a DLC-coated bottle, it became less than 0.02 cc/ bottle/day. Low-cost and high mass production are needed for the DLC film to be applicable to PET bottles. To realize these, Mitsubishi Electric Co., Ltd. developed the continuous processor for the CVD method using a high-frequency power source with a rotary table. This continuous processor has production capacity of 12000/h or higher [75]. The safety of the DLC film used for PET bottles has been confirmed safety, and the authorization of the United States Food and Drug Administration has been obtained for the DLC films. The DLC film is also now limited used in the containers warm beverages in Japan.

DLC is researched as a medical device material. For example, Thomson et al. reported that the DLC film suppressed the proliferation of macrophages [76]. Attention is also focused on the composition of DLC films. Many other elements for doping DLC have been examined for biocompatibility. Hasebe et al. reported that the adsorption of protein in blood is decreased when the amount of fluorine in the DLC film is increased [77]. Kwok et al. reported that the doping of calcium or phosphorus in the DLC film by the ion-implantation method decreases the amount of platelets adhesion [78]. Bendavid et al. reported that the doping of Si in the DLC film by the pulse plasma CVD method resulted in the high proliferation rate of osteoblast cells [79]. The  $sp^3$  carbon to the  $sp^2$  carbon ratio in DLC film excluding the doped elements has been examined. Jelinek et al. reported that the ratio of the  $sp^3$  carbon in the DLC film prepared by the pulse laser method is high and the film shows a high proliferation rate of fibroblasts [80]. For these findings, the DLC films are expected to have application in medical materials. However, there was a possibility of sacrificing mechanical compatibility when giving priority to surface-interface compatibility.

Therefore, a method that changes only the structure of the surface and acquiring surface interface compatibility was used to prevent the loss of mechanical compatibility. The plasma surface treatment technique was practically used. There are many unanswered questions regarding the origin of species, and it is not clear how cells appeared. A cell is chiefly composed of lipids, amino acids, and DNA. The Miller-Urey experiment points out the possibility that the lipids and the amino acids were generated from methane contained in the

ancient atmosphere as induced by the electrical discharge energy of lightning [81, 82]. Therefore, using the discharge phenomenon in hydrocarbon is one of the simple methods with the possibility of creating the basic structure of biomaterial. Then, this study aims to further develop implants, and attention is focused on DLC with expectations of its application in materials for various medical treatments.

#### **1.4. Interaction between organisms and medical materials**

A biological system is subdivided into the organism, organ, tissue, and cell. The basic functional unit of a living organism is the cell. There about 60 trillion cells in the human body. The cell mainly consists of proteins, polysaccharids, and phospholipids. The cell is covered with the cell membrane of about 10 nm thickness. The inside of the cell is filled with the cytoplasm and contains various organelles such as, the cell nucleus. Proteins are found in the lipid bilayer such as phospholipids and cholesterol, in cell membrane. Singer–Nicolson developed a fluid mosaic model [83]. Integrin is among the proteins existing in the cell membrane. Integrin is transported across the cell membrane and is a heterodimer of the  $\alpha\beta$  type that transmits information from the outside of the cell to the inside.

Cells bond to each other, except blood corpuscle cells or extracellular matrix to form body tissues. The recognition of other cells or the extracellular matrix is important for cells to form bonds. Therefore, a cell receives external information via its adjacent cells through the surface of the cell membrane.

A typical mechanism of cellular adhesion is the interaction among the cell membrane, integrin, cellular adhesion protein, and extracellular matrix. Ruoslahti reported that integrin recognizes the arginine–glycine–aspartic–acid (RGD) site found in fibronectin of the cellular adhesion protein [84]. Thus, the cell bonds to the recognition site of integrin of specific protein contained in the extracellular matrix.

Replacing an artificial material with the extracellular matrix can explain the mechanism of the interaction between an artificial material and the cell. Figure 6 shows a diagram of the pattern of bonding between a cell and an artificial substrate.

The following process shows the process of cellular adhesion to the surface of an artificial material. (1) An artificial material and the body fluid come in contact. (2) Adsorption of the cellular adhesion protein occurs. (3) The cell and the adsorption protein come in contact through integrin in the cell membrane. (4) Adsorption and extension of cell occurs. The cell

thus bonds through integrin induced by a cellular adhesion protein with the RGD site that is adsorbed on the surface of an artificial material. The adsorption of a cellular adhesion protein on the surface of an artificial material is a trigger of cellular adhesion.

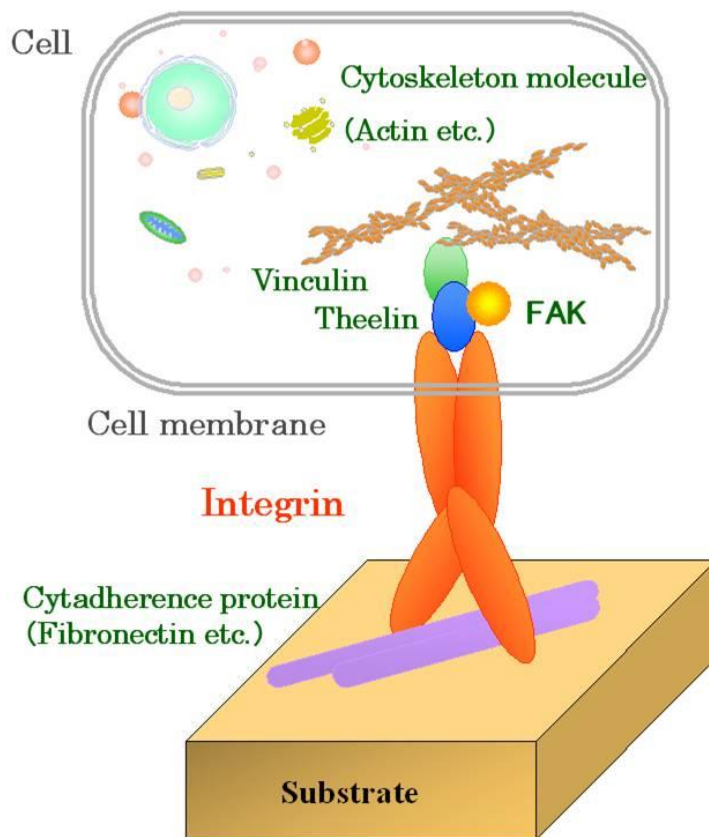


Figure 6. Mechanism of cell bonding on surface of artificial substrate

Regarding the biocompatibility mechanism on the surface of a material, a hydrophilic surface [85, 86], hydrophobe interaction [87, 88], similarity of the surface of cell membrane [89–91], and a non–uniform surface structure [92] are found to be important. In the case of hydrophobic interaction, the hydrophobic molecules cause dehydration because the removal of water is stable and aggregate. Moreover, the water on the surface causes the dehydration and unites when the protein approaches an artificial material. Thus, a specific protein is adsorbed by the surface, which is thought to influences biocompatibility. In addition, because water has polarity, the surface potential of the material influences the absorption of water by electrostatic interactions, Van der Waals interaction, and hydrogen bonding. Therefore, it is necessary to consider these interactions in developing biomaterials.



### **1.5. Purpose of this study**

The materials used in today medical devices cannot unite mechanical compatibility and surface–interface compatibility. The coating technology is examined to unite both compatibilities. However, when the mechanical property is insufficient, problems such as flaking off occurs in the coating material. DLC was selected as the coating material owing to its excelling mechanical property. However, if its mechanical compatibility is insufficient, the problems such as flaking off may occur in this coating material. Then, the method of changing only the structure of the surface and acquiring surface interfacial compatibility may be used to prevent the loss of a mechanical compatibility. The change in the structure of the surface of DLC was examined using the plasma surface treatment technology.

The surface chemical structure of DLC is also important, because it influences its interaction with the living body. However, current analytical techniques for the surface chemical structure of DLC have not been sufficiently developed. Therefore, the surface analysis of DLC by XPS is examined. Also, the biocompatibility of plasma–treated DLC is examined. The first factor evaluated is blood compatibility, which highly demanded for in many medical devices. In addition, to enable the application of implants in dental and orthopedic treatments, bone compatibility is evaluated. The possibility of DLC as a material for medical treatment is examined by evaluating these biocompatibilities *in-vitro*.

This research aims to realize the development of materials for medical devices that can be used to treat various conditions.

## 1.6. References

- [1] Health, Labour and Welfare Ministry. Abridged life table for Japan 2010.  
(<http://www.mhlw.go.jp/english/database/db-hw/lifetb10/index.html>)
- [2] T. Asahara, K. Umeshita, M. Kadota, *Isyoku*, 43 (2006) 45-55, (in Japanese).
- [3] F. Ichida, H. Tanigawa, *KAN-ISYOKU-TEKIOUKIJUN NIHON KAN-ISYOKU TEKIOU KENKYUKAI KIROKU* Arcmedium, Tokyo. (in Japanese)
- [4] K. Takahashi, S. Yamanaka. *Cell*, 126 (2006) 663–676.
- [5] M. Yamato, M. Utsumi, A. Kushida, C. Konno, A. Kikuchi, T. Okano, *Tissue Engineering*, 7 (2001) 473–480.
- [6] K. Nishida, M. Yamato, Y. Hayashida, K. Watanabe, N. Maeda, H. Watanabe, S. Nagai, A. Kikuchi, Y. Tano, T. Okano, *Transplantation*, 77 (2004) 379–385.
- [7] T. Shimizu, H. Sekine, M. Yamato and T. Okano, *Current Pharmaceutical Design*, 15 (2009) 2807–2814.
- [8] Y. Ikada, *SEITAI ZAIRYOU-GAKU*, 1994,53, Sangyou-tosyo,Tokyo, (in Japanese).
- [9] M. Niinomi,T. Hattori,S. Niwa, *Biomaterials in Orthopedics*, Marcel Dekker Inc, (2003) 41–62.
- [10] M. Niinomi, *Journal of the Mechanical Behavior of Biomedical Materials*, 1 (2008) 30–42.
- [11] S. G. Steinemann: *Evaluation of Biomaterials*, Wiley, Chichester, (1980) 1–34.
- [12] Y. Okazaki, Y. Ito, A. Ito, T. Tateishi, *Materials Transactions*, 34 (1993) 1217–1222.
- [13] A. Ito, Y. Okazaki, T. Tateishi Y. Ito, *Journal of Biomedical Materials Research*, 29 (1995) 893–900.
- [14] H. Kyogoku, S. Komatsu, K. Shinohara, H. Jinushi, T. Toda, *Powder Powder Metall*, 41 (1994) 1075–1079, (in Japanese).
- [15] N. Okumori, M. Yoshinari, Y. Oda, *The Shikwa Gakuho*, 100 (2000) 737–753, (in Japanese).
- [16] Kokai number, (1994) 7425, (in Japanese).
- [17] S. Hontsu, T. Hayami, Y. Higuchi, Y. Ohashi, Y. Hashimoto, *Journal of Japanese Society of Oral Implantology*, 23 (2010) 697–708, (in Japanese).
- [18] M. Kitamura, *Japanese Journal of Artificial Organs*, 30 (2001) 1–8, (in Japanese).
- [19] Y. Charbit, C. Hitzig, M. Bolla, C. Bitton, MF. Bertrand, *Biomedical Instrumentation and Technology*, 33 (1999) 71-75.

- [20] Y. Kadoma, N. Nakabayashi, E. Masuhara, J. Yamauchi, *Kobunshi Ronbunshu*, 35 (1978) 423–427, (in Japanese).
- [21] S. Fukushima, Y. Kadoma, N. Nakabayashi, *Kobunshi Ronbunshu*, 40 (1983) 785–793, (in Japanese).
- [22] K. Ishihara, T. Ueda, N. Nakabayashi, *Kobunshi Ronbunshu*, 46 (1989) 591–595, (in Japanese).
- [23] G.W. Stone, S.G. Ellis, D.A. Cox, J. Hermiller, C. O. 'Shaughnessy, J. Tift Mann, M. Turco, R. Caputo, P. Bergin, J. Greenberg, J.J. Popma, M.E. Russell, *The New England Journal of Medicine*, 350 (2004) 221–231.
- [24] J. Gunn, D. Cumberland, *European Heart Journal*, 20, (1999), 1693–1700.
- [25] K. Okamoto, T. Nakatani, S. Yamashita, S. Takabayashi, T. Takahagi, *Surface and Coatings Technology*, 202 (2008) 5750–5752.
- [26] J. H. Wang, *Annals of Thoracic Surgery*, 48 (1989) 55–56.
- [27] S. Aisenberg, R. Chabot, *Journal of Applied Physics*, 42 (1970) 2953–2958.
- [28] W. Jacob, W. Muller, *Applied Physics Letters*, 63 (1993) 1771–1773.
- [29] J. Robertson, *Material Science Engineering R*, 37 (2002) 129–281.
- [30] C. Casiraghi, J. Robertson, A. C. Ferrari, *Materialstoday*, 10 (2007) 44–53.
- [31] J. Robertson, *Surface and Coatings Technology*, 50 (1992) 185–203.
- [32] D. S. Whitmell, R. Williamson, *Thin Solid Films*, 35 (1976) 255–261.
- [33] H. Vora, T.J. Moravec, *Journal of Applied Physics*, 52 (1981) 6151–6157.
- [34] J. Suzuki, S. Okada, *Japanese Journal of Applied Physics*, 34 (1995) 1218–1220.
- [35] T. mori, T. Kumada, Y. Namba, *HYOUMEN-KAGAKU*, 3 (1982) 75–80. (in Japanese)
- [36] Y. Namba, *KINZOKU-HYOUMEN-GIJUTU*, 35 (1984) 572–578, (in Japanese).
- [37] T. Mori, Y. Namba. *Journal of Vacuum Science and Technology A*, 1, (1983) 23–27.
- [38] T. Mori, Y. Namba. *Journal of Applied Physics*, 55, (1984) 3276–3279.
- [39] E. G. Spencer, P. H. Schmidt, D. C. Joy, F. J. Sansalone, *Applied Physics Letters*, 29 (1976) 118–120.
- [40] G. Gautherin, Chr. Weissmantel, *Thin Solid Films*, 50 (1978) 135–144.
- [41] N. Savvides, *Journal of Applied Physics*, 59 (1986) 4133–414.
- [42] I. I. Akesson, V. E. Strel' nitskij, *Surface and Coatings Technology*, 47 (1991) 98–105.
- [43] H. Dimigen, H. Hubsch, R. Memming, *Applied Physics Letters*, 50 (1987) 1056–1059.
- [44] P.J. Kelly, R.D. Arnell, *Vacuum*, 56 (2000) 159–172.

- [45] B. Window, N. Savvides, *Journal of Vacuum Science and Technology A*, 4 (1986) 453–456.
- [46] D. G. Teer, *Surface and Coatings Technology*, 36 (1988) 901–907.
- [47] D. P. Monaghan, D. G. Teer, P. A. Logan, I. Efeoglu, R. D. Arnell, *Surface and Coatings Technology*, 60 (1993) 525–530.
- [48] V. Kouznetsov, K. Maca'k, J. M. Schneider, U. Helmersson, I. Petrov, *Surface and Coatings Technology*, 122 (1999) 290–293.
- [49] U. Helmersson, M. Lattemann, J. Bohlmark, A. P. Ehiasarian, J. T. Gudmundsson, *Thin Solid Films*, 513 (2006) 1–24.
- [50] I. G. Brown, *Annual Review of Materials Science*, 28 (1998) 243–269.
- [51] D. Drescher, J. Koskinen, H. J. Scheibe, A. Mensch, *Diamond and Related Materials*, 7 (1998) 1375–1380.
- [52] M. Janotta, F. Vogt, H. S. Voraberger, W. Waldhauser, J. M. Lackner, C. Stotter, M. Beutl, B. Mizaikoff, *Analytical Chemistry*, 76 (2004) 384–391.
- [53] M. Janotta, D. Rudolph, A. Kueng, C. Kranz, H. S. Voraberger, W. Waldhauser, B. Mizaikoff, *Langmuir*, 20 (2004) 8634–8640.
- [54] M. Shinohara, K. Cho, Y. Matsuda, H. Fujiyama, K. Okamoto, T. Nakatani, *Transactions of the Materials Research Society of Japan*, 32 (2006) 473–476.
- [55] M. Shinohara, K. Cho, H. Shibata, K. Okamoto, T. Nakatani, Y. Matsuda, H. Fujiyama, *Thin Solid Films*, 516 (2008) 4379–4383.
- [56] F. Tuinstra, J. L. Koenig, *Journal of Chemical Physics*, 53 (1970) 1126–1130.
- [57] A. C. Ferrari, J. Robertson, *Physical Review B*, 61 (2000) 14095–14107.
- [58] N. Wada, P. J. Gaczi, S. A. Solin, *Journal of Non-Crystalline Solids*, 35–36 (1980) 543–548.
- [59] S. R. Sails, D. J. Gardiner, M. Bowden, J. Savage, D. Rodway, *Diamond and Related Materials*, 5 (1996) 589–591.
- [60] F. Mauri, A. D. Corso, *Applied Physics Letters*, 75 (1999) 644–646.
- [61] A. C. Ferrari, J. Robertson, *Philosophical Transactions Royal Society London A*, 362 (2004) 2477–2512.
- [62] A. C. Ferrari, J. Robertson, *Physical Review B*, 64 (2001) 075414.
- [63] S. T. Jackson, R. G. Nuzzo, *Applied Surface Science*, 90 (1995) 195–203.
- [64] J. Diaz, G. Paolicelli, S. Ferrer, F. Comin, *Physical Review B*, 54 (1996) 8064–8069.

- [65] P. Merel, M. Tabbal, M. Chaker, S. Moisa, J. Margot, *Applied Surface Science*, 136 (1998) 105–110.
- [66] R. Haerle, E. Riedo, A. Pasquarello, A. Baldereschi, *Physical Review B*, 65 (2002) 045101–045109.
- [67] S. Doniach, M. Sunjic, *Journal of Physics C*, 3 (1970) 285–291.
- [68] J. G. Hong, S. Lee, C. Cardinaud, G. Turban, *Journal of Non-Crystalline Solids*, 265 (2000) 125–132.
- [69] S. Tashima R. Shimizu H. Koto, H. Ebino, S. Okazaki S. Ueki, *Mazda Technical Review*, 21 (2003) 18–23, (in Japanese).
- [70] T. Nakatani, K. Okamoto, A. Araki, T. Washimi, *New Diamond and Frontier Carbon Technology*, 16 (2006) 187–200.
- [71] H. Ohara, Y. Utsumi, T. Saito, Y. Fujinami, Y. Tano, *Nissin Electronic Technical Review*, 53 (2008) 46–50, (in Japanese).
- [72] Kokai number (2001) 279466, (in Japanese).
- [73] N.Akita, Y. Konishi, S. Ogura, M. Imamura, Y.H. Hu, X. Shi, *Diamond and Related Materials*, 10 (2001) 1017–1023.
- [74] Patent number 4050648, (in Japanese).
- [75] A. Ueda, M. Nakachi, S. Goto, H. Yamakoshi, A. Shirakura, *Mitsubishi Heavy Industries Technical Review*, 42 (2005) 42–43, (in Japanese).
- [76] L.A. Thomson, F.C. Law, N. Rushton, J. Franks, *Biomaterials*, 12 (1991) 37-40.
- [77] T. Hasebe, S. Yohena, A. Kamijo, Y. Okazaki, A. Hotta, K. Takahashi, T. Suzuki, *Journal of Biomedical Materials Research Part A*, 4 (2007) 1192–1199.
- [78] S.C.H. Kwok, P.C.T. Ha, D.R. McKenzie, M.M.M. Bilek, P.K. Chu, *Diamond and Related Materials*, 15 (2006) 893–897.
- [79] A. Bendavid, P. J. Martin, C. Comte, E. W. Preston, A. J. Haq, F. S. M. Ismail, R.K. Singh, *Diamond and Related Materials*, 16 (2007) 1616–1622.
- [80] M. Jelinek, K. Smetanac, T. Kocourek, B. Dvořankovac, J. Zemeka, J. Remsaa, T. Luxbacher, *Materials Science and Engineering B*, 169 (2010) 89–93.
- [81] S. L. Miller, *Science*, 117 (1953) 528–529.
- [82] S. L. Miller, H. C. Urey, *Science*, 130 (1959) 245–251.
- [83] S. J. Singer, G. L. Nicolson, *Science*, 175 (1972) 720–731.
- [84] P. Bacher, E. Ruoslahti, *Nature*, 309 (1984) 30–33.

- [85] E. W. Merrill, E. W. Salzman, *ASAIO Journal*, 28 (1982) 482–485.
- [86] T. Furuzono, K. Senshu, A. Kishida, T. Matsumoto, M. Akashi, *Polymer Journal*, 29 (1997) 201–209.
- [87] D. R. Lu, S. J. Lee, K. Park, *Journal of Biomaterials Science, Polymer Edition*, 3 (1991) 127–147.
- [88] E. Kulk, Y. Ikada, *J. Biomedical Materials Research*, 30 (1996) 295–304.
- [89] Y. Kadoma, N. Nakabayashi, E. Masuhara, J. Yamauchi, *Kobunshi Ronbunshu*, 35 (1978) 423–427.
- [90] K. Ishihara, R. Takayama, N. Nakabayashi, K. Fukumoto, J. Aoki, *Biomaterials*, 13 (1992) 235–239.
- [91] H. Kitano, T. Mori, S. Tada, M. Gemmei-Ide, M. Tanaka, *Macromolecular Bioscience*, 5 (2005) 314–321.
- [92] T. Okano, S. Nishiyama, I. Shinohara, T. Akaike, Y. Sakurai, K. Kataoka, T. Tsuruta, *J. Biomedical Materials Research*, 15 (1981) 393–403.

## Chapter 2

# Surface Analysis of Carbon–Hydrogen Bonds in Diamond-like Carbon by X-ray Photoelectron Spectroscopy

### 2.1. Introduction

When DLC films are applied to medical devices, their surface chemical structure is the most important factor for achieving biocompatibility. X-ray photoelectron spectroscopy (XPS) is one of the suitable methods of analyzing the surface chemical structure. DLC is composed of  $sp^3$  and  $sp^2$  carbons and hydrogen, making the analysis of the structure complex. Thus, XPS is an analytical method for determining the surface chemical structure of DLC films. When an X-ray energy of  $h\nu$  is emitted, the inner orbital electrons are excited, and photoelectrons are discharged with an energy of  $E_k$ . The relationship between these parameters is shown by equation (1), with  $E_B$  as the binding energy of the photoelectron,  $\Phi$  as the work function, and  $C$  as the amount of electrification.

$$E_B = h\nu - E_K - \Phi - C \quad (1)$$

$E_B$  is generally evaluated because it is fixed by each orbit, whereas  $E_K$  depends on the energy of the excited X-ray. In addition,  $E_B$  is affected by the electrical charge distribution near the target atom and is shifted. Therefore, the chemical–bonding state of a limited part of the object atom can be analyzed by analyzing the  $E_B$  shift. Equation (2) shows the decay of a photoelectron that passes in the material.

$$\phi(z) = c \exp\left(-\frac{z}{\lambda \cos \theta}\right) \quad (2)$$

The photoelectron intensity  $I(x)$  detected from the surface is shown by equation (3).

$$I(x) = \frac{\int_0^x \phi(z) dz}{\int_0^\infty \phi(z) dz} = \frac{\int_0^x \exp\left(-\frac{z}{\lambda \cos \theta}\right) dz}{\int_0^\infty \exp\left(-\frac{z}{\lambda \cos \theta}\right) dz} = 1 - \exp\left(-\frac{x}{\lambda \cos \theta}\right) \quad (3)$$

Therefore, the depth that corresponds to 95% of total photoelectron intensity becomes  $x = 3\lambda \cos \theta$ , and it becomes  $3\lambda$  at  $\theta = 0^\circ$ .

Next, the detection depth when DLC is analyzed by XPS is examined. The nonelasticity mean free path  $\lambda$  of the photoelectron of C1s of the carbon is 3.11 nm [1]. When the emission angle  $\theta$  is adjusted to  $45^\circ$ , it is shown to contain information on the carbon atom of  $d = 3\lambda \cos \theta = 6.6$  nm in the detection depth. Also, the integrated intensity of 50% corresponds to the surface within the shallow range of 1.5 nm [2]. Thus, it is shown that XPS is extremely effective for analyzing the surface chemical structure of DLC. Moreover, angle-resolved XPS (AR-XPS) is a method of adjusting the escape depth of a photoelectron from the surface of the sample by changing the emission angle of the photoelectron by applying this spectroscopic characteristic. Figure 1 shows the outline of the AR-XPS method.

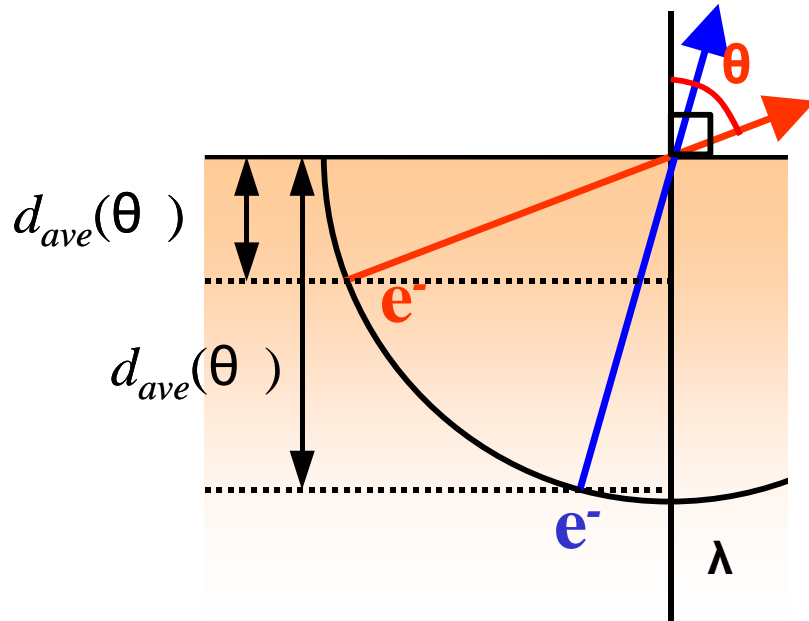


Figure 1 Relation between emission angle and detection depth of photoelectron by AR-XPS method



The analysis of  $sp^2$  and  $sp^3$  carbons in DLC has been reported. First, the AR-XPS analysis of the C1s spectra highly oriented pyrolytic graphite (HOPG) showed that the  $sp^2$  carbon is divided into two elements [2–4]. Next, it was reported for the  $sp^3$  carbon that the peak is divided into two elements of 283.8 and 285.3 eV [5–8]. On the other hand, for the DLC, it was reported that the C1s spectra is divided into two elements of  $sp^2$  and  $sp^3$  carbons [9–11]. Results of AR-XPS analysis showed that the surface element and the bulk element are different. Also, it is assumed that the  $sp^3$  and  $sp^2$  carbons exist respectively on the surface and the bulk, as already shown by the results for the carbon material.

Results of the XPS analysis of DLC obtained by a different group have been reported. They are consistent with the observation that the  $sp^3$  carbon is on the high-binding-energy side from the  $sp^2$  carbon, and the difference in the peak energy between these carbons is 0.9 eV, as determined from the results. It is considered that the reason for these results is that disorder increases because of the increase in the number of  $sp^3$  carbon elements, and the energy level difference between both orbit carbons was enhanced. As for XPS, differentiation between  $sp^2$  and  $sp^3$  carbons is possible, although the  $sp^2$  and  $sp^3$  carbons are difficult to distinguish in Raman spectroscopic analysis. However, because the hydrogen that originates in the raw material is contained in DLC, practical analysis is more complex. Thus, We proposed the chemical structure analysis of four elements that compose DLC by the AR-XPS using the Doniach-Šunjić function convoluted with a Gaussian function [12]. The valence band ( $V_B$ ) electron near the Fermi potential ( $E_F$ ) is excited to the conduction band ( $C_B$ ), and the energy of the system is absorbed because innumerable electron–hole pairs are formed for the metal and semimetal. The wave form of a photoelectron spectrum becomes asymmetric owing to this effect. The C1s spectrum of DLC containing the  $sp^2$  and  $sp^3$  carbons shows asymmetric diversity because this DLC contains a conductive element. The analysis of such a material uses the Doniach-Šunjić function that describes the asymmetric diversity [13].

$$DS(E_{BE}, \Gamma_L, \alpha) = I_0 \Gamma (1 - \alpha) \frac{\cos \left\{ \frac{\pi \alpha}{2} + (1 - \alpha) \tan^{-1} \left( \frac{E_0 - E_{BE}}{\frac{\Gamma_L}{2}} \right) \right\}}{\left\{ (E_0 - E_{BE})^2 + \left( \frac{\Gamma_L}{2} \right)^2 \right\}^{\frac{1-\alpha}{2}}} \quad (4)$$

$\Gamma(x)$  is a Gamma function.  $\Gamma_L$  is the half-bandwidth of the Lorentz function.  $\Gamma_G$  is the half-bandwidth of the Gauss function.  $\alpha$  is a singularity index. The peak position is  $E_0$  at  $\alpha=0$ .  $I_0$  is the intensity of proportionality constant. The singularity index  $\alpha$  of the DŠ function is the parameter that expresses the spectrum asymmetric diversity and it is related to the electronic density of states near the Fermi potential. The spectroscopic characteristic is also superimposed on these in the actual measurement. Then, the equation to make them superimpose the Gauss function that expresses these various characteristics in the DŠ function is used.

$$\begin{aligned}
& DS(E_{BE}, \Gamma_L, \alpha) \otimes G(E_{BE}, \Gamma_G) \\
&= \int_{-\infty}^{+\infty} DS(E') G(E_{BE} - E') dE' \\
&= \int_{-\infty}^{+\infty} DS(E_{BE} - E') G(E') dE' \\
&= I_0 \int_{-\infty}^{+\infty} \frac{\Gamma(1-\alpha) \cos\left\{\frac{\pi\alpha}{2} + (1-\alpha) \tan^{-1}\left(\frac{E_0 - (E_{BE} - E')}{\frac{\Gamma_L}{2}}\right)\right\}}{\left\{(E_0 - (E_{BE} - E'))^2 + \left(\frac{\Gamma_L}{2}\right)^2\right\}^{\frac{1-\alpha}{2}}} \cdot \frac{2\sqrt{\ln 2}}{\sqrt{\pi}\Gamma_G} \exp\left\{-4 \ln 2 \left(\frac{E_{BE} - E_0}{\Gamma_G}\right)^2\right\}}{dE'} \quad (5) \\
&= I_0 \Gamma(1-\alpha) \frac{2\sqrt{\ln 2}}{\sqrt{\pi}\Gamma_G} \int_{-\infty}^{+\infty} \frac{\cos\left\{\frac{\pi\alpha}{2} + (1-\alpha) \tan^{-1}\left(\frac{E_0 - (E_{BE} - E')}{\frac{\Gamma_L}{2}}\right)\right\} \exp\left\{-4 \ln 2 \left(\frac{E_{BE} - E_0}{\Gamma_G}\right)^2\right\}}{\left\{(E_0 - (E_{BE} - E'))^2 + \left(\frac{\Gamma_L}{2}\right)^2\right\}^{\frac{1-\alpha}{2}}} dE'
\end{aligned}$$

The parameters of the DŠ function are five elements, namely,  $\Gamma_L, \Gamma_G, \alpha, E_0$  and  $I$ . The commonness of  $\Gamma_G$  and  $\Gamma_L$  of each element is assumed for simplification. It is assumed in a previous report on DLC that only the  $sp^2$  carbon of the conductive element shows an asymmetric diversity. Also, it cannot be confirmed whether DLC of the amorphous substance is separate from the conductive and nonconductive elements. Thus, it is assumed that  $\alpha$  of each element is common. The  $sp^2$  carbon is assigned into two elements by AR-XPS analysis and from the  $h\nu$  dependence of the C 1s spectra of HOPG [14–16]. The  $sp^3$  carbon is assigned into two elements of 283.8 and 285.3 eV from the analysis of C 1s spectra of diamond [17, 18].  $E_0$  of each element was assigned with the bulk layer  $sp^3$  carbon (283.8 eV), bulk layer  $sp^2$  carbon (284.3 eV), surface coat  $sp^2$  carbon (284.8 eV), and surface coat  $sp^3$  carbon (285.3

eV) on the basis of current reports.

In addition, the dependence of the surface layer element on hydrogen concentration, as shown in the C 1s spectra, was examined using DLC films with different hydrogen concentrations. In other words, the relationship between the two-layer structural model and the actual chemical structure was examined [19]. The amount of surface layer elements increases when the CH<sub>4</sub>/Ar gas ratio increases, as shown by analyzing the spectra of DLC films with different hydrogen concentration distributions by the above-mentioned technique, and the amount of bulk layer elements decreases. Thus, it was suggested that the surface layer element has some relationship with the hydrogen atom in the DLC film. Also, the peak of 285.3 eV corresponds to the hydrogen-carbon bond caused by the hydrogen termination on the diamond surface, according to the report on the analysis of diamond [20–22]. Assignments of the C1s spectrum of the DLC film were revised from those mentioned above to C–C *sp*<sup>3</sup> carbon (283.8 eV), C–C *sp*<sup>2</sup> carbon (284.3 eV), H–C *sp*<sup>2</sup> carbon (284.8 eV), and H–C *sp*<sup>3</sup> carbon (285.3 eV).

In principle, it is impossible to detect hydrogen directly by XPS. Therefore, a method of analyzing hydrogen by another technique has been reported. For example, elastic recoil detection (ERD) is possible for the depth distribution analysis of hydrogen concentration at the atomic level with a high resolution of 0.28 nm [23]. ERD is a technique for analyzing the amount of hydrogen by detecting the hydrogen atoms that fly out when the accelerated heavy atomic ion impinged on the hydrogen atom in the thin film. However, the combination of DLC structures is complex with the C–C *sp*<sup>3</sup> carbon, C–C *sp*<sup>2</sup> carbon, H–C *sp*<sup>2</sup> carbon, and H–C *sp*<sup>3</sup> carbon. Then, the result of the above-mentioned AR-XPS method that used the D<sup>3</sup> function for analyzing four elements at a time was compared with the actual hydrogen concentration in the DLC film with a different hydrogen concentration distribution determined using the ERD method.

## 2.2. Methods and experimentation

Two types of DLC film were prepared as follows. One film of the first type was prepared on a Si wafer by the ionized deposition method, and was designated as an “ID-DLC” film. The operation gas was used C<sub>6</sub>H<sub>6</sub>. The base pressure of the chamber was maintained below  $1 \times 10^{-3}$  Pa, and operation pressure was about  $1.3 \times 10^{-1}$  Pa. The substrate bias voltage adjusted to -2 kV. DLC film was deposited on a single-crystal of n-Si (111). Three films of the

second type were prepared on Si wafers by the unbalanced magnetron sputtering (UBMS) method, and were designated as “UBMS-DLC” films. The target was graphite fixed in the chamber, and the CH<sub>4</sub>/Ar gas ratio in the chamber was varied to control the concentration of hydrogen incorporated, with values of 0, 0.06, and 0.12 [19, 20]. AR-XPS measurements were conducted on a surface area with a diameter of 0.8mm using an ULVAC-PHI PHI1600 system. The system had an unmonochromated Al K $\alpha$  line (1486.6 eV) with a voltage of 15 kV and a power of 400 W.

All measurements were performed at room temperature and a pressure below  $4.0 \times 10^{-9}$  torr. The emission angle was varied as 10, 30, 45, 60, and 75° with respect to the surface normal. The Shirley method was used to subtract the background lines [21]. The energy resolution of the spectrometer was estimated by analyzing the Fermi edge spectrum of a Au plate using the Fermi–Dirac distribution function convoluted with a Gaussian function. The fullwidth at half maximum (FWHM) of the Gaussian function was 0.6 eV.

Before each AR-XPS measurement, a few microliters of a dilute aqueous solution of Au nanocolloids were dropped on a local surface area of the DLC film to calibrate the binding energy [17, 22]. The droplet was gradually dried in vacuo, leaving Au nanocolloids adsorbed on the surface as a calibrant. The C 1s spectrum of the DLC film was observed at another surface area without the Au nanocolloids. The observed C 1s binding energy was calibrated by tuning the Au 4f 7/2 binding energy of the Au nanocolloids to 84.0 eV. The charge difference between the areas with and without Au nanocolloids was also calibrated by comparing the difference in the C 1s binding energy between the two areas.

### **2.3. Results and discussion**

Figure 2 shows the (a) ERD spectra and (b) hydrogen depth profiles of the UBMS–DLC films prepared with different CH<sub>4</sub>/Ar gas ratios in the plasma during the preparation process. The results demonstrate that a higher CH<sub>4</sub>/Ar gas ratio results in DLC films with a higher hydrogen concentration. Hydrogen atoms in every film are homogeneously distributed along the depth axis except for a slight increase in the concentration at the surface.

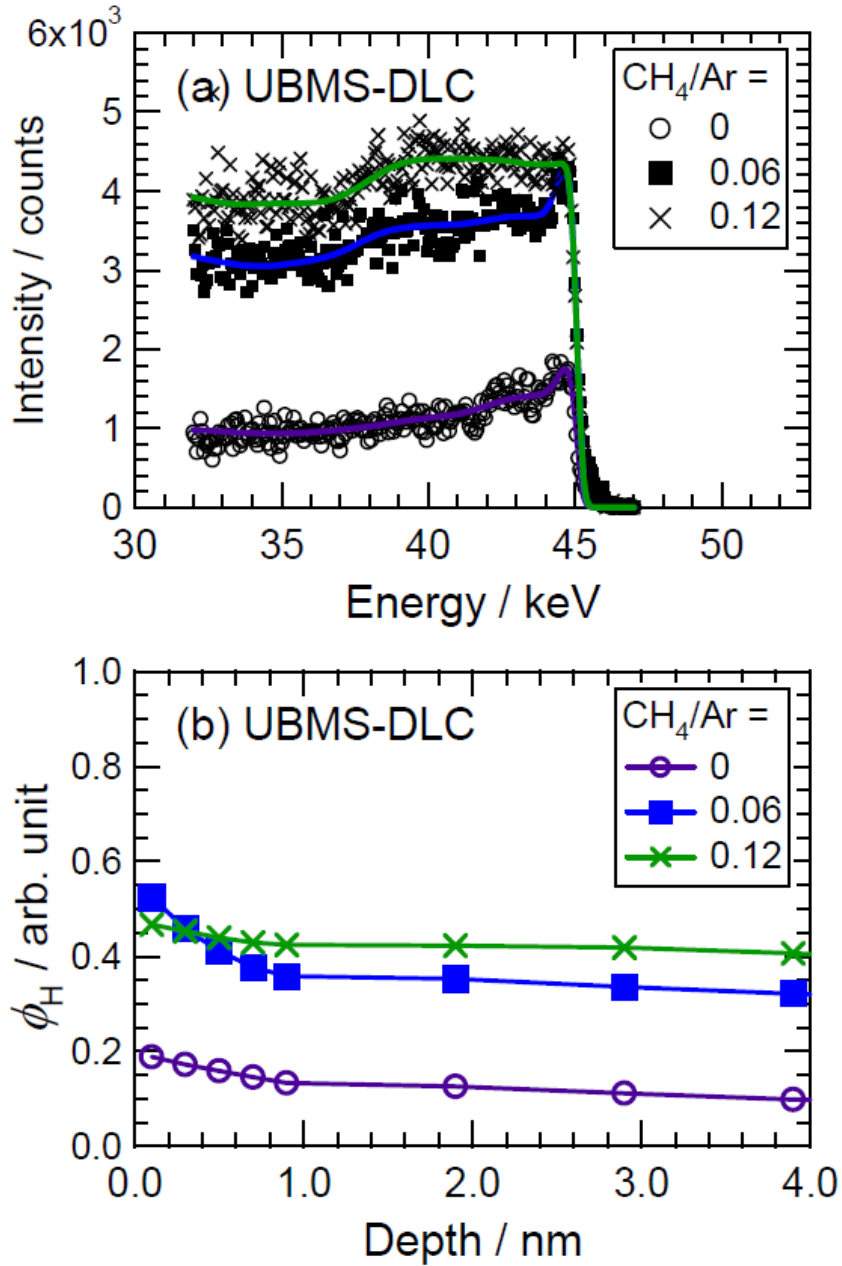


Figure 2. (a) ERD spectra and (b) hydrogen depth profile of the UBMS-DLC films prepared with different  $\text{CH}_4/\text{Ar}$  gas ratios in the plasma during the preparation process:  $\circ$  0,  $\blacksquare$  0.06, and  $\times$  0.12. “Copyright (2009) The Japan Society of Applied Physics”

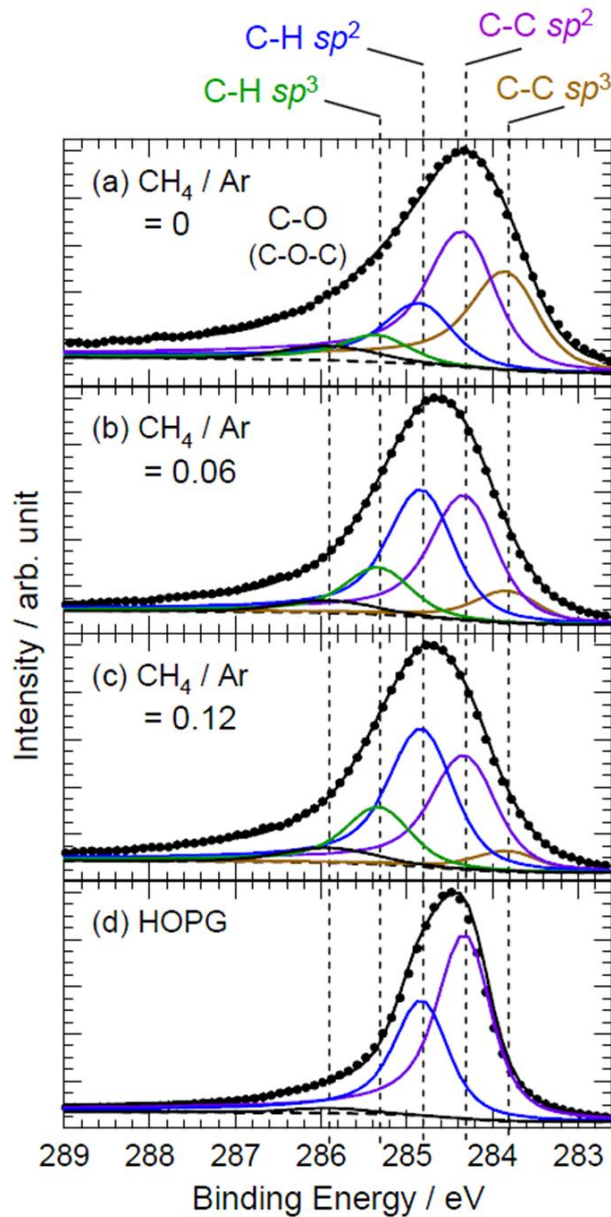


Figure 3. C 1s spectra of (a)–(c) the UBMS–DLC films and (d) a freshly-cleaved HOPG film where the fitting curves of the chemical components are represented by the proposed XPS analysis using the DS function convoluted with a Gaussian function. The UBMS-DLC films were prepared with the following CH<sub>4</sub>/Ar gas ratios in the plasma : (a) 0, (b) 0.06, and (c) 0.12. The emission angle is 45°. The peak assignments are follows: C–C *sp*<sup>3</sup> carbon (283.8 eV), C–C *sp*<sup>2</sup> carbon (284.3 eV), C–H *sp*<sup>2</sup> carbon (284.8 eV), C–H *sp*<sup>3</sup> carbon (285.3 eV), and C–O (or C–O–C) bonds (285.9 eV). “Copyright (2009) The Japan Society of Applied Physics”

Figure 3 shows the C 1s spectra of UBMS-DLC films and a freshly-cleaved HOPG film, which is composed of  $sp^2$  carbon only, with the fitting curves corresponding to the chemical components. The emission angle was fixed at  $45^\circ$ . All the C 1s spectra of the UBMS-DLC films show almost no dependence on the emission angle, and the spectra observed at  $45^\circ$  were almost the same as those observed at the other angles. The spectrum of the HOPG film was decomposed into two chemical components related to  $sp^2$  carbon and a very small C–O component [23, 24]. The spectra of the UBMS-DLC films were wider than that of the HOPG film, suggesting that two chemical components related to  $sp^3$  carbon exists at either side of the pair of the  $sp^2$  carbon components, which is similar to the results of the Artirradiated HOPG film mentioned above [25]. Each component is represented by the DŠ function convoluted with a Gaussian function as equation (5).

Generally, XPS photoelectron signals from materials decay exponentially along the depth axis. Thus if XPS can detect hydrogen bound to carbon directly, the total hydrogen intensity  $I_H(\theta)$  is estimated by

$$I_H(\theta) = \int_0^{\infty} \varphi_H(Z) \exp\left(-\frac{Z}{\lambda \cos \theta}\right) dZ, \quad (6)$$

where  $\varphi_H(Z)$  is the hydrogen distribution intensity at the depth  $Z$ ,  $\theta$  is the emission angle, and  $\lambda$  is the inelastic mean free path (IMFP). In these experiments,  $\lambda$  is estimated to be 2.0 nm by assuming that the C 1s binding energy is  $\sim 285$  eV and the kinetic energy is  $\sim 1200$  eV [26]. If we apply equation (6) to the analysis of the hydrogen depth profiles in Figure 2 (b), and the correlation of the concentration of hydrogen was evaluated by XPS and ERD analyses. Figure 4 shows the correlation of the UBMS-DLC films at the emission angle of  $45^\circ$ . The hydrogen concentration estimated by the XPS curve-fitting analysis is expressed as  $R_{C-H}$ , which is the area ratio of the C–H components (all hydrogen) to the sum of the C–H and C–C components (all carbon). A correlation is obtained between the XPS and ERD analyses, suggesting that XPS can analyze hydrogen as an atom bound to a carbon atom. As a result, the differences in the features of the C 1s spectra in Figure 3 arise from the difference in bond formation between carbon and hydrogen.

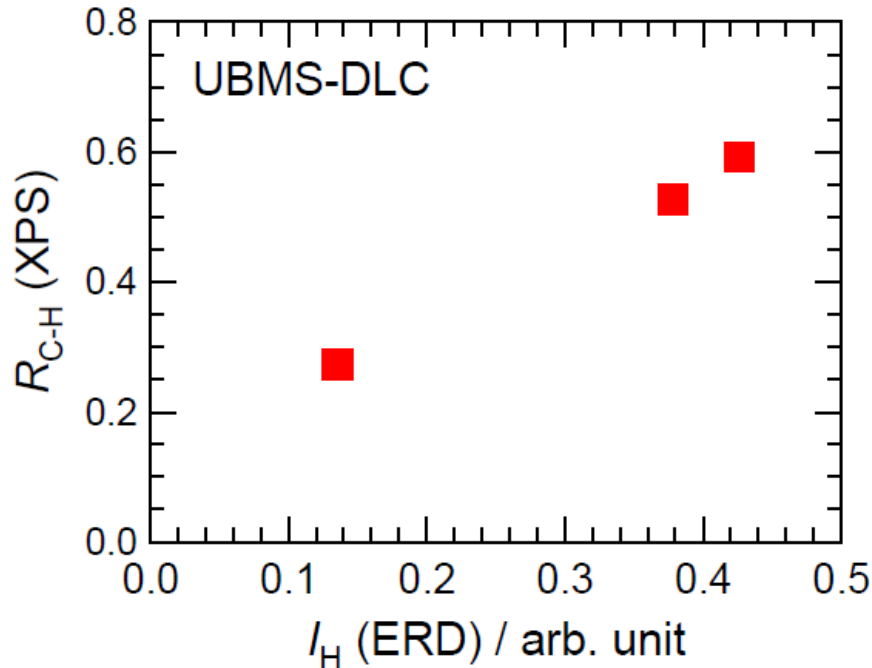


Figure 4. Correlation between the hydrogen concentrations obtained by the XPS and ERD analyses of the UBMS-DLC films with a homogeneous hydrogen distribution. “Copyright (2009) The Japan Society of Applied Physics”

Figures 5 (a) and 5 (b) show the ERD spectrum and hydrogen depth profile of the ID-DLC film, respectively. In contrast to the result of the UBMS-DLC films, a sharp and strong peak was observed in the ERD spectrum. This result demonstrates that, in the ID-DLC film, hydrogen atoms are inhomogeneously distributed along the depth axis and are more concentrated at the surface.

Figures 6 (a) and 6 (b) show the C 1s AR-XPS spectra of the ID-DLC film with the fitting curves of the chemical components determined in the same way as in figure 3. In contrast to the results of the UBMS-DLC films, the spectra change as a function of the emission angle. It was reported previously [12] that the surface and bulk components of the same ID-DLC film are different and that the chemical components of the C 1s spectrum are bulk  $sp^3$ , bulk  $sp^2$ , surface  $sp^2$ , and surface  $sp^3$ , carbons. The above discussion of DLC films with different hydrogen concentrations suggests that the surface component is related to the carbon with carbon–hydrogen bonds and the bulk component to the carbon with carbon–carbon bonds [16].



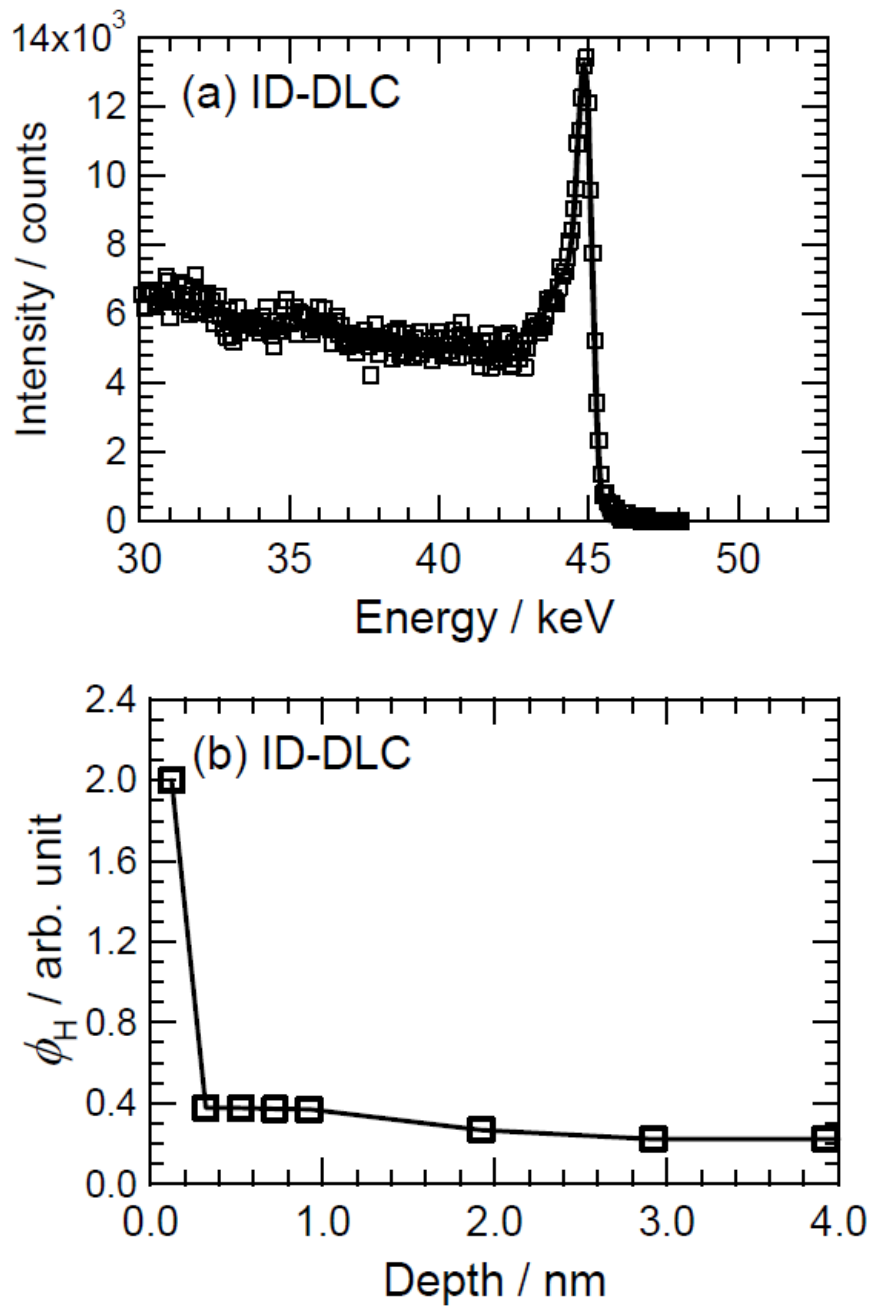


Figure 5. (a) ERD spectrum and (b) hydrogen depth profile of ID-DLC film. “Copyright (2009) The Japan Society of Applied Physics”

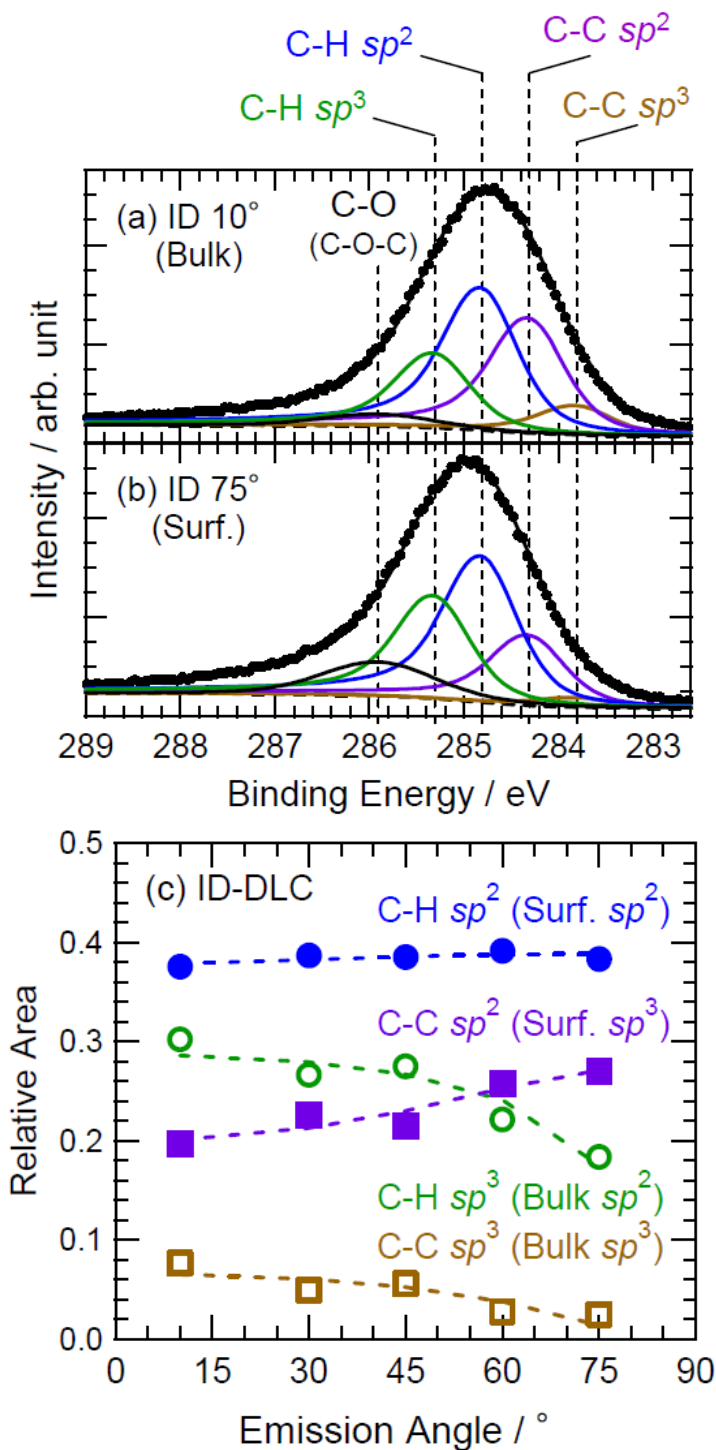


Figure 6. Relative intensities of the chemical components as a function of the emission angle: C-C  $sp^3$  (bulk  $sp^3$ ) carbon, C-C  $sp^2$  (bulk  $sp^2$ ) carbon, C-H  $sp^2$  (surface  $sp^2$ ) carbon, and C-H  $sp^3$  (surface  $sp^3$ ) carbon. “Copyright (2009) The Japan Society of Applied Physics”

Taking these relationships into account, Figure 6 (c) shows the relative intensities of the chemical components as a function of the emission angle. The dashed lines are the theoretical AR-XPS analysis curves calculated by

$$\begin{cases} I_S = I_S^0 \left[ 1 - \exp\left(-\frac{d}{\lambda_{S,S} \cos \theta}\right) \right], \\ I_B = I_B^0 \exp\left(-\frac{d}{\lambda_{B,S} \cos \theta}\right), \end{cases} \quad (7)$$

where the fitting parameters are the intensities of the surface and bulk components ( $I_S$  and  $I_B$ ), the standard intensities of the surface and bulk components ( $I_S^0$  and  $I_B^0$ ), the imaginary thickness of the surface atomic layers ( $d$ ), the IMFPs through  $d$  of the surface and bulk components ( $\lambda_S^0$  and  $\lambda_B^0$ ), and the emission angle ( $\theta$ ).

Figure 7 shows the correlation between the hydrogen concentrations obtained by the XPS and ERD analyses of the ID-DLC film, as obtained in the same way as in Figure 3, but with  $\theta$  being varied. The correlation suggests that our XPS analysis can also explain the behavior of the DLC film where hydrogen is distributed inhomogeneously. The present analysis has clarified that the correspondence of the surface (bulk) component to the carbon with carbon–hydrogen (carbon–carbon) bonds in the ID-DLC film is due to the inhomogeneous distribution of hydrogen in the film.

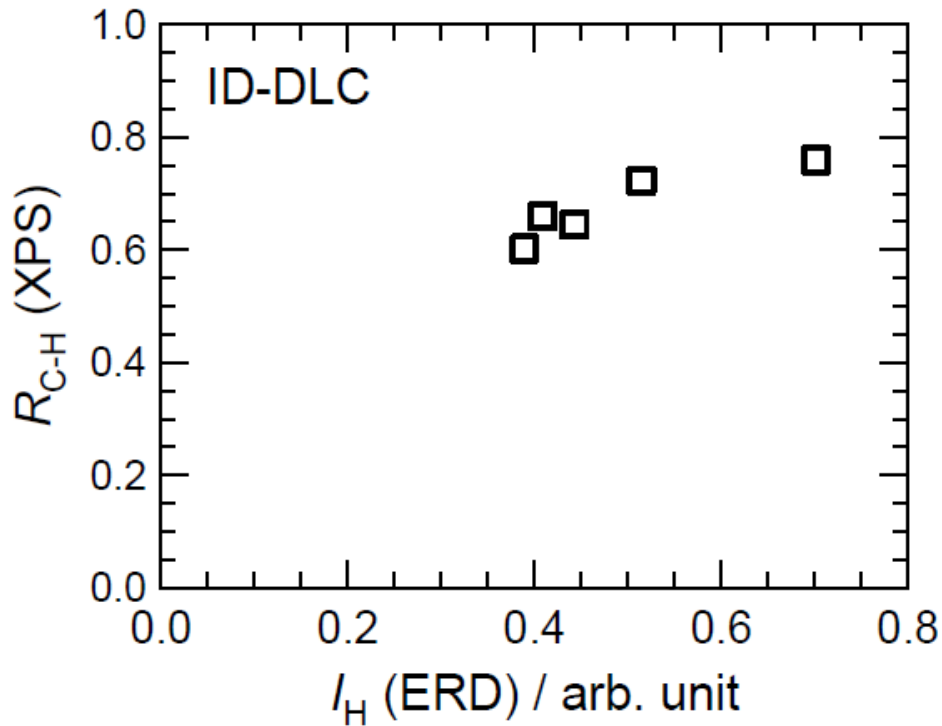


Figure 7. Correlation between the hydrogen concentrations obtained by the XPS and ERD analyses of the ID-DLC films with an inhomogeneous hydrogen distribution. “Copyright (2009) The Japan Society of Applied Physics”

Figure 8 shows the correlation between the hydrogen concentrations obtained by the XPS and ERD analyses of DLC films with both the homogeneous and inhomogeneous hydrogen distributions. A continuative correlation is obtained, suggesting that our proposed XPS analysis can explain the behaviors of the DLC films where the hydrogen distributions are different each other. However, it should be noted that the present XPS analysis can not distinguish the variation in the coordination number of of C–H bonds, –CH, –CH<sub>2</sub>, and –CH<sub>3</sub>, which may vary for different types of films.

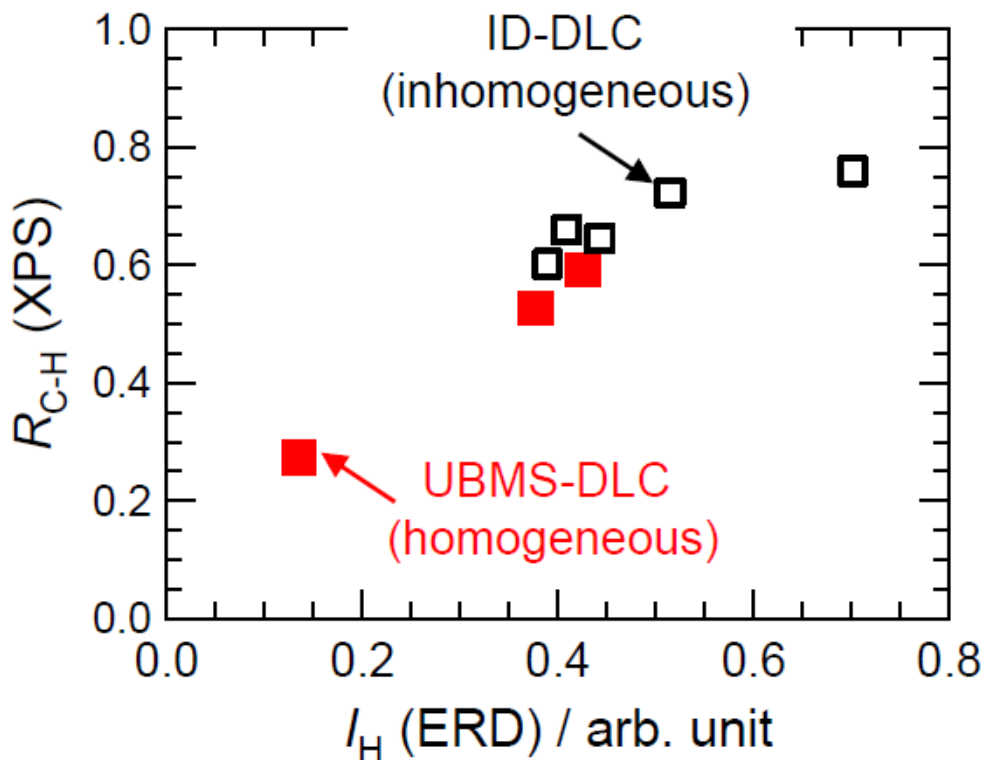


Figure 8. Correlation between the hydrogen concentrations obtained by the XPS and ERD analyses of ■ the UBMS-DLC films with a homogeneous hydrogen distribution and □ the ID-DLC films with an inhomogeneous hydrogen distribution.

“Copyright (2009) The Japan Society of Applied Physics”

## 2.4. Conclusion

The correlation between XPS and ERD was studied for different DLC that hydrogen is distributed in homogeneously or inhomogeneously. AR-XPS analysis using the  $D\check{S}$  function convoluted with a Gaussian function can be used for examining the behavior of hydrogen in ID-DLC films regardless of the hydrogen concentration distributions. This XPS analysis method was suggested to be useful for the comprehensive surface analysis of ID-DLC films and other carbon materials. Moreover, it contributes to the development of the functional surface including the biocompatibility function. This method for analyzing the C1s spectrum enabled the identification of four elements (C–C  $sp^3$  carbon, C–C  $sp^2$  carbon, C–H  $sp^2$  carbon, and C–H  $sp^3$  carbon) composing DLC. Moreover, when the functional group is analyzed from

the C1s spectrum, for example, the hydroxyl spectrum is found to overlaps with the spectrum of the C–H  $sp^3$  carbon. It is effective for the accurate examination of a functional group element by assigning the chemical constitution of DLC. This technique is useful for the structural analysis of not only DLC but also the bulk carbon material.

## **.2.5. References**

- [1] S. Tanuma, C. J. Powell and D. R. Penn, *Surface Interface Analysis*, 11 (1988) 577–589.
- [2] K. C. Prince, I. Ulrych, M. Peloi, B. Ressel, V. Chab, C. Crotti, and C. Comincioli, *Physical Review B*, 62 (2000) 6866–6868.
- [3] T. Balasubramanian, J. N. Andersen, and L. Wallden, *Physical Review B* 64 (2001) 205420.
- [4] R. A. P. Smith, C. W. Armstrong, G. C. Smith, and P. Weightman, *Physical Review B*, 66 (2002) 245409.
- [5] P. Reinke, G. Francz, P. Oelhafen, and J. Ullmann, *Physical Review B*, 54 (1996) 7067–7073.
- [6] K. Bobrov, G. Comtet, G. Dujardin, L. Hellner, P. Bergonzo, and C. Mer, *Physical Review B*, 63 (2001) 165421.
- [7] K. Bobrov, A. Mayne, G. Comtet, G. Dujardin, L. Hellner, and A. Hoffman, *Physical Review B*, 68 (2003) 195416.
- [8] J. Díaz, G. Paolicelli, S. Ferrer, and F. Comin, *Physical Review B*, 54 (1996) 8064-8069.
- [9] J. Díaz, S. Anders, X. Zhou, E. J. Moler, S. A. Kellar, and Z. Hussain, *Physical Review B*, 64 (2001) 125204
- [10] R. Haerle, A. Pasquarello, and A. Baldereschi, *Comput. Materials Science*, 22 (2001) 67–72.
- [11] R. Haerle, E. Riedo, A. Pasquarello, and A. Baldereschi, *Physical Review B*, 65 (2002) 045101.
- [12] S. Takabayashi, K. Motomitsu, T. Takahagi, A. Terayama, K. Okamoto, and T. Nakatani, *Journal of Applied Physics*, 101 (2007) 103542.
- [13] S. Doniach and M. Šunjić, *Journal of Physics C*, 3 (1970) 285–291.
- [14] E. J. McGuire, *Physical Review*, 185 (1969) 1.
- [15] S. Takabayashi, K. Okamoto, H. Sakaue, T. Takahagi K. Shimada, and T. Nakatani, *Journal of Applied Physics*, 104 (2008) 043512.
- [16] S. Takabayashi, K. Okamoto, K. Shimada, K. Motomitsu, H. Motoyama, T. Nakatani, H. Sakaue, H. Suzuki, and T. Takahagi, *Japanese Journal of Applied Physics*, 47 (2008) 3376.
- [17] S. Takabayashi, K. Okamoto, K. Motomitsu, A. Terayama, T. Nakatani, H. Sakaue, H. Suzuki, and T. Takahagi, *Applied Surface Science*, 254 (2008) 2666.
- [18] K. Kimura, K. Nakajima and H. Imura, *Nuclear Instruments and Methods in Physics*

- Research Section B, 140 (1998) 397–401.
- [19] R. D. Mansano, M. Massi, L. S. Zambom, P. Verdonck, P. M. Nogueira, H. S. Maciel, and C. Otani, *Thin Solid Films*, 373 (2000) 243.
- [20] M. Massi, H. S. Maciel, C. Otani, R. D. Mansano, and P. Verdonck, *Journal of Materials Science: Materials in Electronics*, 12 (2001) 343–346.
- [21] D. A. Shirley, *Physical Review B*, 5 (1972) 4709.
- [22] S. Takabayashi, K. Okamoto, T. Nakatani, H. Sakaue, and T. Takahagi, *TANSO*, 235 (2008) 280-289.
- [23] T. Balasubramanian, J. N. Andersen and L. Wallden, *Physical Review B*, 64 (2001) 205420.
- [24] R. A. P. Smith, C. W. Armstrong, G. C. Smith and P. Weightman, *Physical Review B*, 66 (2002) 245409.
- [25] G. Speranza, L. Minati, and M. Anderle, *Journal of Applied Physics*, 102 (2007) 043504.
- [26] S. Tanuma, C. J. Powell and D. R. Penn, *Surface Interface Analysis*, 37 (2005) 1-14.



## Chapter 3

# Chemical Structure and Physical Properties of Plasma-Treated Diamond-like Carbon Film Surface

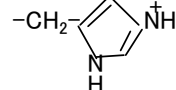
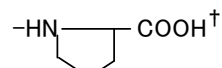
### 3.1. Introduction

The interaction between an artificial material and a cell has the following issues. A typical cell bonding mechanism is an interaction of a cellular adhesion protein and integrin. In this case, it is triggered by the adsorption of the protein on the material surface. As for the adsorption mechanism on the surface of the material, which is a hydrophilic surface, hydrophobic interaction, similar to that on the surface of the cell membrane, and a nonuniform surface structure are shown [1–8]. The chemical composition of the material surface is especially important. It is necessary to match the chemical composition on the DLC surface to an individual cell and the appropriate protein to obtain biocompatibility.

The surface of the cell is negatively charged in general. As for proteins, their structures differ depending on their type, and their potentials are also different. A protein is composed of 20 types of amino acid. The carbon skeleton of an amino acid molecule has amino and carboxyl groups. Amino acids show different characteristics, such as hydrophobicity and hydrophilicity, depending on the structure of this basic carbon skeleton and the side chain. Table 1 shows a list of amino acids [9]. In addition, aspartic acid and glutamic acid show a negative electric potential, whereas lysine, histidine, and arginine show a positive electric potential. Therefore, the potential of a protein changes depending on the amino acids that compose the protein.

For the DLC coating, it is considered that its interaction with a cell and the adsorptive behavior of a protein are changed if the surface potential and hydrophilicity can be freely controlled. The purpose of this study is to control the surface potential of DLC by introducing amino and carboxyl groups onto the DLC surface. These functional groups are common to the amino acid structure; the carboxyl group generally shows a negative charge, and the amino group shows a positive charge. Therefore, an arbitrary surface potential is obtained by controlling the amounts of these functional groups on the DLC surface.

Table 1. 20 kinds of amino acids that compose protein [9]

Character	Name	Structure of side chain	
Neutral	Glycine	-H	
Hydrophile	Positive electric charge	Histidine	
		Lysine	$-(\text{CH}_2)_4-\text{NH}_3^+$
		Arginine	$-(\text{CH}_2)_3-\text{NH}-\text{C}=\overset{+}{\text{N}}\text{H}_2$   N    NH <sub>2</sub>
	Negative electric charge	Aspartic acid	$-\text{CH}_2-\text{COO}^-$
		Glutamic acid	$-\text{CH}_2-\text{CH}_2-\text{COO}^-$
	Amid is contained.	Asparagine	$-\text{CH}_2-\text{CO}-\text{NH}_2$
		Glutamine	$-\text{CH}_2-\text{CH}_2-\text{CO}-\text{NH}_2$
	Hydroxy radical is contained.	Serine	$-\text{CH}_2\text{OH}$
		Threonine	$-\text{CH}_2-\text{CH}(\text{OH})-\text{CH}_3$
	Hydrophobe	The aromatic ring is contained.	Phenylalanine
Tyrosine			$-\text{CH}_2-$ attached to a benzene ring with an -OH group.
Tryptophane			$-\text{CH}_2-$ attached to an indole ring system.
Sulfur is contained.		Methionine	$-\text{CH}_2-\text{CH}_2-\text{S}-\text{CH}_3$
		Cysteine	$-\text{CH}_2-\text{SH}$
Aliphatic character		Alanine	$-\text{CH}_3$
		Leucine	$-\text{CH}_2-\text{CH}(\text{CH}_3)_2$
		Isoleucine	$-\text{CH}(\text{CH}_3)-\text{CH}_2-\text{CH}_3$
		Valine	$-\text{CH}(\text{CH}_3)_2$
		Proline	

It is difficult to directly measure the surface potential of a material. Thus, zeta potential was measured as an alternative characteristic [10]. When the charged material is put in an electrobath, an ion of opposite charge is drawn to the surface, and an electric double layer is formed. The bias of the charge is canceled with increasing distance from the surface of the base material. Then, the numbers of positive and negative ions become the same. This layer is a diffusion zone. Under such a condition, when the electric field is applied, the particle on the surface of the base material and a part of the diffusion zone move together. However, the particle that does not move begins to exist while moving away from the surface in the diffusion zone. The boundary of the potential between the particle that moves together and the particle that does not move is defined as the glide plane. The potential in the glide plane is defined as the zeta potential. Figure 1 shows a diagram of the electric double-layer model and various potentials.

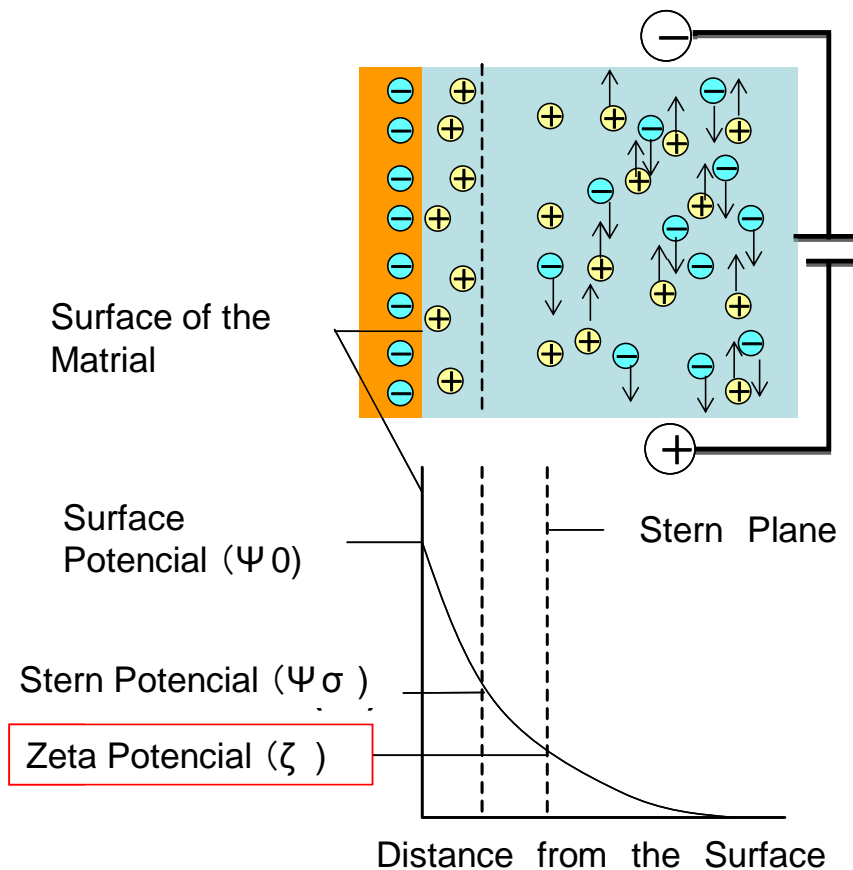


Figure 1. Diagram of electric double layer model and various potential.

Plasma surface treatment is used as a means of introducing a functional group. The equipment used for this purpose has a simple composition, that is, a vacuum chamber and a plasma power supply. Therefore, DLC has an advantage compared with a material that requires a large-scale plant, such as a polymeric material. If plasma surface treatment can satisfy the demand of various biocompatibilities using DLC that controls the surface chemical structure, the biocompatibility problem that many medical treatment devices have becomes surmountable. In addition, the achievement of a tailor-made medical treatment device that matches the state of a patient's disease is expected.

### 3.2. Methods and experimentation

Figure 2 shows diagram of experimental apparatus of the plasma surface treatment. The base pressure was set to 2 Pa by using rotary vacuum pump system, and the working pressure was set to 130 Pa. The operation gases used Ar, C<sub>2</sub>H<sub>2</sub>, and O<sub>2</sub>. The RF power was 30 W. In the case of high vacuum, base pressure was set to 10<sup>-3</sup> Pa, and the working pressure was set to 4 Pa by using turbo molecular pump system. RF power was 100 W. The process chamber was connected to RF power supply with an excitation frequency 13.56 MHz. RF power of 30W and 100W was injected to generate plasmas. CCP (Capacitively Coupled Plasmas) was generated by means of two parallel plate electrodes. The operational gases used were O<sub>2</sub>, Ar, NH<sub>3</sub> and C<sub>2</sub>H<sub>2</sub>. These gases were introduced into the chamber via a mass flow controller. In the experiments, the plasma treatment duration was 15 seconds with each gas, making duration of 30 seconds when two gases were used. Table 2 shows details of the plasma treatment conditions. DLC thin films used for plasma surface modification were prepared by ionization-assisted deposition. The operational gases used were benzene gases. The film thickness was about 40nm.

The composition ratio of the DLC samples that modified by the plasma modification was analyzed by an XPS (JPS-9010, JOEL). The XPS measurements condition was mean voltage of 10 kV and current of 10 mA with an unmonochromated AlK $\alpha$  line. The measurements focused on the C 1s, N 1s, O 1s and O=C-O carbon. The C1s spectrum was first assigned into four elements (C-C *sp*<sup>3</sup> (283.8 eV), C-C *sp*<sup>2</sup> (284.3 eV), C-H *sp*<sup>2</sup> (284.8 eV), and C-H *sp*<sup>3</sup> (285.3 eV)) [11–13]. The static contact angle was measured with a contact angle meter (DM300, Kyowa Interface Science). Pure water was used to measure contact angle. Then, amount of the dropped water was 1  $\mu$ l. The zeta potential on ID-DLC films surface was

measuring a zeta potential meter (ELS-Z, Otsuka Electronics). Solution used sodium chloride of 10mM. Solvent used pure water. The distance of the electrode was 15 mm. Average electric field was 17.3 V / m.

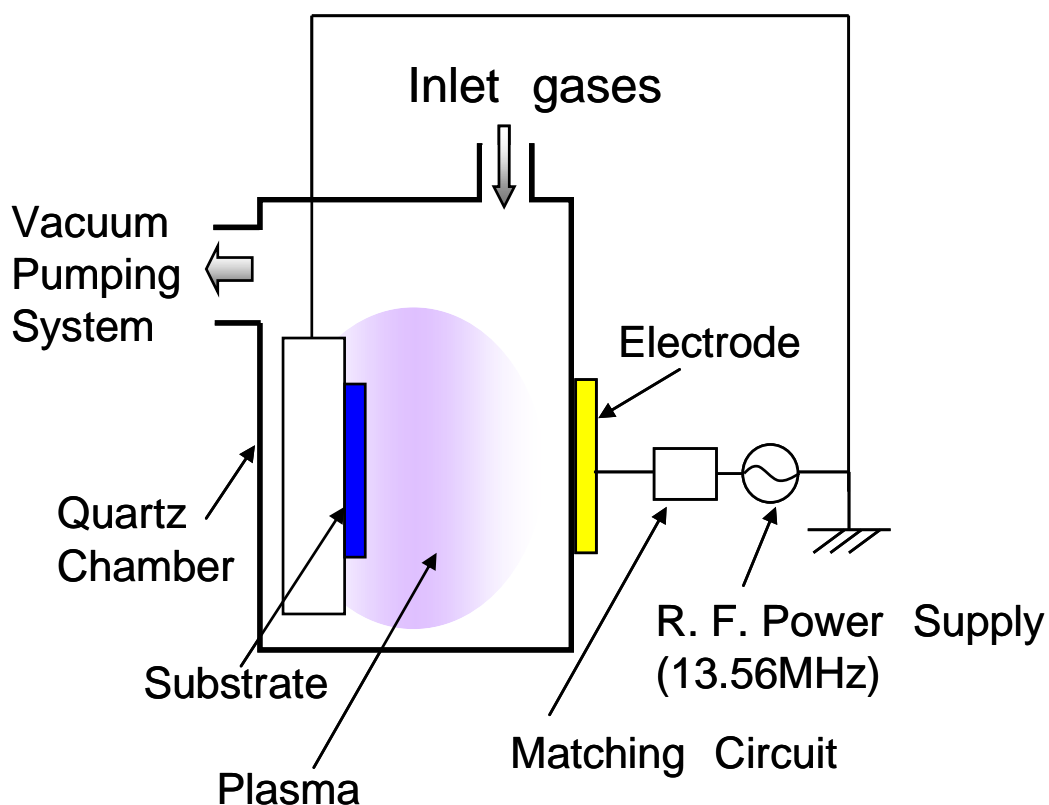


Figure 2. Diagram of experimental apparatus of the plasma surface treatment.

Table 2. ID-DLC sample group and preparation condition

Group	Sample	Plasma source	Plasma condition
A	a	O <sub>2</sub>	Low vacuum
	b	Ar	
	c	Ar + NH <sub>3</sub>	
B	d	C <sub>2</sub> H <sub>2</sub>	Low vacuum
	e	C <sub>2</sub> H <sub>2</sub> + O <sub>2</sub>	
C	f	NH <sub>3</sub>	High vacuum (TMP)
	g	O <sub>2</sub> + NH <sub>3</sub>	

TMP: Turbo Molecular Pump

### 3.3. Results and discussion

#### 3.3.1. Results of XPS spectrum measurement

Figure 3 and 4 shows the result of XPS measurement after plasma treatment. Figure 3 shows the XPS spectra of treated ID-DLC in C 1s, O 1s and N 1s observed when the sample was given C<sub>2</sub>H<sub>2</sub> plasma treatment followed by O<sub>2</sub> plasma treatment. The composition rate of C 1s, O 1s and N 1s were 0.78, 0.22 and 0 respectively. Nitrogen was not observed from N 1s spectrum. The C 1s spectrum can be assigned to the binding energy of C–O, C=O and O=C–O bonded network respectively [14, 15].

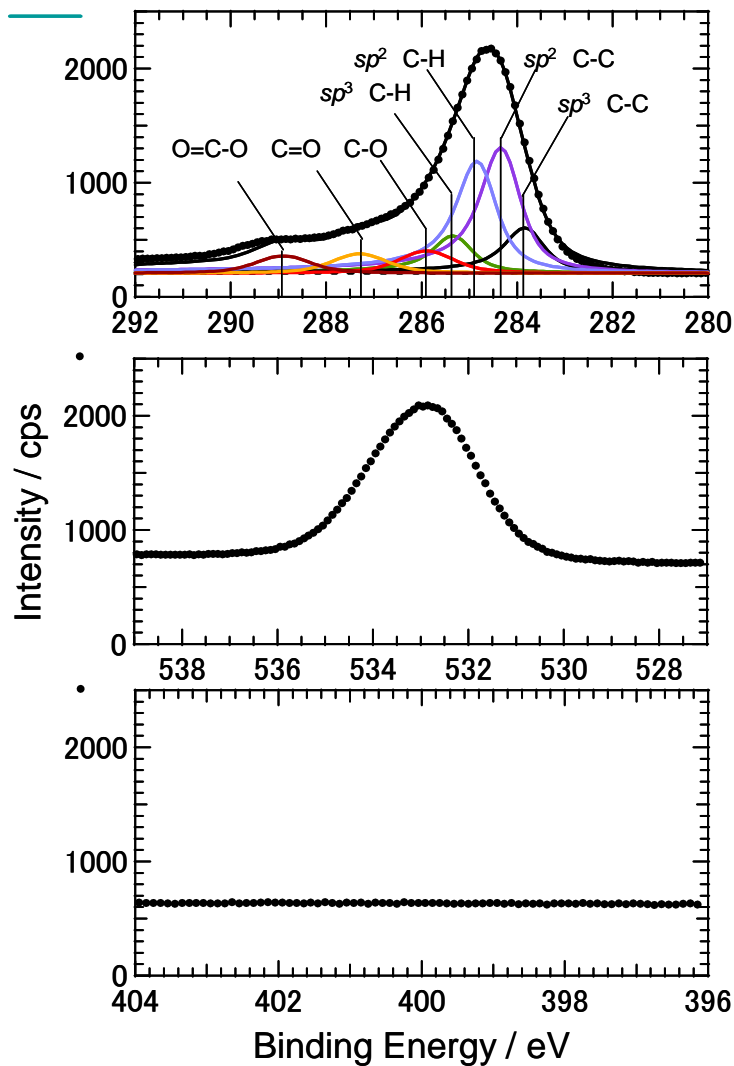


Figure 3. The XPS spectra of plasma treated ID-DLC observed when the sample was given C<sub>2</sub>H<sub>2</sub> plasma treatment followed by O<sub>2</sub> plasma treatment. (Upper spectrum is C 1s, middle spectrum is O 1s and lower spectrum is N 1s)

The composition rate of C–O/C, C=O/C and O=C–O/C were 0.08, 0.05 and 0.04 respectively. Since the composition rate of C–O/C, C=O/C and O=C–O/C in an untreated ID-DLC were 0.06, 0.02 and under 0.01, it is evident that the C–C bonds and C–H bonds were cleaved by radicals, electrons and ions in the plasma, and that thereby oxidation reactions such as C–O, C=O and O=C–O bonds were promoted. Particularly, substrate bias was 0 V when plasma treatment was performed in this experiment. It was considered that O<sub>2</sub> or O radicals in plasma mainly drawn H from C–H bonds. Amount of C–C bonds or C–H bonds in DLC thin films were dependence on functional group introduced to ID-DLC surface. Therefore it is considered that amount of functional groups introduced to DLC thin films surface can be controlled by controlling amount of C–C bonds or C–H bonds in ID-DLC thin films. It can also be seen that the O=C–O peaks were peaks stemming from the carboxyl groups and were, approximately, over three times more numerous compared with an untreated ID-DLC sample. From this result, it will be seen that carboxyl groups can be introduced efficiently onto the surface of ID-DLC thin films by plasma surface modification.

Figure 4 shows the XPS spectra of ammonia plasma treated ID-DLC in C 1s, O 1s and N 1s. The composition rate of C 1s, O 1s and N 1s were 0.86, 0.03 and 0.11 respectively. It is observed that N 1s spectrum was remarkable, in contrast to the C<sub>2</sub>H<sub>2</sub> + O<sub>2</sub> plasma treatment. It is considered that the C–H bonds or C–C bonds were severed by radicals, electron and ion in the NH<sub>3</sub> plasma. It will be seen from the foregoing that we are now able to generate both carboxyl groups and amino groups on the surface of ID-DLC thin films. In these results, possibility for controlling the zeta potential was suggested.

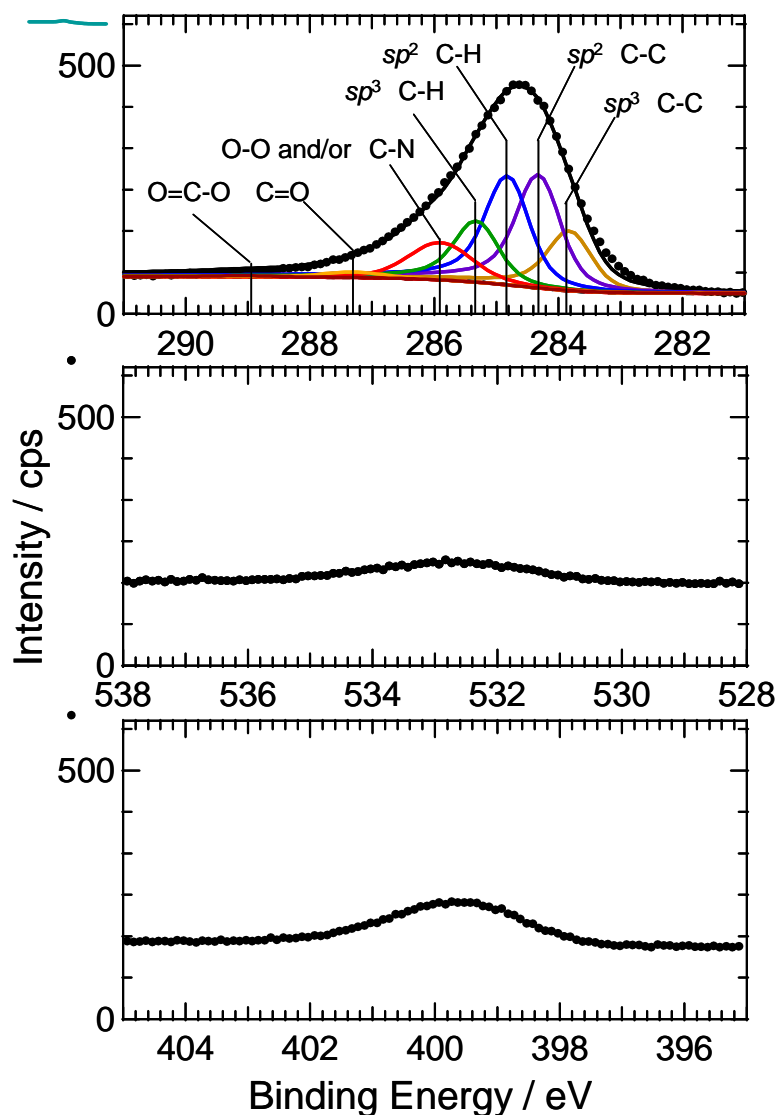


Figure 4. The XPS spectra of plasma treated ID-DLC in C 1s, O 1s and N 1s were observed when the sample was modified by ammonia plasma treatment.  
(Upper spectrum is C 1s, middle spectrum is O 1s and lower spectrum is N 1s)

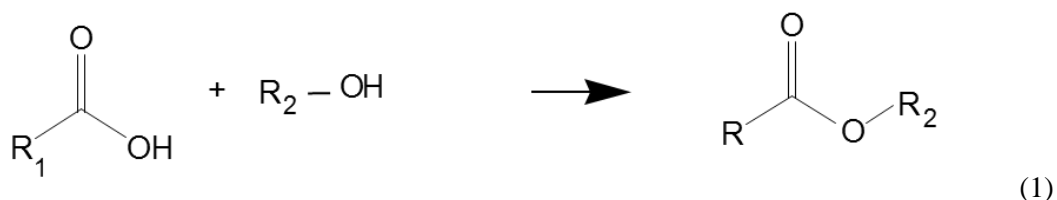
### 3.3.2. Results of chemical modification XPS method

The carboxyl groups and the ester bonds cannot be distinguished by the C 1s spectrum of XPS analysis. In this study, the chemical modification XPS method is evaluated. The feature in this analysis is the labeling element reacts to the target functional group [16, 17]. As for the label element, it must not be contained in the measuring object, and it should have a large photoionization cross section. Fluorine is an element not contained in DLC and the functional



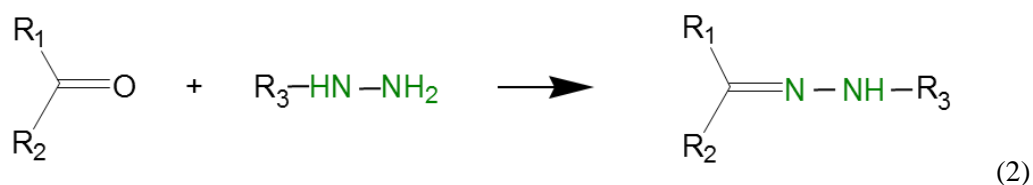
group. Moreover, the photoionization cross section of fluorine is four times the carbon. Fluorine is especially suitable for the labeling element in this study. Then, analysis of the carboxyl groups and the carbonyl groups on the plasma-treated ID-DLC surfaces prepared by  $C_2H_2 + O_2$  plasma was evaluated by using the reagent including the fluorine of the labeling element.

Trifluorethanol (TFE,  $CH_2CF_3OH$ ) is reported as a reagent of the analysis of the carboxyl group [18, 19]. Chemical equation of a carboxyl group and a primary alcohol is shown in equation (1).



The analysis of carboxyl groups that used TFE was as follows. TFE of 0.5 ml, pyridine of 1ml, and dicyclohexylcarbodiimide of 200 mg are measured. These measured reagents are added to the methylene chloride of 15 ml. Next, plasma treated ID-DLC and untreated ID-DLC samples were put in the reagent solution, and the samples soaked it during 24 hours in the room temperature. The samples washed three times with the diethyl ether, and the samples were dried. Next, the fluorine was analyzed by the XPS.

Tetrafluorophenylhydrazine (TFPH,  $C_6HF_4NHNH_2$ ) is known as a reagent of the analysis of the carbonyl groups [18, 19]. Chemical equation of a carbonyl group and a hydrazine is shown in equation (2).



The analysis of the carbonyl group that used TFPH was as follows. TFPH of 150 mg and a small amount of hydrochloric acid was added to the ethanol of 15ml. Next, plasma treated DLC and untreated DLC samples were put in the reagent solution, and the samples soaked it during 24 hours in the room temperature. The samples washed three times with the ethanol,

and the samples were dried. Next, the fluorine was analyzed by the XPS.

Figure 5 shows the state after chemical modification reacts. Three fluorine atoms per one carboxyl group are united and four fluorine atoms per one carbonyl group are united.

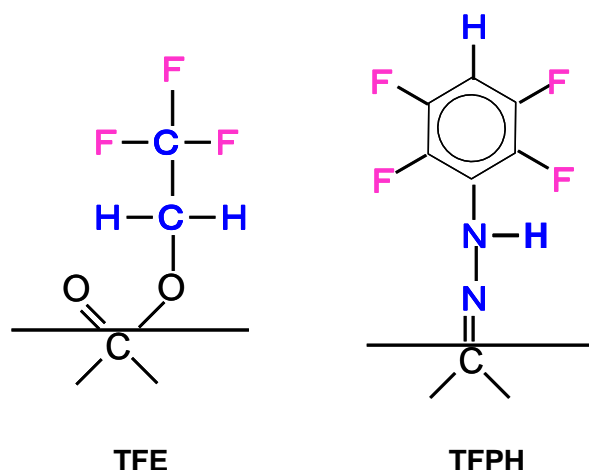


Figure 5. The state after chemical modification reacts of TFE and TFPH.

Photoelectron intensity of the carbon detects all depth areas. Meanwhile, the photoelectron intensity of fluorine is observed only from the surface. Therefore, it is necessary to know the ratio of photoelectron intensity of the carbon on the surface to all photoelectron intensity.

Then, it is assumed that DLC is a regularly atomic arrangement structured model, and calculates the depth distance of one atom carbon layer from the density of DLC. The ratio of all integrated photoelectron intensity of carbon and integrated photoelectron intensity by the depth of one atom carbon layer is calculated from the depth distance of one atom carbon layer. The surface coverage of functional groups on the plasma-treated DLC surface is obtained by multiplying this ratio by the amount of the observation of fluorine, and dividing in the number of fluorine a labeling molecule.

The thickness of one atom carbon layer is obtained from equation (3). Then,  $A_c$  is atomic weight of carbon,  $N$  is Avogadro's number,  $T_c$  is depth distance of one atom carbon layer,  $D$  is atom density of DLC.

$$T_c = \frac{1}{\sqrt[3]{\left(\frac{D}{A_c} \times N\right)}} \quad (3)$$

The density of ID-DLC was 2.14 g/cm<sup>3</sup> according to X-ray reflectivity method. The thickness of one atom carbon layer is obtained.

$$Tc = \frac{1}{\sqrt[3]{\left(\frac{2.14 \text{ g/cm}^3}{12 \text{ g/cm}^3} \times 6.02 \times 10^{23} \text{ atom/cm}^3\right)}} = 0.21 \text{ nm}$$

Next, the attenuation of the photoelectron to the mileage in the material is obtained in equation (4).

$$\phi(z) = c \exp\left(-\frac{z}{\lambda \cos \theta}\right) \quad (4)$$

Equation (5) shows integrated photoelectron intensity obtained when the mileage of the photoelectron in the material is assumed to be  $x$ .

$$I(x) = \frac{\int_0^x \phi(z) dz}{\int_0^\infty \phi(z) dz} = \frac{\int_0^x \exp\left(-\frac{z}{\lambda \cos \theta}\right) dz}{\int_0^\infty \exp\left(-\frac{z}{\lambda \cos \theta}\right) dz} = 1 - \exp\left(-\frac{x}{\lambda \cos \theta}\right) \quad (5)$$

As for the carbon, non-elasticity mean free path  $\lambda$  of the photoelectron is reported to be 3.11 nm [16]. The taking off angle  $\theta$  of the photoelectron to the sample normal was 0 degree. The thickness of one atom carbon layer that had been obtained according to the density of DLC was 0.21 nm. Therefore, photoelectron intensity radiated from one atom carbon layer is 0.934, and the integrated intensity is 0.021. Also, all integrated intensities of the carbon are 0.321.

Therefore, the surface coverage of functional groups on the DLC is obtained from the following equation (6).  $SC_F$  is surface coverage of functional groups,  $C$  is all integrated intensities of the carbon,  $C_S$  is integrated intensity radiated from one atom carbon layer  $C'$  is

ratio of the functional group to the total carbon.  $F'$  is amount of fluorine.  $n_F$  is number of fluorine that labeling reagent molecule contains.

$$SC_F = C \times \frac{C}{C_S} = \frac{F'}{n_F} \times \frac{C}{C_S} = \frac{F'}{n_F} \times \frac{0.321}{0.021} \quad (6)$$

Figure 6 shows chemical labeling measurement result of  $C_2H_2 + O_2$  plasma treatment. Amount of carboxyl and carbonyl groups was measured with trifluoroethanol and tetrafluorophenylhydrazine. From this result, it was observed that carbonyl and carboxyl groups were increased by plasma treatment. It was found that carboxyl groups were introduced to DLC surface by  $O_2$  Plasma.

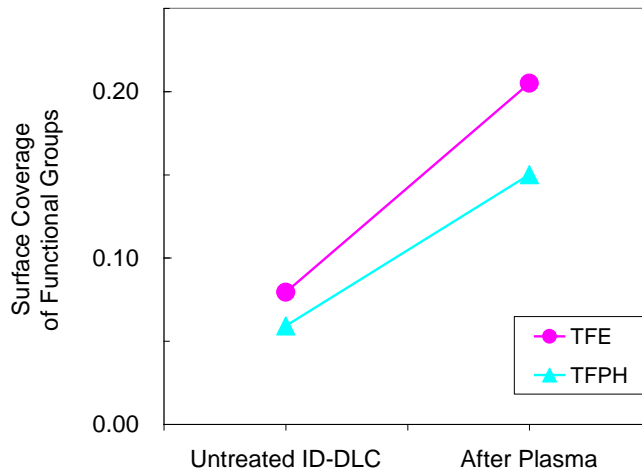


Figure 6. The chemical labeling result for  $C_2H_2 + O_2$  plasma treated DLC film. It was observed that carboxyl groups and carbonyl groups were increasing after plasma treatment.

### 3.3.3. Results of contact angle measurement

Figure 7 shows the contact angles measurement result when the amount of carboxyl groups is varied. The proportions of such groups were determined by plasma surface modification with different gases and measuring the resulting samples with the XPS. The contact angles are the values immediately after plasma treatment.

It can be observed that the contact angle tends to decrease with increasing in amount of  $O=C-O$ . Also, the DLC thin films surface becomes adequately hydrophilic with increasing in

the carboxyl groups, since the contact angle of ID-DLC thin films is around 70°. As C–O bonds such as C–O, C=O, O=C–O are known to be hydrophilic, the cause is considered to be that the hydrophilicity of the ID-DLC thin films surface increases with increasing in such bonds. The contact angle of the C<sub>2</sub>H<sub>2</sub> plasma was higher than that of ID-DLC. Hydrophilicity was increased by the plasma treatment, which introduces the carboxyl groups and the hydroxyl groups on the surface of ID-DLC. Moreover, the functional group is introduced by bonding with the carbon. Therefore, it is suggested that the C<sub>2</sub>H<sub>2</sub> plasma forms another structure including many carbon–hydrogen uniting on the ID-DLC.

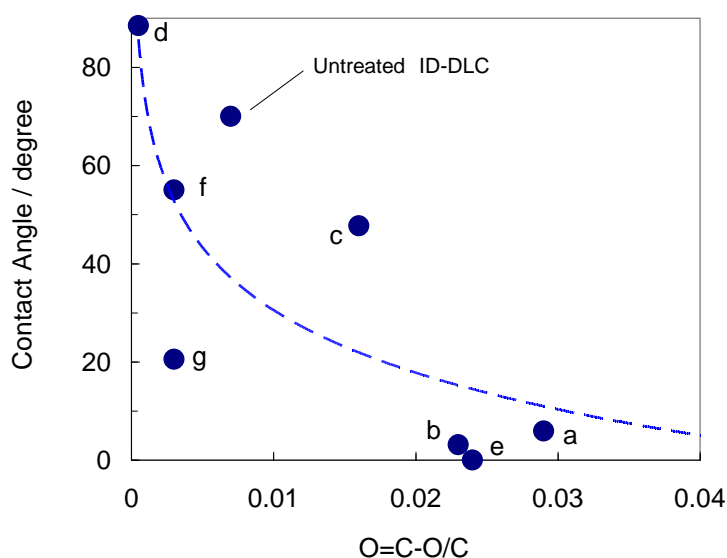


Figure 7. The proportions of such groups were determined by plasma surface treatment with different gases and measuring the resulting samples with XPS. The static contact angles are the values immediately after plasma treatment. The static contact angle values were decreasing with increasing in carboxyl groups.

Figure 8 shows the contact angle measurement result when ID-DLC surface was modified by NH<sub>3</sub> plasma. The contact angle of NH<sub>3</sub> plasma treatment was lower than that of untreated DLC. The contact angle was saturated when N/C ratio was about 0.07. However even the lowest value of contact angle was about 30°, the contact angle was higher than that of ID-DLC introduced carboxyl groups. Therefore it is considered that either the contact angle was mainly dependence on amount of O=C–O. It was found that the contact angle can be controlled by controlling the amount of the carboxyl groups.

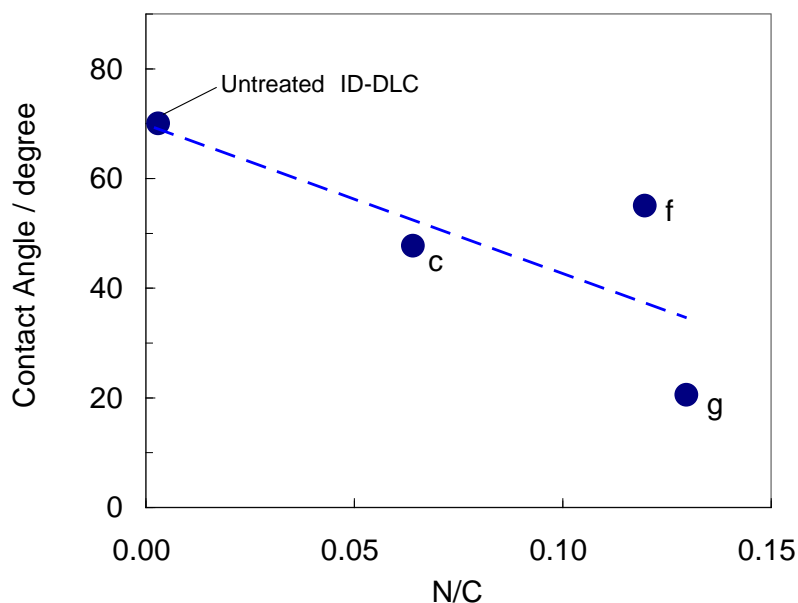


Figure 8. The static contact angle measurement result when ID-DLC surface was treated by  $\text{NH}_3$  Plasma. The static contact angle values of  $\text{NH}_3$  plasma treatment were lower than that of untreated ID-DLC. The static contact angle values were saturated when N/C ratio was about 0.07. However even the lowest value of contact angle values was about  $30^\circ$ , the contact angle was higher than that of introduced carboxyl groups.

### 3.3.4. Results of zeta potential measurement

Figure 9 shows the results of zeta potential measurement for various carboxyl group amounts. Zeta potential was measured. The carboxyl group amount was measured under various plasma modification conditions, and the zeta potential in each case was measured. The N/C ratio in the various cases is also shown in the figure. The N/C and O=C–O/C ratio were the values immediately after plasma treatment. It can be observed that the zeta potential was decreased approximately twice as much as untreated sample with increasing in the O=C–O/C ratio. It is known that where the carboxyl group  $-\text{COOH}$  is present it will generally dissociate thus:



and samples to which carboxyl groups have attached will be negatively charged due to the  $-\text{COO}^-$ . Therefore, it is considered that the zeta potential was decreased with increasing in the carboxyl groups, compared with untreated ID-DLC thin films. It can also be observed that when  $\text{N/C} = 0.06$  and  $0.12$  the zeta potential increases greatly compared with an untreated DLC thin films, particularly at  $\text{N/C} = 0.12$ , where the zeta potential turns positive. Generally, amino groups unite in solution with the proton as follows.



It is known that where the amino group  $-\text{NH}_3^+$  with bonded protons is present on the surface of a sample, the sample will generally be positively charged. Therefore, it was considered to account for the marked increase in the surface potential of the DLC thin films when the amino groups were introduced.

These results indicate that it is possible to control the zeta potential of DLC thin films by controlling the amounts of the carboxyl groups and amino groups. It may thus be said to have discovered a possibility for development of a new biocompatible material.

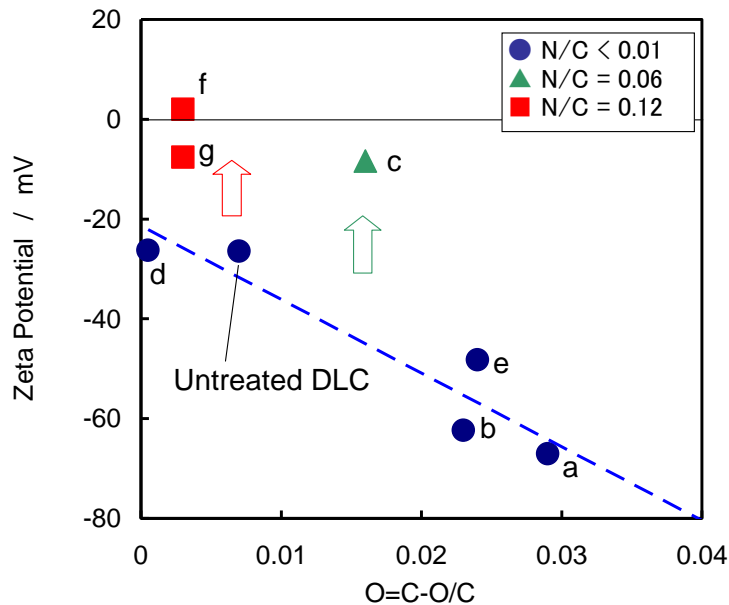


Figure 9. Correlation between the zeta potential and O=C–O/C ratio with different N/C ratio of plasma treated ID-DLC surfaces.

### **3.4. Conclusion**

The purpose of this research was the controlling of the zeta potential of DLC surface by introducing the amino groups and the carboxyl groups onto the surface of DLC. The plasma surface treatment technology can be used to introduce carboxyl groups and functional groups derived from nitrogen onto the ID-DLC film surface. Moreover, the amount of these functional groups can be controlled by changing the condition of plasma treatment.

Regarding the results of zeta potential measurement, the ID-DLC film surface became negatively charged when the carboxyl groups are introduced, and ID-DLC film surface became positively charged when the functional groups derived from nitrogen are introduced. The zeta potential of the ID-DLC film surface was controlled easily by controlling the amount of carboxyl groups and functional groups derived from nitrogen.

From these results, a unique material similar to amino acids where the positive and negative charges existed together at the same time could be obtained.



### 3.5 References

- [1] E. W. Merrill, E. W. Salzman, *ASAIO Journal*, 28 (1982) 482–485.
- [2] E. Kulk, Y. Ikada, *Journal of Biomedical Materials Research*, 30 (1996) 295–304.
- [3] T. Okano, S. Nishiyama, I. Shinohara, T. Akaike, Y. Sakurai, K. Kataoka, T. Tsuruta, *Journal of Biomedical Materials Research*, 15 (1981) 393–403.
- [4] T. Furuzono, K. Senshu, A. Kishida, T. Matsumoto, M. Akashi, *Polymer Journal*, 29 (1997) 201–209.
- [5] Y. Kadoma, N. Nakabayashi, E. Masuhara, J. Yamauchi, *Kobunshi Ronbunshu*, 35 (1978) 423–427, (in Japanese).
- [6] K. Ishihara, R. Takayama, N. Nakabayashi, K. Fukumoto, J. Aoki, *Biomaterials*, 13 (1992) 235–239.
- [7] H. Kitano, T. Mori, S. Tada, M. Gemmei-Ide, M. Tanaka, *Macromolecular Bioscience*, 5 (2005) 314–321.
- [8] D. R. Lu, S. J. Lee, K. Park, *Journal of Biomaterials Science, Polymer Edition*, 3 (1992) 127–147.
- [9] T. Tamura, M. Muramatsu, *KISO BUNSHI SEIBUTSU-GAKU*, 2007, Tokyo Kagaku Doujin, Tokyo, (in Japanese).
- [10] K. Furusawa, *Bunseki*, 5 (2004) 247–254, (in Japanese).
- [11] S. Takabayashi, K. Motomitsu, T. Takahagi, A. Terayama, K. Okamoto, and T. Nakatani, *Journal of Applied Physics*, 101 (2007) 103542.
- [12] S. Takabayashi, K. Okamoto, K. Motomitsu, A. Terayama, T. Nakatani, H. Sakaue, H. Suzuki, T. Takahagi, *Applied Surface Science*, 254 (2008) 2666.
- [13] S. Takabayashi, K. Okamoto, T. Nakatani, H. Sakaue, T. Takahagi, *TANSO*, 235 (2008) 280–289, (in Japanese).
- [14] W. Chuang, J. Lin, *Journal of Biomedical Material Research, Part A*, 82 (2007) 820–830.
- [15] T. Takahagi, A. Ishitani, *Carbon* 22 (1984) 43–46.
- [16] D.S. Everhert, C.N. Reilly, *Analytical Chemistry*, 53 (1981) 665–676.
- [17] T. Takahagi, A. Ishitani, *Carbon*, 26 (1988) 389–395.
- [18] Y. Nakayama, T. Takahagi, F. Soeda, K. Hatada, S. Nagaoka, J. Suzuki, A. Ishitani, *Journal of Polymer Science, Polymer Chemistry*, 26 (1988) 559–572.
- [19] S. Tanuma, C. J. Powell and D. R. Penn, *Surface Interface Analysis*, 11 (1988) 577–589.

## Chapter 4

# Introduction of Carboxyl Groups onto Diamond-like Carbon Films Doped with Silicon

### 4.1. Introduction

Silicon doping is reported as one of the methods of improving the mechanical properties of DLC films [1–3]. It is applied to automotive parts with good mechanical characteristics [4]. Moreover, Bendavid et al. reported that the silicon contained in the DLC film increases the proliferation rate of osteoblast cells [5]. It is expected that the silicon contained in the DLC film is good for application to medical equipment from the viewpoint of mechanical property and biocompatibility.

The previous chapter showed that a functional group could be introduced onto the DLC film surface by plasma surface treatment. When the functional group was introduced, it was shown that the zeta potential can be controlled. However, the effect of the introduced functional group on the doping of silicon into the DLC film is unclear. Then, the DLC film with a different silicon content was prepared, and the functional group was introduced by the plasma surface treatment. The effect on the ratio of the carboxyl group introduced was examined when the silicon content was changed.

### 4.2. Methods and experimentation

The DLC was prepared by ionized deposition method. Si wafers were placed in the chamber of an ionized deposition apparatus, and argon gas was introduced to the chamber. Then, bombardment cleaning was implemented by plasma discharge. Plasma discharge operational conditions were controlled of negative DC bias voltage to 2 kV and the electric power of the filament was 300W. The deposition pressure adjusted to  $1 \times 10^{-1}$  Pa. Subsequently, operation gases were switched to tetramethylsilane ( $\text{Si}(\text{CH}_3)_4$ ) and benzene ( $\text{C}_6\text{H}_6$ ) and adjusting the flow ratio between  $\text{C}_6\text{H}_6$  and  $\text{Si}(\text{CH}_3)_4$  used as material gases coated the DLC films having four different silicon contents. Four types of ID-DLC films were deposited on the Si wafer.

The amount of silicon was measured by using the auger spectrum analysis (AES, PHI-660, PHYSICAL ELECTRONICS). AES measurement condition of electron gun was accelerating

voltage of 10kV and current of 500 nA.

Next, the C 1s and Si 2p spectra measured using the XPS (JPS-9010, JEOL) on ID-DLC film surface. The XPS measurements condition of X-ray source was a voltage of 12.5 kV and current of 15 mA with an unmonochromated AlK $\alpha$  (1486.3 eV) line. The charge correction was determined by first dropping Au colloids on a part of the substrate surface and allowing them to dry. The amount of shift was determined from the binding energy of Au 4f 7/2 [6]. Next, functional groups modification was conducted on ID-DLC films surfaces with different amounts of doped silicon by using the plasma surface treatment technology in the same manner as chapter 3, and the relationship between the composition of the surface and the amount of the functional groups introduced was examined.

Functional groups were introduced on the surface by first applying plasma using gases containing Ar mixed with 3% flow rate O<sub>2</sub>, and then by applying plasma using only O<sub>2</sub> gas. The working pressure was set to 133 Pa, the RF power was 30 W, and the irradiation time was 15 seconds. Different XPS method was used to divide the peaks of C 1s spectrum with O=C–O, C=O and C–O bonds for quantitative measurement of the carboxyl groups obtained [7]. The amount of carboxyl groups introduced on the surface was obtained by determining the ratio of the intensity of the peak of O=C–O bonding to the intensity of the maximum peak of C 1s spectrum.

### **4.3. Results and discussion**

The concentration of silicon of ID-DLC films were 28 atom %, 19 atom %, 3 atom % and 0 atom % respectively by using AES. Tetramethylsilane gas was not used when ID-DLC films of 0 atom % was prepared. Next, a comparison of the binding energy of XPS C 1s spectrum carboxyl groups was conducted on a substrate subjected to functional groups modification through ID-DLC films surface treatment using plasma.

Figure 1 shows the XPS C 1s spectrum where plasma treated ID-DLC films. As a result, a peak of O=C–O bonding was found on the ID-DLC films surface, and the introduction of carboxyl groups was observed. Furthermore, it was determined that the amount of O=C–O bonding decreased as the amount of doped silicon increased.

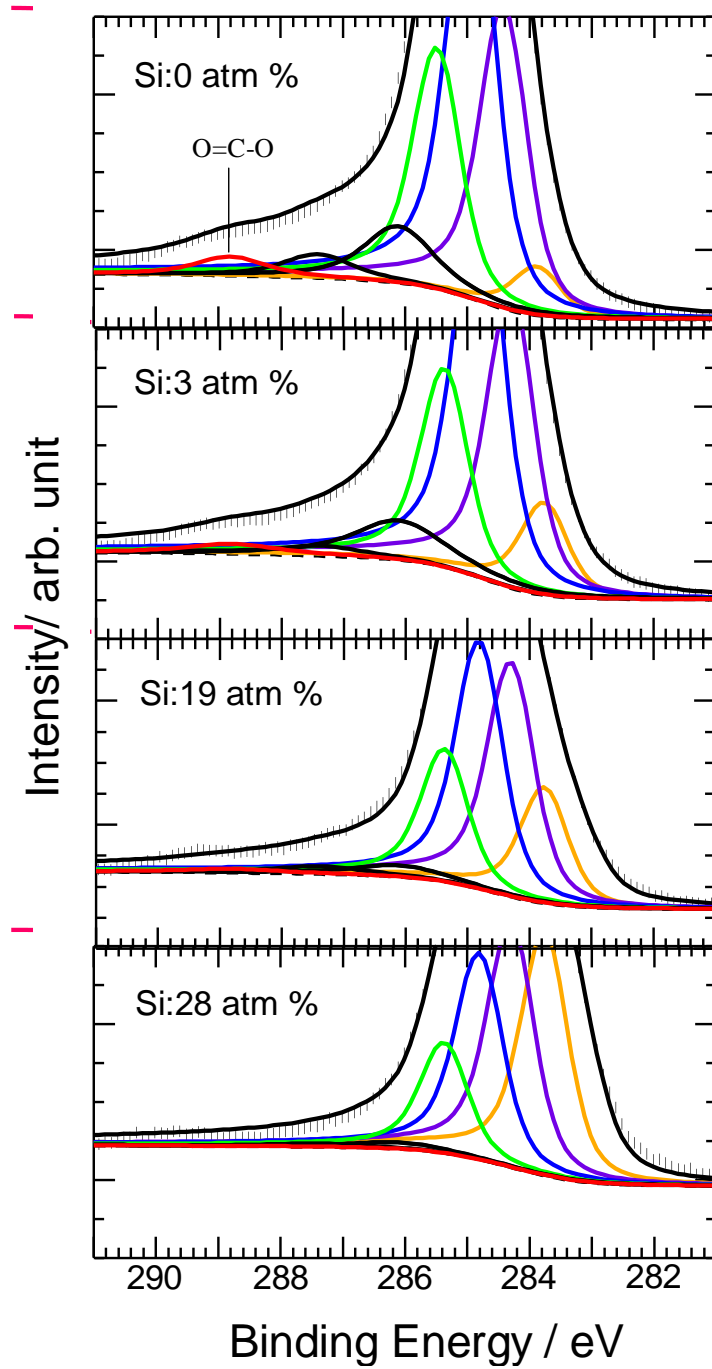


Figure 1. C 1s spectrum of ID-DLC films with different amounts of doped silicon subjected to plasma surface treatment.

Figure 2 shows the relationship of O=C–O/C ratio of C 1s spectrum and different silicon contents. O=C–O/C ratio is decrease when silicon concentration is increasing.

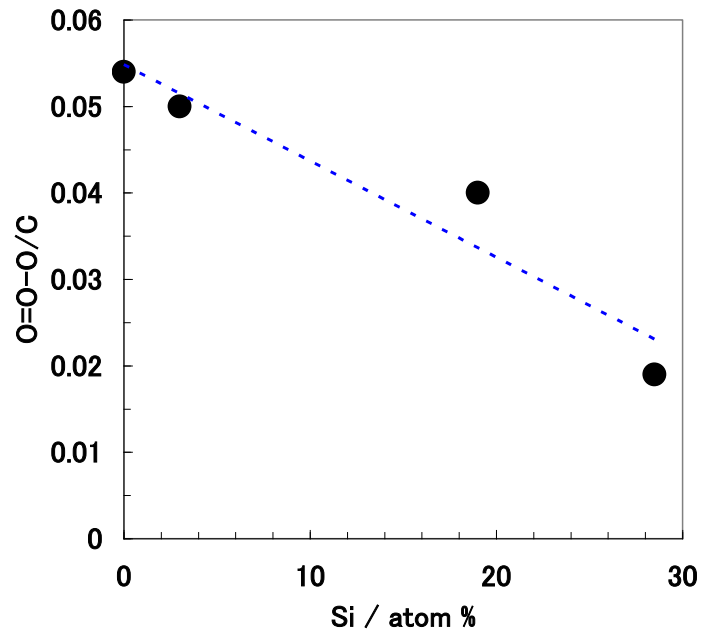


Figure 2. Correlation between O=C–O/C ratio and silicon concentration after plasma treatment.

Figure 3 shows the difference Si 2p spectrum of ID-DLC films after the plasma treatment. In addition, a peak of SiO<sub>2</sub> was obtained on Si 2p spectrum after the plasma treatment, indicating the oxidation of Si–C.

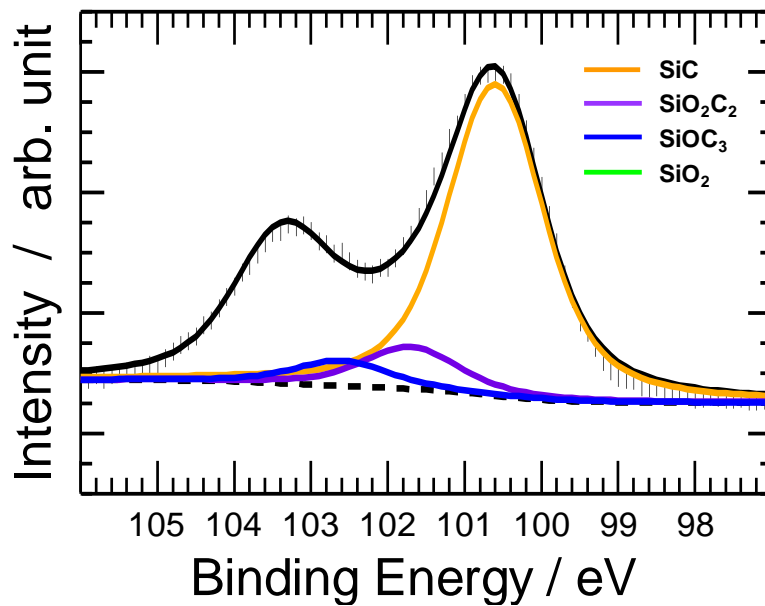


Figure 4–3. Si 2p spectrum of plasma treated ID-DLC with 19% silicon.

Figure 4 shows relationship of SiO<sub>2</sub> and different silicon contents. SiO<sub>2</sub> is increase when silicon concentration is increasing. Silicon is oxidized to form SiO<sub>2</sub> through the surface treatment using oxygen plasma and obstruct to the introduction of carboxyl groups. In addition, increasing the silicon content relatively decreases the proportion on the carbon surface. When a silicon and carbon are compared, electolonegativity (Pauling) of silicon (1.9) is lower than carbon (2.55) [8]. Therefore we deduce silicon to be oxidized first more than carboxyl groups are introduced.

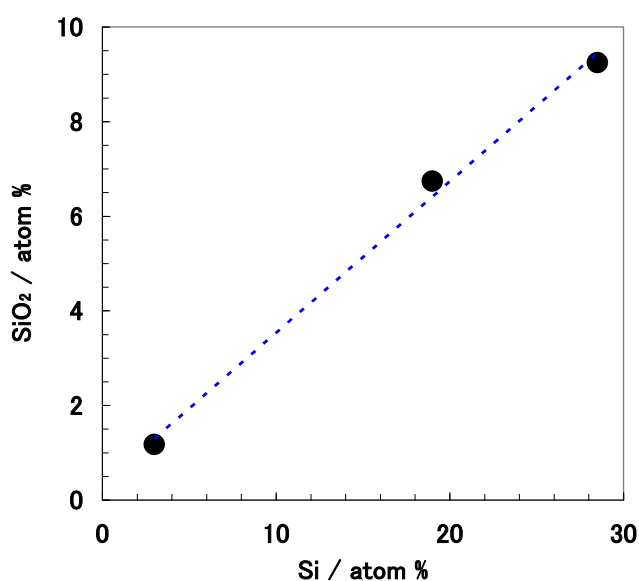


Figure 4. Corelation between amount of generation SiO<sub>2</sub> and silicon concentration after plasma treatment..

#### 4.4. Conclusion

In this study, the introduction of carboxyl groups onto ID-DLC films doped with silicon through surface treatment technology using oxygen plasma was tried. The introduction of carboxyl groups onto the ID-DLC films doped with silicon by surface treatment technology using oxygen plasma was tried. It was found that silicon is obstructive in the case of DLC used as the base of functional group introduction. As a reason, the oxidation of silicon first occur, inhibiting carboxyl group generation.

#### 4.5. References

- [1] T. Nakatani, K. Okamoto, A. Araki, T. Washimi, *New Diamond and Frontier Carbon Technology*, 16 (2006) 187–200.
- [2] H. Mori, H. Tachikawa, *Surface and Coatings Technology*, 149 (2002) 225–230.
- [3] K. Nakanishi, H. Mori, H. Tachikawa, K. Itou, M. Fujoka, Y. Funaki, *Surface and Coatings Technology*, 200 (2006) 4277–4281.
- [4] K. Hayashida, *JTEKT Engineering Journal*, 1007 (2009) 8–14, (in Japanese).
- [5] A. Bendavid, P. J. Martin, C. Comte, E. W. Preston, A. J. Haq, F. S. M. Ismail, R.K. Singh, *Diamond and Related Materials*, 16 (2007) 1616–1622.
- [6] S. Takabatashi, K. motomitsu, T. takahagi, A. terayama, K. okamoto and T, nakatani, *Journal of Applied physics*, 101 (2007) 103542.
- [7] S. Kodama, H. Habaki, H. Sekiguchi, J. Kawasaki, *Thin Solid Films*, 407 (2002) 151–155.
- [8] L. Pauling, *Journal of the American Chemical Society*, 54 (1932) 3570-3582.

## Chapter 5

### Blood Compatibility of Plasma Surface Treated Diamond-like Carbon *in-vitro*

#### 5.1. Introduction

Medical devices come in contact with blood *in vivo*. Therefore, an important characteristic of a medical device is blood compatibility. That is, the medical material should satisfy requirements related to platelet adhesion and blood coagulation. The platelet behaviors include activation and sticking when a foreign substance is recognized in the blood. Research on the control of platelet adhesion is advanced in the field of polymer materials. Positive and negative polarity groups in relation to the lecithin of the phosphorus lipid that comprises the cell membrane exist. A methacryloyloxyethylphosphorylcholine (MPC) polymer was used to imitate the chemical construction of a cell membrane with good platelet adhesion [1, 2]. Kitano et al. showed that a betaine polymer has zwitterionic groups with good platelet adhesion. They insisted that such an ionic structure does not destroy the boundary water structure [3]. However, the chemical construction of the polymer is not easily changed during mass production. Therefore, polymer materials are difficult to apply in a chemical structure in accordance with the treatment purpose and patient's condition, and the biocompatibility cannot be modified. In this research, we examined the biocompatibility of the surface functional group structure on the basis of these reports. In chapter 4, it was suggested that, in the plasma-surface-treated ID-DLC, the ratio of the surface functional groups was arbitrarily changed with the simple device. In the plasma-surface-treated ID-DLC, it is possible that the blood compatibility can be arbitrarily controlled.

Concerning the activation mechanism of the blood coagulation system, the first two steps are known. The coagulation factor is activated when prekallikrein and kininogen come in contact on the negatively charged surface and the prekallikrein changes into kallikrein [4]. On the other hand, in the plasma-surface-treated ID-DLC, the possibility of the control of the zeta potential according to the existence ratio of the functional group on the surface was suggested in chapter 3. The kallikrein-like activity of blood plasma provides important information on the predominant pathway of the generation of TAT [5].

Thus, if the blood compatibility can be freely controlled by plasma-surface-treated



ID-DLC, developing new biocompatible materials that can be matched with treatment purposes and the patient's conditions becomes possible. Then, the platelet adhesion and blood coagulation characteristics of various plasma-surface-treated ID-DLCs were evaluated, and the blood compatibility was examined.

## 5.2. Methods and experimentation

ID-DLC film for blood compatibility tests was prepared on a SUS 316L stainless steel disc with a 46 mm diameter using benzene as the carbon source. The deposition of carbon was carried out as follows. The SUS 316L disc was placed in the chamber of an ionized deposition apparatus, and argon gas was introduced to the chamber. Then, bombardment cleaning was implemented for about 30 min by discharge. Subsequently, tetramethylsilane ( $\text{Si}(\text{CH}_3)_4$ ) and benzene ( $\text{C}_6\text{H}_6$ ) were passed in, adjusting the deposition pressure to  $1 \times 10^{-1}$  Pa, and thus an amorphous DLC film was deposited on the disc. In the deposition process, the DC bias voltage was  $-2$  kV and the electric power of the filament was 300W.

Table 1. ID-DLC sample group and preparation condition.

Group	Sample	Plasma source	Plasma condition
ID-DLC	a	$\text{O}_2$	Low vacuum
	b	Ar	
	c	Ar	High vacuum (TMP)
	d	$\text{NH}_3$	
	e	$\text{O}_2 + \text{NH}_3$	
	f	Untreated	
Control	SUS316L PET glass		

TMP: Turbo Molecular Pump

Functional group modification was performed on ID-DLC films surfaces using plasma surface treatment technology. Plasma treatment of the ID-DLC surface was performed under high vacuum with a turbo molecular pump (TMP) or under low vacuum with a rotary pump (RP). The base pressures in the treatment chamber were  $1 \times 10^{-3}$  Pa (TMP) or 3 Pa (RP). The process chamber was connected to an RF power supply (13.56 MHz: AX-300, Adtec Plasma Technology), and the RF power to generate the gas plasma was 30W (for low vacuum) and 100W (for high vacuum). Capacitively coupled plasma was generated by means of two

parallel plate electrodes. The operation gases were oxygen (O<sub>2</sub>), argon (Ar), acetylene (C<sub>2</sub>H<sub>2</sub>) and ammonia (NH<sub>3</sub>), which were introduced into the chamber through a mass flow controller under an operation pressure of 1 Pa (TMP) or 130 Pa (RP). The duration time of plasma irradiation was 15 s for each gas or 30 s when two gases were used. Thus, in this work, the gas plasma-treated DLC surfaces are classified into three groups according to the preparation method; treated under low-vacuum condition, and treated under high-vacuum condition, as shown in Table 1.

Determination of the elements and functional groups on the DLC surfaces was carried out by X-ray photoelectron spectroscopy (JPS-9010, JEOL). The X-ray source was monochromatized Al K $\alpha$ . The X-ray gun was operated at 10 kV and the anode power was 100 W. The photoelectron take-off angle (TOA) was 90° for all measurements.

The zeta potential of the DLC surfaces was measured using a zeta potential meter (ELS-Z, Otsuka Electronics). The plasma-treated ID-DLC plate was attached to a chamber, and the chamber was filled with a 10 mM NaCl solution, in which monitoring particles were suspended. Electrophoresis of the particles was carried out, and the apparent velocity distribution in the chamber was determined. The conditions of electrophoresis were as follows; mean electric field intensity 17.33 V/cm and average current 1.02 mA.

The static contact angle of water on the DLC surfaces was measured using a contact angle goniometer (Face CA-A, Kyowa Interface Science, Tokyo, Japan) at room temperature. The volume of water droplet was 10  $\mu$ l. The contact angle was read from a protractor of the equipment through a microscope by the naked eye at five different places of each sample surface, and the values were averaged.

The blood compatibility of DLC was evaluated in terms of platelet adhesion and the generation of thrombin-antithrombin III complex (TAT). The blood used was drawn from healthy volunteers using a blood collection tube (Venoject II, Terumo). The platelet adhesion test was performed according to our previous article [6].

Briefly, the method is shown below. Whole blood was anticoagulated by 3.8% sodium citrate solution at the mixing ratio of blood to a citrate solution (97.5/2.5 vol/vol), and was centrifuged at 1500 rpm for 10 min at room temperature. The supernatant layer was platelet rich plasma (PRP). Centrifugation of PRP at 3000 rpm for 10 min gave platelet-poor plasma (PPP) as an upper layer. The number of platelets in the plasmas was counted by a hemacytometer (K-1000, Sysmex Co.), and a platelet-suspended plasma for the adhesion

test was prepared by adjusting the number to  $1 \times 10^5$  platelets/ $\mu\text{l}$  when mixing PRP and PPP. An aliquot amount of the plateletsuspended plasma was placed on the samples and incubated for 60 min at 37 °C. After the sample was washed, it was immersed in 1 % glutaraldehyde in a phosphate-buffered saline (PBS) for 60 min at 4 °C to fix the adherent platelets. The sample was freeze-dried and sputtercoated using gold, prior to observation by a scanning electron microscope (JSM-840, JEOL). Five SEM images were taken for each sample, and the number of adherent platelets on the five images was averaged.

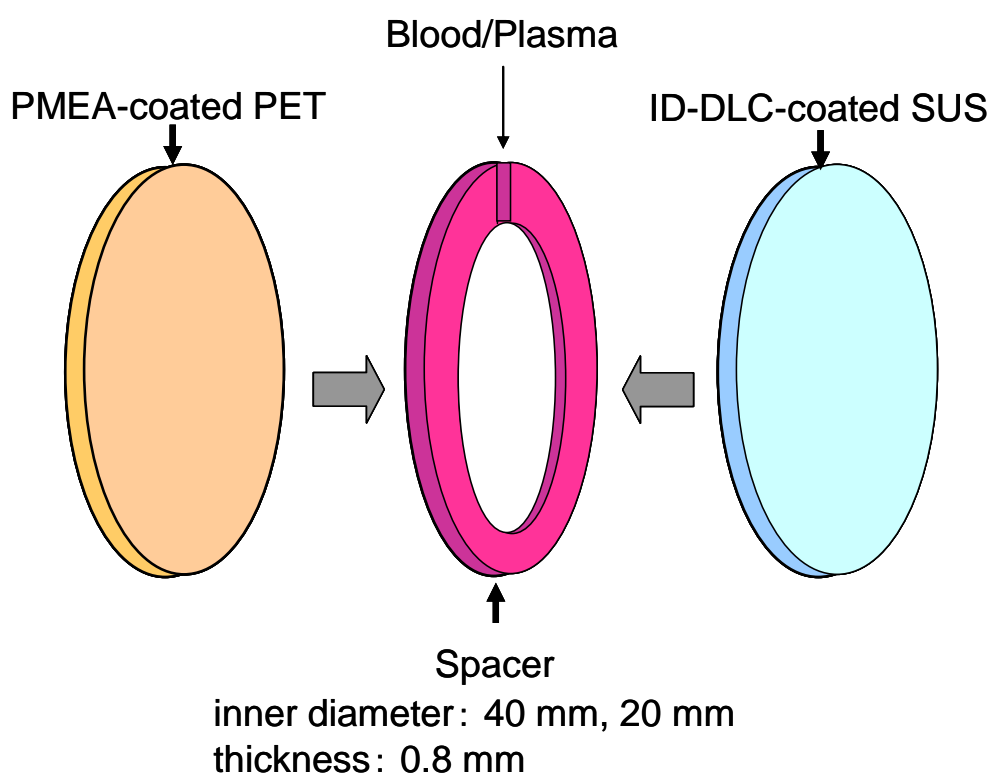


Figure 1. Structure of chamber for evaluation of blood compatibility.

Sample plate and PMEA-coated PET film adhered to a spacer, resulting in a chamber.

A volume of 1000  $\mu\text{l}$  (40 mm in diameter) or 400  $\mu\text{l}$  (20 mm in diameter).

The method to determine TAT generation was as follows. Heparinized whole blood (1000  $\mu\text{l}$ , 2 IU/ml) was pipetted into an inhouse-built chamber with 1307  $\text{mm}^2$  of DLC surface area (40 mm diameter), the chamber being composed of a poly (2-methoxyethyl acrylate) (PMEA)-coated PET wall, a DLC-coated SUS wall and a spacer. As PMEA (Figure 1) is inert

and activation of the coagulation system by its surface is very low [7], the influence of the wall on the determination of TAT generated by the DLC surface is negligibly small. The chamber was rotated vertically at 47 rpm at 37 °C for 120 min to avoid sedimentation of blood cells during incubation. After incubation, the blood was moved to a micro test-tube, followed by the addition of 10% sodium citrate solution. The blood was centrifuged at 3000 rpm for 10 min to obtain blood plasma. The level of TAT in the plasma was evaluated using an ELISA kit (TAT-EIA, Enzyme Research Laboratories).

The kallikrein-like activity of plasma was determined in order to investigate the activation pathway of the coagulation system. Heparinized whole blood (2 IU/ml) was centrifuged at 3000 rpm and platelet-poor plasma was obtained. Filtration of the plasma through a membrane filter with a 0.2 µm pore size (Minisart 17597, Sartorius AG) yielded platelet-free plasma (PFP). The PFP (3 ml) was diluted with a pH 7.8 Tris-buffer (9 ml), and 400 µl of the diluted plasma was pipetted into the sample chamber. The chamber has a similar structure to the one shown in Figure 1 except for the spacer diameter, 20 mm. After incubation of the sample chamber for 1 h at 37 °C, the plasma was pipetted into a 96-well multiplate and a chromogenic reagent (S-2302, Chromogenix) (50 µl) was pipetted into the wells. The absorbance of the sample was monitored at 405 nm using a multiplate reader (Thermo Max, Molecular Device). This procedure was carried out in accordance with the maker's protocol.

It is very important to know the performance level of new material in comparison with conventional biomaterials. As control materials, poly(ethylene terephthalate)(PET) and SUS 316L stainless steel were adopted in this work. Both materials are very popular and important biomaterials in clinical use, for both implant and single-use devices. In addition, in this work, SUS 316L was used as a substrate where DLC was coated. Thus, these controls are good for the evaluation of blood compatibility of plasma-treated DLCs. PET film was supplied by Toray.

### **5.3. Results and discussion**

#### **5.3.1. Surface chemical structure**

The XPS surface analysis of the ID-DLC is discussed first. The surface chemical compositions of the ID-DLC deposited on the substrates were determined from wide-scan spectra and are shown in Table 2.

Table 2. Surface chemical structure of plasma treated ID-DLC and untreated ID-DLC.

Sample	XPS analysis composition ratio				Zeta potential / mV
	Elements <sup>a</sup> comprising DLC			O=C-O/C <sup>b</sup>	
	C	N	O		
a	0.87	>0.007	0.12	0.03	-67
b	0.87	>0.008	0.13	0.02	-62
c	0.88	0.03	0.08	0.01	Unmeasurement
d	0.86	0.10	0.04	0.00	2
e	0.86	0.11	0.03	0.00	-7
f	0.92	>0.003	0.08	0.01	-26

a Determined from wide-scan spectra.

b Determined by deconvolution of C1s peak at 288.8 eV (narrow-scan).

Table 2 shows that all of the surfaces are composed of carbon, nitrogen and oxygen atoms were observed. It was positively found that the oxygen and ammonia plasma treatments bring about high concentration of oxygen and nitrogen at the surface when compared with other gas plasma treatments. However, all of the DLC surfaces has 3–13 atom % oxygen and 0–11 atom % nitrogen, regardless of the plasma species. That is, for DLC samples b, c, and f, oxygen atoms were observed, even though those DLC surfaces were not treated with oxygen plasma. These results are caused by the reactions with oxygen in the air via dangling bonds after the deposition or the plasma treatments. Consequently, it is difficult to determine the contribution ratio of the ammonia plasma and oxygen plasma to the surface chemical composition with accuracy. From the narrow-scan of XPS for C1s, we determined the chemical species (functional groups) composing the plasma-treated ID-DLC surfaces. The functional group on the surface of ID-DLC was decided from the XPS narrow spectrum of C1s. The C1s peak was decomposed to peaks of three 285.9 eV, 287.3 eV, and 288.8 eV, and, they were assigned to –C–H / –C–C / –C=C, –C–O and –COOH respectively. The peak of –C–O relates to carbon of C–H (alcohol) and O–C–O (ether), and, in addition, relates to carbon nitride (C–N), in addition to the carbon atoms of alcohol (C–OH) and ether (C–O–C), so we did not carry out further investigation [8, 9]. Similarly, from the narrow-scan peak of N1s, it is difficult to assign amino nitrogen and carbon nitride nitrogen, so we did not analyze the narrow-scan of N 1s. Thus, the functional groups introduced by the ammonia plasma treatment cannot be clarified from the result of XPS, which does not deny the presence of –NO, –NO<sub>2</sub>, and –CNO groups. However, the zeta potential described below suggests that the

species introduced is a group that can change the electrical state of the surface. On the other hand, it is known that the peak at 288.8 eV is due to a carboxyl (COOH) carbon, and that any carbon bonding to a nitrogen atom does not show a peak at this bond energy. Consequently, it is obvious from the XPS results that the plasma-treated DLC has a COOH group at the surface, regardless of the plasma species.

### 5.3.2. Physicochemical property of surface

Plotting the contact angle against the concentration of COOH carbon on the DLC surfaces gave Figure 2.

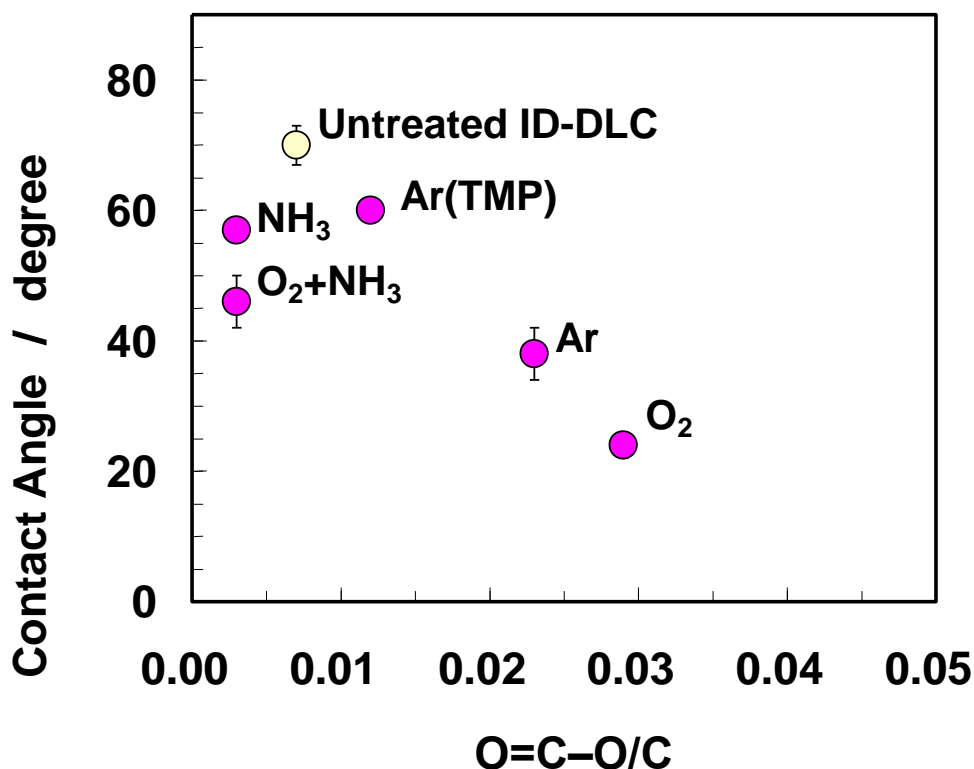


Figure 2. Correlation between the contact angle and O=C-O/C ratio of ID-DLC.

The contact angles are on the same curve and decreased gradually from 70° to 30° with an increase in the COOH carbon concentration from 0 to 4 atom%, indicating that the plasma species had little effect on the contact angle. These results indicate that the contact angle is strongly affected by a small amount of COOH and that the decrease in the contact angle

depends not only on the amount of COOH at the surface but also on other factors. One of the factors may be oxygen-based functional groups, such as a hydroxyl group. The existence of such a group is suggested by the C 1s narrow-scan of XPS and the estimated concentration is shown in Table 2. Again, from these results it is concluded that the exposure to plasma brings about the formation of a carboxyl group and a hydroxyl group on the ID-DLC surface, resulting in an increase in hydrophilicity. However, the predominant factor for the contact angle is not clear. The combination of these functional groups may lead to the observed result.

The effect of ammonia plasma treatment on the surface property of ID-DLC was investigated in terms of zeta potential, by using ID-DLC deposited on a glass substrate, where the condition of the plasma treatment was the same as for the DLC samples prepared under the condition in Table 1. The relationship between the zeta potential of the ID-DLC surface and the concentrations of COOH carbon atoms and nitrogen atoms is shown in Table 2. When argon plasma-treated ID-DLC, a, was compared with non-treated DLC, it was clearly found that the treatment increased the concentration of COOH carbon ratio from 0.01 to 0.03, resulting in the drop of the zeta potential to  $-67$  mV. On the other hand, the treatment with ammonia plasma caused a significant increase in the concentration of nitrogen atoms ratio at the DLC surfaces, from 0.003 to 0.10–0.11 and raised the zeta potential from  $-26$  to  $-7$  to  $+2$  mV. From the fact that the zeta potential is affected by an ionic functional group at a material surface, it is reasonable to consider that these drastic changes in zeta potential are caused by the ionic groups at the DLC surface. Consequently, it is summarized that some of the nitrogen atoms introduced by the ammonia plasma have a cationic property. However, in this work, we could not determine the type of functional group expressing the cationic property nor its real concentration.

### **5.3.3. Evaluation of platelet adhesion of ID-DLC**

The platelet compatibility of DLC was compared with that of the control materials from the viewpoint of platelet adhesion and the results were shown in Figures 3–6. Figure 3 (the adhesion numbers on the sample surfaces) shows that the plasma-treated ID-DLC exhibits lower platelet adhesion than those on PET, SUS and untreated ID-DLC. In addition, this result shows that the types of plasma species have little effect on the adhesion number. It is well known that morphology of adherent platelets on a sample surface gives important information about the activation level of platelets [10]. The activation of adherent platelets on the ID-DLC

was investigated from the viewpoint of platelet morphology shown in Figure 5, where representative images are shown. In the images, plasma-treated DLC samples are a, and c as representatives in Table 1, respectively, and the control materials are SUS and PET, and untreated ID-DLC. In the cases of the plasma-treated DLC, the platelets show that pseudopod form and the spread form are not found. The morphological change of the platelets is on the same level, regardless of the plasma species. On untreated ID-DLC and SUS surfaces the adherent platelets exhibit stellate or pseudopod form. From these results it is concluded that the activation of adherent platelets on surfaces treated with gas plasmas is weaker than that on common materials (SUS). The morphological changes of adherent platelets and the number of adherent platelets indicate that the compatibility of the surface is in the following order: plasma-treated ID-DLC > SUS > untreated ID-DLC  $\geq$  PET.

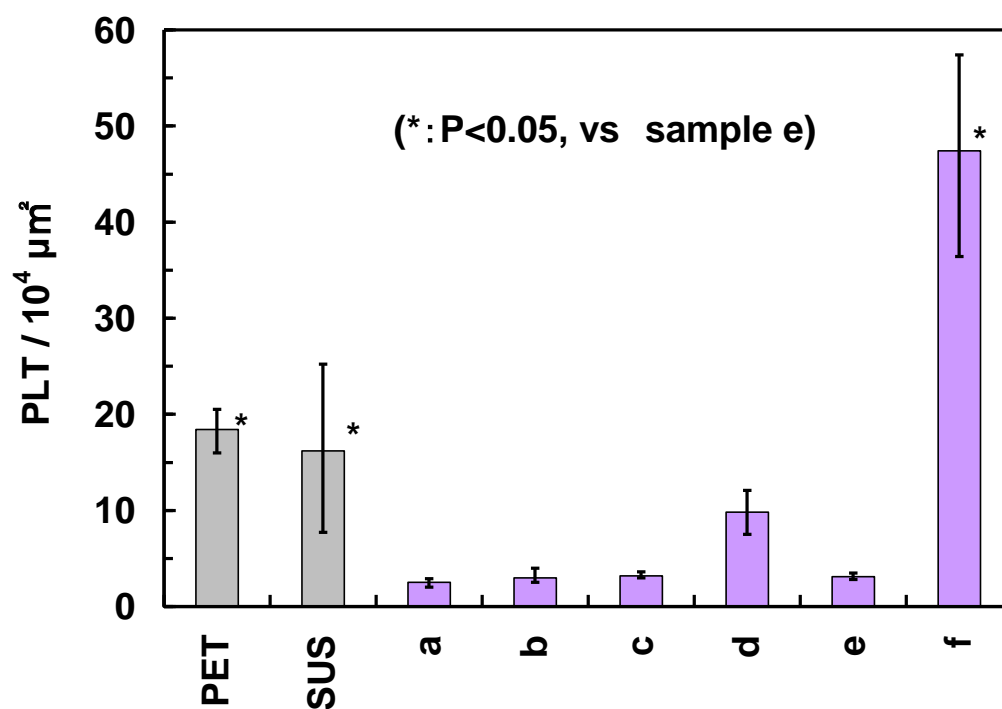


Figure 3. Comparison of ID-DLC with common biomaterials in terms of platelet adhesion.

Label in the y-axis: the number of adherent platelets on the surface.



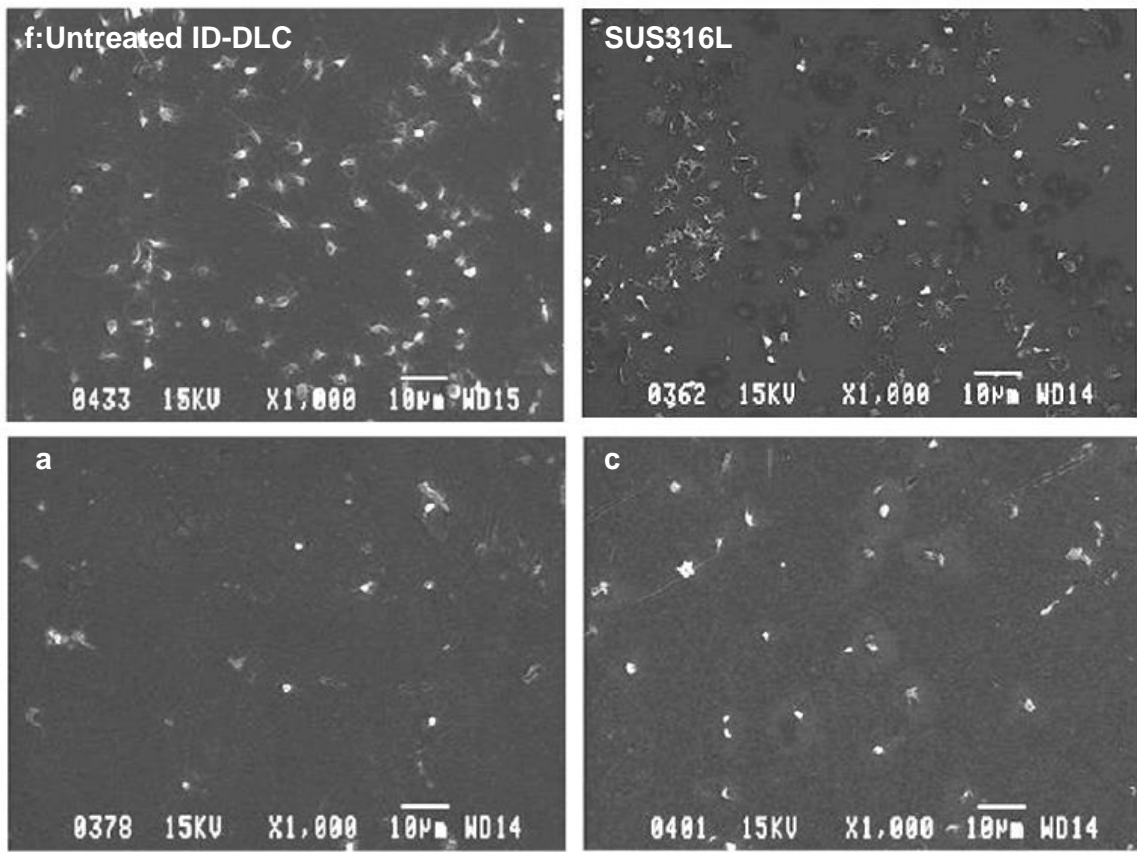


Figure 4 the SEM image of platelet morphology on the surface of DLC and SUS 316L.

It is well known that platelets easily adhere to a hydrophobic surface compared with hydrophilic ones [11]. Thus, the platelet adhesion property of the ID-DLCs was investigated from the viewpoint of the hydrophilicity/hydrophobicity, or the contact angle. Plotting the number of adherent platelets against the contact angle (Figure 5) indicates the following. As for untreated ID-DLC, significant platelet adhesion was observed. Moreover, the contact angle of untreated ID-DLC is larger. The hydrophobe molecule coheres by the hydrophobe interaction that causes dehydration in water. Similarly, when the protein approaches a hydrophobe artificial material, it unites by the hydrophobe interaction. Therefore, it is suggested that untreated ID-DLC adsorbs cell adhesion molecules that consists of the protein relates to the platelet by the hydrophobe interaction, and caused the platelet adhesion. As mentioned earlier, untreated ID-DLC has no anionic group or carboxyl group, resulting in a highly hydrophobic surface (Figure 2). This surface property causes poor compatibility.

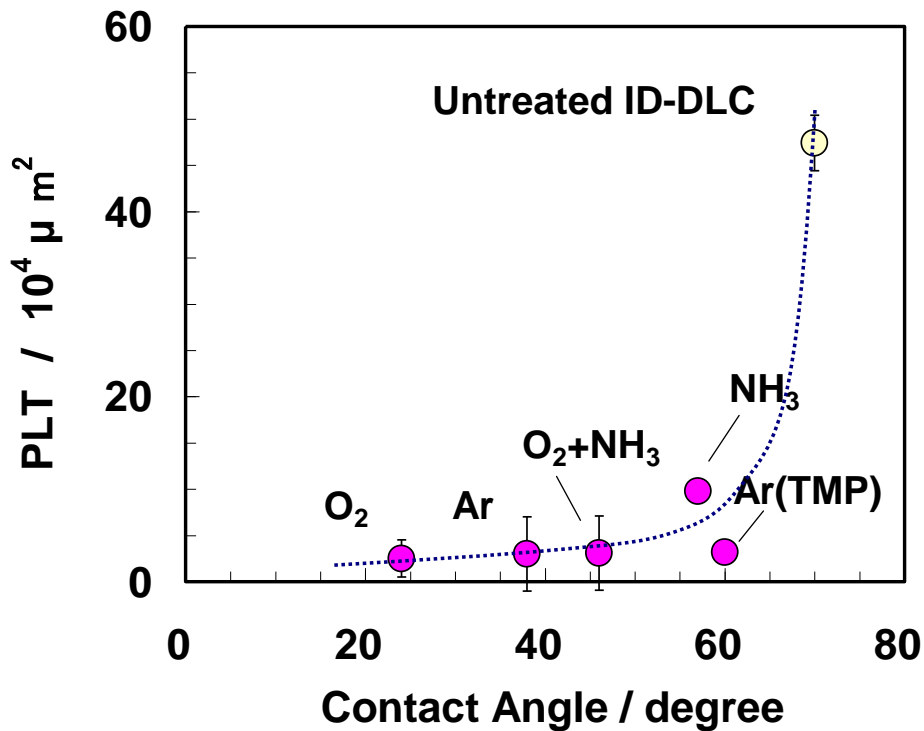


Figure 5. Correlation between the adherent platelet number and contact angle.

#### 5.3.4. Evaluation of blood coagulation of ID-DLC

The compatibility of plasma-treated ID-DLC with the coagulation system was investigated in terms of generation of TAT. The amount of TAT corresponds to the amount of thrombin generated by the contacting blood, because the thrombin generated is immediately inactivated by antithrombin-III, resulting in the formation of thrombin-antithrombin III complex [12]. The activation of the coagulation system by biomaterial is not fully understood in terms

of physicochemical surface properties. It is said that the factors affecting the activation are electrical surface charge, hydrophobicity/hydrophilicity, chemical functional group, roughness, and so on. First, a comparison of TAT generation by a DLC surface with that by common biomaterials is described. The results are shown in Figure 7. As for the control materials, PET shows low TAT generation, suggesting good compatibility, and SUS generated a significant amount of TAT, meaning poor compatibility. On the other hand, in the case of plasma-treated ID-DLC, the activation level of the coagulation system depends on the surfaces and that the concentration of TAT varies in the range of from 600 pM to 6500 pM. From this result, one can classify DLC into two groups by the capability to activate the

coagulation system; one has high potency and the other has low. The potency of the former group is comparable to SUS and has proven to have very poor compatibility in terms of the generation of TAT. On the other hand, the potency of the latter group is on the same level as PET, relatively good compatibility.

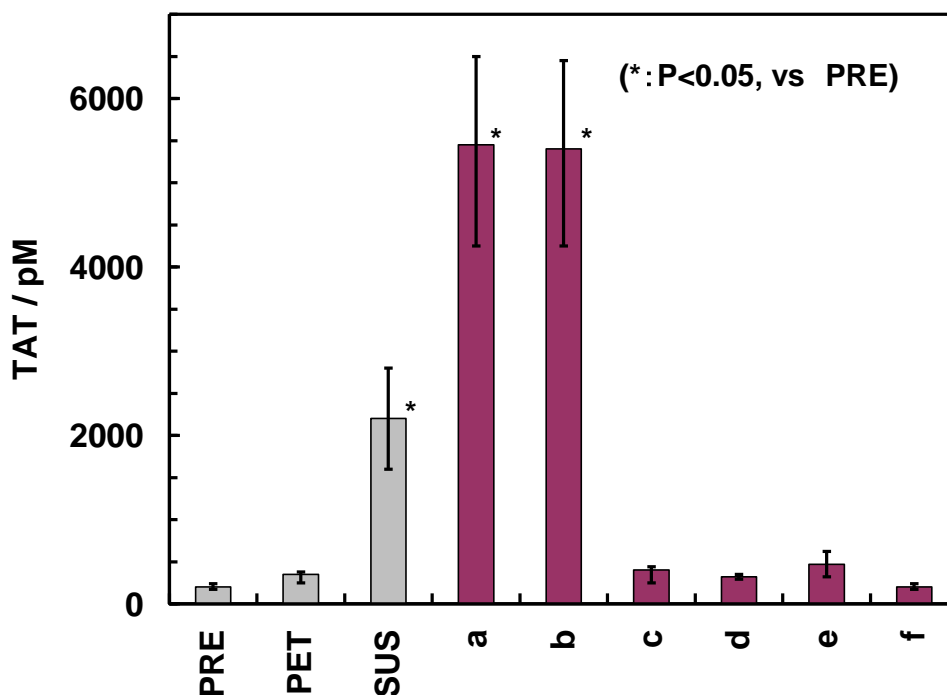


Figure 7. Comparison of ID-DLC with common biomaterials in terms of generation of TAT.

Label in the y-axis: the concentration of TAT (picomol/liter),

PRE: the value before contact with a sample

Next, from the viewpoint of hydrophilicity/hydrophobicity the TAT generation is discussed. From Figures 2 and 7, TAT generation seems to be depressed when the contact angle of the DLC surface is over  $40^\circ$  (samples c, d, and e), however, there is no clear difference between sample b and sample e in contact angle in spite of their significant difference in TAT generation. This means that TAT generation is not explained by the contact angle. Thus, it is concluded that the contribution of hydrophilicity/hydrophobicity to TAT generation is small, and that there are other dominant factors which activate the coagulation system. On the basis of these results, the TAT generation by the DLC was described from the zeta potential of ID-DLC. Plotting the TAT concentration against the zeta potential (Figure 8) shows that the

zeta potential increases from 600 to 6500 pM with an higher in the zeta potential than -50 mV, and in regions of less than -50 mV of zeta potential, the level of TAT is kept low (ca. 600 pM).

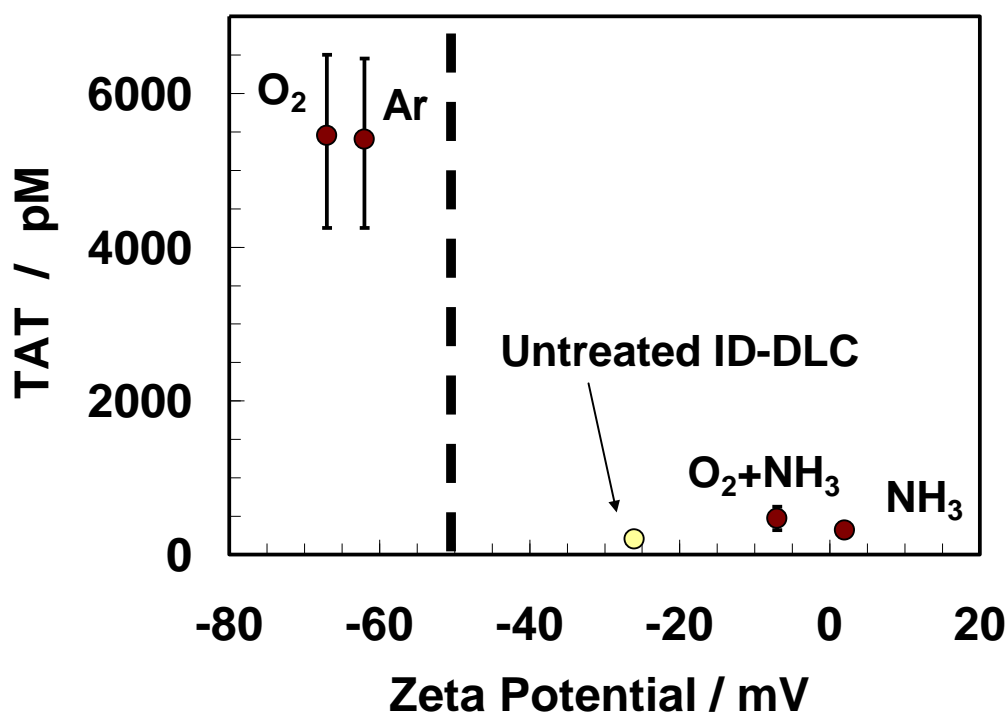


Figure 8. Correlation between the TAT generation and the zeta potential.

### 5.3.5. Evaluation of kallikrein-like activity of ID-DLC

It is well known that the coagulation system is activated via the intrinsic pathway comprising contact activation or the extrinsic pathway where tissue factor plays a key role [13]. In the contact activation, high molecular weight kininogen, prekallikrein, and factor IIX are involved and the activations of these molecules require a negatively charged surface such as zeolite or glass in vitro. Factor IIX is activated by adsorption onto the surface and FIIXa converts prekallikrein to kallikrein. The activation of the intrinsic pathway proceeds in cascade reactions, resulting in thrombin generation and clotting. Thus, when the fact that the plasma-treated DLC has a carboxyl group is considered, the measurement of the kallikrein-like activity of the blood plasma gives important information. That is, from the level of the activity, it is suggested which pathway is dominant in generation of TAT by DLC.

The results of kallikrein-like activity are shown in Figure 9, where absorbance at 405 nm is plotted, and an increase in absorbance corresponds to a rise in kallikrein activity. Figure 9 expresses the results of the activation of the contact phase in the coagulation system by the various surfaces. From this figure and Figure 7, ID-DLC that generates TAT significantly seems to activate the contact phase.

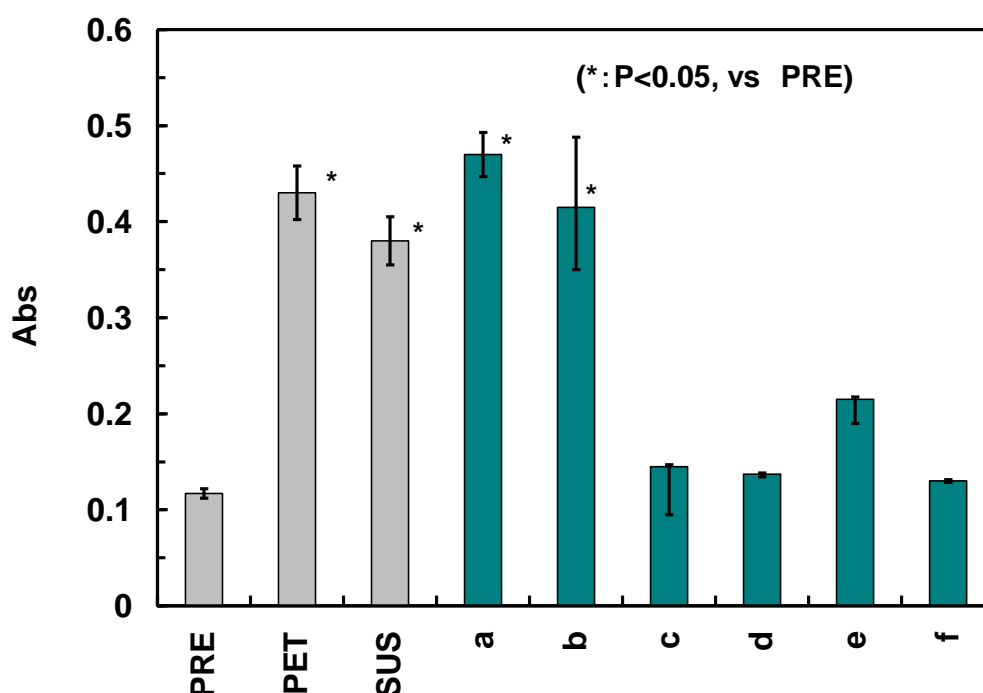


Figure 9. Kallikrein-like activity of blood plasma contacting various surfaces.

Label in the y-axis: the absorbance at 405 nm, corresponding to the strength of the activity in plasma. n=4, mean  $\pm$  SE (standard error), glass: glass plate, PRE: the value before contact with a sample

Figure 10 shows that absorbance increases with an increase in the zeta potential, when the zeta potential is over -50 mV, except for ID- DLC of d and e treated with  $\text{NH}_3$  plasma. That is, ID-DLC treated with ammonia plasma exhibits low ability to activate the contact phase. In our experiment, we also measured the kallikrein-like activity for a glass plate as a control, and the absorbance was over 0.4. The absorbance observed for DLC with low compatibility is close to the absorbance for a glass plate. The reason for the good compatibility of DLC d and e can be explained from the result of the surface physicochemical property of DLC deposited

on a glass substrate. As shown in Table 2, the ammonia plasma-treated surfaces show very high zeta potential ( $-7-2$  mV) compared to other DLC having a high concentration of COOH (their zeta potential is less than  $-50$  mV). This implies that the COOH group on the surface is neutralized by ammonia plasma. A similar phenomenon occurs in the case of the plasma-treated ID-DLC surface on the SUS substrate which was used for the blood compatibility tests. Thus, the neutralized surface results in the low generation of TAT though the surface has a high concentration of the COOH group.

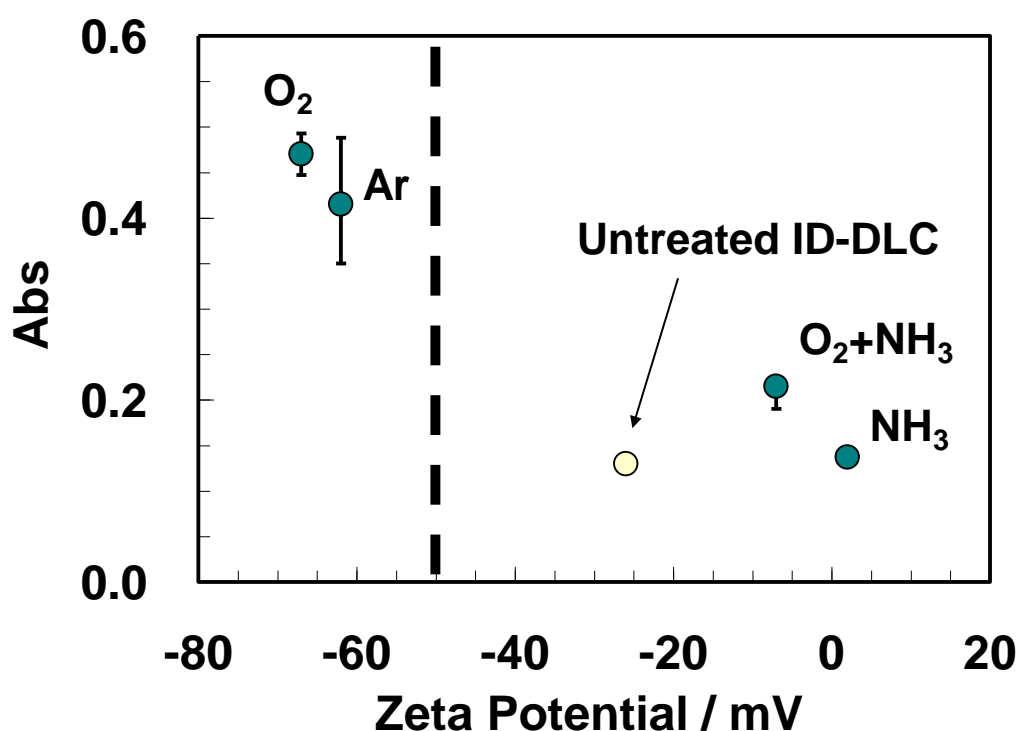


Figure 10. Correlation between the kallikrein-like activity and the zeta potential.

#### 5.4. Conclusion

In this study, the blood compatibility of plasma surface treated ID-DLC that used various gases was investigated. Hydrophilicity was increased by the plasma treatment, which introduces the carboxyl groups and the hydroxyl groups on the surface of ID-DLC. The platelet adhesion proof property was observed in plasma surface treated ID-DLC. Meanwhile, untreated ID-DLC was observed significant platelet adhesion. It is suggested that untreated

ID-DLC adsorbs cell adhesion molecules that consists of the protein relates to the platelet by the hydrophobe interaction, and caused the platelet adhesion. Moreover, the influence of the zeta potential is a little for platelet adhesion property. Next, the tendency to blood coagulation property has divided the zeta potential at -50 mV. Moreover, kallikrein-like activity and the TAT generation were the same behavior. It was suggested that kallikrein-like activity of the early response is triggered in cascade of coagulation reaction. And coagulation reaction continues to TAT generation closing phase. Moreover, it is known that coagulation reaction is occurred when prekallikrein and factor XII adsorbs on negatively charged surface. It was suggested that prekallikrein behavior on the ID-DLC surface is also similar. Moreover, ID-DLC that adjusted the zeta potential to -50 mV or more can inhibit kallikrein-like activity, and acquire characteristic of blood coagulation. These findings suggest that plasma treated ID-DLC inhibits both platelet adhesion and blood coagulation. Moreover, it is suggested that arbitrary blood compatibility may be obtained in plasma surface treated ID-DLC by controlling the amount of the functional group on the ID-DLC surface.

## 5.5. References

- [1] S. Fukushima, Y. Kadoma, N. Nakabayashi, *Kobunshi Ronbunshu*, 40 (1983) 785–793.
- [2] K. Ishihara, R. Aragaki, T. Ueda, A. Watanabe, N. Nakabayashi *Journal of Biomedical Materials Research*, 24 (1990) 1069–1077.
- [3] H. Kitano, T. Mori, Y. Takeuchi, S. Tada, M. G. Ide, Y. Yokoyama, M. Tanaka, *Molecular Bioscience*, 5 (2005) 314–321.
- [4] M.B. Gorbet, M.V. Sefton, *Biomaterials*, 25 (2004) 5681–5703.
- [5] T. Sugo, N. Ikari, H. Kato, S. Inagawa, S. Fujii, *Biochemistry*, 19 (1980) 3215–3220.
- [6] M. Tanaka, A. Mochizuki, N. Ishii, T. Motomura, T. Hatakeyama, *Biomacromolecules*, 3 (2002) 36–41.
- [7] M. Tanaka, T. Motomura, M. Kawada, T. Anzai, Y. Kasori, T. Shiroya, K. Shimura, M. Onishi, A. Mochizuki, *Biomaterials*, 21 (2000) 1471–1481.
- [8] G. Jama, A. Alkhawwam, A.-S. Loir, P. Goudmand, O. Dessaux, L. Gengembre, J. Grimblot, *Surface Interface Analysis*, 31 (2001) 815–824.
- [9] H. Cachet, C. Debiemme-Chouvy, C. Deslouis, A. Lagrini, V. Vivier, *Surface Interface Analysis*, 38 (2006) 815–818.
- [10] M. Fedel, A. Motta, D. Maniglio, C. Magliaresi, *Journal of Biomedical Materials Research B*, 90B (2009) 338–349.
- [11] N. Yayapour, and H. Nygren, *Colloids and Surfaces B: Biointerfaces*, 15 (1999) 127–138.
- [12] J.H. Griffin, in: M.A. Lichtman, E. Beutler, T.J. Kipps, U. Seligsohn, K. Kaushansky, J.T. Prchal (Eds.), *Williams Hematology*, 7th edition, McGraw-Hill, New York, (2006) 1703.
- [13] M.B. Gorbet, M.V. Sefton, *Biomaterials* 25 (2004) 5681–5703.



## Chapter 6

### Bone Compatibility of Diamond-like Carbon *in-vitro*

#### 6.1. Introduction

Diamond-like carbon (DLC) are widely used in industrial applications, such as automobile parts with high wear resistance [1,2]. Moreover, DLC has been considered as one of the excellent biocompatible coating materials for medical devices [3–12]. It is known that DLC has a wide composition in a material composed of  $sp^2$  carbon,  $sp^3$  carbon, and hydrogen. Moreover, a functional group can be introduced using the carbon bond of DLC. Then, I examined the functionality of DLC for dental implant surface treatment by plasma treatment. This plasma treatment technics can control the zeta potential within the wide range in the results of chapter 3. In addition, the characteristics of platelet adhesion and fibrin coagulation can be controlled on the basis of the functional group introduction ratio and zeta potential in the result of chapter 3. The result showing blood compatibility suggests the possibility of applying to various implants that come in contact with blood.

Currently, various implants are applied by dental and orthopedic operations. The dental implant fixture often reduces infection and an inappropriate occlusal force because the period until fixture is long. Therefore, urgent requirements are to develop a technology that improves the growth of the bone and to complete a treatment in a short period. Therefore, we applied DLC used by controlling blood compatibility and aimed at the development of a technology that controlled the differentiation of osteoblast. In an actual experiment aimed at the functionalization of DLC to introduce a functional group into a surface by plasma surface treatment, we examined the effect of the differentiation capability of osteoblast. And the purpose of this study is to obtain the unique material of bone compatibility for application to endosseous implant.

#### 6.2. Method and experimentation

ID-DLC film for cell differentiation tests was prepared on pure titanium (JIS type2) disk disc with 12 mm diameter. The titanium discs were placed in the chamber of an ionized deposition apparatus, and argon gas was introduced to the chamber. Then, bombardment cleaning was implemented by plasma discharge. Plasma discharge operational conditions were controlled

of negative DC bias voltage to 2 kV and the electric power of the filament was 300W. The deposition pressure adjusted to  $1 \times 10^{-1}$  Pa. Subsequently, operation gases were switched to tetramethylsilane ( $\text{Si}(\text{CH}_3)_4$ ) and benzene ( $\text{C}_6\text{H}_6$ ) in sequence. ID-DLC films were deposited on the titanium disc.

Next, functional group modification was conducted on ID-DLC film surface using the plasma treatment technology, and the composition ratio of functional groups introduced was examined. The equipment of plasma treatment was same manner as chapter 3. Condition of plasma treatment is as follows. Base pressure was  $1 \times 10^{-3}$  Pa. Operating gases were  $\text{O}_2$  and  $\text{NH}_3$ , and operating pressure adjusted 4 Pa. RF power supplied 100 W. Figure 1 shows the appearance of test pieces used to experiment.



Figure 1. The appearance of test pieces used to experiment.

In order from the left, pure titanium, untreated ID-DLC,  $\text{O}_2$  plasma treated ID-DLC and ammonia plasma treated ID-DLC.

ID-DLC surface was analyzed by XPS system (JOEL, JPS9010) with non-monochromatized  $\text{AlK}\alpha$  lines. The  $\text{C}1s$  spectrum was first assigned into four elements ( $\text{C-C } sp^3$  (283.8 eV),  $\text{C-C } sp^2$  (284.3 eV),  $\text{C-H } sp^2$  (284.8 eV), and  $\text{C-H } sp^3$  (285.3 eV)) [13–15]. Then, the  $\text{C}1s$  spectrum was analyzed so that the ratio of the total area of  $\text{C-O}$  ( $\text{O-C-O}$ ) (285.9 eV),  $\text{C=O}$  (287.3 eV), and  $\text{O=C-O}$  (288.8 eV), to the area of  $\text{C-N}$  may be the same as the ratio of oxygen and nitrogen to carbon. The analysis of ID-DLC was carried out by the angle resolved XPS method. Then, the emission angle was varied as 0 and  $75^\circ$ .

To examine the effect of ID-DLC on osteoblast differentiation, osteoblastic cell line; MC3T3-E1 was used in the present study. MC3T3-E1 cell line was purchased from the European Collection of Cell Cultures (Wiltshire). MC3T3-E1 cells were cultured in

alpha-MEM supplemented with an antibiotic mixture (Invitrogen), 10% fetal bovine serum (Biological Industries) and 50 ug/ml L-ascorbic acid (Sigma). MC3T3-E1 were maintained at 37 °C under 5 % CO<sub>2</sub> / 95 % air for an experiment. The cell were seeded to the surfaces of titanium specimens placed on the bottoms of 24-well plates at a density of 5.0 x 10<sup>4</sup> cells/well titanium specimens and well was extracted using TRIzol reagent maintained for 7 days [16].

Total RNA of each well was extracted using TRIzol reagent (Invitrogen), and first-strand cDNA from total RNA (100 ng) using ReverTra Ace reverse transcriptase (Toyobo). RT-PCR analysis for runt-related transcription factor 2 (Runx2), type I collagen was performed using Colbet (Qiagen).

Runx2 is known the main gene that influences from the first stage of the osteoblastic differentiation to a final bone formation stage. Type I collagen is known a marker which express to the first stage of the differentiation [17]. The sequences of the primers used in these analyses are previously described [18]. Differences between mean values of groups were subjected to a one-way analysis-of-variance (ANOVA) and Tukey's multiple range test.

## **6.3. Results and discussion**

### **6.3.1. Surface structures**

Figure 2 shows the profile used to analyze the C1s spectra of untreated ID-DLC by the angle-resolved XPS method. The C1s spectra was analyzed and the bonds of C-O (O-C-O), C=O, and O-C=O were fitted. It was shown by angle-resolved XPS that many elements of O-C=O, C=O, and C-O (O-C-O) existed on the surface. It was suggested that the dangling bond on ID-DLC surface bonded with oxygen when the coating of ID-DLC was completed, and the chamber was opened to the atmosphere and it was terminated.

Table 1 shows the atomicity ratios of carbon, oxygen, and nitrogen, and composition ratios of O=C-O/C bonds obtained before and after the plasma treatment. O<sub>2</sub> plasma has increased the ratio of oxygen and increased the O=C-O ratio clearly. Also, ammonia plasma introduced nitrogen.

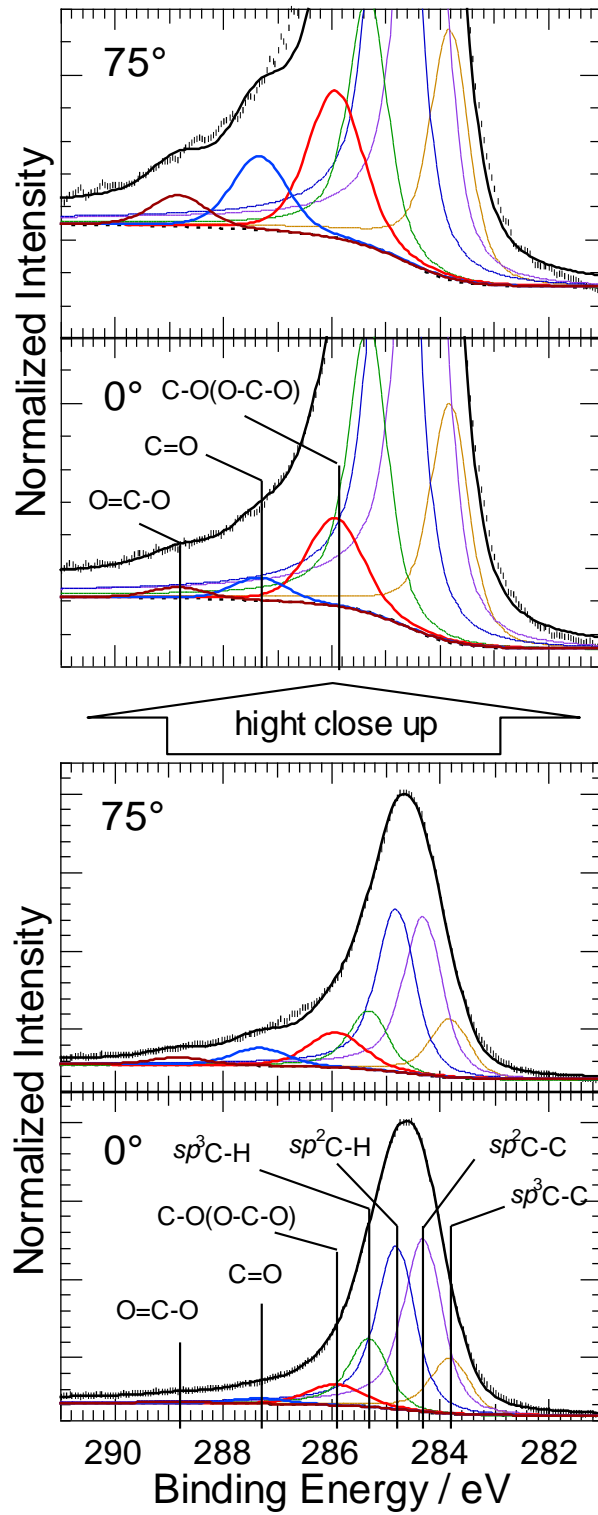


Figure 2. The C1s spectra of untreated ID-DLC used to analyze by the angle-resolved XPS method.

Table 1. Atomicity ratios of carbon, oxygen and nitrogen and composition ratios of O=C–O/C by XPS analysis of functionalized ID-DLC by plasma surface treatment.

		atomicity ratio			composition ratio
		C	O	N	O=C-O/C
No.1	ID-DLC(Untreated)	0.92	0.08	>0.003	>0.007
No.2	O <sub>2</sub> Plasma	0.90	0.10	>0.002	0.04
No.3	NH <sub>3</sub> Plasma	0.86	0.04	0.10	>0.005

### 6.3.2. Differentiation capability evaluation in osteoblastic cells

The mRNA expressions of Runx2 and type I collagen in MC3T3-E1 cells cultured on pure titanium of the control or three kinds of ID-DLC with different composition ratio of the functional group element (No.1, No.2, and No.3) were examined.

Figure 3 shows the level of the mRNA expression of Runx2 and type I collagen about control–titanium and ID-DLC. The mRNA expressions of Runx2 and type I collagen in MC3T3-E1 cells cultured on sample of No.1 (untreated ID-DLC) was about eighteen and twenty–four times, as compared those cultured on pure titanium, respectively (ANOVA,  $p < 0.01$ ). On the other hand, these expressions in MC3T3-E1 on the sample of No.2 and No.3 (plasma surface treated ID-DLC) were almost the same as those on pure titanium (ANOVA,  $p > 0.05$ ). It was suggested that the level of the osteoblast differentiation might be dependent on the composition ratio of the surface functional group in ID-DLC.

Untreated ID-DLC observed salient platelet adhesion in chapter 5. Meanwhile, platelet–rich plasma in dental implant treatment is known to act on the bone growth factor and to stimulate periodontal regeneration [19–21]. However, the platelet has not acted directly because cow's serum medium is used in this study, and the platelet is not included. The reason for the good compatibility of untreated ID-DLC is not clear. In addition, the adhesive platelet on the surface of ID-DLC releases the growth factor because ID-DLC coating implants comes in contact with blood in actual clinical application, and a further enhanced differentiation and the cell proliferation are expected.

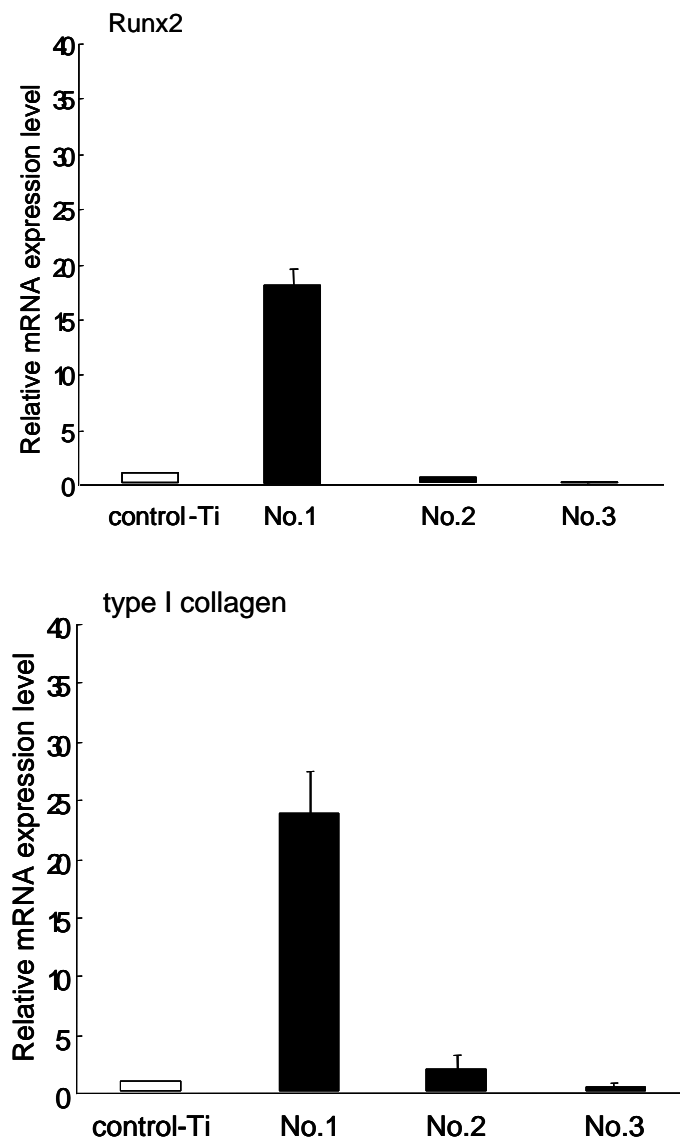


Figure 3. Effects of ID-DLC with different composition ratio of the functional group element on the titanium surface on the expression levels of dependent on mRNAs for Runx2 and type I collagen in MC3T3-E1 cells.

#### 6.4. Conclusion

In this study, bone compatibility was evaluated *in-vitro* by using different ID-DLC based on blood compatibility evaluation in chapter 5. Effect of different ID-DLC was examined by using the mRNA expression of type I collagen and Runx2 known as the marker of the osteoblastic differentiation. The mRNA expression level of Runx2 and type I collagen in

MC3T3-E1 cells cultured on an untreated ID-DLC sample with a low composition ratio of the functional groups were about eighteen and twenty-four times as those in cells cultured on pure titanium. Untreated ID-DLC showed platelet adhesion, and the results on blood compatibility was not satisfactory. However, the bone compatibility was excellent.

It is known that the platelet-rich plasma promotes the bone growth. However, the platelet has not acted directly because cow's serum medium is used in this study, and the platelet is not included. The reason for the good compatibility of untreated ID-DLC is not clear. However, it is forecast that the cell adhesion molecule adsorbs the surface of ID-DLC easily as described in chapter 5. Therefore, cell adhesion molecule or cytokine in the serum related to both of the platelet and osteoblast cell is adsorbed by the surface, and it was guessed that the differentiation of osteoblast cell may be caused.

The possibility of controlling the various biocompatibilities by optimizing the composition ratio of functional groups on the ID-DLC film surface was also suggested.

## 6.5. References

- [1] T. Nakatani, K. Okamoto, A. Araki, T. Washimi, *New Diamond and Frontier Carbon Technology*, 16 (2006) 187–200.
- [2] C. Weissmantel, K. Bewilogua, K. Breuer, D. Dietrich, U. Ebersbach, H. J. Erler, B. Rau and G. Reisse, *Thin Solid Films*, 96 (1996) 31–44.
- [3] D. P. Maguire, J. A. McLaughlin, T. I. T. Okpalugo, P. Lemoine, P. Papakonstantinou, E. T. McAdams, M. Needham, A. A. Ogwu, M. Ball, G. A. Abbas, *Diamond and Related materials*, 14 (2005) 1277–1288.
- [4] B. Balram, N. R. Krishna, K. Ganesan, R. Raghava, M. Sundeep Mishra, S. Sandeep W. Ron Waksman, V. Renu, B. Somaraju, *Catheterization and Cardiovascular Interventions*, 67 (2006) 698–702.
- [5] A. Shirakura, M. Nakaya, Y. Koga, H. Kodama, T. Hasebe and T. Suzuki, *Thin Solid Films*, 494 (2006) 84–91.
- [6] R. Hauert, *Tribology International*, 37 (2004) 991–1003.
- [7] R. Hauert, *Diamond and Related Materials*, 12 (2003) 583–589.
- [8] M. I. Jones, I. R. McColl, D. M. Grant, K. G. Parker, T. L. Parkar, *J. Biomedical Material Reserch*, 52 (2000) 413–421.
- [9] N. Nurdin, P. Francois, Y. Mugnier, J. Krumeich, M. Moret, B. O. Aronsson and P. Discounts, *European Cells and Materials*, 5 (2003) 17–28.
- [10] D. Antonucci, A. Bartorelli, R. Valenti, P. Montorsi, G. M Santoro, F. Fabbicocchi, L. Bolognese, A. Loaldi, M. Trapani, D. Trabattoni, G. Moschi, S. Galli, *Am. J. Cardiol.*, 85 (2000) 821–825.
- [11] T. Nakatani, K. Okamoto, I. Omura, S. Yamashita, *J. Photopolymer Science and Technology*, 20 (2007) 221–228.
- [12] T. Nakatani, K. Okamoto, I. Omura, S. Yamashita, *New Diamond and Frontier Carbon Technology*, 17 (2007) 289–300.
- [13] S. Takabayashi, K. Motomitsu, T. Takahagi, A. Terayama, K. Okamoto, and T. Nakatani, *Journal of Applied Physics*, 101 (2007) 103542.
- [14] S. Takabayashi, K. Okamoto, K. Motomitsu, A. Terayama, T. Nakatani, H. Sakaue, H. Suzuki, T. Takahagi, *Applied Surface Science*, 254 (2008) 2666.
- [15] S. Takabayashi, K. Okamoto, T. Nakatani, H. Sakaue, T. Takahagi, *TANSO*, 235 (2008) 280–289, (in Japanese).



- [16] S. Makihira, Y. Mine, H. Nikawa, T. Shuto, E. Kosaka, M. Sugiyama, R. Hosokawa, *Journal of Materials Science: Materials in Medicine*, 21 (2010) 647–653.
- [17] S. Yamada, Y. Hayashi, *SEITAI IKOU-GAKU*, 44 (2006) 490–495, (in Japanese).
- [18] Y. Mine, S. Makihira, H. Nikawa, H. Murata, R. Hosokawa, A. Hiyama, S. Mimura. *Journal of Prosthodontic Research*. 54 (2010) 1–6.
- [19] R. Marx, E. R. Carlson, R. M. Eichstaedt, S. R. Schimmele, J. E. Strauss, K. R. Georrgoff, *Oral Surgery, Oral Medicine, Oral Pathology*, 85 (1998) 638–646.
- [20] L. Boyapati, H. Wang, *Implant Dentistry*, 15 (2006) 160–170.
- [21] W. S. Pietrzak, B. L. Epply, *Journal of Craniofacial Surgery*, 16 (2005) 1043–1054.

## Chapter 7

### Concluding Remarks

Medical materials should have biocompatibility with the interface at living organisms in addition to mechanical property. However, this requirement cannot sufficiently satisfy even with the commercial materials. In this research, it is aimed to harmonize the mechanical property of the base material and surface-interface compatibility by applying the coating technology in this research. Plasma surface treated ID-DLC was concretely used.

Plasma surface treated ID-DLC was improved and examined with the aim of applying it to medical device materials. It was considered that the plasma surface treatment technology is effective as a method of acquiring surface-interface compatibility without impairing the mechanical property. The surface chemical structure of DLC is more important for advancing this research. Therefore, the surface analytical technique for DLC by XPS was examined. The biocompatibility of plasma surface treated DLC was also examined. The first factor evaluated is blood compatibility, which is highly demanded for in many medical devices. In addition, to enable the application of implants in dental and orthopedic treatments, bone compatibility is evaluated. The possibility of ID-DLC as a material for medical treatments is examined by evaluating these biocompatibilities *in-vitro*. The results of this research are described as follows.

1) AR-XPS analysis using the  $D\check{S}$  function convoluted with a Gaussian function can be used for examining the behavior of hydrogen in ID-DLC films regardless of the hydrogen concentration distributions. This XPS analysis method was suggested to be useful for the comprehensive surface analysis of ID-DLC films and other carbon materials. Moreover, it contributes to the development of the functional surface including the biocompatibility function. This method for analyzing the C1s spectrum enabled the identification of four elements (C–C  $sp^3$  carbon, C–C  $sp^2$  carbon, C–H  $sp^2$  carbon, and C–H  $sp^3$  carbon) composing DLC. Moreover, when the functional group is analyzed from the C1s spectrum, for example, the hydroxyl spectrum is found to overlaps with the spectrum of the C–H  $sp^3$  carbon. It is effective for the accurate examination of a functional group element by assigning the chemical constitution of DLC. This technique is useful for the structural analysis of not only

DLC but also the bulk carbon material.

2) The plasma surface treatment technology can be used to introduce carboxyl groups and functional groups derived from nitrogen onto the ID-DLC film surface. Moreover, the amount of these functional groups can be controlled by changing the condition of plasma treatment.

Regarding the results of the zeta potential measurement, the ID-DLC film surface became negatively charged when the carboxyl groups are introduced, and ID-DLC film surface became positively charged when the functional groups derived from nitrogen are introduced. The zeta potential of the ID-DLC film surface was controlled easily by controlling the amount of carboxyl groups and functional groups derived from nitrogen.

From these results, a unique material similar to amino acids where the positive and negative charges existed together at the same time could be obtained.

3) The introduction of carboxyl groups onto the ID-DLC films doped with silicon by surface treatment technology using oxygen plasma was tried. It was found that silicon is obstructive in the case of DLC used as the base of functional group introduction. As a reason, the oxidation of silicon first occur, inhibiting carboxyl group generation.

4) Hydrophilicity was increased by the plasma treatment, which introduces the carboxyl groups and the hydroxyl groups on the surface of ID-DLC. The platelet adhesion proof property was observed in plasma surface treated ID-DLC. Meanwhile, untreated ID-DLC was observed significant platelet adhesion. It is suggested that untreated ID-DLC adsorbs cell adhesion molecules that consists of the protein relates to the platelet by the hydrophobe interaction, and caused the platelet adhesion. Moreover, the influence of the zeta potential is a little for platelet adhesion property. Next, the tendency to blood coagulation property has divided the zeta potential at  $-50$  mV. Moreover, kallikrein-like activity and the TAT generation were the same behavior. It was suggested that kallikrein-like activity of the early response is triggered in cascade of coagulation reaction. And coagulation reaction continues to TAT generation closing phase. Moreover, it is known that coagulation reaction is occurred when prekallikrein and factor XII adsorbs on negatively charged surface. It was suggested that prekallikrein behavior on the ID-DLC surface is also similar. Moreover, ID-DLC that adjusted the zeta potential to  $-50$  mV or more can inhibit kallikrein-like activity, and acquire

characteristic of blood coagulation. These findings suggest that plasma treated ID-DLC inhibits both platelet adhesion and blood coagulation. Moreover, it is suggested that arbitrary blood compatibility may be obtained in plasma surface treated ID-DLC by controlling the amount of the functional group on the ID-DLC surface.

5) The mRNA expression level of Runx2 and type I collagen in MC3T3-E1 cells cultured on an untreated ID-DLC sample with a low composition ratio of the functional groups were about eighteen and twenty-four times as those in cells cultured on pure titanium. Untreated ID-DLC showed platelet adhesion, and the results on blood compatibility was not satisfactory. However, the bone compatibility was excellent. It is known that the platelet-rich plasma promotes the bone growth. However, the platelet has not acted directly because cow's serum medium is used in this study, and the platelet is not included. The reason for the good compatibility of untreated ID-DLC is not clear. However, it is forecast that the cell adhesion molecule adsorbs the surface of ID-DLC easily as described in chapter 5. Therefore, cell adhesion molecule or cytokine in the serum related to both of the platelet and osteoblast cell is adsorbed by the surface, and it was guessed that the differentiation of osteoblast cell may be caused. The possibility of controlling the various biocompatibilities by optimizing the composition ratio of functional groups on the ID-DLC film surface was also suggested.

In this study, the possibility of developing a unique material for medical treatments matching usage and the patient's conditions was shown by applying the plasma surface treated ID-DLC. Moreover, surface structural analysis by XPS to clarify the characteristics of the DLC film surface was extremely effective. Moreover, it succeeded in not changing mechanical compatibility and acquisition of interfacial compatibility. However, the mechanism underlying the biocompatibility is not clarified in this research. These will promote future research to realize better biocompatible materials for all patients needing such materials.

## Acknowledgements

First of all, I wish to thank as well as extend my gratitude to Professor Dr. Takayuki Takahagi for his supervision and encouragement on the completion of this study. I would like to express my appreciation to Professor Dr. Tatsuyuki Nakatani (Okayama University of Science) for his leadership and useful deep discussion. I would like to my gratitude to Professor Dr. Hiroki Nikawa for his constructive advice and useful suggestion regarding dental materials and biocompatibility. I also would like to express my gratitude to Professor Dr. Yutaka Kadoya, Professor Dr. Yoshitake Takane, Associate Professor Dr. Hitoshi Suzuki, and Assistant Professor Dr. Hiroyuki Sakaue for their useful comment and suggestion. I would like to express my appreciation to Mr. Yuki Nitta (TOYO Advanced technologies) for his help with plasma treatment experiments, the zeta potential analysis and useful discussion. I thank Professor Dr. Akira Mochizuki (Tokai University) for his suggestions regarding biomaterials and biocompatibility. I thank Research Assistant Professor Dr. Susumu Takabayashi (Tohoku University) for his suggestions regarding analysis technics of DLC and useful discussion. I thank Associate Professor Dr. Seicho Makihira (Kyusyu University) for his suggestions regarding cell differentiation and dental materials. I thank two researchers Dr. Shuzo Yamashita and Mr. Ikuo Omura for their advice regarding coating technology for medical devices. I thank Toyo Advanced Technology Corporation for the financial support on this study. And I thank two superiors at that time Mr. Masayoshi Murai, and Mr. Yoshinori Abe who gave chance of this research for me. I thank Professor Dr. Kohei Shiraishi (Kinki University) for his sugestion regarding biomaterials and plasma surface treatment technology. I thank Professor Dr. Noriyoshi Satoh (Tohoku University) for his suggestion regarding plasma technology. I thank Professor Dr. Keishi Kawabata (Hiroshima Institute of Technology) for his advice regarding plasma technology.

Chapter 6 of this study supported by Regional Innovation Creation Research and Development programs of Ministry of Economy, Trade and Industry in Japan.

Finally, I receive encouragement from my families, Yumi, Nayuta, Shoyo and Yukiko who always supported me.

# 公表論文

- (1) Differentiation Capability Evaluation of Osteoblast by Functionalized DLC Thin Films with Plasma Processing  
Keishi Okamoto, Tatsuyuki Nakatani, Yuki Nitta, Seicho Makihira, Satoshi Iwata, Hiroki Nikawa, Takayuki Takahagi,  
Journal of Photopolymer Science and Technology, 23 (2010) 591–594.
  
- (2) Diamond-like carbon thin film with controlled zeta potential for medical material application  
Yuki Nitta, Keishi Okamoto, Tatsuyuki Nakatani, Hideo Hoshi, Akihiko Homma, Eisuke Tatsumi, Yosiyuki Taenaka,  
Diamond and Related Materials, 17 (2008) 1972–1976.
  
- (3) Blood Compatibility of Gas Plasma treated Diamond-like Carbon Surface-Effect of Physicochemical Properties of DLC Surface on Blood Compatibility  
Akira Mochizuki, Tatsuhisa Ogawa, Keishi Okamoto, Tatsuyuki Nakatani, Yuki Nitta,  
Materials Science and Engineering, C31 (2011) 567–573.

# Differentiation Capability Evaluation of Osteoblast by Functionalized DLC Thin Films with Plasma Processing

Keishi Okamoto<sup>†\*\*</sup>, Tatsuyuki Nakatani, Yuki Nitta,  
Seicho Makihira\*, Satoshi Iwata\*, Hiroki Nikawa\* and Takayuki Takahagi<sup>\*\*</sup>

<sup>†</sup>Toyoto Advanced Technologies Co., Ltd.

5-3-38 Ujina-higashi, Minami-ku, Hiroshima 734-8501, Japan

\* Graduate School of Biomedical Sciences Hiroshima University

1-2-3 Kasumi, Minami-ku, Hiroshima 734-8553, Japan

\*\* Graduate School of Advanced Sciences of Matter Hiroshima University

1-3-1 Kagamiyama, Higashi-Hiroshima, Hiroshima, 739-8530, Japan

[nakatani.t@toyoto-at.co.jp](mailto:nakatani.t@toyoto-at.co.jp)

**Keywords: Diamond-like carbon, osteoblast, biocompatibility, dental implant**

## 1. Introduction

Diamond-like carbon (DLC) are widely used in industrial applications, such as automobile parts with high wear resistance [1,2]. Moreover, DLC has been considered as one of the excellent biocompatible coating materials for medical devices in recent years [3-13]. It is known that DLC has a wide composition in a material composed of  $sp^2$  carbon,  $sp^3$  carbon, and hydrogen. Moreover, a functional group can be introduced using the carbon bond of DLC. Then, we examined the functionality of DLC for dental implant surface treatment by plasma processing. Fig. 1 shows the model of the functional group introduction into the surface of DLC using by  $O_2$  and/or  $NH_3$  plasma. Radicals and ions are generated with plasma, and the functional group terminates the carbon bond of DLC [14]. This plasma processing can control the zeta potential within the wide range of -45

to +10mV [15]. In addition, we report that the characteristics of platelet adhesion and fibrin coagulation can be controlled on the basis of the functional group introduction ratio and zeta potential [16]. The result showing blood compatibility suggests the possibility of applying to various implants that come in contact with blood.

Currently, various implants are applied by dental and orthopedic operations. The dental implant fixture often reduces infection and an inappropriate occlusal force because the period until fixture is long. Therefore, urgent requirements are to develop a technology that improves the growth of the bone and to complete a treatment in a short period. Moreover, platelet-rich plasma is known to act on the bone growth factor and to stimulate periodontal regeneration [17,18]. Therefore, we applied DLC used by controlling blood compatibility and aimed at the development of a technology that controlled the differentiation of osteoblast. In an actual experiment aimed at the functionalization of DLC to introduce a functional group into a surface by plasma surface treatment, we examined the effect of the differentiation capability of osteoblast.

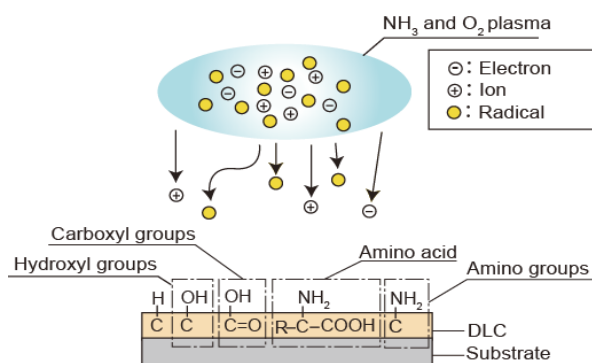


Fig.1 Schematic of DLC thin films surface with introduced functional groups.

## 2. Experimental setup and conditions

DLC coating used ionized-assisted deposition of the plasma-enhanced chemical vapor deposition method. The pressure of the chamber used was adjusted to 0.2Pa using  $C_6H_6$  as the operation gas. The electric power of the

Base pressure:	$1 \times 10^{-3}$ Pa
Operational pressure:	4 Pa
RF power:	100 W
Treatment time:	15 s
Operational gas:	O <sub>2</sub> , NH <sub>3</sub>

Table 1 Surface treatment conditions by plasma.

filament was 300W, and the bias voltage of the substrate was 2kV. The test piece material used the pure Ti (JIS TP340C).

Next, functional group modification was conducted on DLC surfaces using the plasma surface treatment technology, and the relationship between the composition of the surface and the composition ratio of functional groups introduced was examined. The equipment used was a capacitively coupled plasma surface treatment system with a radio-frequency power source. Table 1 shows the plasma surface treatment conditions used in this experiment.

DLC surface was analyzed by X-ray photoelectron spectroscopy (JOEL JPS9010) with non-monochromatized AlK<sub>α</sub> rays. The C1s spectrum was first assigned into four elements (C-C *sp*<sup>3</sup> (283.8eV), C-C *sp*<sup>2</sup> (284.3eV), C-H *sp*<sup>2</sup> (284.8eV), and C-H *sp*<sup>3</sup> (285.3eV)) [19-21]. Then, the C1s spectrum was analyzed so that the ratio of the total area of C-O (O-C-O), C=O (287.3eV), and O=C-O (288.8eV), to the area of C-N may be the same as the ratio of oxygen and nitrogen to carbon. The analysis of DLC was carried out by the angle resolved XPS method. Then, the emission angle was varied as 0 and 75°.

To examine the effect of DLC on osteoblast differentiation, osteoblastic cell line; MC3T3-E1 was used in the present study. MC3T3-E1 cell line was purchased from the European Collection of Cell Cultures (Wiltshire). MC3T3-E1 cells were cultured in alpha-MEM supplemented with an antibiotic mixture (Invitrogen), 10% fetal bovine serum (Biological Industries) and 50 ug/ml L-ascorbic acid (Sigma). MC3T3-E1 were maintained at 37°C under 5% CO<sub>2</sub>/95% air for an experiment. The cells were seeded to the surfaces of Ti specimens placed on the bottoms of 24-well plates at a density of 5.0 x 10<sup>4</sup> cells/well titanium specimens and well was extracted using TRIZol reagent maintained for 7 days [22]. Total RNA of each well was extracted using TRIZol reagent (Invitrogen), and first-strand cDNA from total RNA (100 ng) using ReverTra

Ace reverse transcriptase (Toyobo). Real-time quantitative RT-PCR analysis for runt-related transcription factor 2 (Runx2), type I collagen and β-actin were performed using Colbet (Qiagen). β-actin was chosen as an internal control against which to standardize the variability in amplification owing to slight differences in starting total RNA concentrations. The sequences of the primers used in these analyses are previously described [23]. Differences between mean values of groups were subjected to a one-way analysis-of-variance (ANOVA) and Tukey's multiple range test.

### 3. Result and discussion

Table 2 shows the atomicity ratios of functionalized DLC by plasma surface treatment for C, O, and N. Then, the emission angle was 0°. O<sub>2</sub> plasma has increased the ratio of oxygen a little. Moreover, NH<sub>3</sub> plasma introduced nitrogen.

		atomicity ratio		
		C	O	N
No.1	DLC(Untreated)	0.92	0.08	>0.003
No.2	O <sub>2</sub> Plasma	0.90	0.10	>0.002
No.3	NH <sub>3</sub> Plasma	0.86	0.04	0.10

Table 2 Atomicity ratio of functionalized DLC by plasma surface treatment.

Fig. 2 shows the profile used to analyze the C1s spectra of untreated DLC by the angle-resolved XPS method. The C1s spectra was analyzed and the bonds of C-O (O-C-O), C=O, and O=C=O were fitted. It was shown by angle-resolved XPS that many elements of O=C=O, C=O, and C-O (O-C-O) existed on the surface. It was suggested that the dangling bond on the DLC surface bonded with oxygen when the coating of DLC was completed, and the chamber was opened to the atmosphere and it was terminated.

Table 3 shows the composition ratio obtained before and after the plasma treatment. The O<sub>2</sub> plasma showed increases in the ratio of C=O, and O=C-O bonds. The NH<sub>3</sub> plasma showed increases in the ratio of C-N bond. Next, the mRNA expressions of Runx2 and type I collagen in MC3T3-E1 cells cultured on pure Ti of the control or three kinds of DLC with



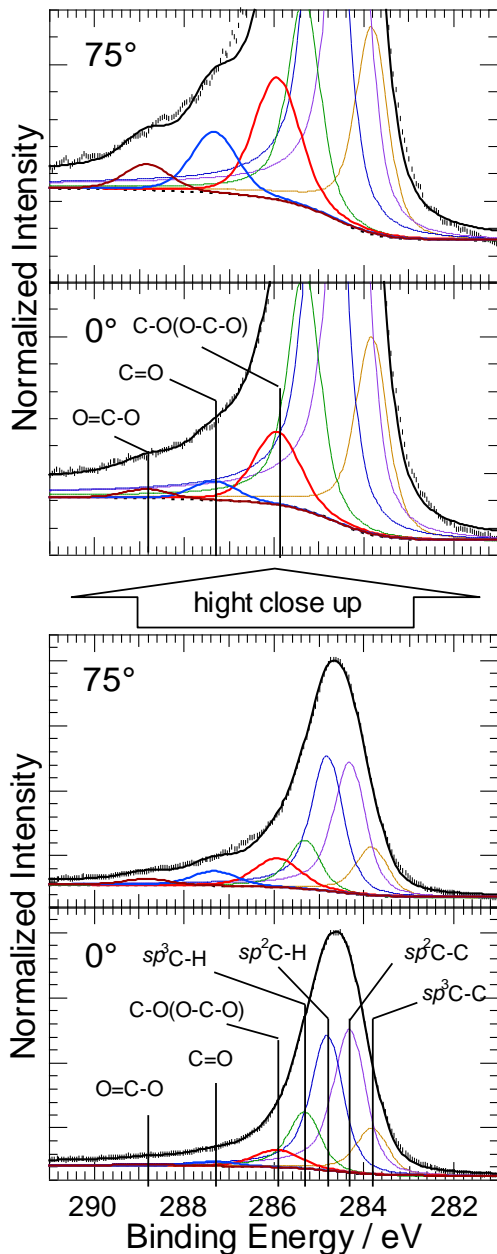


Fig. 2 The C1s spectra of untreated DLC used to analyze by the angle-resolved XPS method.

		composition ratio				
		C-O (O-C-O)	C=O	O=C-O	C-N	(C-C+O-H)
No.1	DLC(Untreated)	0.06	0.02	>0.007	-	0.91
No.2	O <sub>2</sub> Plasma	0.07	0.04	0.04	-	0.86
No.3	NH <sub>3</sub> Plasma	0.03	0.02	>0.005	0.15	0.79

Table 3 Composition ratio of functionalized DLC by plasma surface treatment.

different composition ratio of the functional group element (No.1, No.2, and No.3) were examined.

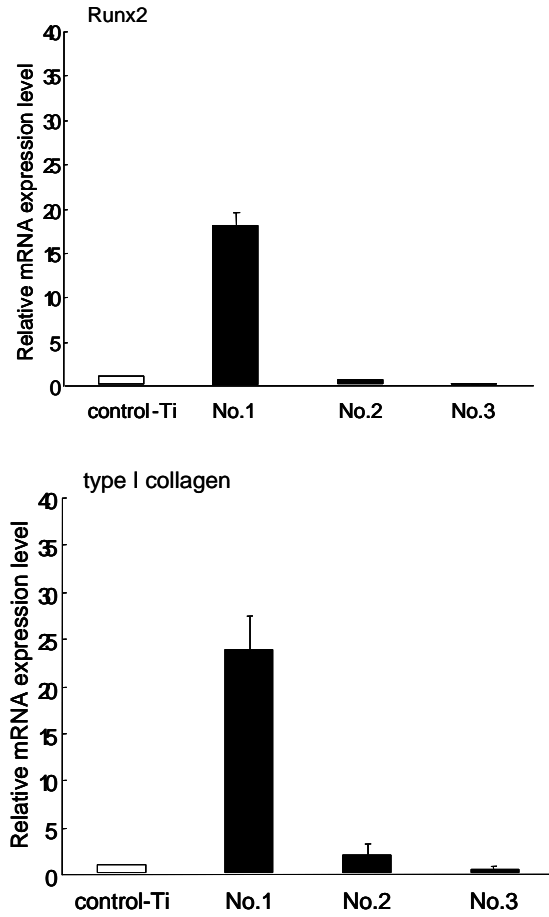


Fig.3 Effects of the DLC with different composition ratio of the functional group element on the titanium surface on the expression levels of dependent on mRNAs for Runx2 and type I collagen in MC3T3 E1 cells.

Fig. 3 shows the level of the mRNA expression of Runx2 and type I collagen about control-Ti and DLC. The mRNA expressions of Runx2 and type I collagen in MC3T3-E1 cells cultured on sample of No.1 was about eighteen and twenty-four times, as compared those cultured on pure Ti, respectively (ANOVA,  $p < 0.01$ ). On the other hand, these expressions in MC3T3-E1 on the sample of No.2 and No.3 were almost the same as those on pure Ti (ANOVA,  $p > 0.05$ ). It was suggested that the level of the osteoblast differentiation might be dependent on the composition ratio of the surface functional group in DLC.

#### 4. Conclusion

The effect of DLC thin films to introduce a functional group into surface using the plasma surface treatment technology on the expressions

of Runx2 and type I collagen known as the markers for osteoblast differentiation was examined in the present study. A difference in differentiation marker appearance was obtained in the outcome of an experiment depending on the amount of functional groups introduced into the surface of DLC. As a result, the possibility of controlling the differentiation of osteoblast by optimizing the composition ratio of functional groups on the surface of DLC was suggested.

#### Acknowledgements

The result of the actual experiment was achieved by the cooperation of the regional innovation creation research and development business program of the Ministry of Economy, Trade and Industry in Japan.

#### References

1. T. Nakatani, K. Okamoto, A. Araki, T. Washimi, *New Diamond and Frontier Carbon Technology*, **16** (2006) 187.
2. C. Weissmantel, K. Bewilogua, K. Breuer, D. Dietrich, U. Ebersbach, H. J. Erler, B. Rau and G. Reisse, *Thin Solid Films*, **96** (1996) 31.
3. D. P. Maguire, *Diamond and Related materials*, **14** (2005) 1277.
4. B. Balram, et al., *Catheterization and Cardiovascular Interventions*, **67** (2006) 698.
5. A. Shirakura, M. Nakaya, Y. Koga, H. Kodama, T. Hasebe and T. Suzuki, *Thin Solid Films*, **494** (2006) 84.
6. T. Hasebe, A. Kamijo, A. Hotta, K. Takahashi, T. Suzuki, *Chemistry and Chemical Industry*, **59** (2006) 1064.
7. R. Hauert, *Tribology International*, **37** (2004) 991.
8. R. Hauert, *Diamond and Related Materials*, **12** (2003) 583.
9. M. I. Jones, I. R. McColl, D. M. Grant, K. G. Parker, T. L. Parkar, *J. Biomedical Material Reserch*, **52** (2000) 413.
10. N. Nurdin, P. Francois, Y. Mugnier, J. Krumeich, M. Moret, B. O. Aronsson and P. Descouts, *European Cells and Materials*, **5** (2003) 17.
11. D. Antoniucci, et al., *Am. J. Cardiol.*, **85** (2000) 821.
12. T. Nakatani, K. Okamoto, I. Omura, S. Yamashita, *J. Photopolymer Science and Technology*, **20** (2007) 221.
13. T. Nakatani, K. Okamoto, I. Omura, S. Yamashita, *New Diamond and Frontier Carbon Technology*, **17** (2007) 289.
14. K. Okamoto, T. Nakatani, S. Yamashita, S. Takabayashi, T. Takahagi, *Surface and Coating Technology*, **202** (2008) 5750.
15. T. Nakatani, K. Okamoto, Y. Nitta, A. Mochizuki, H. Hoshi and A. Homma, *J. Photopolymer Science and Technology*, **21** (2008) 225.
16. Y. Nitta, K. Okamoto, T. Nakatani, H. Hoshi, A. Homma, E. Tatsumi and Y. Taenaka, *Diamond and Related Materials*, **17** (2008) 1972.
17. L. Boyapati, H. Wang, *Implant Dentistry*, **15** (2006) 160.
17. W. S. Pietrzak, B. L. Epply, *J. of Craniofacial Surgery*, **16** (2005) 1043.
18. S. Takabatashi, K. motomitsu, T. takahagi, A. terayama, K. okamoto and T. nakatani, *J. Applied Physics*, **101** (2007) 103542.
19. S. Takabayashi, K. Okamoto, K. Motomitsu, A. Terayama, T. Nakatani, H. Sakaue, H. Suzuki, T. Takahagi, *Applied Surface Science*, **254** (2008) 2666.
20. S. Takabayashi, K. Okamoto, T. Nakatani, H. Sakaue, T. Takahagi, *TANSO*, **235** (2008) 280. (in Japanese)
21. S. Makihira, Y. Mine, H. Nikawa, T. Shuto, E. Kosaka, M. Sugiyama, R. Hosokawa. *J Mater Sci Mater Med.* **21** (2010) 647.
22. Y. Mine, S. Makihira, H. Nikawa, H. Murata, R. Hosokawa, A. Hiyama, S. Mimura. *J Prosthodont Res.* **54** (2010) 1.



## Diamond-like carbon thin film with controlled zeta potential for medical material application

Yuki Nitta<sup>a,\*</sup>, Keishi Okamoto<sup>a</sup>, Tatsuyuki Nakatani<sup>a</sup>, Hideo Hoshi<sup>b</sup>, Akihiko Homma<sup>b</sup>, Eisuke Tatsumi<sup>b</sup>, Yoshiyuki Taenaka<sup>b</sup>

<sup>a</sup> TOYO Advanced Technologies Co., Ltd., 5-3-38 Ujina-higashi Minami-ku, Hiroshima 734-8501, Japan

<sup>b</sup> National Cardiovascular Center Research Institute Advanced Medical Engineering Center Department of Artificial Organs, 5-7-1 Fujishiro-dai, Suita, Osaka 565-8565, Japan

### ARTICLE INFO

#### Article history:

Received 21 January 2008

Received in revised form 7 May 2008

Accepted 28 May 2008

Available online 8 June 2008

#### Keywords:

Diamond-like carbon

Biomaterials

Surface characterization

### ABSTRACT

With the purpose of applying diamond-like carbon (DLC) thin films as a biocompatible material, we experimented with introducing functional groups such as amino and carboxyl groups to the surface of DLC thin films by plasma surface treatment. From the results, it was found that the contact angle values of the DLC thin films surface were decreased with increasing in the O=C–O bonded network on the surface. Measurement of the zeta potential when the amounts of the functional groups were varied showed that this successfully varied the zeta potential over the wide range of  $-48$  mV to  $+12$  mV. It was found that when carboxyl groups are introduced by  $O_2$  plasma modification of the DLC thin films surface, the zeta potential was lower than that of untreated DLC thin films sample. It was also found that amino groups can be introduced to the DLC thin films surface by  $NH_3$  plasma treatment, the zeta potential was higher than that of untreated DLC thin films sample. This means that zeta potential of the DLC thin films can also be controlled by controlling these two functional groups. Therefore, we have succeeded in developing a multifunctional DLC thin films that does not use polymers and is suitable as a biocompatible material.

© 2008 Elsevier B.V. All rights reserved.

### 1. Introduction

DLC (diamond-like carbon) thin films are amorphous thin films with both graphite bonds and diamond bonds. It has interesting characteristic, such as a low friction coefficient, wear resistance, and a wide band gap. Accordingly it is already used widely for industrial purposes, such as in dies of various types and in automobile parts [1,2]. Additionally, since DLC thin films have characteristics such as biocompatibility and antithrombogenicity, its application to the medical and biological fields has received a great deal of attention in recent years [3–9], and study for clarification of the deposition mechanisms [10,11] and surface conditions of such films have been well-practiced [12].

Meanwhile, the needs for medical devices that are in contact with the blood, such as artificial hearts and blood pumps, has increased with the development of medical technology. However, such medical devices have the problem that when they are inserted inside the body, blood clotting may form, or biological tissue attachment to them, causing their functioning to decrease markedly. Therefore, it is considered important to impart blood compatibility to medical devices. Currently, polymers are mainly used to impart blood

compatibility, however they have problems, namely that their blood compatibility is not necessarily outstanding, and their adhesion will not be of the best to metallic substrate. Consequently, development of a new medical material that has superior adhesion to base materials and high blood compatibility is viewed as an urgent task [13].

Accordingly, we have tried to develop new biocompatible materials that utilizes DLC thin films, having noted that DLC thin films is a chemically stable amorphous hydrocarbon thin films that is smooth and atomic flatness and moreover has superior compatibility with tissue and blood, as well as extremely superior adherence to metals [14]. DLC thin films itself is reported to have adequate biocompatibility [15], however is not effective in all situations. Therefore, account must be taken of the interactions between the DLC thin films surface and the cells in order for imparting higher biocompatibility to medical materials. One important parameter for this is the zeta potential between the cell and DLC thin films surfaces.

Cells are generally negatively charged, and their surface potential varies depending on the individual cell. Therefore, it will be possible to reduce stimulation to the cells by controlling the zeta potential of the DLC thin films. A method of controlling the zeta potential of the DLC thin films is to introduce functional groups such as amino and carboxyl groups into the DLC thin films surface by plasma surface treatment. We had already succeeded in introducing carboxyl groups into the DLC thin films surface, and had found that the DLC thin films

\* Corresponding author. Tel.: +81 82 252 5215; fax: +81 82 256 0264.  
E-mail address: [nitta.y@toyo-at.co.jp](mailto:nitta.y@toyo-at.co.jp) (Y. Nitta).

**Table 1**

The operational gases were used oxygen, argon, ammonia and acetylene

Base pressure [Pa]	2
Gas	NH <sub>3</sub> , O <sub>2</sub> , C <sub>2</sub> H <sub>2</sub> , Ar
Operational pressure [Pa]	130
Applied power [W]	30
Treatment time [s]	15, 30

These gases were introduced into the chamber via a mass flow controller. In the experiments, the plasma treatment duration was 15 s with each gas, making duration of 30 s when two gases were used.

were rendered superhydrophilic [16]. Carboxyl groups generally have the effect of increasing negative charge, and amino groups that of increasing positive charge. Hence, if the quantities of these functional groups can be controlled at the DLC thin films surface, it will be possible to control the zeta potential. This method is applied plasma surface modification to a sample on which DLC thin films has been formed. Thus, unlike the traditional techniques using polymers, it does not require the use of plant etc. It is impossible to develop outstandingly biocompatible materials with extremely simple techniques. In this experiment, we experimented with performing plasma surface treatment on DLC thin films so as to introduce functional groups into its surface. We also measured the zeta potential of the DLC thin films when the carboxyl groups and amino groups had been introduced into it.

In this paper, we report X-ray photoelectron spectroscopy (XPS) deconvolution results of the amounts of functional groups generated, the relationship between the amounts of functional groups generated and the static contact angle, and also the zeta potential measurement results of the samples.

## 2. Experimental apparatus and condition

The chamber of plasma surface modification was evacuated to no more than 5 Pa with a rotary pumps, the base pressure was measured with a Pirani gauge. The process chamber was connected to RF power supply with an excitation frequency 13.56 MHz at maximum electrical power of 300 W. RF power of 30 W was injected to generate plasmas. CCP (Capacitively Coupled Plasmas) was generated by means of two parallel plate electrodes. The operational gases used were O<sub>2</sub>, Ar, NH<sub>3</sub> and C<sub>2</sub>H<sub>2</sub>. These gases were introduced into the chamber via a mass flow controller. In the experiments, the plasma treatment duration was 15 s with each gas, making duration of 30 s when two gases were used. Table 1 shows details of the plasma treatment conditions. DLC thin films used for plasma surface modification were prepared by ionization-assisted deposition. The operational gases used were benzene gases. The film thickness was

**Table 2**

The XPS, contact angle and zeta potential measurement conditions

Measurement condition	
<i>XPS measurement condition</i>	
Measurement atoms	C1s, N1s, O1s
X-ray source	Al (Aluminum)
Accelerating voltage [V]	12.5
Emission current [mA]	15
Base pressure [Pa]	Below 1 × 10 <sup>-6</sup>
<i>Zeta potential measurement condition</i>	
Measurement cell	NELS flat panel cell 15
Average electric field [V/m]	17.33
Average current [mA]	1.02
Monitoring particle	10 mm sodium chloride (NaCl)
Solvent	Pure water
<i>Contact angle measurement condition</i>	
Measurement liquid	Pure water
Amount of liquid [μl]	1

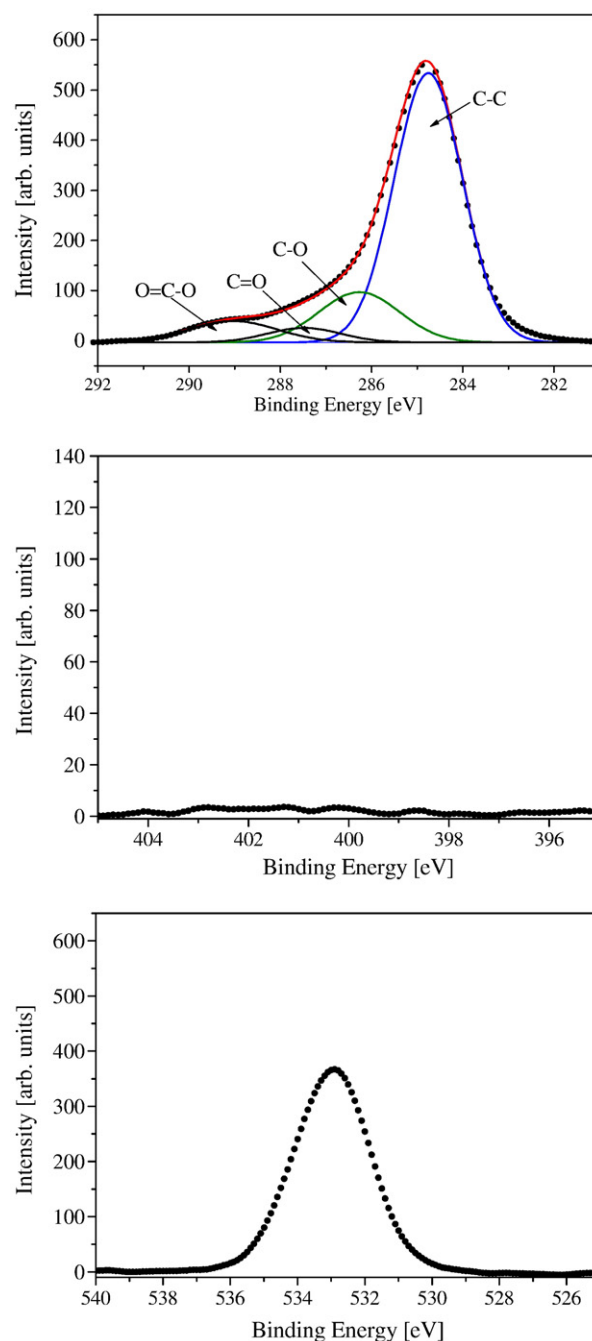


**Fig. 1.** The XPS spectra of treated DLC in C1s, N1s and O1s waveforms observed when the sample was given C<sub>2</sub>H<sub>2</sub> plasma treatment followed by O<sub>2</sub> plasma treatment. It is not observed that N1s peak, the C1s and O1s peaks were predominate. The C1s peak can be assigned to the binding energy of C–C, C–O, C=O and O=C–O bonded network respectively. The binding amounts were 71.8 at.%, 18.6 at.%, 2.9 at.% and 6.5 at.% respectively.

about 40 nm. We have already succeeded in applying this film to coronary artery drug-eluting stent [16].

The composition ratio of the DLC samples that modified by the plasma treatment was analyzed by an XPS (photoelectron spectroscopy, JPS-9010MC), and the static contact angle under the various conditions was measured with a contact angle meter (DM300, Kyowa Interface Science). Pure water was used to measure contact angle. The zeta potential of the samples was measured by a zeta potentiometer (ELS-Z, Otsuka Electronics). Table 2 shows these measurement conditions.

### 3. Results and discussion

#### 3.1. XPS measurement result

Figs. 1 and 3 show the results of XPS measurement after plasma treatment.

Fig. 1 shows the XPS spectra of treated DLC in C1s, N1s and O1s waveforms observed when the sample was given  $C_2H_2$  plasma treatment followed by  $O_2$  plasma treatment. Table 3 shows the composition ratio. It is not observed that N1s peak, the C1s and O1s peaks were predominate. The C1s peak can be assigned to the binding energy of C–C, C–O, C=O and O=C–O bonded network respectively [17,18]. The binding amounts were 71.8 at.%, 18.6 at.%, 2.9 at.% and 6.5 at.% respectively. Since the binding amounts in an untreated DLC sample were 82.7 at.%, 11.7 at.%, 3.8 at.% and 1.7 at.% respectively, it is evident that the C–C bonds or C–H bonds were cleaved by radicals, electrons and ions in the plasma, and that thereby oxidation reactions such as C–O, C=O and O=C–O were promoted. Particularly, substrate bias was 0 V when plasma treatment was performed in this experiment. It was considered that  $O_2$  or O radicals in plasma mainly drew H from C–H bonds. Amount of C–C bonds or C–H bonds in DLC thin films were dependence on functional groups introduced to DLC surface. Therefore it is considered that amount of functional groups introduced to DLC thin films surface can be controlled by controlling amount of C–C bonds or C–H bonds in DLC thin films. It can also be seen that the O=C–O peaks were peaks stemming from the carboxyl groups and were, approximately, over three times more numerous compared with an untreated DLC sample. From this result, it will be seen that carboxyl groups can be introduced efficiently onto the surface of DLC thin films by plasma surface treatment.

Fig. 2 shows chemical labeling measurement result of  $C_2H_2+O_2$  plasma treatment. Amount of carboxyl and carbonyl groups was measured with trifluoroethanol and tetrafluorophenylhydrazine [19,20]. From this result, it was observed that carbonyl and carboxyl groups were increased by plasma treatment. It was found that carboxyl groups were introduced to DLC surface by  $O_2$  plasma treatment.

Fig. 3 shows the XPS spectra of treated DLC in C1s, N1s and O1s waveforms were observed when the sample was modified by  $C_2H_2$  plasma followed by  $NH_3$  plasma treatment. Table 3 shows composition ratio.

The C1s peak was assigned in the same manner as above, and binding amounts were 79.1 at.%, 11.6 at.%, 7.2 at.% and 2 at.% respectively. Compared with the above-described  $C_2H_2+O_2$  plasma treatment, the C–C bonds were larger than that of  $C_2H_2+O_2$  plasma

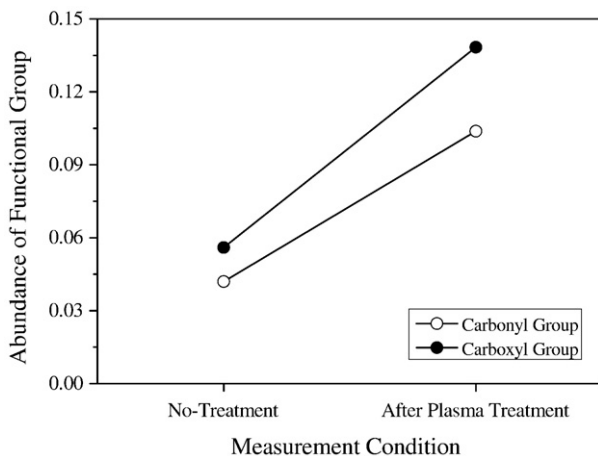


Fig. 2. The chemical labeling result for  $C_2H_2+O_2$  plasma treatment. It was observed that carbonyl groups and carboxyl groups were increased after plasma treatment.

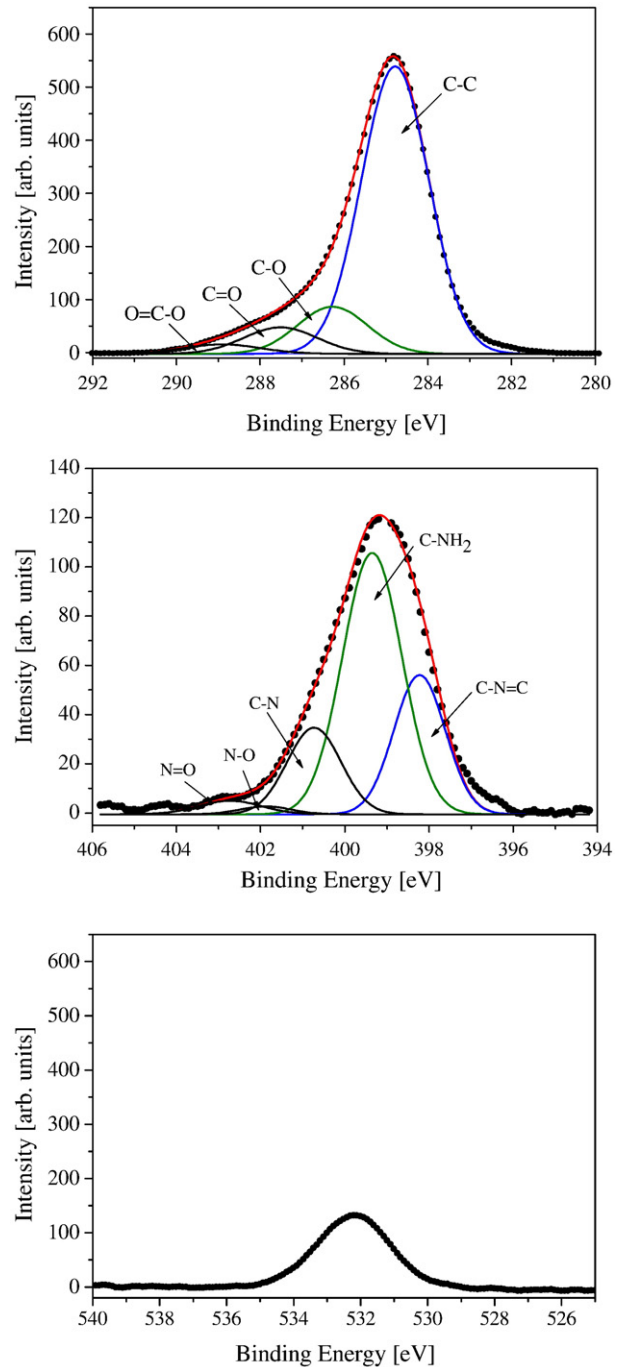


Fig. 3. The XPS spectra of treated DLC in C1s, N1s and O1s waveforms were observed when the sample was modified by  $C_2H_2$  plasma followed by  $NH_3$  plasma treatment. The N1s peak can be assigned to the binding energy of C–N=C, C–NH<sub>2</sub>, C–N, N–O, N=O bonded network respectively. The binding amounts were 20.7 at.%, 58.7 at.%, 16.3 at.%, 1.7 at.% and 2.6 at.% respectively. It was observed that C–NH<sub>2</sub> was dominated.

treatment and the amount of carboxyl groups were decreased. However, as Fig. 3 shows, it is observed that N1s peak was remarkable, in contrast to the  $C_2H_2+O_2$  plasma treatment. It is considered that the

Table 3  
The composition ratio of XPS measurement results

	C1s	N1s	O1s
$C_2H_2+O_2$	80.6	0.6	18.8
$C_2H_2+NHO_3$	63.05	22.5	14.45

C–H bonds or C–C bonds were severed by radicals, electron and ion in the NH<sub>3</sub> plasma, and nitrogen was introduced into the DLC thin films surface. N1s peak can be assigned to the binding energy of C–N=C, C–NH<sub>2</sub>, C–N, N–O, N=O bonded network respectively [21–23]. The binding amounts were 20.7 at.%, 58.7 at.%, 16.3 at.%, 1.7 at.% and 2.6 at.% respectively. From this result, it was found that C–NH<sub>2</sub> was dominated. Also, it was observed that amino groups were introduced to DLC surface by chemical method. Therefore, it is possible to generate amino groups preponderantly on the DLC thin films surface with these conditions.

It will be seen from the foregoing that we are now able to generate both carboxyl groups and amino groups on the surface of DLC thin films. Therefore, we have discovered a possibility for controlling the zeta potential on DLC surface.

3.2. Contact angle measurement results

Fig. 4 shows the static contact angles values measurement result when the amount of carboxyl groups is varied. The proportions of such groups were determined by plasma surface modification with different gases and measuring the resulting samples with the XPS. The contact angles are the values immediately after plasma treatment.

It can be observed that the contact angle tends to decrease with increasing in amount of O=C–O. Also, the DLC thin films surface becomes adequately hydrophilic with increasing in the carboxyl groups, since the contact angle of conventional DLC thin films is around 70°. As C–O bonds such as C–O, C=O, O=C–O are known to be hydrophilic, the cause is considered to be that the hydrophilicity of the DLC thin films surface increases with increasing in such bonds.

Fig. 5 shows the contact angle measurement result when DLC surface was treated by NH<sub>3</sub> plasma. The contact angle values of NH<sub>3</sub> plasma treatment were lower than that of untreated DLC. The contact angle was saturated when N/C ratio was about 0.07. However even the lowest value of contact angle values was about 30°, the contact angle was higher than that of DLC introduced carboxyl groups. Therefore it is considered that either the contact angle was mainly dependence on amounts of O=C–O. It was found that the static contact angle values can be controlled by controlling the amount of the carboxyl groups.

3.3. Zeta potential measurement results

Fig. 6 shows the results of zeta potential measurement for various carboxyl group amounts. Zeta potential was measured using an ELS-Z made by Otsuka Electronics. The carboxyl group amount was

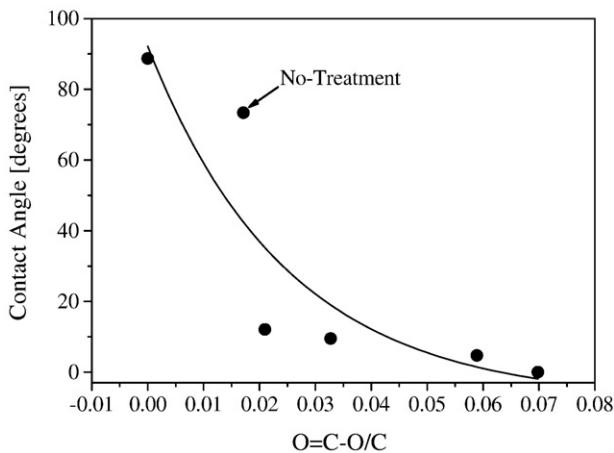


Fig. 4. The proportions of such groups were determined by plasma surface treatment with different gases and measuring the resulting samples with the XPS. The static contact angles are the values immediately after plasma treatment. The static contact angle values were decreasing with increasing in carboxyl groups.

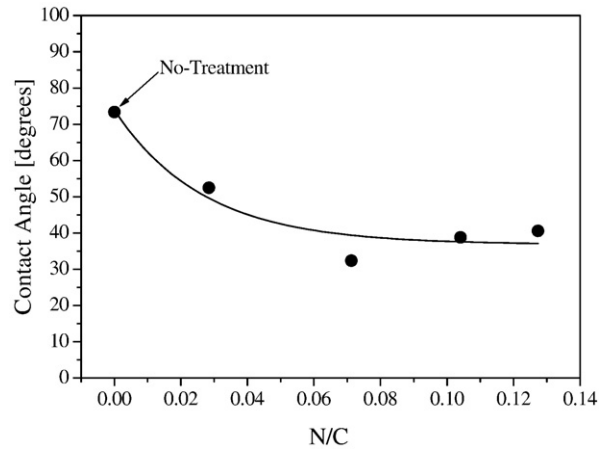
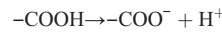


Fig. 5. The static contact angle measurement result when DLC surface was treated by NH<sub>3</sub> plasma. The static contact angle values of NH<sub>3</sub> plasma treatment were lower than that of no treatment. The static contact angle values were saturated when N/C ratio was about 0.07. However even the lowest value of contact angle values was about 30°, the contact angle was higher than that of DLC introduced carboxyl groups.

measured under various plasma modification conditions, and the zeta potential in each case was measured. The N/C ratio in the various cases is also shown in the figure. The N/C and O=C–O/C ratio were the values immediately after plasma treatment.

It can be observed that the zeta potential was decreased approximately twice as much as untreated sample with increasing in the O=C–O/C ratio. It is known that where the carboxyl group –COOH is present it will generally dissociate thus:



and samples to which carboxyl groups have attached will be negatively charged due to the –COO<sup>-</sup>. Therefore, it is considered that the zeta potential was decreased with increasing in the carboxyl groups, compared with untreated DLC thin films. It can also be observed that when N/C=0.04 and 0.36 the zeta potential increases greatly compared with an untreated DLC thin films, particularly at N/C=0.36, where the zeta potential turns positive. It is known that where the amino group –NH<sub>3</sub><sup>+</sup> with bonded protons is present on the surface of a sample, the sample will generally be positively charged. Therefore, it was considered to account for the marked increase in the surface potential of the DLC thin films when the amino groups were introduced.

These results indicate that it is possible to control the zeta potential of DLC thin films by controlling the amounts of the carboxyl groups

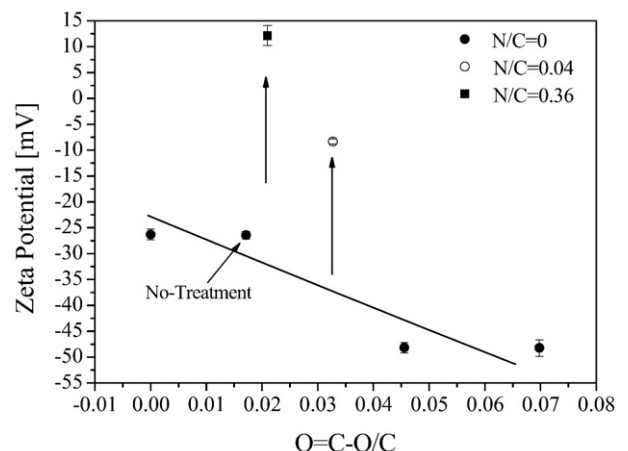


Fig. 6. Dependence of zeta potential on O=C–O/C.

and amino groups. It may thus be said to have discovered a possibility for development of a new biocompatible material.

#### 4. Summary

The purpose of this experiment was to introduce functional groups into the surface of DLC thin films. The results showed that it is possible to introduce amino and carboxyl groups into a DLC surface by plasma surface treatment. It was also found that the amounts of these functional groups can be controlled by varying the plasma treatment conditions.

From measurements of the zeta potential, it was found that the DLC surface is negatively charged when carboxyl groups are introduced to it, and positively charged when amino groups are introduced to it. We succeeded in controlling the zeta potential over a wide range by varying the amounts of these functional groups. Therefore, we have discovered through this study that development of a new biocompatible material for application to medical materials that are in contact with the blood is possible.

#### Acknowledgements

The authors would like to thank the following persons for their technical support and assistance in the execution of this study: Emeritus Prof. Noriyoshi Sato of Tohoku University regarding plasma technology, Prof. Takayuki Takahagi of Hiroshima University regarding DLC surface evaluation methods, and Prof. Kouhei Shiraishi of Kinki University regarding deconvolution technique of the zeta potential.

#### References

- [1] C. Weissmantel, K. Bewilogua, K. Breuer, D. Dietrich, U. Ebersbach, H.J. Erler, B. Rau, G. Reisse, *Thin Solid Films* 96 (1996) 31.

- [2] T. Nakatani, K. Okamoto, A. Araki, T. Washimi, *New Diamond and Frontier Carbon Technology* 16 (2006) 187.
- [3] D.P. Maguire, *Diamond and Related Materials* 14 (2005) 1277.
- [4] A. Shirakura, M. Nakaya, Y. Koga, H. Kodama, T. Hasebe, T. Suzuki, *Thin Solid Films* 494 (2006) 84.
- [5] T. Hasebe, A. Kamijo, A. Hotta, K. Takahashi, T. Suzuki, *Chemistry and Chemical Industry* 59 (2006) 1064.
- [6] R. Hauert, *Tribology International* 37 (2004) 991.
- [7] R. Hauert, *Diamond and Related Materials* 12 (2003) 583.
- [8] M.I. Jones, I.R. McColl, D.M. Grant, K.G. Parker, T.L. Parkar, *Journal of Biomedical Material Research* 52 (2000) 413.
- [9] N. Nurdin, P. Francois, Y. Mugnier, J. Krumeich, M. Moret, B.O. Aronsson, P. Descouts, *European Cells and Materials* 5 (2003) 17.
- [10] M. Shinohara, K. Cho, Y. Matsuda, H. Fujiyama, K. Okamoto, T. Nakatani, *Transactions of the Materials Research Society of Japan* 32 (2) (2007) 473.
- [11] M. Shinohara, H. Shibata, K. Cho, T. Nakatani, K. Okamoto, Y. Matsuda, H. Fujiyama, *Applications of Surface Science* 253 (2007) 6242.
- [12] S. Takabayashi, K. motomitsu, T. Takahagi, A. Terayama, K. Okamoto, T. Nakatani, *Journal of Applied Physics* 101 (2007) 103542.
- [13] Yang Jung-Hoon, Song Kwang-Soup, Zhang Guo-Jun, Degawa Muneori, Sasaki Yoshinori, Ohdomari Iwao, Kawarada Hiroshi, *Langmuir* 22 (2006) 11245.
- [14] T. Nakatani, K. Okamoto, I. Omura, S. Yamashita, *Journal of Photopolymer Science and Technology* 20 (2) (2007) 221.
- [15] R. Hauert, *Diamond and Related Materials* 12 (2003) 583.
- [16] T. Nakatani, K. Okamoto, I. Omura, S. Yamashita, *New Diamond and Frontier Carbon Technology* 17 (6) (2007) 289.
- [17] Wen-His Chuang, Jui-Che Lin, *Journal of Biomedical Material Research* 82 (2007) 820.
- [18] T. Takahagi, A. Ishitani, *Carbon* 22 (1984) 43.
- [19] D.S. Everhart, C.N. Reilly, *Analytical Chemistry* 53 (1981) 665.
- [20] T. Takahagi, et al., *Carbon* 26 (1988) 389.
- [21] G. Beshkov, D.B. Dimitrov, St. Georgiev, D. Juan-Cheng, P. Petrov, N. Velchev, V. Krastev, *Diamond and Related Materials* 8 (1999) 591.
- [22] R. Ohta, K.H. Lee, N. Saito, Y. Inoue, H. Sugimura, O. Takai, *Thin Solid Films* 434 (2003) 296.
- [23] Zhimin Zhou, Lifang Xia, Mingren Sun, *Diamond and Related Materials* 13 (2004) 14.



Contents lists available at ScienceDirect

## Materials Science and Engineering C

journal homepage: [www.elsevier.com/locate/msec](http://www.elsevier.com/locate/msec)

# Blood compatibility of gas plasma-treated diamond-like carbon surface—Effect of physicochemical properties of DLC surface on blood compatibility

Akira Mochizuki <sup>a,\*</sup>, Tatsuhisa Ogawa <sup>a</sup>, Keishi Okamoto <sup>b</sup>, Tatsuyuki Nakatani <sup>b</sup>, Yuki Nitta <sup>b</sup><sup>a</sup> Department of Bio-Medical Engineering, Tokai University, Nishino 317, Numazu, Shizuoka 410-0395, Japan<sup>b</sup> Toyo Advanced Technologies Co., Ltd., Ujina-Higashi 5-3-38, Minami-ku, Hiroshima 734-8501, Japan

## ARTICLE INFO

## Article history:

Received 4 June 2010

Received in revised form 9 September 2010

Accepted 20 November 2010

Available online 27 November 2010

## Keywords:

Diamond-like carbon

Zeta potential

Gas plasma treatment

Blood compatibility

Platelet

Coagulation system

## ABSTRACT

From the knowledge that zwitterion-type polymers show good blood compatibility, the introduction of both cationic and anionic functional groups onto diamond-like carbon (DLC) surface is expected to improve blood compatibility. Thus, DLC films were treated with oxygen and ammonia gas plasmas. The surfaces were characterized in terms of chemical composition by XPS, contact angle, and zeta potential. XPS analysis showed the introductions of a carboxyl group by oxygen plasma treatment and nitrogen atoms by ammonia plasma treatment. The evaluation of blood compatibility for the DLC surfaces was carried out in terms of platelets and the coagulation system. Excellent improvement of platelet compatibility was observed by the treatment with the gas plasmas, regardless of the plasma species. As for the compatibility with the coagulation system, DLC surfaces with a high concentration of carboxyl groups (COOH) markedly activated the system via the intrinsic pathway. However, the surfaces treated with ammonia plasma did not activate the system even though they had high COOH concentration. Measurement of the zeta potential revealed that the ammonia plasma treatment raised the potential from a negative value to a positive one. Though the introduction of amino groups to the surface was not detected directly, the treatment of ammonia plasma changed the electrical state of the DLC surface having COOH group, causing a difference in blood compatibility among the DLCs obtained by various plasma conditions.

© 2010 Elsevier B.V. All rights reserved.

## 1. Introduction

Carbon is known to be one of the good blood-compatible materials and is used in several medical devices. For example, pyrolytic carbon is applied to the artificial heart valve. Among the carbon materials, diamond-like carbon (DLC) that consists of carbon and hydrogen has recently been expected to be used as a medical coating because of its chemical stability, low friction coefficient, and high hardness/wear resistance, in addition to its good bio-compatibility [1]. Thus, many applications to implants such as hip joints and coronary stents are under investigation. DLC coating can be carried out on a targeted surface (substrate) by depositing carbon by radio-frequency plasma-enhanced chemical vapor deposition and so on. As the thickness of a DLC coating is usually on the nm order, only the surface properties of the substrate can be improved without deterioration of its mechanical property. Recently, in order to improve the bio-compatibility of DLC, many efforts have been made from the viewpoint of its atomic structure and composition. The former example is an attempt based on varying the  $sp^2/sp^3$  ratio of carbons [2]. The latter example is the introduction of hetero-atoms such as silicon, fluorine, calcium, and

phosphor to DLC [3–5]. On the other hand, there are many proposals and investigations with regard to the bio-compatible surfaces composed of polymeric materials or low-molecular-weight organic compounds. In such studies, it is known that surfaces having zwitterionic groups show good blood compatibility and low protein adsorption. Kitano et al. [6] showed that the betaine polymer has good compatibility, the reason being that they insisted that such an ionic structure does not destroy the water structure. Chung et al. [7] reported that phosphorylcholine (PC)-terminated self-assembled monolayer (SAM) showed excellent property for the adhesion of platelets. PC is a component forming bio-membrane and has two moieties, an anionic phosphate group and a cationic ammonium group. Chuang et al. [8] investigated SAM composed of both amine and carboxylic acid-terminated functionalities and found that SAM with surface amine mole fractions of 0.5 exhibits the least platelet adhesion. These reports indicate that a better surface for blood compatibility can be provided when the surface has both an anionic group and a cationic group at a mole ratio near 1:1. Consequently, it is worth applying these findings observed in organic materials to a DLC surface; that is, it is interesting to introduce both anionic and cationic functional groups to a DLC surface at a ratio of 1:1 in order to create blood-compatible DLC. One of the possible methods for introducing the groups to a DLC surface is plasma treatment using ammonia and oxygen gases. Nakatani et al. [9,10] found that the zeta potential of

\* Corresponding author. Tel.: +81 55 968 1211; fax: +81 55 968 1156.  
E-mail address: [azmochi@wing.ncc.u-tokai.ac.jp](mailto:azmochi@wing.ncc.u-tokai.ac.jp) (A. Mochizuki).



DLC varies in a wide range by treatment with these gas plasmas. When the application of this method to medical devices is considered, coronary stents made of metal are one of the expected devices; for this purpose, the evaluation of its blood compatibility should be carried out using DLC deposited on the metal substrate. One of the physicochemical surface properties which suggest the introduction of both cationic and anionic groups is the zeta potential. However, in general, it is difficult to measure the zeta potential of DLC deposited on a metal substrate because of the conductivity of the substrate. In addition, in our laboratory we cannot prepare DLC films on non-conductive substrates under the same conditions that allow the preparation of DLC on a conductive substrate. Therefore, we prepared them by different methods and equipments, and the effect of the zeta potential on blood compatibility is elucidated. Thus, in this work, we compared blood compatibility between the plasma-treated DLC and common biomaterials to know their compatibility level as biomaterials, and in addition, investigated the relationship between the surface structure of DLC and blood compatibility to clarify the dominant factor determining the compatibility.

## 2. Experimental

### 2.1. Preparation of DLC films and plasma treatment

DLC film for blood compatibility tests was prepared on a SUS 316L stainless steel disc with a 46-mm diameter using benzene as the carbon source. The deposition of carbon was carried out as follows. The SUS 316L disc was placed in the chamber of an ionized deposition apparatus, and argon gas was introduced to the chamber to render the pressure at  $10^{-1}$  to  $10^{-3}$  Pa. Then, bombardment cleaning was implemented for about 30 min by discharge. Subsequently, tetramethylsilane ( $\text{Si}(\text{CH}_3)_4$ ) and benzene ( $\text{C}_6\text{H}_6$ ) were passed in, adjusting the deposition pressure to  $10^{-1}$  Pa at a rate of 30 ml/min, and thus an amorphous DLC film was deposited on the disc. In the deposition process, the DC bias voltage was  $-1.5$  kV and the temperature was about  $160^\circ\text{C}$ . The thickness of the DLC layer was estimated to be ca. 30 nm from the deposition time.

DLC film for the measurement of the zeta potential was prepared on a glass plate ( $15 \times 40$  mm) using acetylene as the carbon source. The deposition of carbon was carried out as follows. The glass plate was placed in the chamber of an ionized deposition apparatus, and argon gas was introduced to the chamber to clean the surface for 300 s at 2 Pa. Subsequently, acetylene ( $\text{C}_2\text{H}_2$ ) gas was passed in, adjusting the deposition pressure to 3 Pa and thus an amorphous DLC film was deposited on the plate. The thickness of the DLC layer was estimated to be ca. 130 nm from the deposition time (in 180 s).

Plasma treatment of the DLC surface was performed under high vacuum with a turbo molecular pump (TMP) or under low vacuum with a rotary pump (RP). The base pressures in the treatment chamber were  $1 \times 10^{-3}$  Pa (TMP) or 3 Pa (RP). The process chamber was connected to an RF power supply (13.56 MHz: AX-300, Adtec Plasma Technology, Fukuyama, Japan), and the RF power to generate the gas plasma was 30 W (for low vacuum) and 100 W (for high vacuum). Capacitively coupled plasma was generated by means of two parallel plate electrodes. The operation gases were oxygen ( $\text{O}_2$ ), argon (Ar), acetylene ( $\text{C}_2\text{H}_2$ ) and ammonia ( $\text{NH}_3$ ), which were introduced into the chamber through a mass flow controller under an operation pressure of 1 Pa (TMP) or 130 Pa (RP). The duration time of plasma irradiation was 15 s for each gas or 30 s when two gases were used.

Thus, in this work, the gas plasma-treated DLC surfaces are classified into three groups according to the preparation method; A: treated under low-vacuum condition, B: treated with acetylene-based plasma, and C: treated under high-vacuum condition, as shown in Table 1.

**Table 1**  
DLC sample group and plasma treatment condition.

Group	Sample	Plasma source	Plasma condition
A	a	$\text{O}_2$	Low vacuum
	b	Ar	
B	c	$\text{C}_2\text{H}_2$	Low vacuum
	d	$\text{C}_2\text{H}_2 + \text{O}_2$	
	e	$(\text{C}_2\text{H}_2 + \text{O}_2) + \text{O}_2^*$	
C	f	Ar	High vacuum (TMP)
	g	$\text{NH}_3$	
	h	$\text{O}_2 + \text{NH}_3$	
Control	DLC SUS316L PET	Non-plasma-treated	

TMP: turbo molecular pump.

\* After the treatment with ( $\text{C}_2\text{H}_2 + \text{oxygen}$ ) plasma, oxygen plasma treatment was carried out.

### 2.2. Surface characterization

Determination of the elements and functional groups on the DLC surfaces was carried out by X-ray photoelectron spectroscopy (Quantum 2000-TK, Physical Electronics Inc., Chanhassen, MN, USA). The X-ray source was monochromatized Al  $K\alpha$ . The X-ray gun was operated at 14 kV and the anode power was 25 W. Pass energy of 23.50 eV was chosen for high-resolution spectrum acquisition (C1s). The photoelectron take-off angle (TOA) was  $45^\circ$  (about 7 nm of the sampling depth) for all measurements.

The zeta potential of the DLC surfaces was measured using a zeta potential meter (ELS-Z, Otsuka Electronics, Osaka, Japan). The plasma-treated DLC plate was attached to a chamber, and the chamber was filled with a 10 mM NaCl solution, in which monitoring particles were suspended. Electrophoresis of the particles was carried out, and the apparent velocity distribution in the chamber was determined. The conditions of electrophoresis were as follows; mean electric field intensity 17.33 V/cm and average current 1.02 mA.

The static contact angle of water on the DLC surfaces was measured using a contact angle goniometer (Face CA-A, Kyowa Interface Science, Tokyo, Japan) at room temperature. The volume of water droplet was 10  $\mu\text{l}$ . The contact angle was read from a protractor of the equipment through a microscope by the naked eye at five different places of each sample surface, and the values were averaged.

### 2.3. Evaluation of blood compatibility

The blood compatibility of DLC was evaluated in terms of platelet adhesion and the generation of thrombin–antithrombin III complex (TAT). The blood used was drawn from healthy volunteers using a blood collection tube (Venoject II, Terumo, Tokyo, Japan). The platelet adhesion test was performed according to our previous article [11]. Briefly, the method is shown below. Whole blood was anticoagulated by 3.8% sodium citrate solution at the mixing ratio of blood to a citrate solution (97.5/2.5 vol/vol), and was centrifuged at 1500 rpm for 10 min at room temperature. The supernatant layer was platelet rich plasma (PRP). Centrifugation of PRP at 3000 rpm for 10 min gave platelet-poor plasma (PPP) as an upper layer. The number of platelets in the plasmas was counted by a hemacytometer (K-1000, Sysmex Co., Kobe, Japan), and a platelet-suspended plasma for the adhesion test was prepared by adjusting the number to  $1 \times 10^5$  platelets/ $\mu\text{l}$  when mixing PRP and PPP. An aliquot amount of the platelet-suspended plasma was placed on the samples and incubated for 60 min at  $37^\circ\text{C}$ . After the sample was washed, it was immersed in 1% glutaraldehyde in a phosphate-buffered saline (PBS) for 60 min at  $4^\circ\text{C}$  to fix the adherent platelets. The sample was freeze-dried and sputter-coated using gold, prior to observation by a scanning electron microscope (JSM-840, JEOL, Tokyo, Japan). Five SEM images were

taken for each sample, and the number of adherent platelets on the five images was averaged.

The method to determine TAT generation was as follows. Heparinized whole blood (1000  $\mu$ l, 2 IU/ml) was pipetted into an in-house-built chamber with 1307 mm<sup>2</sup> of DLC surface area (40-mm diameter), the chamber being composed of a poly(2-methoxyethyl acrylate) (PMEA)-coated PET wall, a DLC-coated SUS wall and a spacer. As PMEA (Fig. 1) is inert and activation of the coagulation system by its surface is very low [12], the influence of the wall on the determination of TAT generated by the DLC surface is negligibly small. The chamber was rotated vertically at 47 rpm at 37 °C for 120 min to avoid sedimentation of blood cells during incubation. After incubation, the blood was moved to a micro test-tube, followed by the addition of 10% sodium citrate solution. The blood was centrifuged at 3000 rpm for 10 min to obtain blood plasma. The level of TAT in the plasma was evaluated using an ELISA kit (TAT-EIA, Enzyme Research Laboratories, South Bend, IN, USA).

#### 2.4. Determination of plasma kallikrein-like activity

The kallikrein-like activity of plasma was determined in order to investigate the activation pathway of the coagulation system. Heparinized whole blood (2 IU/ml) was centrifuged at 3000 rpm and platelet-poor plasma was obtained. Filtration of the plasma through a membrane filter with a 0.2- $\mu$ m pore size (Minisart 17597, Sartorius AG, Goettingen, Germany) yielded platelet-free plasma (PFP). The PFP (3 ml) was diluted with a pH 7.8 Tris-buffer (9 ml), and 400  $\mu$ l of the diluted plasma was pipetted into the sample chamber. The chamber has a similar structure to the one shown in Fig. 1 except for the spacer diameter, 20 mm. After incubation of the sample chamber for 1 h at 37 °C, the plasma was pipetted into a 96-well multiplate and a chromogenic reagent (S-2302, Chromogenix, Milano, Italy) (50  $\mu$ l) was pipetted into the wells. The absorbance of the sample was monitored at 405 nm using a multiplate reader (Thermo Max, Molecular Device, Sunnyvale, CA, USA). This procedure was carried out in accordance with the maker's protocol.

#### 2.5. Statistical analysis in evaluation of blood compatibility

All data on the evaluation of blood compatibility were obtained from several independent experiments and are expressed as mean  $\pm$  SE (standard error) in the figures. A paired t-test was employed to evaluate the statistical significance of the differences. The software used was Excel® (Microsoft, Redmond, WA, USA).

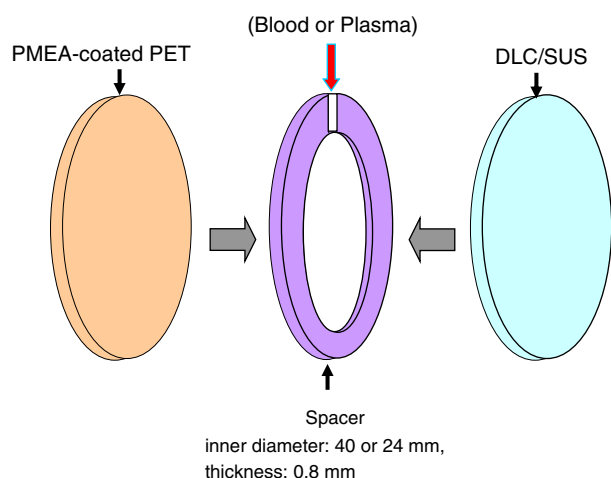


**Fig. 1.** Structure of chamber for evaluation of blood compatibility. Sample plate and PMEA-coated PET film adhered to a spacer, resulting in a chamber. A volume of 1000  $\mu$ l (40 mm in diameter) or 400  $\mu$ l (20 mm in diameter).

#### 2.6. Control materials

It is very important to know the performance level of new material in comparison with conventional biomaterials. As control materials, poly(ethylene terephthalate)(PET) and SUS 316L stainless steel were adopted in this work. Both materials are very popular and important biomaterials in clinical use, for both implant and single-use devices. In addition, in this work, SUS 316L was used as a substrate where DLC was coated. Thus, these controls are good for the evaluation of blood compatibility of plasma-treated DLCs. PET film was supplied by Toray (Tokyo, Japan).

### 3. Results and discussion

#### 3.1. Surface structure

The XPS surface analysis of the DLC is discussed first. The surface chemical compositions of the DLC deposited on the SUS and glass substrates were determined from wide-scan spectra and are shown in Tables 2 and 3, respectively. Table 2 shows that all of the surfaces are composed of carbon, nitrogen and oxygen atoms, and for some of the DLCs a small amount of Si was observed. It was positively found that the oxygen and ammonia plasma treatments bring about high concentration of oxygen and nitrogen at the surface when compared with other gas plasma treatments. However, all of the DLC surfaces have 0.3–10 atom% nitrogen atoms and 10–23% oxygen atoms, regardless of the plasma species. That is, for DLC samples **b**, **c**, and **f**, oxygen and nitrogen atoms were observed, even though those DLC surfaces were not treated with oxygen and/or ammonia plasma. Similarly, increases in the concentration of oxygen and nitrogen atoms by plasma treatments were observed for DLC deposited on a glass substrate (Table 3). These results are caused by the reactions with oxygen or nitrogen in the air via dangling bonds after the deposition or the plasma treatments. Consequently, it is difficult to determine the contribution ratio of the ammonia plasma and oxygen plasma to the surface chemical composition with accuracy. From the narrow-scan of XPS for C1s, we determined the chemical species (functional groups) composing the plasma-treated DLC surfaces. The C1s spectrum of DLC sample **h** was shown in Fig. 2 as representative. The C1s peak was decomposed into three peaks at 284.9, 287.9, and 289.1 eV, and they were assigned to  $\text{-C-H/-C-C/-C=C}$ ,  $\text{-C-O}$  and  $\text{-COOH}$ , respectively. In reality, the 'C-O' peak involves carbon nitride ( $\text{-C-N}$ ), in addition to the carbon atoms of alcohol ( $\text{C-OH}$ ) and ether ( $\text{C-O-C}$ ), so we did not carry out further investigation [13,14]. Similarly, from the narrow-scan peak of N1s, it is difficult to assign amino nitrogen and carbon nitride nitrogen, so we did not analyze the narrow-scan of N1s. Thus, the functional groups introduced by the

**Table 2**  
Surface chemical structure of DLC deposited on SUS 316L.

Sample	XPS analysis (atom%)					
	Elements <sup>a</sup> comprising DLC				Carboxyl carbon <sup>b</sup>	C-O-carbon <sup>c</sup>
	C	N	O	Si		
<b>a</b>	82.35	0.31	16.21	0.33	3.85	12.82
<b>b</b>	82.19	1.62	17.81	0	3.71	13.00
<b>c</b>	76.42	1.30	20.43	1.23	2.25	21.19
<b>d</b>	74.40	1.61	22.87	0	3.20	19.07
<b>e</b>	74.06	2.74	23.20	0	3.32	23.58
<b>f</b>	77.69	2.74	18.41	1.16	2.09	17.14
<b>g</b>	74.22	10.08	14.29	1.42	3.03	21.36
<b>h</b>	74.35	4.44	18.72	2.49	3.20	22.69
DLC	83.42	1.98	10.77	3.31	0	10.77

<sup>a</sup> Determined from wide-scan spectra.

<sup>b</sup> Determined by deconvolution of C1s peak at 289.1 eV (narrow-scan).

<sup>c</sup> Carbon bonded to oxygen and nitrogen with single bond; amount was determined by deconvolution of C1s peak at 287.9 eV (narrow-scan).

**Table 3**  
Surface chemical structure of DLC deposited on glass plate.

Sample	XPS analysis (atom%)						Zeta potential (mV)
	Elements <sup>a</sup> comprising DLC				Carboxyl carbon <sup>b</sup>	C–O–carbon <sup>c</sup>	
	C	N	O	Si			
a <sub>gla</sub>	80.02	4.06	15.32	0.35	3.79	7.74	–67.1
f <sub>gla</sub>	79.20	3.76	16.71	0.2	3.38	9.96	–32.1
g <sub>gla</sub>	75.21	12.23	12.38	0.18	3.60	23.90	2.0
h <sub>gla</sub>	75.40	9.11	15.00	0	2.92	9.16	–7.6
DLC <sub>gla</sub>	84.75	2.30	11.92	0	2.60	6.70	–26.4

The condition of plasma treatment is the same as for the DLC in Table 1.

- <sup>a</sup> Determined from wide-scan spectra.
- <sup>b</sup> Determined by deconvolution of C1s peak at 289.1 eV (narrow-scan).
- <sup>c</sup> Carbon bonded to oxygen and nitrogen with single bond; amount was determined by deconvolution of C1s peak at 287.9 eV (narrow-scan).

ammonia plasma treatment cannot be clarified from the result of XPS, which does not deny the presence of –NO, –NO<sub>2</sub>, and –CNO groups. However, the zeta potential described below suggests that the species introduced is a group that can change the electrical state of the surface (e.g., amino group, etc.). On the other hand, it is known that the peak at 289.1 eV is due to a carboxyl (COOH) carbon, and that any carbon bonding to a nitrogen atom does not show a peak at this bond energy. Consequently, it is obvious from the XPS results that the plasma-treated DLC has a COOH group at the surface, regardless of the plasma species.

### 3.2. Physicochemical property of surface

Plotting the contact angle against the concentration of COOH carbon on the DLC surfaces gave Fig. 3. The figure shows that the contact angle behavior of the three DLC groups is classified into two types. The contact angles for “groups A and C DLC” are on the same curve and decreased gradually from 70° to 30° with an increase in the COOH carbon concentration from 0 to 4 atom%, indicating that the plasma species had little effect on the contact angle. In the case of “group B DLC” (treated with acetylene-based plasma), the contact angle decreased a great deal, with a small increase in the COOH carbon

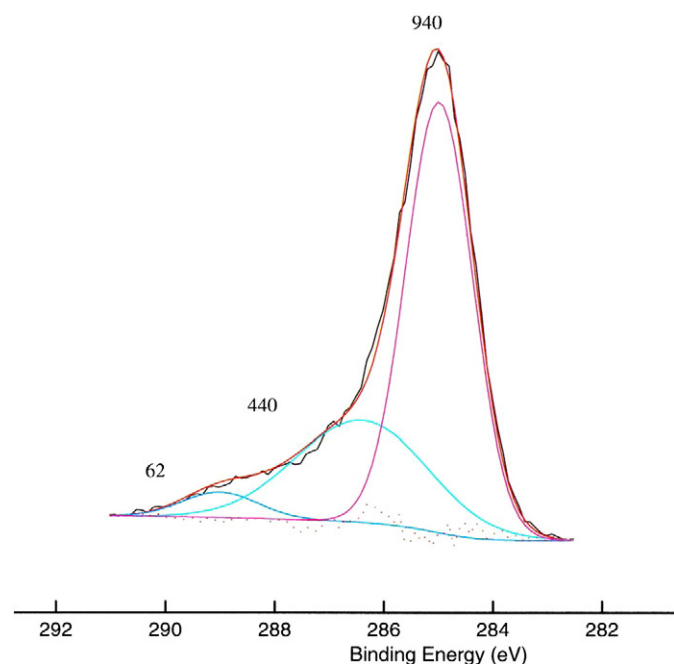


**Fig. 2.** Representative XPS C1s spectrum of plasma-treated DLC surface. Sample: DLC treated with ammonia and oxygen plasmas (sample: h) deconvolution of C1s peak: CH, C–C at 284.9 eV, C–O at 287.9 eV, COOH at 289.1 eV.

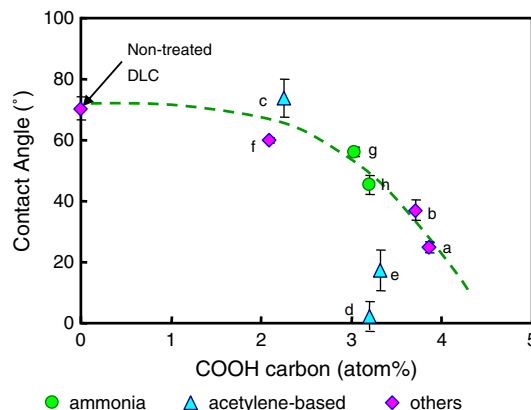


**Fig. 3.** Dependence of contact angle on concentration of carboxyl carbon on DLC surface. ● ammonia: DLC treated with ammonia plasma, ▲ acetylene-based: DLC treated with acetylene-based plasma and ◆ others: DLC treated with Ar or O<sub>2</sub> plasma, and non-treated DLC. n = 5, mean ± SD (standard deviation).

atoms from 2.25 to 3.32 atom%. These results indicate that the contact angle is strongly affected by a small amount of COOH and that the decrease in the contact angle depends not only on the amount of COOH at the surface but also on other factors. One of the factors may be oxygen-based functional groups, such as a hydroxyl group. The existence of such a group is suggested by the C1s narrow-scan of XPS and the estimated concentration is shown in Table 2. Again, from these results it is concluded that the exposure to plasma brings about the formation of a carboxyl group and a hydroxyl group on the DLC surface, resulting in an increase in hydrophilicity. However, the predominant factor for the contact angle is not clear. The combination of these functional groups may lead to the observed result.

The effect of ammonia plasma treatment on the surface property of DLC was investigated in terms of zeta potential, by using DLC deposited on a glass substrate, where the condition of the plasma treatment was the same as for the DLC samples prepared under the condition in Table 1. The relationship between the zeta potential of the DLC surface and the concentrations of COOH carbon atoms and nitrogen atoms is shown in Table 3. When argon plasma-treated DLC, f<sub>gla</sub>, was compared with non-treated DLC, it was clearly found that the treatment increased the concentration of COOH carbon from 2.6 to 3.4 atom%, resulting in the drop of the zeta potential to –32 mV. On the other hand, the treatment with ammonia plasma caused a significant increase in the concentration of nitrogen atoms at the DLC surfaces, from 2.3 to 9.1–12.2 atom% and raised the zeta potential from –32.1 to –7.6 to +2.0 mV, even though the carboxyl carbon content was high enough (2.9–3.6 atom%). From the fact that the zeta potential is affected by an ionic functional group at a material surface, it is reasonable to consider that these drastic changes in zeta potential are caused by the ionic groups at the DLC surface. Consequently, it is summarized that some of the nitrogen atoms introduced by the ammonia plasma have a cationic property. However, in this work, we could not determine the type of functional group expressing the cationic property nor its real concentration.

### 3.3. Blood compatibility of DLC

The platelet compatibility of DLC was compared with that of the control materials from the viewpoint of platelet adhesion and the results were shown in Figs. 4–6. Fig. 4 (the adhesion numbers on the sample surfaces) shows that the plasma-treated DLC exhibits lower platelet adhesion than those on PET, SUS and plasma-non-treated DLC. In addition, this result shows that the types of plasma species have little effect on the adhesion number. It is well known that morphology of adherent platelets on a sample surface gives important

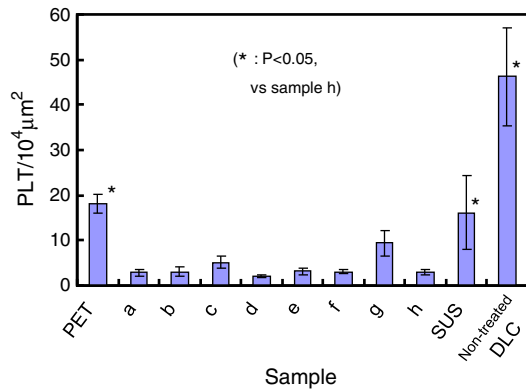


**Fig. 4.** Comparison of DLC with common biomaterials in terms of platelet adhesion. Label in the y-axis: the number of adherent platelets on the surface, n=5, mean ± SE (standard error).

information about the activation level of platelets [15]. The activation of adherent platelets on the DLC was investigated from the viewpoint of platelet morphology shown in Fig. 5, where representative images are shown. In the images, plasma-treated DLC samples are **a**, **c**, and **h** as representatives of groups A, B, and C listed in Table 1, respectively, and the control materials are PET, SUS, and non-treated DLC. In the cases of the plasma-treated DLC, the platelets show that pseudopod form and the spread form are not found. The morphological change of the platelets is on the same level, regardless of the plasma species. On the other hand, in the case of PET, most of the adherent platelets are significantly spread, and it is hard to observe pseudopod form platelets. On non-treated DLC and SUS surfaces the adherent platelets exhibit stellate or pseudopod form. From these results it is concluded that the activation of adherent platelets on surfaces treated with gas plasmas is weaker than that on common materials (PET and SUS). The morphological changes of adherent

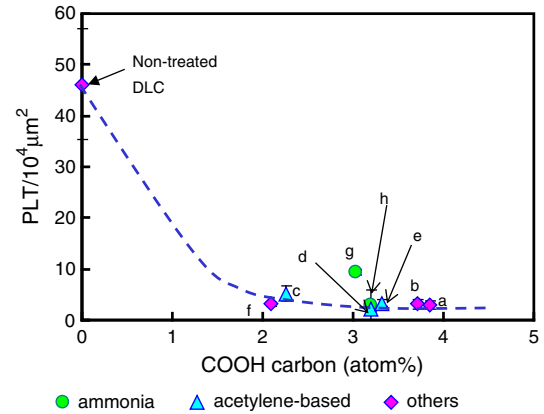


**Fig. 6.** Relationship between concentration of carboxyl carbon on DLC surfaces and adherent platelet number. ● ammonia: DLC treated with ammonia plasma, ▲ acetylene-based: DLC treated with acetylene-based plasma and ◆ others: DLC treated with Ar or O<sub>2</sub> plasma, and non-treated DLC, n=5, mean ± SE (standard error).

platelets and the number of adherent platelets indicate that the compatibility of the surface is in the following order: plasma-treated DLC > SUS > non-treated DLC ≥ PET.

It is well known that platelets easily adhere to a hydrophobic surface compared with hydrophilic ones. Thus, the platelet adhesion property of the DLCs was investigated from the viewpoint of the hydrophilicity/hydrophobicity, or the contact angle. From Figs. 3 and 4, DLC samples **c** and **f** show the lower platelet adhesion even though the contact angles are high and close to that of non-plasma-treated DLC, ca.70°. The number of adhesions of non-treated DLC is significantly larger. These facts observed in the plasma-treated DLC cannot be explained only by hydrophilicity/hydrophobicity and suggest a strong contribution of other factors of the surface properties to the platelet adhesion. Therefore, as for the plasma-treated DLC, the

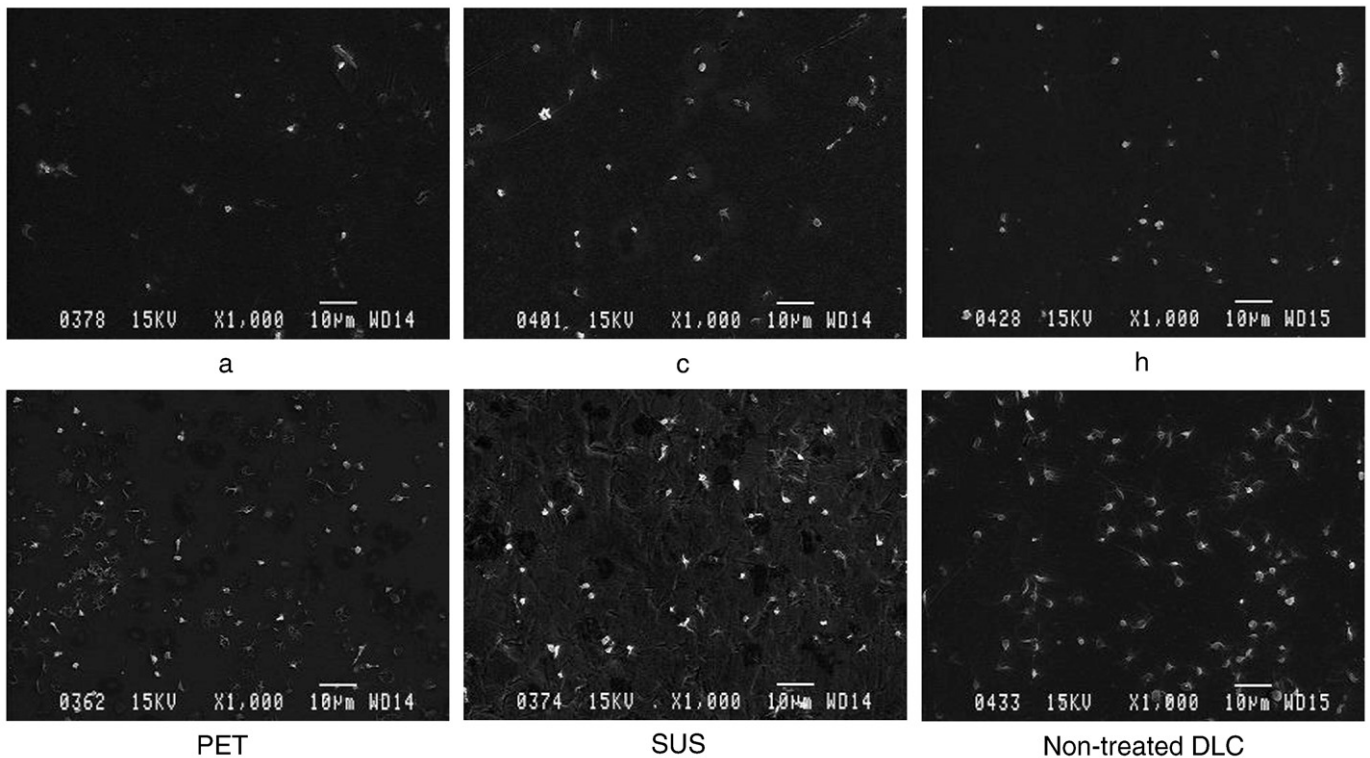


**Fig. 5.** Representative SEM images of adherent platelets on DLC and common biomaterials.

effect of surface chemical structure on the platelet adhesion was investigated. Plotting the number of adherent platelets against the concentration of COOH carbon (Fig. 6) indicates the following. As for DLC treated with gas plasma, the platelet adhesion is at a good level regardless of the concentration of COOH carbon. This can be explained by the knowledge that the cell tends not to adhere to an anionic surface but easily adheres to a cationic surface because of the anionic charge on the cell surface [16]. On the other hand, as for plasma-non-treated DLC, significant platelet adhesion was observed. As mentioned earlier, non-treated DLC has no anionic group or carboxyl group, resulting in a highly hydrophobic surface (Fig. 3). This surface property causes poor compatibility.

The compatibility of plasma-treated DLC with the coagulation system was investigated in terms of generation of TAT. The amount of TAT corresponds to the amount of thrombin generated by the contacting blood, because the thrombin generated is immediately inactivated by antithrombin-III, resulting in the formation of thrombin-antithrombin III complex [17]. The activation of the coagulation system by biomaterial is not fully understood in terms of physicochemical surface properties. It is said that the factors affecting the activation are electrical surface charge, hydrophobicity/hydrophilicity, chemical functional group, roughness, and so on. First, a comparison of TAT generation by a DLC surface with that by common biomaterials is described. The results are shown in Fig. 7. As for the control materials, PET shows low TAT generation, suggesting good compatibility, and SUS generated a significant amount of TAT, meaning poor compatibility. On the other hand, in the case of plasma-treated DLC, the activation level of the coagulation system depends on the surfaces and that the concentration of TAT varies in the range of from 600 pM to 6500 pM. From this result, one can classify DLC into two groups by the capability to activate the coagulation system; one has high potency and the other has low. The potency of the former group is comparable to SUS and has proven to have very poor compatibility in terms of the generation of TAT. On the other hand, the potency of the latter group is on the same level as PET, relatively good compatibility.

Next, from the viewpoint of hydrophilicity/hydrophobicity the TAT generation is discussed. From Figs. 3 and 7, TAT generation seems to be depressed when the contact angle of the DLC surface is over 40° (samples **c**, **f**, **g**, and **h**), however, there is no clear difference between sample **b** and sample **h** in contact angle in spite of their significant difference in TAT generation. This means that TAT generation is not explained by the contact angle. Thus, it is concluded that the contribution of hydrophilicity/hydrophobicity to TAT generation is small, and that there are other dominant factors which activate the coagulation system. On the basis of these results, the TAT generation by the DLC was described from the surface chemical structure of DLC.

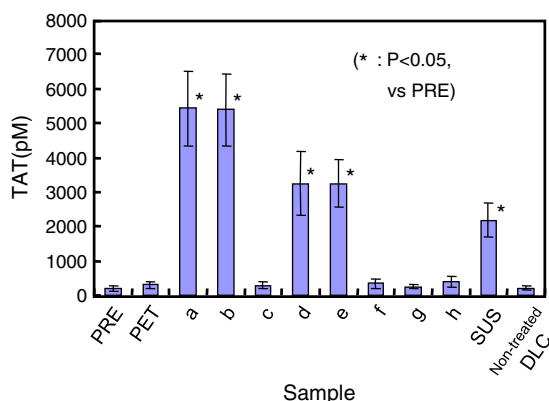


Fig. 7. Comparison of DLC with common biomaterials in terms of generation of TAT. Label in the y-axis: the concentration of TAT (picomol/liter),  $n=6$ , mean  $\pm$  SE (standard error), PRE: the value before contact with a sample.

The DLC with poor compatibility tends to have a high COOH concentration, while the DLC with better compatibility seems to have a lower COOH concentration. Plotting the TAT concentration against the concentration of COOH carbon (Fig. 8) shows that the concentration increases from 600 to 6500 pM with an increase in the amount of COOH carbon from 2 to 4 atom%, and in regions of less than 2 atom% of carbon, the level of TAT is kept low (ca. 600 pM). However, DLC **g** and **h**, treated with ammonia plasma, show lower activation potential to the coagulation system though their surfaces have more than 3 atom% of COOH carbon.

It is well known that the coagulation system is activated via the intrinsic pathway comprising contact activation or the extrinsic pathway where tissue factor plays a key role [18]. In the contact activation, high molecular weight kininogen, prekallikrein, and factor IIX are involved and the activations of these molecules require a negatively charged surface such as zeolite or glass in vitro. Factor IIX is activated by adsorption onto the surface and FIIXa converts prekallikrein to kallikrein. The activation of the intrinsic pathway proceeds in cascade reactions, resulting in thrombin generation and clotting. Thus, when the fact that the plasma-treated DLC has a carboxyl group is considered, the measurement of the kallikrein-like activity of the blood plasma gives important information. That is, from the level of the activity, it is suggested which pathway is dominant in generation of TAT by DLC. The results of kallikrein-like activity are shown in Fig. 9, where absorbance at 405 nm is plotted, and an increase in absorbance corresponds to a rise in kallikrein activity. Fig. 9 expresses the results of the activation of the contact phase in the coagulation system by the various surfaces. From this figure and Fig. 7, DLC that generates TAT significantly seems to activate the contact phase. Fig. 10 shows that absorbance increases with an increase in the concentration of COOH carbon, when the concentration is over 2 atom %, except for DLC of **g** and **h** treated with NH<sub>3</sub> plasma. That is, DLC treated with ammonia plasma exhibits low ability to activate the contact phase. In our experiment, we also measured the kallikrein-like activity for a glass plate as a control, and the absorbance was over 0.4. The absorbance observed for DLC with low compatibility is close to the absorbance for a glass plate. The reason for the good compatibility of DLC **g** and **h** can be explained from the result of the surface physicochemical property of DLC deposited on a glass substrate. As shown in Table 3, the ammonia plasma-treated surfaces show very high zeta potential ( $-10\sim 0$  mV) compared to other DLC having a high concentration of COOH (their zeta potential is less than  $-40$  mV). This implies that the COOH group on the surface is neutralized by ammonia plasma. A similar phenomenon occurs in the

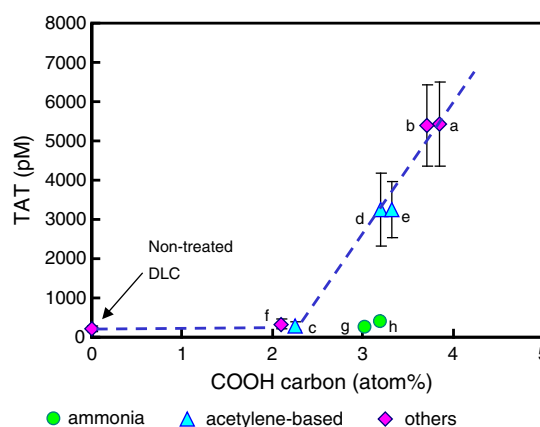
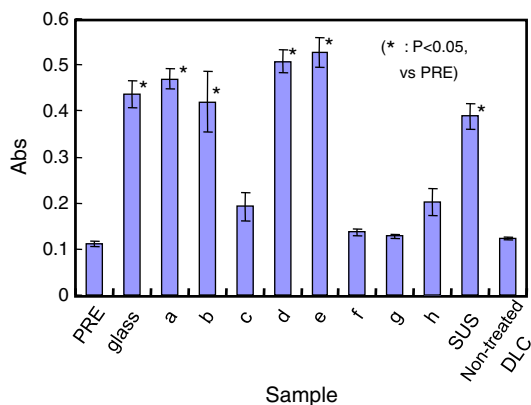


Fig. 8. Relationship between concentration of carboxyl carbon and TAT generation. Label in the y-axis: the concentration of TAT (picomol/liter). ● ammonia: DLC treated with ammonia plasma, ▲ acetylene-based: DLC treated with acetylene-based plasma and ◆ others: DLC treated with Ar or O<sub>2</sub> plasma, and non-treated DLC,  $n=6$ , mean  $\pm$  SE (standard error).



**Fig. 9.** Kallikrein-like activity of blood plasma contacting various surfaces. Label in the y-axis: the absorbance at 405 nm, corresponding to the strength of the activity in plasma. n = 4, mean ± SE (standard error), glass: glass plate, PRE: the value before contact with a sample.

case of the plasma-treated DLC surface on the SUS substrate which was used for the blood compatibility tests. Thus, the neutralized surface results in the low generation of TAT though the surface has a high concentration of the COOH group.

#### 4. Conclusion

DLC surfaces were treated with oxygen, acetylene, and/or ammonia gas plasmas and the blood compatibility of the surfaces was investigated. The treatment with oxygen plasmas reduced the contact angle due to the formation of COOH groups. The treatment with ammonia plasma increased the zeta potential from a negative value to a positive one, suggesting the introduction of a cationic functional group. Thus, cationic and anionic functional groups can be introduced to the DLC surface by using ammonia/oxygen plasma. Good platelet compatibility (low adhesion) was observed for plasma-treated DLC, regardless of the types of gas plasmas, when compared with common biomaterials and non-treated DLC. As for compatibility with the coagulation system, DLC having a high concentration of COOH at the surface showed poor performance, while the treatment with ammonia plasma improved the performance. It was shown that the activation of the coagulation system started via the intrinsic pathway. Consequently, though the presence of amino groups was not detected directly, the treatment of ammonia plasma changed the electrical state of the DLC surface having a COOH group, causing a difference in blood compatibility among the DLCs obtained by various plasma conditions.

#### Acknowledgements

We thank the Technical Service Coordination Office in Tokai University for their technical support in the XPS measurements. We

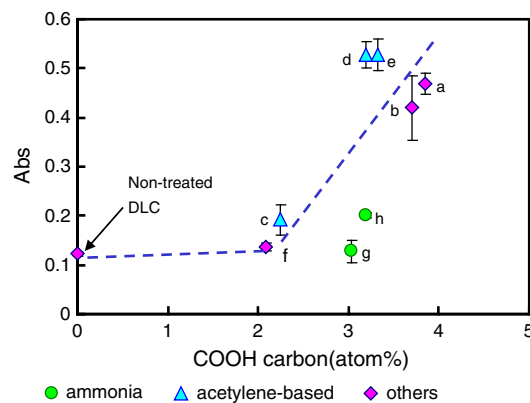


**Fig. 10.** Dependence of kallikrein-like activity on concentration of carboxyl carbon on DLC surfaces. ● ammonia: DLC treated with ammonia plasma, ▲ acetylene-based: DLC treated with acetylene-based plasma and ◆ others: DLC treated with Ar or O<sub>2</sub> plasma, and non-treated DLC. n = 4, mean ± SE (standard error).

also thank Education and Research Support Center, Tokai University for their technical support in the SEM observation.

#### References

- [1] F.Z. Cui, D.J. Li, *Surf. Coat. Technol.* 131 (2000) 481.
- [2] T.I.T. Okpalugo, A.A. Ogwu, P.D. Maguire, J.A.D. McLaughlin, D.G. Hirst, *Diamond Relat. Mater.* 13 (2004) 1088.
- [3] S.C.H. Kwok, P.C.T. Ha, D.R. McKenzie, M.M.M. Bilek, P.K. Chu, *Diamond Relat. Mater.* 15 (2006) 893.
- [4] T. Hasebe, A. Shimada, T. Suzuki, Y. Matsuoka, T. Saito, S. Yohena, A. Kamijo, N. Shiraga, M. Higuchi, K. Kimura, H. Yoshimura, S. Kuribayashi, *J. Biomed. Mater. Res. A* 76A (2006) 86.
- [5] T. Hasebe, S. Yohena, A. Kamijo, Y. Okazaki, A. Hotta, K. Takahashi, T. Suzuki, *J. Biomed. Mater. Res. A* 83A (2007) 1192.
- [6] H. Kitano, T. Mori, Y. Takeuchi, S. Tada, M. Genmei-Ide, Y. Yokoyama, M. Tanaka, *Macromol. Biosci.* 5 (2005) 314.
- [7] Y.C. Chung, Y.H. Chiu, Y.W. Wu, Y.T. Tao, *Biomaterials* 26 (2005) 2313.
- [8] W.H. Chuang, J.C. Lin, *J. Biomed. Mater. Res. A* 82A (2007) 820.
- [9] T. Nakatani, K. Okamoto, Y. Nitta, A. Mochizuki, H. Hoshi, A. Homma, *J. Photopolym. Sci. Technol.* 21 (2008) 225.
- [10] Y. Nitta, K. Okamoto, T. Nakatani, H. Hoshi, A. Homma, E. Tatsumi, Y. Taenaka, *Diamond Relat. Mater.* 17 (2008) 1972.
- [11] M. Tanaka, A. Mochizuki, N. Ishii, T. Motomura, T. Hatakeyama, *Biomacromolecules* 3 (2002) 36.
- [12] M. Tanaka, T. Motomura, M. Kawada, T. Anzai, Y. Kasori, T. Shiroya, K. Shimura, M. Onishi, A. Mochizuki, *Biomaterials* 21 (2000) 1471.
- [13] G. Jama, A. Alkhwam, A.-S. Loir, P. Goudmand, O. Dessaux, L. Gengembre, J. Grimblot, *Surf. Interface Anal.* 31 (2001) 815.
- [14] H. Cachet, C. Debienne-Chouvy, C. Deslouis, A. Lagrini, V. Vivier, *Surf. Interface Anal.* 38 (2006) 815.
- [15] M. Fedel, A. Motta, D. Maniglio, C. Magliaresi, *J. Biomed. Mater. Res. B* 90B (2009) 338.
- [16] R.D. Falb, R.I. Leininger, J.P. Crowley, *Ann. NY Acad. Sci.* 283 (1977) 396.
- [17] J.H. Griffin, in: M.A. Lichtman, E. Beutler, T.J. Kipps, U. Seligsohn, K. Kaushansky, J.T. Prchal (Eds.), *Williams Hematology*, 7th ed., McGraw-Hill, New York, 2006, p. 1703.
- [18] M.B. Gorbet, M.V. Sefton, *Biomaterials* 22 (2004) 5681.

# 参考論文

- (1) Surface Analysis of Carbon–Hydrogen Bonds in Diamondlike Carbon Films by X–ray Photoelectron Spectroscopy  
Susumu Takabayashi, Keishi Okamoto, Tatsuyuki Nakatani, Hiroyuki Sakaue, Takayuki Takahagi,  
Japanese Journal of Applied Physics, 48 (2009) 092304.
  
- (2) Development of surface–functionalized drug–eluting stent with diamond–like carbon nanocoated by using PECVD method  
Keishi Okamoto, Tatsuyuki Nakatani, Syuzo Yamashita, Susumu Takabayashi, Takayuki Takahagi,  
Surface and Coatings Technology, 202 (2008) 5750–5752.
  
- (3) Qualitative analysis of a diamondlike carbon film by angle-resolved x-ray photoelectron spectroscopy  
Susumu Takabayashi, Kunihiko Motomitsu, Takayuki Takahagi, Akira Terayama, Keishi Okamoto, and Tatsuyuki Nakatani,  
Journal of Applied Physics, 101 (2007) 103542.
  
- (4) Chemical Structural Analysis of Diamondlike Carbon Films with Different Electrical Resistivities by X-ray Photoelectron Spectroscopy  
Susumu Takabayashi, Keishi Okamoto, Kenya Shimada, Kunihiko Motomitsu, Hiroaki Motoyama, Tatsuyuki Nakatani, Hiroyuki Sakaue, Hitoshi Suzuki, and Takayuki Takahagi,  
Japanese Journal of Applied Physics, 47 (2008) 3376–3379.

# Surface Analysis of Carbon–Hydrogen Bonds in Diamondlike Carbon Films by X-ray Photoelectron Spectroscopy

Susumu Takabayashi<sup>1\*</sup>, Keishi Okamoto<sup>1,2</sup>, Tatsuyuki Nakatani<sup>2</sup>, Hiroyuki Sakaue<sup>1</sup>, and Takayuki Takahagi<sup>1</sup>

<sup>1</sup>Department of Quantum Matter, Graduate School of Advanced Sciences of Matter, Hiroshima University, 1-3-1 Kagamiyama, Higashihiroshima, Hiroshima 739-8530, Japan

<sup>2</sup>Toyo Advanced Technologies Co., Ltd., 5-3-38 Ujina-Higashi, Minami-ku, Hiroshima 734-8501, Japan

Received May 14, 2009; accepted June 26, 2009; published online September 24, 2009

X-ray photoelectron spectroscopy (XPS) was used to analyze the carbon–hydrogen bonds near the surfaces of two types of diamondlike carbon (DLC) film with different hydrogen distribution, which were prepared by the unbalanced magnetron sputtering (UBMS) and ionized deposition (ID) methods, respectively. Elastic recoil detection (ERD) analysis revealed that, in the UBMS films, hydrogen is distributed homogeneously along the depth axis, while in the ID film it is distributed inhomogeneously and concentrated at the surface. The C 1s spectra of the UBMS films with different hydrogen concentrations suggested that the spectra are decomposed into four components, corresponding to the carbon–hydrogen and carbon–carbon bonds of the  $sp^2$  and  $sp^3$  carbons. A correlation between the hydrogen concentrations obtained by the XPS and ERD analyses was observed. The C 1s spectrum of the ID film depended on the emission angle, suggesting that the carbon–hydrogen bonds concentrate at the surface. This result agreed with the ERD result. Both correlations suggested that XPS can analyze hydrogen as an atom bound to a carbon atom and be a comprehensive surface analytical tool for DLC films. © 2009 The Japan Society of Applied Physics

DOI: 10.1143/JJAP.48.092304

## 1. Introduction

Diamondlike carbon (DLC) is an amorphous carbonaceous material composed of  $sp^2$  carbon,  $sp^3$  carbon, and hydrogen.<sup>1,2</sup> Its unique characteristics such as surface lubrication, flatness, and hardness, have been shown to be very useful, and the films have been applied as surface coating for industrial products,<sup>3</sup> and more recently, for medical tools.<sup>4–6</sup> The composition ratio of  $sp^2/sp^3$  carbons is often used for the characterization, while the contribution of hydrogen is also important for the electrical resistivity, optical gap, and internal compressive stress. Thus a comprehensive analysis of the interactions among the three elements is necessary. Fourier transform infrared spectroscopy (FT-IR) has been used to analyze the carbon–hydrogen bonds of DLC films.<sup>7–13</sup> FT-IR is, however, sensitive to the bulk properties rather than to the surface properties. For the further development of the above surface applications, it is necessary to elucidate the depth profile of the three elements near the surface, and relate it with the physical properties of DLC.

We previously reported<sup>14</sup> the qualitative analysis of a DLC film by angle-resolved X-ray photoelectron spectroscopy (AR-XPS). The binding energy of the C 1s spectrum was found to shift by varying the emission angle, suggesting that the DLC film has two types of chemical component, namely, surface and bulk components: the former is located at a higher binding energy and the latter at a lower. DLC has two types of carbon:  $sp^2$  and  $sp^3$  carbons. Thus, it was expected that the DLC film contains at least “ $2 \times 2 = 4$ ” unique chemical bonds. As a result, the C 1s spectra of the DLC film are decomposed into four chemical components, corresponding to the surface and bulk components of the  $sp^2$  and  $sp^3$  carbons: bulk  $sp^3$ , bulk  $sp^2$ , surface  $sp^2$ , and surface  $sp^3$  carbons.

In order to assign the surface and bulk components to the corresponding chemical structures, further XPS analysis of DLC films with different electrical resistivities has been

undertaken and distinctive features of the C 1s spectra have been reported.<sup>15,16</sup> The C 1s spectra are varied owing to the asymmetry and position of the constituent peaks depending on electrical resistivity. Mansano *et al.* reported<sup>17,18</sup> that the electrical resistivity of DLC films can be varied experimentally by controlling the concentration of incorporated hydrogen. The amount of the surface component assigned above increased with that of methane in the plasma as the hydrogen source, while that of the bulk decreased. These results suggested that the surface component is related to the carbon with carbon–hydrogen bonds and the bulk component to the carbon with carbon–carbon bonds. Hence, we have assumed<sup>16,19</sup> four chemical components of the C 1s spectra of DLC films:  $sp^3$  carbon with carbon–carbon bonds (C–C  $sp^3$  carbon),  $sp^2$  carbon with carbon–carbon bonds (C–C  $sp^2$  carbon),  $sp^2$  carbon with carbon–hydrogen bonds (C–H  $sp^2$  carbon), and  $sp^3$  carbon with carbon–hydrogen bonds (C–H  $sp^3$  carbon). We numerically analyzed the C 1s spectra taking into account previous reports on highly oriented pyrolytic graphite (HOPG) and crystalline diamond. The C 1s spectra of HOPG were decomposed into the surface and bulk components.<sup>20,21</sup> For diamond, a new peak at a higher binding energy than that of bulk diamond emerged in the C 1s spectra by hydrogen plasma treatment and was assigned to multivalent hydrocarbon species ( $CH_x$ ), while another peak emerged at a lower binding energy by annealing in an ultrahigh vacuum or  $Ar^+$ -bombardment.<sup>22–26</sup> The  $Ar^+$ -irradiation treatment of a HOPG film demonstrated that two new chemical components emerged at 283.9 and 285.3 eV, which was located on either side of the main peak of HOPG.<sup>27</sup> These assignments have succeeded in explaining the thermal emission of hydrogen from a DLC film in an ultrahigh vacuum investigated by thermal desorption spectroscopy (TDS).<sup>28</sup>

However, in principle, it is impossible for XPS to detect hydrogen directly.<sup>29</sup> In order to confirm our XPS analysis, another technique, which directly observes hydrogen, is necessary. Elastic recoil detection (ERD) is such a technique.<sup>30,31</sup> Its latest depth resolution is 0.28 nm,<sup>32,33</sup> which is comparable to the interatomic distance and the depth

\*E-mail address: stak@hiroshima-u.ac.jp



resolution of XPS.<sup>34,35</sup> In this paper, the potential of XPS as a comprehensive surface analytical tool for DLC films is discussed by comparing XPS and ERD analyses.

### 2. Experimental Procedure

Two types of DLC film were prepared as follows. Three films of the first type were prepared on Si wafers by the unbalanced magnetron sputtering (UBMS) method,<sup>15,16</sup> and were designated as “UBMS-DLC” films. The target was graphite fixed in the chamber, and the CH<sub>4</sub>/Ar gas ratio in the chamber was varied to control the concentration of hydrogen incorporated, with values of 0, 0.06, and 0.12.<sup>17,18</sup> One film of the second type was prepared on a Si wafer by the ionized deposition (ID) method,<sup>14,28</sup> and was designated as an “ID-DLC” film. The carbon source was 30 sccm of benzene gas. The DC bias voltage applied to the substrate was -2 kV, and the temperature was 180 °C.

ERD measurements were conducted with a KOBERCO HRBS500 system. A 240-keV N<sub>2</sub><sup>+</sup> beam with a current of 2 nA irradiated the DLC films at 70° with respect to the surface normal. Hydrogen ions recoiled at 30° in the forward direction were observed.

AR-XPS measurements were conducted on a surface area with a diameter of 0.8 mm using an ULVAC-PHI PHI1600 system. The system had an unmonochromated Al K $\alpha$  line (1486.6 eV) with a voltage of 15 kV and a power of 400 W. All measurements were performed at room temperature and a pressure below 4.0 × 10<sup>-9</sup> Torr. The emission angle was varied as 10, 30, 45, 60, and 75° with respect to the surface normal. The Shirley method was used to subtract the background lines.<sup>36,37</sup> The energy resolution of the spectrometer was estimated by analyzing the Fermi edge spectrum of a Au plate using the Fermi–Dirac distribution function convoluted with a Gaussian function. The full-width at half maximum (FWHM) of the Gaussian function was 0.6 eV.

Before each AR-XPS measurement, a few microliters of a dilute aqueous solution of Au nanocolloids were dropped on a local surface area of the DLC film to calibrate the binding energy.<sup>15,19</sup> The droplet was gradually dried *in vacuo*, leaving Au nanocolloids adsorbed on the surface as a calibrant. The C 1s spectrum of the DLC film was observed at another surface area without the Au nanocolloids. The observed C 1s binding energy was calibrated by tuning the Au 4f<sub>7/2</sub> binding energy of the Au nanocolloids to 84.0 eV. The charge difference between the areas with and without Au nanocolloids was also calibrated by comparing the difference in the C 1s binding energy between the two areas.

### 3. Results and Discussion

Figure 1 shows the (a) ERD spectra and (b) hydrogen depth profiles of the UBMS-DLC films prepared with different CH<sub>4</sub>/Ar gas ratios in the plasma during the preparation process. The results demonstrate that a higher CH<sub>4</sub>/Ar gas ratio results in DLC films with a higher hydrogen concentration. Hydrogen atoms in every film are homogeneously distributed along the depth axis except for a slight increase in the concentration at the surface.

Figure 2 shows the C 1s spectra of the UBMS-DLC films and a freshly-cleaved HOPG film, which is composed of sp<sup>2</sup> carbon only, with the fitting curves corresponding to the

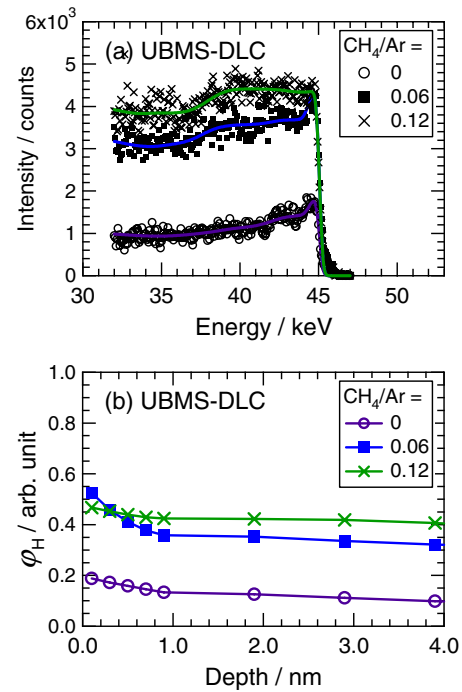


**Fig. 1.** (Color online) (a) ERD spectra and (b) hydrogen depth profiles of the UBMS-DLC films prepared with different CH<sub>4</sub>/Ar gas ratios in the plasma during the preparation process: ○, 0, ■, 0.06, and ×, 0.12.

chemical components. The emission angle was fixed at 45°. All the C 1s spectra of the UBMS-DLC films show almost no dependence on the emission angle, and the spectra observed at 45° were almost the same as those observed at the other angles. The spectrum of the HOPG film was decomposed into two chemical components related to sp<sup>2</sup> carbon and a very small C–O component.<sup>20,21</sup> The spectra of the UBMS-DLC films were wider than that of the HOPG film, suggesting that two chemical components related to sp<sup>3</sup> carbon exists at either side of the pair of the sp<sup>2</sup> carbon components, which is similar to the results of the Ar<sup>+</sup>-irradiated HOPG film mentioned above.<sup>27</sup> Each component is represented by the Doniach–Šunjić (DŠ) function convoluted with a Gaussian function as<sup>14,16,19,38</sup>

$$\begin{aligned}
 & (D\check{S} * G)(E_B) \\
 &= \int_{-\infty}^{+\infty} D\check{S}(E')G(E_B - E') dE' \\
 &= I\Gamma(1 - \alpha) \frac{2}{\Gamma_G} \sqrt{\frac{\ln 2}{\pi}} \\
 & \times \int_{-\infty}^{+\infty} \frac{\cos \left[ \frac{\pi\alpha}{2} + (1 - \alpha) \tan^{-1} \left( \frac{E_0 - E'}{\Gamma_L/2} \right) \right]}{\left[ (E_0 - E')^2 + \left( \frac{\Gamma_L}{2} \right)^2 \right]^{(1-\alpha)/2}} \\
 & \times \exp \left\{ -4 \ln 2 \left[ \frac{E_0 - (E_B - E')}{\Gamma_G} \right]^2 \right\} dE', \quad (1)
 \end{aligned}$$

where the fitting parameters are the binding energy at  $\alpha = 0$  ( $E_0$ ), spectral intensity ( $I$ ), FWHMs of the Lorentzian and Gaussian functions ( $\Gamma_L$  and  $\Gamma_G$ ), and singularity index ( $\alpha$ ). The magnitude of  $\Gamma_L$  represents lifetime broadening, which

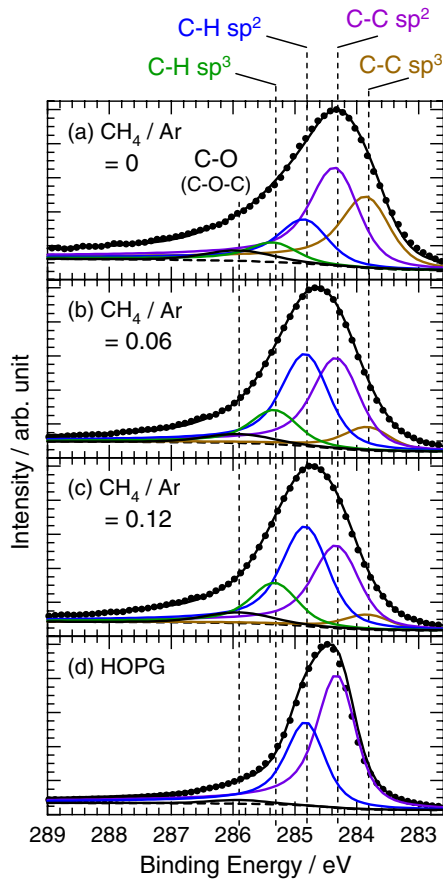


**Fig. 2.** (Color online) C 1s spectra of (a)–(c) the UBMS-DLC films and (d) a freshly-cleaved HOPG film where the fitting curves of the chemical components are represented by the proposed XPS analysis<sup>14,16</sup> using the DS function convoluted with a Gaussian function. The UBMS-DLC films were prepared with the following CH<sub>4</sub>/Ar gas ratios in the plasma: (a) 0, (b) 0.06, and (c) 0.12. The emission angle is 45°. The peak assignments are as follows: C–C sp<sup>3</sup> carbon (283.8 eV), C–C sp<sup>2</sup> carbon (284.3 eV), C–H sp<sup>2</sup> carbon (284.8 eV), C–H sp<sup>3</sup> carbon (285.3 eV), and C–O (or C–O–C) bonds (285.9 eV).

is mainly determined by the Auger transition in the case of C 1s.<sup>39,40</sup> Since DLC is an amorphous compound, we assumed that the Auger transition probability, which is in proportion to the magnitude of the interaction of the valence electrons, is effectively averaged, giving a common  $\Gamma_L$  for these peaks. The magnitude of  $\Gamma_G$  is mostly affected by the amorphousness due to the random variations of the conformations, and is also averaged.<sup>28</sup> As for  $\alpha$ , other authors assumed that it has a finite value for sp<sup>2</sup> carbon and is zero for sp<sup>3</sup> carbon because graphite, which is composed of sp<sup>2</sup> carbon only, is a conductor and diamond, which is composed of sp<sup>3</sup> carbon only, is an insulator.<sup>41–43</sup> In DLC or amorphous films, however, it is more reasonable to assume that the chemical structures are not divided into the crystalline graphite and diamond phases. We, therefore, set  $\alpha$ ,  $\Gamma_L$ , and  $\Gamma_G$  at common values for all curves of the carbon–hydrogen and carbon–carbon bonds.<sup>14,16,19,28</sup> The  $\alpha$  values for the carbon–oxygen bonds, which are mainly derived from the surface functional groups and not an element of DLC, are set at zero (reduction to Lorentzian) because the bonds do not contribute to the electronic states around the Fermi level. Moreover, we have experimentally demonstrated that the intensities and positions of the

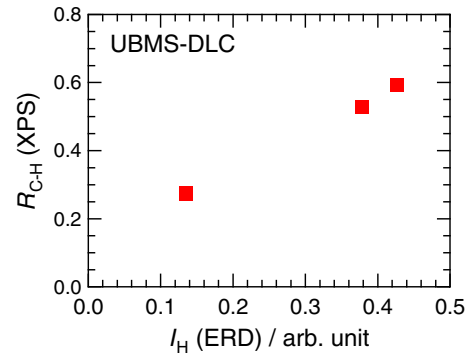


**Fig. 3.** (Color online) Correlation between the hydrogen concentrations obtained by the XPS and ERD analyses of the UBMS-DLC films with a homogeneous hydrogen distribution.

chemical components were almost constant for  $\alpha(\text{sp}^2) : \alpha(\text{sp}^3) = 5 : 5-10 : 0$ , and  $\alpha$  does not affect the quantitative analysis within the range.<sup>14</sup> As a result, the assignments were made as follows: C–C sp<sup>3</sup> carbon (283.8 eV), C–C sp<sup>2</sup> carbon (284.3 eV), C–H sp<sup>2</sup> carbon (284.8 eV), C–H sp<sup>3</sup> carbon (285.3 eV), and C–O (or C–O–C) bonds (285.9 eV).

Generally, XPS photoelectron signals from materials decay exponentially along the depth axis.<sup>29</sup> Thus if XPS can detect hydrogen bound to carbon directly, the total hydrogen intensity  $I_H(\theta)$  is estimated by

$$I_H(\theta) = \int_0^\infty \varphi_H(z) \exp\left(-\frac{z}{\lambda \cos\theta}\right) dz, \quad (2)$$

where  $\varphi_H(z)$  is the hydrogen distribution intensity at the depth  $z$ ,  $\theta$  is the emission angle, and  $\lambda$  is the inelastic mean free path (IMFP). In these experiments,  $\lambda$  is estimated to be 2.0 nm by assuming that the C 1s binding energy is  $\sim 285$  eV and the kinetic energy is  $\sim 1200$  eV.<sup>44</sup> If we apply eq. (2) to the analysis of the hydrogen depth profiles in Fig. 1(b), we can then consider the correlation between hydrogen concentrations obtained by XPS and ERD analyses. Figure 3 shows the correlation of the UBMS-DLC films at the emission angle of 45°. The hydrogen concentration estimated by the XPS curve-fitting analysis is expressed as  $R_{\text{C-H}}$ , which is the area ratio of the C–H components (all hydrogen) to the sum of the C–H and C–C components (all carbon). A correlation is obtained between the XPS and ERD analyses, suggesting that XPS can analyze hydrogen as an atom bound to a carbon atom. As a result, the differences in the features of the C 1s spectra in Fig. 2 arise from the difference in bond formation between carbon and hydrogen.

We subsequently examined whether our proposed XPS analysis is applicable to another type of DLC film. Figures 4(a) and 4(b) show the ERD spectrum and hydrogen depth profile of the ID-DLC film, respectively. In contrast to the result of the UBMS-DLC films, a sharp and strong peak was observed in the ERD spectrum. This result demonstrates that, in the ID-DLC film, hydrogen atoms are inhomogeneously distributed along the depth axis and are more concentrated at the surface.

Figures 5(a) and 5(b) show the C 1s AR-XPS spectra of the ID-DLC film with the fitting curves of the chemical components determined in the same way as in Fig. 2. In

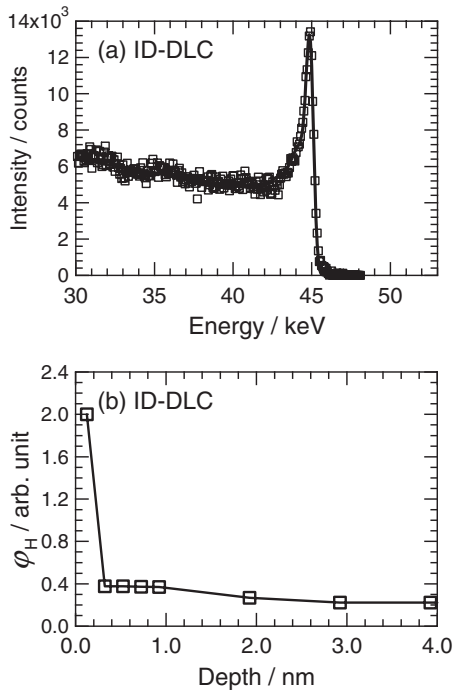


Fig. 4. (a) ERD spectrum and (b) hydrogen depth profile of the ID-DLC film.

contrast to the results of the UBMS-DLC films, the spectra change as a function of the emission angle. We previously reported<sup>14)</sup> that the surface and bulk components of the same ID-DLC film are different and that the chemical components of the C 1s spectrum are bulk sp<sup>3</sup>, bulk sp<sup>2</sup>, surface sp<sup>2</sup>, and surface sp<sup>3</sup> carbons. The above discussion of DLC films with different hydrogen concentrations suggests that the surface component is related to the carbon with carbon–hydrogen bonds and the bulk component to the carbon with carbon–carbon bonds.<sup>16)</sup> Taking these relationships into account, Fig. 5(c) shows the relative intensities of the chemical components as a function of the emission angle. The dashed lines are the theoretical AR-XPS analysis curves calculated by<sup>14,19,45)</sup>

$$\begin{cases} I_S = I_S^0 \left[ 1 - \exp\left(-\frac{d}{\lambda_{S,S} \cos \theta}\right) \right], \\ I_B = I_B^0 \exp\left(-\frac{d}{\lambda_{B,S} \cos \theta}\right), \end{cases} \quad (3)$$

where the fitting parameters are the intensities of the surface and bulk components ( $I_S$  and  $I_B$ ), the standard intensities of the surface and bulk components ( $I_S^0$  and  $I_B^0$ ), the imaginary thickness of the surface atomic layers ( $d$ ), the IMFPs through  $d$  of the surface and bulk components ( $\lambda_{S,S}^0$  and  $\lambda_{B,S}^0$ ), and the emission angle ( $\theta$ ).

Figure 6 shows the correlation between the hydrogen concentrations obtained by the XPS and ERD analyses of the ID-DLC film, as obtained in the same way as in Fig. 3, but with  $\theta$  being varied. The correlation suggests that our XPS analysis can also explain the behavior of the DLC film where hydrogen is distributed inhomogeneously. The present analysis has clarified that the correspondence of the surface (bulk) component to the carbon with carbon–hydrogen (carbon–carbon) bonds in the ID-DLC film is due to the inhomogeneous distribution of hydrogen in the film.

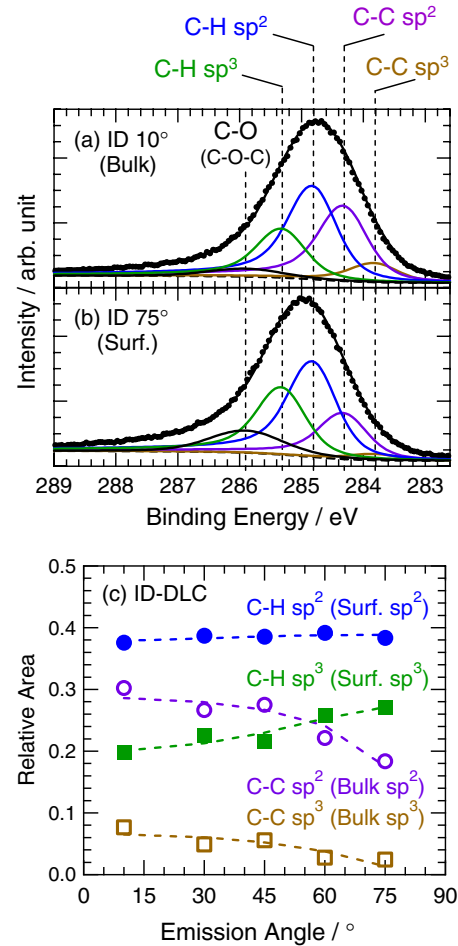


Fig. 5. (Color online) C 1s AR-XPS spectra of the ID-DLC film where the fitting curves of the chemical components are represented by XPS analysis in the same way as in Fig. 2. The emission angles are (a) 10° (for the bulk) and (b) 75° (for the surface). (c) Relative intensities of the chemical components as a function of the emission angle: □ C–C sp<sup>3</sup> (bulk sp<sup>3</sup>) carbon, ○ C–C sp<sup>2</sup> (bulk sp<sup>2</sup>) carbon, ● C–H sp<sup>2</sup> (surface sp<sup>2</sup>) carbon, and ■ C–H sp<sup>3</sup> (surface sp<sup>3</sup>) carbon. The dashed lines are the theoretical curves of the AR-XPS analysis reported previously by using eq. (3).<sup>14,19,45)</sup>

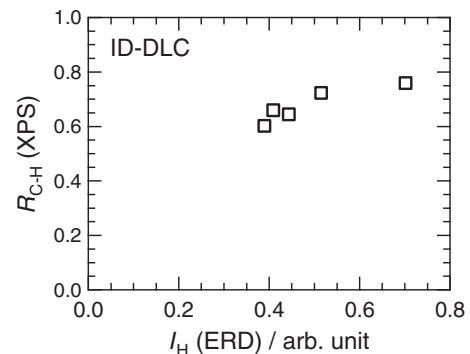
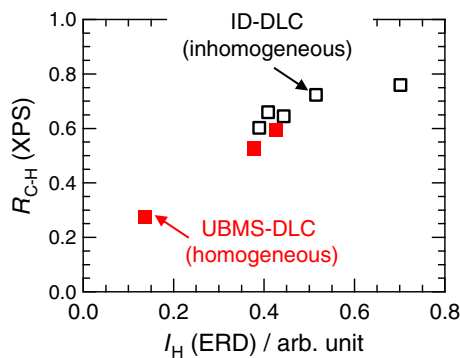


Fig. 6. Correlation between the hydrogen concentrations obtained by the AR-XPS and ERD analyses of the ID-DLC film with an inhomogeneous hydrogen distribution.

Figure 7 shows the correlation between the hydrogen concentrations obtained by the XPS and ERD analyses of DLC films with both the homogeneous and inhomogeneous hydrogen distributions. A continuative correlation is obtained, suggesting that our proposed XPS analysis can



**Fig. 7.** (Color online) Correlation between the hydrogen concentrations obtained by the XPS and ERD analyses of ■ the UBMS-DLC films with a homogeneous hydrogen distribution and □ the ID-DLC film with an inhomogeneous hydrogen distribution.

explain the behaviors of the DLC films where the hydrogen distributions are different each other. However, it should be noted that the present XPS analysis can not distinguish the variation in the coordination number of C–H bonds,  $-\text{CH}$ ,  $-\text{CH}_2$ , and  $-\text{CH}_3$ , which may vary for different types of films.

#### 4. Conclusions

The correlation between the hydrogen concentrations of DLC films obtained by XPS and ERD analyses has been studied with two types of DLC film where hydrogen is distributed homogeneously and inhomogeneously. A continuative correlation is obtained, suggesting that XPS can analyze hydrogen atoms bound to carbon atoms. We have demonstrated that the comprehensive surface analysis of DLC films can be performed by XPS, which contributes to further development of functional surfaces.

#### Acknowledgement

The authors wish to thank Professor Kenya Shimada of Hiroshima Synchrotron Radiation Center, Hiroshima University for valuable advice on XPS analysis.

- 1) S. Aisenberg and R. Chabot: *J. Appl. Phys.* **42** (1971) 2953.
- 2) J. Robertson: *Mater. Sci. Eng. R* **37** (2002) 129.
- 3) T. Nakatani, K. Okamoto, A. Araki, and T. Washimi: *New Diamond Front. Carbon Technol.* **16** (2006) 187.
- 4) T. Saito, T. Hasebe, S. Yohena, Y. Matsuoka, A. Kamijo, K. Takahashi, and T. Suzuki: *Diamond Relat. Mater.* **14** (2005) 1116.
- 5) P. D. Maguire, J. A. McLaughlin, T. I. T. Okpalugo, P. Lemoine, P. Papakonstantinou, E. T. McAdams, M. Needham, A. A. Ogwu, M. Ball, and G. A. Abbas: *Diamond Relat. Mater.* **14** (2005) 1277.
- 6) T. Nakatani, K. Okamoto, I. Omura, and S. Yamashita: *J. Photopolym. Sci. Technol.* **20** (2007) 221.
- 7) A. Grill, V. Patel, and B. S. Meyerson: *J. Electrochem. Soc.* **138** (1991) 2362.
- 8) A. Grill and V. Patel: *Appl. Phys. Lett.* **60** (1992) 2089.
- 9) J. Ristein, R. T. Stief, L. Ley, and W. Beyer: *J. Appl. Phys.* **84** (1998) 3836.
- 10) T. Heitz, B. Drevillon, C. Godet, and J. E. Bouree: *Phys. Rev. B* **58** (1998) 13957.
- 11) M. Shinohara, K. Watsuji, T. Katagiri, H. Shibata, Y. Matsuda, and H. Fujiyama: *Appl. Surf. Sci.* **252** (2006) 8589.
- 12) M. Shinohara, T. Katagiri, K. Iwatsuji, H. Shibata, Y. Matsuda, and H. Fujiyama: *Thin Solid Films* **506** (2006) 710.
- 13) M. Shinohara, K. Cho, H. Shibata, K. Okamoto, T. Nakatani, Y. Matsuda, and H. Fujiyama: *Thin Solid Films* **516** (2008) 4379.
- 14) S. Takabayashi, K. Motomitsu, T. Takahagi, A. Terayama, K. Okamoto, and T. Nakatani: *J. Appl. Phys.* **101** (2007) 103542.
- 15) S. Takabayashi, K. Okamoto, K. Motomitsu, A. Terayama, T. Nakatani, H. Sakaue, H. Suzuki, and T. Takahagi: *Appl. Surf. Sci.* **254** (2008) 2666.
- 16) S. Takabayashi, K. Okamoto, K. Shimada, K. Motomitsu, H. Motoyama, T. Nakatani, H. Sakaue, H. Suzuki, and T. Takahagi: *Jpn. J. Appl. Phys.* **47** (2008) 3376.
- 17) R. D. Mansano, M. Massi, L. S. Zambom, P. Verdonck, P. M. Nogueira, H. S. Maciel, and C. Otani: *Thin Solid Films* **373** (2000) 243.
- 18) M. Massi, H. S. Maciel, C. Otani, R. D. Mansano, and P. Verdonck: *J. Mater. Sci.: Mater. Electron.* **12** (2001) 343.
- 19) S. Takabayashi, K. Okamoto, T. Nakatani, H. Sakaue, and T. Takahagi: *TANSO* **235** (2008) 280 [in Japanese].
- 20) T. Balasubramanian, J. N. Andersen, and L. Wallden: *Phys. Rev. B* **64** (2001) 205420.
- 21) R. A. P. Smith, C. W. Armstrong, G. C. Smith, and P. Weightman: *Phys. Rev. B* **66** (2002) 245409.
- 22) J. F. Morar, F. J. Himpsel, G. Hollinger, J. L. Jordan, G. Hughes, and F. R. McFeely: *Phys. Rev. B* **33** (1986) 1340.
- 23) W. M. Lau, L. J. Huang, I. Bello, Y. M. Yiu, and S. T. Lee: *J. Appl. Phys.* **75** (1994) 3385.
- 24) R. Graupner, F. Maier, J. Ristein, L. Ley, and C. Jung: *Phys. Rev. B* **57** (1998) 12397.
- 25) K. Bobrov, G. Comtet, G. Dujardin, L. Hellner, P. Bergonzo, and C. Mer: *Phys. Rev. B* **63** (2001) 165421.
- 26) K. Bobrov, A. Mayne, G. Comtet, G. Dujardin, L. Hellner, and A. Hoffman: *Phys. Rev. B* **68** (2003) 195416.
- 27) G. Speranza, L. Minati, and M. Anderle: *J. Appl. Phys.* **102** (2007) 043504.
- 28) S. Takabayashi, K. Okamoto, H. Sakaue, T. Takahagi, K. Shimada, and T. Nakatani: *J. Appl. Phys.* **104** (2008) 043512.
- 29) D. Briggs and M. P. Seah: *Practical Surface Analysis: Auger and X-Ray Photoelectron Spectroscopy* (Wiley, Chichester, U.K., 1990) 2nd ed.
- 30) B. Terreault, M. Leroux, J. G. Martel, R. St. Jacques, C. Brassard, C. Cardinal, J. Chabbal, L. Deschenes, J. P. Labrie, and J. L'Ecuyer: *Adv. Chem. Ser.* **158** (1976) 295.
- 31) W. M. A. Bik and F. H. P. M. Habraken: *Rep. Prog. Phys.* **56** (1993) 859.
- 32) K. Kimura, K. Nakajima, and H. Imura: *Nucl. Instrum. Methods Phys. Res., Sect. B* **140** (1998) 397.
- 33) K. Kimura, S. Joumori, Y. Oota, K. Nakajima, and M. Suzuki: *Nucl. Instrum. Methods Phys. Res., Sect. B* **219–220** (2004) 351.
- 34) K. Kimura, K. Nakajima, T. Conard, and W. Vandervorst: *Appl. Phys. Lett.* **91** (2007) 104106.
- 35) K. Kimura, K. Nakajima, M. Zhao, H. Nohira, T. Hattori, M. Kobata, E. Ikenaga, J. J. Kim, K. Kobayashi, T. Conard, and W. Vandervorst: *Surf. Interface Anal.* **40** (2008) 423.
- 36) D. A. Shirley: *Phys. Rev. B* **5** (1972) 4709.
- 37) A. Proctor and P. M. A. Sherwood: *Anal. Chem.* **54** (1982) 13.
- 38) This equation was previously described as eq. (1) in ref. 14 and eq. (4) in ref. 19. However, these expressions were mistyped and have been corrected here. As a matter of course, the previous analyses were performed with the correct equation.
- 39) E. J. McGuire: *Phys. Rev.* **185** (1969) 1.
- 40) M. Cardona and L. Ley: in *Photoemission in Solids I*, ed. M. Cardona and L. Ley (Springer, Berlin, 1978) Chap. 1.
- 41) J. Díaz, G. Paolicelli, S. Ferrer, and F. Comin: *Phys. Rev. B* **54** (1996) 8064.
- 42) R. Haerle, A. Pasquarello, and A. Baldereschi: *Comput. Mater. Sci.* **22** (2001) 67.
- 43) R. Haerle, E. Riedo, A. Pasquarello, and A. Baldereschi: *Phys. Rev. B* **65** (2001) 045101.
- 44) S. Tanuma, C. J. Powell, and D. R. Penn: *Surf. Interface Anal.* **37** (2005) 1.
- 45) This pair of equations was previously described as eqs. (3) and (4) in ref. 14. However, these expressions were mistyped and have been corrected here. As a matter of course, the previous analyses were performed with the correct equations.



Contents lists available at ScienceDirect

## Surface &amp; Coatings Technology

journal homepage: [www.elsevier.com/locate/surfcoat](http://www.elsevier.com/locate/surfcoat)

## Development of surface-functionalized drug-eluting stent with diamond-like carbon nanocoated by using PECVD method

Keishi Okamoto<sup>a,c,\*</sup>, Tatsuyuki Nakatani<sup>a</sup>, Shuzou Yamashita<sup>b</sup>, Susumu Takabayashi<sup>c</sup>, Takayuki Takahagi<sup>c</sup>

<sup>a</sup> TOYO Advanced Technologies Co., Ltd. 5-3-38 Ujina-higashi, Minami-ku, Hiroshima 734-8501, Japan

<sup>b</sup> Japan Stent Technology Co., Ltd., 5303 Haga Okayama 701-1221, Japan

<sup>c</sup> Graduate school of Advanced Science of Matter, Hiroshima University, 1-3-1 Kagamiyama Higashi-Hiroshima, Hiroshima 739-8530, Japan

### ARTICLE INFO

Available online 21 June 2008

#### Keywords:

Diamond-like carbon  
Surface treatment  
Drug-eluting stent  
XPS

### ABSTRACT

We attempted the surface modification of stents using functionalized DLC films in order to improve the adhesion and integrity of drug drug-eluting polymers. We doped Si for the improvement of mechanical properties of DLC films, and modified the surface of DLC films using oxygen plasma. The result of the analysis after the plasma treatment showed that oxidation of Si occurred, and that the introduction of O=C–O bonding decreased as the amount of doped Si increased. We deduced that the reduction of Si concentrations from the surface of DLC films was effective for introducing O=C–O bonding. The results obtained from these composition analyses were applied to drug-eluting stents and it was confirmed that the peeling of polymers did not readily occur.

© 2008 Elsevier B.V. All rights reserved.

### 1. Introduction

Carbon is known to be a biocompatible material. Current clinical applications of carbon include stents using the diamond-like carbon (DLC) films [1–3] and artificial cardiac valves using pyrolytic carbon [4]. In addition, it is known that DLC films can be used as coating films providing high hardness that are applied to automobile parts in order to increase wear resistance [5–6]. When DLC films is used for the stent, the material is required to have enough toughness it undergoes when it is expanded by a balloon-catheter. Another clinical application is drug-eluting stents (DES) that are coated with the drug-containing polymers [7–8]. Sufficient adherence cannot always be achieved between metal and polymer. As a solution to this problem, it is possible to coat the surface of a stent with DLC films so that functional groups are introduced on the surface through carbon bonding. This procedure is expected to provide more tenacious polymer bonds [9]. We have also discussed the analysis of the DLC films surface. At this time we doped Si for the crack prevention of the DLC films [9]. We evaluated the surface by applying X-ray photoelectron spectroscopy (XPS) to the DLC films with the requisite surface characteristics for the efficient introduction of functional groups.

### 2. Methods and experimentation

The DLC films substrate was coated using Si wafers with equipment that utilizes the ionized-assisted deposition of plasma enhanced chemical

vapor deposition (PECVD) method. Plasma operational conditions were controlled of negative DC bias voltage to 1.5 kV and the deposition pressure to  $1.30 \times 10^{-1}$  Pa. Adjusting the flow ratio between  $C_6H_6$  gas and tetramethylsilane gas used as material gases coated the DLC films having different Si contents. Next, the measurements of C 1s and Si 2p spectra were conducted using the XPS. The XPS measurements were conducted on a surface area of diameter of 5 mm with a JEOL JPS-9010 XPS system with an unmonochromated  $AlK_{\alpha}$  (1486.3 eV) line, which had a voltage of 12.5 kV and current of 15 mA. The charge correction was determined by first dropping Au colloids on a part of the substrate surface and allowing them to dry. The amount of shift was determined from the binding energy of Au 4f<sub>7/2</sub> [10]. Next, functional groups were attached to the surface of the Si-doped DLC films using the oxygen plasma, and the relationship between the composition of the surface and the amount of the functional groups introduced was examined. The equipment used was a capacitively coupled plasma surface treatment system with a radio-frequency (RF) power at 13.56 MHz.

Functional groups were introduced on the surface by first applying plasma using gases containing Ar mixed with 3% flow rate  $O_2$ , and then by applying plasma using only  $O_2$  gas. The working pressure was set to 133 Pa, the RF power was 30 W, and the irradiation time was 15 s. We analyzed only the change by the plasma irradiation by using the different XPS method though there was a report concerning the XPS analysis of the plasma treated Si-doped DLC films [11]. Different XPS method was used to divide the peaks of C 1s spectrum with O=C–O, C=O and C–O for quantitative measurement of the O=C–O bonding obtained [12]. The amount of O=C–O bonding introduced on the surface was obtained by determining the ratio of the intensity of the peak of O=C–O bonding to the intensity of the maximum peak of C 1s spectrum.

\* Corresponding author. TOYO Advanced Technologies Co., Ltd. 5-3-38 Ujina-higashi, Minami-ku, Hiroshima 734-8501, Japan. Tel.: +81 82 252 5215; fax: +81 82 256 0264. E-mail address: [okamoto.ke@toyo-at.co.jp](mailto:okamoto.ke@toyo-at.co.jp) (K. Okamoto).

This technology was actually applied to DES using the biodegradable polymers [9]. The thickness of DLC films was set to 50 nm. The Si concentration decreased from the interface with the base metal to the surface, and has facilitated the introduction of the functional groups on the surface keeping mechanical properties of Si-doped DLC films.

The surface of the obtained DLC films was subjected to surface functional groups modification with oxygen plasma and the lactic acid biodegradability polymer was coated by the ultrasonic atomization method of the polymer solution. The film thickness of the polymer was set to 5  $\mu\text{m}$ .

### 3. Results and discussion

A comparison of the binding energy position of XPS C 1s spectrum carboxyl groups was conducted on a substrate subjected to functional groups modification through DLC films surface treatment using plasma. As a result, a peak of O=C–O bonding was found on the DLC films surface, and the introduction of O–C–O bonding was observed. Furthermore, it was determined that the amount of O=C–O bonding decreased as the amount of doped Si increased (Fig. 1). The ratio of the intensity of the peak of O=C–O bonding to that of the maximum peak of C 1s spectrum was: Si (0%)=5.4%, Si (3%)=5.0%, Si (19%)=4.0%, and Si (28.5%)=1.9%. In addition, a peak of SiO<sub>2</sub> was obtained on XPS Si 2p spectrum after the plasma treatment, indicating the oxidation of SiC. Furthermore, a comparison of SiO<sub>2</sub>/SiC on DLC films having different Si contents shows: Si (3%)=0.64, Si (19%)=0.55, and Si (28.5%)=0.48. SiC is oxidized to SiO<sub>2</sub> with the oxygen plasma in an almost constant ratio. SiO<sub>2</sub> is increased by an increase of the SiC concentrations in DLC films, and the introduction of O=C–O bonding decreases. When a Si and carbon are compared, electronegativity (Pauling) of Si (1.9) is lower than carbon (2.55) [13].

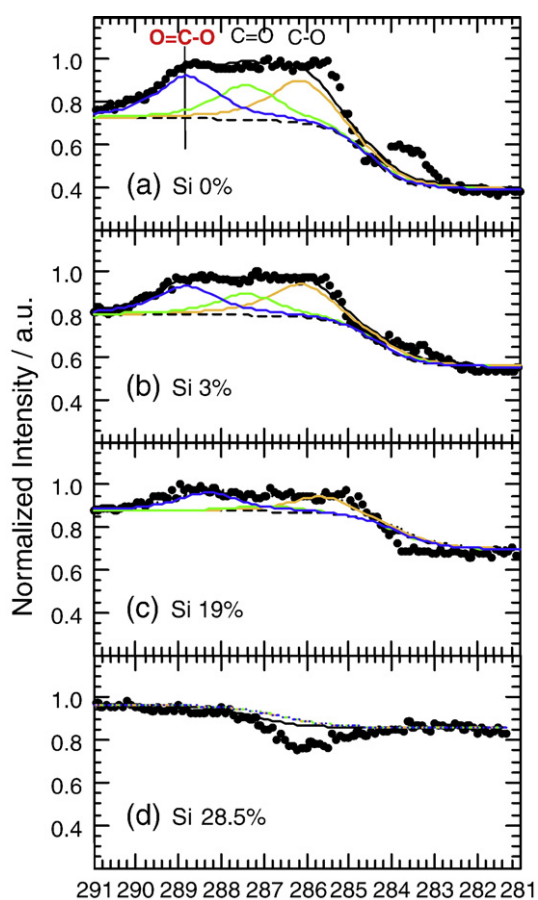


Fig. 1. XPS C 1s spectrum of DLC films with different amounts of doped Si: (a) 0%, (b) 3%, (c) 19%, and (d) 28.5% subjected to plasma surface treatment.

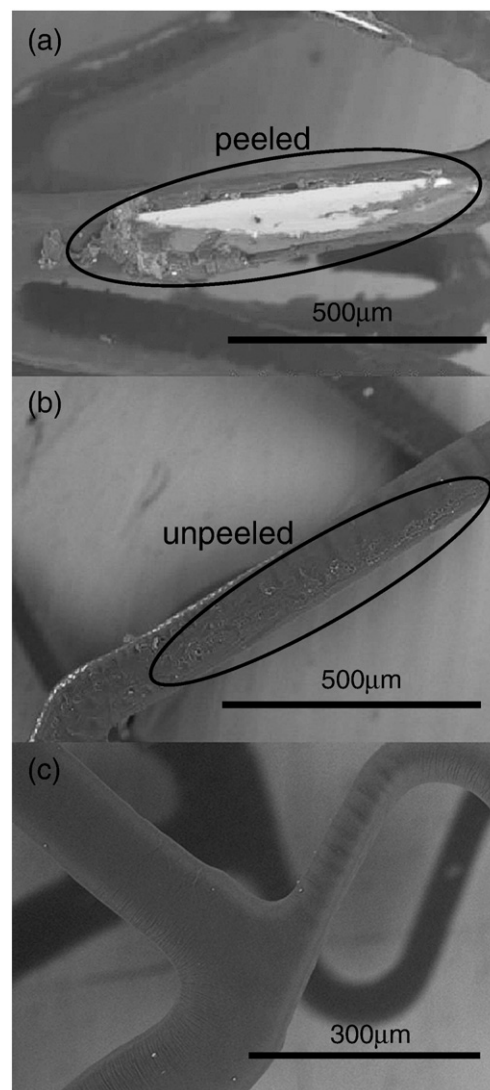


Fig. 2. Results of application to DES. (a) Results of scratching by tweezers: Commercially available coronary artery DES. (b) Results of scratching by tweezers: DES obtained by this experiment. (c) Results of expansion experimental: DES obtained by this experiment.

Therefore we deduce SiC to be oxidized first more than O=C–O bonding are introduced. Fig. 2 shows the results of the comparison with DES that are commercially available. When scratched on surface with tweezers, the polymer of commercially available DES peeled. However, the stents obtained by this experiment remained intact. Additionally, a study was conducted in which the diameter of the stents was expanded from 1.5 mm to 3.0 mm by a balloon-catheter. The results showed that an enough adherence was successfully obtained preventing the polymer from peeling. The calculated maximum distortion factor was estimated to be 170% on the linked segment.

### 4. Conclusion

We attempted the introduction of O=C–O bonding onto Si-doped DLC films through surface treatment technology using oxygen plasma. As a result, the reduction of Si concentrations from the DLC films is effective for introducing O=C–O bonding onto the surface. Furthermore we attempted to apply the process to actual DES: The DES was coated with DLC films having inclined Si concentrations decreasing from the interface with the matrix to the surface. The DES was subjected to the introduction of O=C–O bonding through plasma surface treatment, and then was coated with polymers.

## Acknowledgments

We wish to thank Mr. Ikuo Omura at the Japan Stent Technology Co., Ltd., for his advice regarding polymer-coating technology as well as extend our gratitude to Professor Kohei Shiraishi at the School of Engineering, Kinki University, for his advice regarding plasma surface treatment technology.

## References

- [1] O. Schaefer, C. Lohrmann, J. Winterer, E. Kotter, M. Langer, *Clin. Radiol.* 59 (2004) 1128.
- [2] P.B. Sick, G. Gelbrich, U. Kalnins, A. Erglis, R. Bonan, W. Aengevaeren, D. Elsner, B. Lauer, M. Woinke, O. Brosteanu, G. Schuler, *Am. J. Cardiol.* 93 (2004) 1351.
- [3] P.D. Maguire, J.A. McLaughlin, T.I.T. Okpalugo, P. Lemoine, P. Papakonstantinou, E.T. McAdams, M. Needham, A.A. Ogwu, M. Ball, G.A. Abbas, *Diamond Relat. Mater.* 14 (2005) 1277.
- [4] V.O. Bjork, A. Henze, A. Peterffy, *Eur. Heart J.* 1 (1980) 55.
- [5] T. Nakatani, K. Okamoto, A. Araki, T. Washimi, *New Diam. Front. Carbon Technol.* 16 (2006) 187.
- [6] T. Nakatani, K. Okamoto, S. Ando, T. Washimi, in: *New Diamond* (Ed.), Japan New Diamon Forum, vol. 79, 2005, p. 14.
- [7] G.W. Stone, S.G. Ellis, D.A. Cox, J. Hermiller, C. O. ' Shaughnessy, J. Tift Mann, M. Turco, R. Caputo, P. Bergin, J. Greenberg, J.J. Popma, M.E. Russell, N. E. J. Med. 350 (2004) 221.
- [8] J. Gunn, D. Cumberland, *Eur. Heart J.* 20 (1999) 1693.
- [9] T. Nakatani, K. Okamoto, I. Omura, S. Yamashita, *J. Photopolym. Sci. Tech.* 20 (2007) 221.
- [10] S. Takabatashi, K. motomitsu, T. takahagi, A. terayama, K. okamoto, T. Nakatani, *J. Appl. Phys.* 101 (2007) 103542.
- [11] R.K. Roy, H.W. Choi, S.J. Park, K.R. Lee, *Diamond Relat. Mater.* 16 (2007) 1732.
- [12] S. Kodama, H. Habaki, H. Sekiguchi, J. Kawasaki, *Thin Solid Films* 407 (2002) 151.
- [13] L. Pauling, *J. Am. Chem. Soc.* 54 (1932) 3570.

# Qualitative analysis of a diamondlike carbon film by angle-resolved x-ray photoelectron spectroscopy

Susumu Takabayashi,<sup>a)</sup> Kunihiro Motomitsu, and Takayuki Takahagi

*Department of Quantum Matter, Graduate School of Advanced Sciences of Matter, Hiroshima University, 1-3-1 Kagamiyama, Higashi-Hiroshima, Hiroshima 739-8530, Japan*

Akira Terayama

*Cluster 2, Faculty of Engineering, Hiroshima University, 1-4-1 Kagamiyama, Higashi-Hiroshima, Hiroshima 739-8527, Japan*

Keishi Okamoto and Tatsuyuki Nakatani

*Toyo Advanced Technologies Co., Ltd., 5-3-38 Ujina-Higashi, Minami-ku, Hiroshima-shi, Hiroshima 734-8501, Japan*

(Received 21 December 2006; accepted 25 March 2007; published online 31 May 2007)

Angle-resolved x-ray photoelectron spectroscopy was used to investigate the surface of a diamondlike carbon film prepared by the ionized deposition method. We then analyzed the C 1s spectra using the Doniach-Šunjić (DŠ) [J. Phys. C **3**, 285 (1970)] function convoluted with a Gaussian function. Consequently, we obtained four fitting curves for the carbon components in each spectrum, regardless of the assumption of the singularity index ( $\alpha$ ) in the DŠ function, which expresses the asymmetry of the C 1s spectrum. The curves were assigned in the order of binding energy to bulk  $sp^3$  carbon (283.7–283.8 eV), bulk  $sp^2$  carbon (284.2–284.3 eV), surface  $sp^2$  carbon (284.7–284.8 eV), and surface  $sp^3$  (285.3–285.4 eV) carbon. We further considered the influence of the assumption of  $\alpha$ . Consequently, we suggest that the C 1s spectra can be quantitatively analyzed without considering the influences of  $\alpha$  when the ratio of  $\alpha$  for  $sp^2$  carbon to that for  $sp^3$  carbon [ $\alpha(sp^2) : \alpha(sp^3)$ ] is between 10:0 and 5:5. The distribution in the  $\alpha$  ratio may indicate that the  $sp^2$  and the  $sp^3$  carbon atoms can interact with each other (hybridization) and differ from those highly oriented pyrolytic graphite and diamond, respectively. © 2007 American Institute of Physics. [DOI: 10.1063/1.2735416]

## INTRODUCTION

Diamondlike carbon (DLC) is an amorphous material, which is composed of  $sp^2$  carbon,  $sp^3$  carbon, and hydrogen.<sup>1</sup> Owing to its high lubricity as well as hardness, DLC has been applied to protect the surfaces of a hard disk and a die, and very recently to protect those of medical tools such as stents and guide wires.<sup>2,3</sup> Obviously these characteristics of DLC are mainly derived from the surface characteristics. Raman spectroscopy is the main tool for identifying DLC,<sup>4,5</sup> but is not appropriate for surface analysis because the incident laser irradiation deeply penetrates the sample, and signals (Raman scattering) for several atomic layers at the surface and that for the bulk layers are simultaneously observed and cannot be divided. On the other hand, x-ray photoelectron spectroscopy<sup>6–22</sup> (XPS) is one of the most suitable tools for surface analysis, particularly for quantitative analysis, because it can selectively observe a signal (x-ray-excited photoelectron) for several atomic layers at the surface (the relationship between the Raman spectra and the XPS spectra was also discussed in the references).

XPS core level spectra such as C 1s and O 1s are usually composed of several meaningful curves, each of which is assigned to a unique bond such as carbon-carbon or carbon-oxygen bonds. Thus the core level XPS analysis requires

dividing the spectrum into several meaningful curves, but it is not easy because we must control the number of curves and the free parameters of every curve such as its position, height, width, and symmetry. Thus the qualitative analysis is difficult in contrast to the quantitative analysis. However, angle-resolved (AR-) XPS, which varies the takeoff angles of the electron emission and controls the escape depth of the electrons, gives some useful suggestions for the qualitative analysis because the method gives the difference between the surface component (shallow escape depth) and the bulk component (deep escape depth).<sup>23</sup> Consequently, it is worth using AR-XPS for the qualitative analysis of DLC.

$$\begin{aligned}
 & DS(E_{BE}, \Gamma_L, \alpha) \otimes G(E_{BE}, \Gamma_G) \\
 &= \int_{-\infty}^{+\infty} DS(E_{BE}, \Gamma_L, \alpha) \otimes G(E_{BE} - E', \Gamma_G) dE' \\
 &= I \frac{2}{\Gamma_G} \sqrt{\frac{\ln 2}{\pi}} \\
 &\quad \times \frac{\Gamma(1 - \alpha) \cos[\pi\alpha/2 + (1 - \alpha)\tan^{-1}(E_0 - E_{BE})/(\Gamma_L/2)]}{[(E_0 - E_{BE})^2 + (\Gamma_L/2)^2]^{(1-\alpha)/2}} \\
 &\quad \times \int_{-\infty}^{+\infty} \exp\left\{-4 \ln 2 \left[\frac{(E_{BE} - E') - E_0}{\Gamma_G}\right]^2\right\} dE'. \quad (1)
 \end{aligned}$$

Equation (1) shows the analytical function for an XPS C 1s spectrum of a DLC film, which is the Doniach-Šunjić (DŠ)

<sup>a)</sup> Author to whom correspondence should be addressed; electronic mail: stak@hiroshima-u.ac.jp



function convoluted with a Gaussian function used to consider the instrumental broadening, the phonon interaction, and the chemical disorder.<sup>8,16,18,24</sup> The parameters are as follows:  $\Gamma(x)$  is the gamma function, while  $\alpha$  is the singularity index.  $\Gamma_L$  is the Lorentzian lifetime [expressed as a full width at half maximum (FWHM) of the Lorentzian function].  $E_0$  is the center of the binding energy for the curve at  $\alpha=0$ .  $\Gamma_G$  is the Gaussian broadening (expressed as a FWHM of the Gaussian function).  $I$  is a proportionality constant that is proportional to the incident x-ray intensity and  $E_{BE}$  is the observed binding energy. The singularity index  $\alpha$  of the D $\check{S}$  function is related to the electron density of states (DOS) at the Fermi level ( $E_F$ ) derived from the Anderson catastrophe<sup>25</sup> and the Mahan–Nozières–De Dominicis (MND) theory.<sup>26–28</sup> The D $\check{S}$  function is commonly used to analyze a C 1s spectrum for highly oriented pyrolytic graphite<sup>29–31</sup> (HOPG) (other references are therein), in which  $\alpha$  is a finite value. Otherwise,  $\alpha$  is zero for diamond, which reduces the D $\check{S}$  function to a Lorentzian function.<sup>32–34</sup> For simplicity, herein we assumed that all fitting curves in each C 1s spectrum have common  $\Gamma_L$  and  $\Gamma_G$  values regardless of the type of curve (for  $sp^2$  carbon,  $sp^3$  carbon, and other components). On the other hand, when considering the  $\alpha$ 's for the  $sp^2$  carbon and  $sp^3$  carbon curves in DLC, we assumed some patterns for the ratio of  $\alpha$  for  $sp^2$  carbon [ $\alpha(sp^2)$ ] to that for  $sp^3$  carbon [ $\alpha(sp^3)$ ], that is,  $\alpha(sp^2) : \alpha(sp^3)$ .

To date other authors have assumed  $\alpha(sp^2) : \alpha(sp^3)$ . Diaz *et al.*,<sup>8</sup> Riedo *et al.*,<sup>15</sup> and Haerle *et al.*<sup>18</sup> assumed that  $\alpha(sp^2)$  is a finite value and  $\alpha(sp^3)$  is zero because they felt that the characteristics of the  $sp^2$  carbon atoms of DLC are derived from HOPG, which is solely composed of  $sp^2$  carbon for which  $\alpha$  has a finite value (although the value varies by author),<sup>29–31</sup> while the characteristics of the  $sp^3$  carbon atoms of DLC are derived from diamond, which is composed solely of  $sp^3$  carbon for which  $\alpha$  is zero (then the D $\check{S}$  function is reduced to a Lorentzian function).<sup>32–35</sup> These assumptions would lead to the conclusion that DLC is a simple mixture of HOPG and diamond, which would produce polycrystalline DLC. However, DLC is an amorphous material. Thus, it is unlikely that DLC is composed of complete HOPG structures and complete diamond structures.

On the other hand, Jackson and Nuzzo<sup>6</sup> and Mérel *et al.*<sup>12</sup> assumed that  $\alpha(sp^2) : \alpha(sp^3)$  is 0:0, that is, both curves for  $sp^2$  carbon and  $sp^3$  carbon are symmetric (Lorentzian). However, the C 1s spectrum of every DLC is asymmetric in nature (their spectra were also). Thus, their assumptions are also inadequate.

Consequently, it is worth investigating  $\alpha(sp^2) : \alpha(sp^3)$  to express the interesting amorphous characteristics of DLC. It should be noted that although Kato has calculated<sup>36</sup> the difference between  $\alpha$  for the surface component and that for the bulk component, for a simplified analysis we did not consider the difference.

## EXPERIMENTAL

A DLC film was deposited on a single-crystal Si wafer ( $10 \times 10 \text{ mm}^2$ ) by the ionized deposition method.<sup>37–41</sup> The deposition conditions were as follows. The carbon source

was 30 SCCM (SCCM denotes cubic centimeter per minute at STP) of benzene gas. The dc bias voltage applied to the substrate was  $-2.0 \text{ kV}$  and the temperature was  $180 \text{ }^\circ\text{C}$ . The pressure during the deposition process was about  $1.0 \times 10^{-3} \text{ torr}$  and the deposition time was 12.5 min. The thickness of the DLC film deposited was about 150 nm, which was thick enough for XPS analysis.

Raman spectroscopy were conducted to investigate whether the as-prepared film is a DLC or not with a Horiba-Jobin Yvon T64000 system having a  $\text{Ar}^+$  laser (457.9 and 514.5 nm lines) with a power of 40 mW.<sup>42</sup>

The AR-XPS measurements were conducted on a surface area of  $0.8 \times 2.0 \text{ mm}^2$  of the DLC film with an ULVAC-PHI PHI 1600 system having an unmonochromated  $\text{Al K}\alpha$  (1486.3 eV) line with a voltage of 15 kV and a power of 400 W. The takeoff angles of the electron emission varied from measurement to measurement and ranged between  $10^\circ$  and  $75^\circ$  counted from normal to the surface. All the measurements were carried out at room temperature and a pressure of below  $3.0 \times 10^{-9} \text{ torr}$ . The backgrounds of all spectra were subtracted by the Shirley method.<sup>23,28,43</sup> This method is easy to use and popular, although it includes some error compared to the Tougaard method.<sup>23,28,44</sup> As estimated from the FWHM of the Au  $4f_{7/2}$  spectrum for a Au plate, the energy resolution of the system was 1.1 eV.

Before the AR-XPS measurements, a few microliters of an aqueous solution containing Au particles<sup>45</sup> were dropped on a small local surface area of the DLC film, which measured about  $2 \times 2 \text{ mm}^2$ , using a syringe in air. The surface was then gradually dried *in vacuo*. The observed binding energy of each C 1s spectrum for the surface area of the DLC film was calibrated by setting the observed binding energy of the Au  $4f_{7/2}$  spectrum for the Au particles onto another surface area of the same DLC film to 83.98 eV.<sup>46</sup> The FWHM of each Au  $4f_{7/2}$  spectrum for the Au particles and a Au plate were consistent. Thus, this calibration method is adequate. Furthermore, the method is not only easier but also better than that using a Au film prepared by the vacuum evaporation method because the latter has some carbon contamination on the Au film due to the heated filament, which inevitably affects carbonaceous materials such as DLC, HOPG, and diamond in a negative manner. Of course, every C 1s spectrum was observed on the native surface area of the DLC film without being covered by Au particles.

## RESULTS AND DISCUSSION

Figure 1 shows two Raman spectra of a DLC film excited by the 457.9 and 514.5 nm lines of the  $\text{Ar}^+$  laser with a power of 40 mW. Both excitations gave the similar-shaped spectra having the *G* peaks and the *D* shoulders, however, the 457.9 nm excitation gave the spectrum at higher Raman shift ( $1560 \text{ cm}^{-1}$ ), and the 514.5 nm excitation gave it at slightly lower Raman shift ( $1545 \text{ cm}^{-1}$ ). Ferrari and Robertson proposed to apply the relationship between the *G* peak and the excitation wavelength to identify the kind of DLC, which is called “*G* peak dispersion.”<sup>5</sup> The *G* peak dispersion indicates that our DLC film is a kind of ta-C:H.

Figure 2 shows the AR-XPS C 1s spectra of a DLC film.

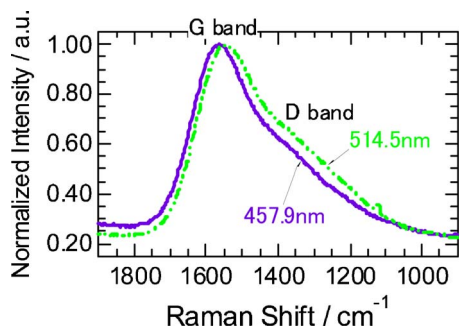


FIG. 1. (Color online) Raman spectra of a DLC film excited by the 457.9 and 514.5 nm lines of the Ar<sup>+</sup> laser with a power of 40 mW.

The takeoff angles of the electron emission counted from normal to the surface were 30°, 60°, and 75°. The C 1s spectrum was shifted to higher binding energy with increasing the takeoff angle. This tendency suggests that at least one curve for the surface component is immanent at higher binding energy in the spectrum and at least one curve for the bulk component at lower binding energy.

Figure 3 shows the AR-XPS C 1s spectra of a DLC film. Each spectrum fitting curve is analyzed by Eq. (1). Here  $\alpha(sp^2)$  and  $\alpha(sp^3)$  are assumed to have the same finite value, that is,  $\alpha(sp^2):\alpha(sp^3)=5:5$ . At this stage, the adequacy for this assumption is unclear, but the assumption makes it easy to analyze the spectra because it is unnecessary to decide in advance whether each fitting curve is for  $sp^2$  carbon or  $sp^3$  carbon. The results demonstrate that the C 1s spectrum is composed of four fitting curves, which have binding energies at 283.7–283.8, 284.2–284.3, 284.7–284.8, and 285.3–285.4 eV. It should be noted that the  $\alpha$ 's for the other very small curves are at 286.1–286.2 and 286.9–287.1 eV. These small curves are probably due to oxygen-bonded carbon, i.e., carbonyl and carboxyl, and were set to zero. The total intensity of these curves in each spectrum is 1.5% of the entire intensity. This value is in good agreement with that calculated from the survey spectrum (not shown). Thus, these very small curves were not further analyzed.

In the AR analysis, a larger takeoff angle (counted from normal to the surface) of the electron emission enhances surface components and a smaller one enhances the bulk components according to Eq. (2)<sup>23</sup>

$$\lambda_i = \lambda_i^0 \cos \theta, \quad (2)$$

where  $\lambda_i$  is the inelastic mean free path (IMFP) for component  $i$  at takeoff angle  $\theta$  counted from normal to the surface

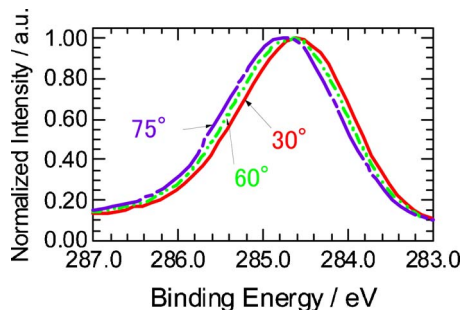


FIG. 2. (Color online) AR-XPS C 1s spectra of a DLC film. The takeoff angles of the electron emission counted from normal to the surface were 30°, 60°, and 75°.

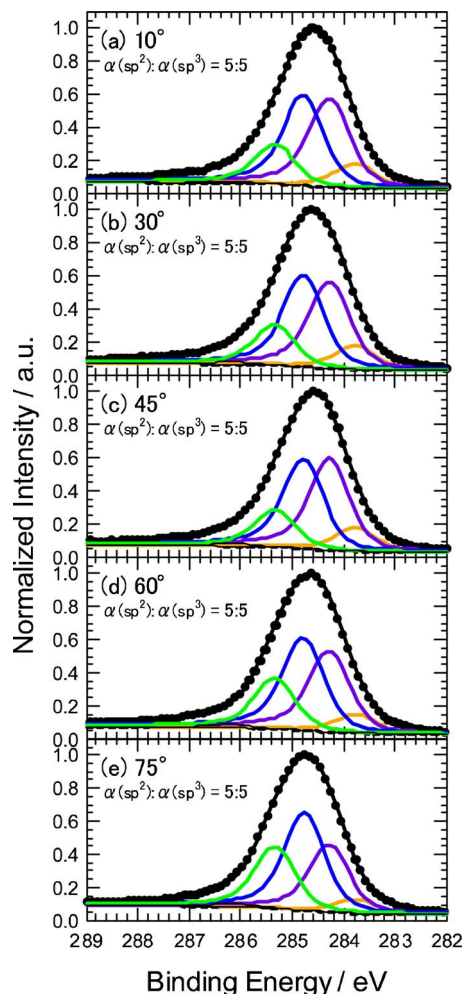


FIG. 3. (Color online) AR-XPS C 1s spectra of a DLC film. Each of which includes its fitting curves analyzed using the D $\check{S}$  function convoluted with a Gaussian function.  $\alpha$ 's of the D $\check{S}$  function for  $sp^2$  carbon [ $\alpha(sp^2)$ ] and for  $sp^3$  carbon [ $\alpha(sp^3)$ ] are assumed to have the same value. Takeoff angles of the electron emission counted from normal to the surface are (a) 10°, (b) 30°, (c) 45°, (d) 60°, and (e) 75°.

and  $\lambda_i^0$  is the standard IMFP (or the IMFP at 0°). Equation (2) suggests that a component for which the intensity increases with  $\theta$  is a surface component, while the intensity of a bulk component decreases with  $\theta$ . Thus, at this stage, the four fitting curves in the order of binding energy are bulk (283.7–283.8 eV), bulk (284.2–284.3 eV), surface (284.7–284.8 eV), and bulk (285.3–285.4 eV) components.

Regarding the assignment of  $sp^2$  carbon, Balasubramanian *et al.*<sup>29</sup> have previously investigated the surface and bulk components of HOPG using synchrotron radiation with various energies. They obtained two fitting curves in each spectrum using the D $\check{S}$  function convoluted with a Gaussian function, as shown in Eq. (1), and then assigned the curve at the higher binding energy to surface  $sp^2$  carbon and the curve at the lower binding energy to bulk  $sp^2$  carbon. A year later Smith *et al.*<sup>30</sup> employed the same AR-XPS method that we used and reported results that support the findings of Balasubramanian *et al.* (It should be noted that Smith *et al.* counted the takeoff angle of the electron emission from the surface, which differs from our case. In their case,  $\cos \theta$  in Eq. (2) is corrected with  $\sin \theta$ ). They also concluded that the

difference in binding energy between the curves for surface  $sp^2$  carbon (observed at a higher binding energy) and for bulk  $sp^2$  carbon (observed at a lower binding energy) of HOPG is 0.47 eV, which agrees with our analysis and demonstrates the difference in binding energy between 284.7–284.8 eV and 284.2–284.3 eV. Thus, the curves at 284.2–284.3 eV and at 284.7–284.8 eV are assigned to bulk  $sp^2$  carbon and surface  $sp^2$  carbon, respectively.

Regarding the assignment of bulk  $sp^3$  carbon, Bobrov *et al.* have reported<sup>35</sup> that the binding energy of the C 1s spectrum for a hydrogenated diamond surface prepared from a natural single-crystal diamond in a microwave hydrogen plasma is 284.5–284.7 eV. Reinke *et al.* have reported<sup>47</sup> that the binding energy of the XPS C 1s spectrum for a diamond film prepared in a mixture of 1% CH<sub>4</sub> in hydrogen by the chemical vapor deposition (CVD) method is 283.8 eV, and Saw and de Plussis have reported 283.3 eV using a similar method.<sup>48</sup> The binding energy of a C 1s spectrum for diamond depends on the preparation method and varies widely (283.7–289.3 eV).<sup>49</sup> At this stage, we assumed that the curve at 283.7–283.8 eV is assigned to bulk  $sp^3$  carbon. To identify surface  $sp^3$  carbon, we must consider the two cases reported by Bobrov *et al.*:<sup>34,35</sup> One case is the surface carbon dimer, which is observed only on a clean diamond surface where the curve is located at a binding energy that is 0.75–0.9 eV lower than that for the bulk component (284.5–284.7 eV). The other is the nonmonohydride CH<sub>x</sub> species, which is observed only on an *ex situ* prepared diamond surface and for which the curve is located at a binding energy that is 0.8 eV higher than that for the bulk component. The latter case may be consistent with our case. Very recently, Paik assigned<sup>20</sup> the fitting curve at 283.8 eV obtained to SiC when he obtained the XPS C 1s spectra of his DLC films prepared with the magnetron sputter-type negative ion source (MSNIS). However, we did not find any peaks for Si in the survey spectra of our DLC films (although the spectra are not shown here), and the films are thick enough for the XPS analysis. Thus, this assignment is inadequate. Consequently, the curves at 283.7–283.8 and 285.3–285.4 eV are assigned to bulk  $sp^3$  carbon and surface  $sp^3$  carbon, respectively.

Figure 4 shows the same AR-XPS C 1s spectra of a DLC film, as shown in Fig. 3, but each includes its fitting curves based on the different assumptions, which  $\alpha(sp^2)$  and  $\alpha(sp^3)$  are a finite value and zero, respectively or  $\alpha(sp^2):\alpha(sp^3) = 10:0$ . The results demonstrate that the C 1s spectrum is composed of four fitting curves. It is noteworthy that each spectrum gave the same binding energy as that based on the assumption that  $\alpha(sp^2):\alpha(sp^3) = 5:5$ , as shown in Fig. 1, and the order of binding energies are 283.7–283.8, 284.2–284.3, 284.7–284.8, and 285.3–285.4 eV. It should be noted that the  $\alpha$ 's for the other very small curves at 286.1–286.2 and 286.9–287.1 eV, which are shown in Fig. 3 and are most likely for oxygen-bonded carbon, did not vary and are not considered in the analysis.

Figure 5 shows the relationships between the fraction intensities (not areas) for the carbon components of the DLC film and the takeoff angle of the electron emission derived from the results in Figs. 3 and 4. The theory of the relation-

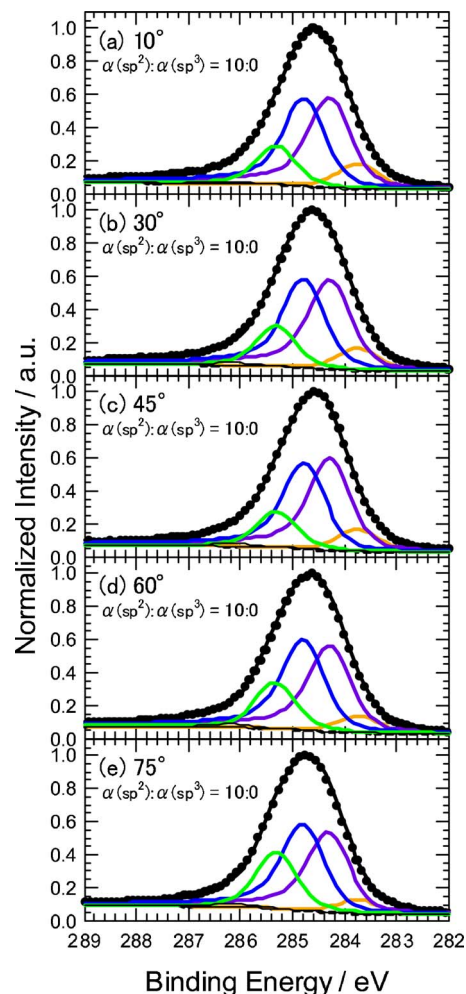


FIG. 4. (Color online) AR-XPS C 1s spectra shown in Fig. 1 for the DLC film, but each includes fitting curves analyzed using the different assumptions,  $\alpha(sp^2)$  and  $\alpha(sp^3)$  are assumed to be a finite value and zero, respectively. Takeoff angles of the electron emission counted from normal to the surface are (a) 10°, (b) 30°, (c) 45°, (d) 60°, and (e) 75°.

ship between the component and the takeoff angle is expressed by Eq. (3) (for a surface component) and Eq. (4) (for a bulk component) when the overlayer film analysis of a heterogeneous double-layer material composed of a thin layer A on a substrate B (A/B) is applied to the analysis of the DLC film imaginarily divided into a thin surface and thick bulk components (S/B).<sup>23</sup> It should be noted that the surface of a DLC film is assumed to be flat and we did not consider the influences of surface roughness on the analysis.

$$I_S = I_S^0 \left\{ 1 - \exp \left[ \frac{1}{(\lambda_{S,S}^0/d) \cos \theta} \right] \right\}, \quad (3)$$

$$I_B = I_B^0 \left\{ -\exp \left[ \frac{1}{(\lambda_{B,S}^0/d) \cos \theta} \right] \right\}, \quad (4)$$

where  $I_S$  and  $I_B$  are the intensities for the surface and bulk components, respectively.  $I_S^0$  and  $I_B^0$  are the standard intensities for the surface and bulk components, respectively, while  $d$  is the imaginary thickness of the surface atomic layers.  $\lambda_{S,S}^0$  and  $\lambda_{B,S}^0$  are the IMFPs through  $d$  of the surface and bulk components, respectively, and  $\theta$  is the takeoff angle of the

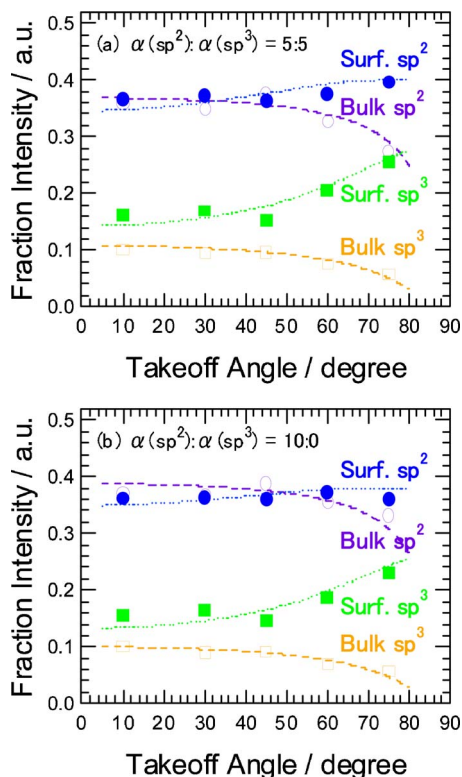


FIG. 5. (Color online) Relationships between the fraction intensities for the carbon components of the DLC film and the takeoff angle of the electron emission derived from the results in Figs. 1 and 2: (a) assumes that  $\alpha(sp^2)$  and  $\alpha(sp^3)$  are a finite value and zero, respectively; (b) assumes that  $\alpha(sp^2)$  and  $\alpha(sp^3)$  have the same value. ■, □, ●, and ○ indicate the fraction intensities for surface  $sp^2$  carbon, bulk  $sp^2$  carbon, surface  $sp^3$  carbon, and bulk  $sp^3$  carbon, respectively.

electron emission. It should be noted that for DLC,  $d$  is assumed to be the thickness of the surface atomic layers in which the  $sp^2$  and  $sp^3$  carbon atoms are homogeneously dispersed and do not vary the values of  $\lambda_{s,s}^0$  and  $\lambda_{B,S}^0$  at a given point. The intensity  $I$  is the peak height and not the area because the area includes information on the asymmetry of the spectrum, which is related to the property of the electrons at  $E_F$ .

Both the results of Fig. 5(a) and 5(b) are consistent with Eq. (3) and (4). Thus, the analysis of the four fitting curves appears to be adequate. These results also gave nearly the same tendency for the relationship between the fraction intensity and the takeoff angle, suggesting that the properties of the photoelectrons emitted from the core C 1s states are almost the same between the assumptions, except for the influences of the holes left on the electrons at  $E_F$ .<sup>25–27</sup>

Figure 6 shows the same XPS C 1s spectra of a DLC film at a takeoff angle of  $45^\circ$ , but each is analyzed on different assumptions of  $\alpha(sp^2):\alpha(sp^3)$ . Figure 7 shows the relationships of the intensities (not areas) for the carbon components of the DLC film and the ratio of  $\alpha(sp^2)$  to  $\alpha(sp^3)$  derived from the results in Fig. 4. It should be noted that the “ratio of  $\alpha(sp^2)=1.0$ ” in the figure expresses that  $\alpha(sp^2):\alpha(sp^3)=10:0$  and “=0.5” expresses that  $\alpha(sp^2):\alpha(sp^3)=5:5$ . Every fraction intensity of the component is constant between ratio of  $\alpha(sp^2)=1.0-0.5$ . These results suggest that quantitative analysis does not vary when

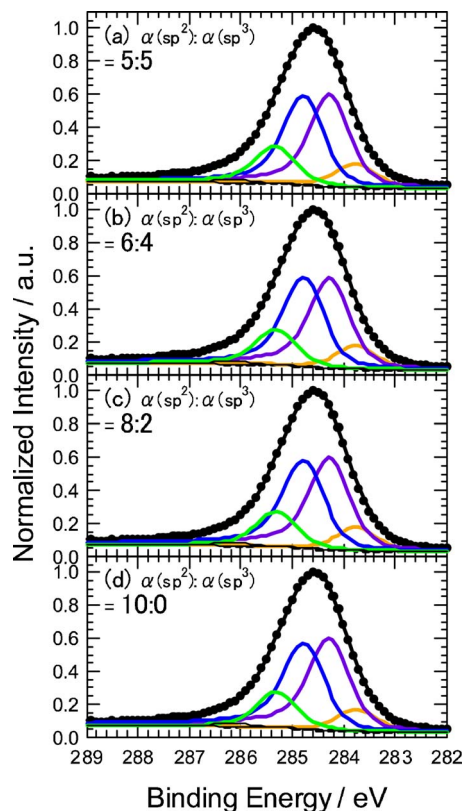


FIG. 6. (Color online) Same XPS C 1s spectra of the DLC film at a takeoff angle of  $45^\circ$ , but each is analyzed on the different assumptions for the ratio of  $\alpha(sp^2)$  to  $\alpha(sp^3)$ ,  $\alpha(sp^2):\alpha(sp^3)$ .  $\alpha(sp^2):\alpha(sp^3)$  are (a) 5:5, (b) 6:4, (c) 8:2, and (d) 10:0.

$\alpha(sp^2):\alpha(sp^3)=10:0-5:5$  and is not influenced by the assumption of the asymmetric property of the spectrum. DLC is an amorphous material. Thus, the distribution in  $\alpha$  of  $\alpha(sp^2):\alpha(sp^3)=10:0-5:5$  may indicate that the  $sp^2$  and  $sp^3$  carbon atoms interact with each other (hybridization) and differ from HOPG and diamond, respectively.

## CONCLUSION

We analyzed the angle-resolved XPS (AR-XPS) C 1s spectra of a DLC film prepared by the ionized deposition

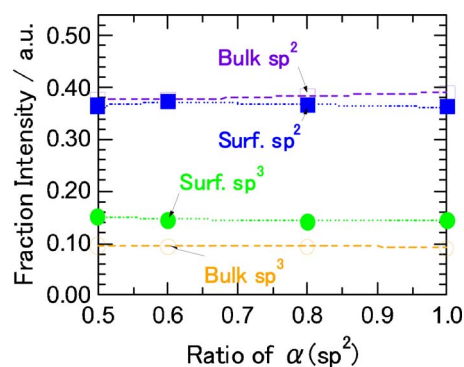


FIG. 7. (Color online) Relationships of the fraction intensities for the carbon components of the DLC film and the assumption of the ratio of  $\alpha(sp^2)$  to  $\alpha(sp^3)$  derived from the results in Fig. 4. ■, □, ●, and ○ indicate the intensities for surface  $sp^2$  carbon, bulk  $sp^2$  carbon, surface  $sp^3$  carbon, and bulk  $sp^3$  carbon, respectively. It should be noted that the “ratio of  $\alpha(sp^2)=1.0$ ” expresses  $\alpha(sp^2):\alpha(sp^3)=10:0$ ; and “=0.5” expresses  $\alpha(sp^2):\alpha(sp^3)=5:5$ .

method. The spectra were analyzed using the Doniach-Šunjić function convoluted with a Gaussian function. The analysis demonstrated that the C 1s spectrum of the DLC film was composed of four components, which in the order of the binding energy are bulk  $sp^3$  carbon (283.7–283.8 eV), bulk  $sp^2$  carbon (284.2–284.3 eV), surface  $sp^2$  carbon (284.7–284.8 eV), and surface  $sp^3$  carbon (285.3–285.4 eV). We also investigated the influences of the assumption on the relationship between the singularity index  $\alpha$  for  $sp^2$  carbon [ $\alpha(sp^2)$ ] and  $sp^3$  carbon [ $\alpha(sp^3)$ ] in the analysis of the C 1s spectrum, and demonstrated that the C 1s spectrum can be quantitatively analyzed without considering the influences of  $\alpha$  between  $\alpha(sp^2):\alpha(sp^3)=10:0$  and 5:5. Finally, the distribution in  $\alpha$  where  $\alpha(sp^2):\alpha(sp^3)=10:0-5:5$  may indicate that the  $sp^2$  and  $sp^3$  carbon atoms interact with each other (hybridization) and differ from HOPG and diamond, respectively.

## ACKNOWLEDGMENTS

The authors wish to thank Dr. Kenya Shimada, Dr. Masashi Nakatake of Hiroshima Synchrotron Radiation Center, Hiroshima University, Dr. Shin-ichi Wada, and Dr. Ken-ichirou Tanaka of Graduate School of Science, Hiroshima University, for valuable discussions and advices.

<sup>1</sup>J. Robertson, *Mater. Sci. Eng.*, **R**, **37**, 129 (2002).

<sup>2</sup>T. Saito, T. Hasebe, S. Yohena, Y. Matsuoka, A. Kamijo, K. Takahashi, and T. Suzuki, *Diamond Relat. Mater.* **14**, 1116 (2005).

<sup>3</sup>P. D. Maguire *et al.*, *Diamond Relat. Mater.* **14**, 1277 (2005).

<sup>4</sup>E. H. Lee, D. M. Hembree, G. R. Rao, and L. K. Mansur, *Phys. Rev. B* **48**, 15540 (1993).

<sup>5</sup>A. C. Ferrari and J. Robertson, *Philos. Trans. R. Soc. London, Ser. A* **362**, 2477 (2004).

<sup>6</sup>S. T. Jackson and R. G. Nuzzo, *Appl. Surf. Sci.* **90**, 195 (1995).

<sup>7</sup>J. Schäfer *et al.*, *Phys. Rev. B* **53**, 7762 (1996).

<sup>8</sup>J. Díaz, G. Paolicelli, S. Ferrer, and F. Comin, *Phys. Rev. B* **54**, 8064 (1996).

<sup>9</sup>V. N. Apakina *et al.*, *Diamond Relat. Mater.* **6**, 564 (1997).

<sup>10</sup>S. Bhattacharyya, J. Hong, and G. Turban, *J. Appl. Phys.* **83**, 3917 (1998).

<sup>11</sup>S. Bhattacharyya, C. Cardinaud, and G. Turban, *J. Appl. Phys.* **83**, 4491 (1998).

<sup>12</sup>P. Mérel, M. Tabbal, M. Chaker, S. Moisa, and J. Margot, *Appl. Surf. Sci.* **136**, 105 (1998).

<sup>13</sup>P. Petrov, D. B. Dimitrov, D. Papadimitriou, G. Beshkov, V. Krastev, and C. Georgiev, *Appl. Surf. Sci.* **151**, 233 (1999).

<sup>14</sup>M. Ramm, M. Ata, K. W. Brzezinka, T. Gross, and W. Unger, *Thin Solid Films* **354**, 106 (1999).

<sup>15</sup>E. Riedo, F. Comin, J. Chevrier, F. Schmithusen, S. Decossas, and M.

Sancrotti, *Surf. Coat. Technol.* **125**, 124 (2000).

<sup>16</sup>J. G. Hong, S. Lee, C. Cardinaud, and G. Turban, *J. Non-Cryst. Solids* **265**, 125 (2000).

<sup>17</sup>J. Díaz, S. Anders, X. Zhou, E. J. Moler, S. A. Kellar, and Z. Hussain, *Phys. Rev. B* **64**, 125204 (2001).

<sup>18</sup>R. Haerle, E. Riedo, A. Pasquarello, and A. Baldereschi, *Phys. Rev. B* **65**, 045101 (2002).

<sup>19</sup>B. Bouchet-Fabre, E. Marino, G. Lazar, K. Zellama, M. Clin, D. Ballutaud, F. Abel, and C. Godet, *Thin Solid Films* **482**, 167 (2005).

<sup>20</sup>N. Paik, *Surf. Coat. Technol.* **200**, 2170 (2005).

<sup>21</sup>S. S. Roy, R. McCann, P. Papakonstantinou, P. Maguire, and J. A. McLaughlin, *Thin Solid Films* **482**, 145 (2005).

<sup>22</sup>F. C. Tai, S. C. Lee, C. H. Wei, and S. L. Tyan, *Mater. Trans.* **47**, 1847 (2006).

<sup>23</sup>D. Briggs and M. P. Seah, *Practical Surface Analysis*, 2nd. ed. (Wiley, Chichester, 1990), Vol. 1.

<sup>24</sup>S. Doniach and M. Šunjić, *J. Phys. C* **3**, 285 (1970).

<sup>25</sup>P. W. Anderson, *Phys. Rev. Lett.* **18**, 1049 (1967).

<sup>26</sup>G. D. Mahan, *Phys. Rev.* **163**, 612 (1967).

<sup>27</sup>P. Nozières and C. T. De Dominicis, *Phys. Rev.* **178**, 1097 (1969).

<sup>28</sup>S. Hüfner, *Photoelectron Spectroscopy: Principle and Applications*, 3rd. ed. (Springer-Verlag, Berlin, 2003).

<sup>29</sup>T. Balasubramanian, J. N. Andersen, and L. Wallden, *Phys. Rev. B* **64**, 205420 (2001).

<sup>30</sup>R. A. P. Smith, C. W. Armstrong, G. C. Smith, and P. Weightman, *Phys. Rev. B* **66**, 245409 (2002).

<sup>31</sup>D.-Q. Yang and E. Sacher, *Langmuir* **22**, 860 (2006).

<sup>32</sup>J. F. Morar, F. J. Himpsel, G. Hollinger, J. L. Jordan, G. Hughes, and F. R. McFeely, *Phys. Rev. B* **33**, 1340 (1986).

<sup>33</sup>R. Graupner, F. Maier, J. Ristein, L. Ley, and C. Jung, *Phys. Rev. B* **57**, 12397 (1998).

<sup>34</sup>K. Bobrov, A. Mayne, G. Comtet, G. Dujardin, L. Hellner, and A. Hoffman, *Phys. Rev. B* **68**, 195416 (2003).

<sup>35</sup>K. Bobrov, G. Comtet, G. Dujardin, L. Hellner, P. Bergonzo, and C. Mer, *Phys. Rev. B* **63**, 165421 (2001).

<sup>36</sup>M. Kato, *Phys. Rev. B* **38**, 10915 (1988).

<sup>37</sup>T. Mōri and Y. Namba, *J. Vac. Sci. Technol. A* **1**, 23 (1983).

<sup>38</sup>T. Mōri and Y. Namba, *J. Appl. Phys.* **55**, 3276 (1984).

<sup>39</sup>Y. Namba and T. Mōri, *J. Vac. Sci. Technol. A* **3**, 319 (1985).

<sup>40</sup>Y. Namba, J. Wei, T. Mohri, and E. A. Heidarpour, *J. Vac. Sci. Technol. A* **7**, 36 (1989).

<sup>41</sup>A. Tsuchiyama, M. Minami, H. Hasuyama, Y. Shima, Y. Takatani, in *Surface Treatment IV*, edited by C. A. Brebbia and J. M. Kenny (WIT Press, Southampton, UK, 1999).

<sup>42</sup>M. Yoshikawa, K. Iwagami, T. Matsunobe, N. Morita, Y. Yamaguchi, Y. Izumi, and J. Wagner, *Phys. Rev. B* **69**, 045410 (2004).

<sup>43</sup>D. A. Shirley, *Phys. Rev. B* **5**, 4709 (1972).

<sup>44</sup>S. Tougaard, *Surf. Interface Anal.* **11**, 453 (1988).

<sup>45</sup>G. Tsutsui, S. J. Huang, H. Sakaue, S. Shingubara, and T. Takahagi, *Jpn. J. Appl. Phys., Part 1* **40**, 346 (2001).

<sup>46</sup>M. P. Seah, *Surf. Interface Anal.* **14**, 488 (1989).

<sup>47</sup>P. Reinke, G. Francz, P. Oelhafen, and J. Ullmann, *Phys. Rev. B* **54**, 7067 (1996).

<sup>48</sup>K. G. Saw and J. du Plessis, *Mater. Lett.* **58**, 1344 (2004).

<sup>49</sup>G. Speranza and N. Laidani, *Diamond Relat. Mater.* **13**, 445 (2004).

## Chemical Structural Analysis of Diamondlike Carbon Films with Different Electrical Resistivities by X-ray Photoelectron Spectroscopy

Susumu TAKABAYASHI<sup>1\*</sup>, Keishi OKAMOTO<sup>1,2</sup>, Kenya SHIMADA<sup>3</sup>, Kunihiro MOTOMITSU<sup>1</sup>,  
Hiroaki MOTOYAMA<sup>1</sup>, Tatsuyuki NAKATANI<sup>2</sup>, Hiroyuki SAKAUE<sup>1</sup>, Hitoshi SUZUKI<sup>1</sup>, and Takayuki TAKAHAGI<sup>1</sup>

<sup>1</sup>Department of Quantum Matter, Graduate School of Advanced Sciences of Matter, Hiroshima University,  
1-3-1 Kagamiyama, Higashihiroshima, Hiroshima 739-8530, Japan

<sup>2</sup>Toyo Advanced Technologies Co., Ltd., 5-3-38 Ujina-Higashi, Minami-ku, Hiroshima 734-8501, Japan

<sup>3</sup>Hiroshima Synchrotron Radiation Center, Hiroshima University, 2-313 Kagamiyama, Higashihiroshima, Hiroshima 739-0046, Japan

(Received October 1, 2007; revised December 26, 2007; accepted January 9, 2008; published online May 16, 2008)

The chemical structure of diamondlike carbon (DLC) has been clarified by means of the quantitative analysis of the C 1s X-ray photoelectron spectra of the DLC films with different electrical resistivities prepared by the unbalanced magnetron sputtering (UBMS) method. The observed C 1s spectra showed asymmetric shapes and shifts of peak positions depending on the electrical resistivity of the films. Every spectrum was decomposed into four chemical components that were represented by the Doniach–Šunjić (DŠ) function convoluted with a Gaussian function. The structures corresponding to the chemical components were analyzed by considering that the electrical resistivity of DLC increases as the amount of hydrogen increases. The assignments of the chemical components are as follows: in order of binding energy, sp<sup>3</sup> carbon with carbon–carbon bonds (C–C sp<sup>3</sup> carbon, 283.7–283.8 eV), sp<sup>2</sup> carbon with carbon–carbon bonds (C–C sp<sup>2</sup> carbon, 284.2–284.3 eV), sp<sup>2</sup> carbon with hydrogen–carbon bonds (H–C sp<sup>2</sup> carbon, 284.7–284.8 eV), and sp<sup>3</sup> carbon with hydrogen–carbon bonds (H–C sp<sup>3</sup> carbon, 285.3–285.4 eV). [DOI: 10.1143/JJAP.47.3376]

KEYWORDS: diamondlike carbon (DLC), unbalanced magnetron sputtering (UBMS), X-ray photoelectron spectroscopy (XPS), electrical resistivity, chemical structure

### 1. Introduction

Diamondlike carbon (DLC) is an amorphous carbonaceous material composed of sp<sup>2</sup> carbon, sp<sup>3</sup> carbon, and hydrogen.<sup>1)</sup> The chemical structure of DLC corresponding to the ratio of the three components plays an important role in applications,<sup>2,3)</sup> such as surface coating materials for industrial products and medical tools. A number of preparation methods of DLC to control the chemical structure have been reported,<sup>4–6)</sup> but the correlation between the characteristics and the chemical structure is still unclear.<sup>7)</sup>

One of the main tools to analyze DLC is X-ray photoelectron spectroscopy (XPS).<sup>8–24)</sup> The binding energy ( $E_B$ ) shift in the XPS spectrum of a material, which is mainly influenced by neighboring atoms of the target atom,<sup>25,26)</sup> gives useful information about the chemical structure. Specifically, C 1s XPS spectra of DLC show asymmetric shapes similar to the XPS spectra of metals<sup>27)</sup> and semi-metallic graphite.<sup>28–31)</sup> The asymmetry also provides useful information about the electronic state at the Fermi level ( $E_F$ ), which is related to the electron–hole pair creation, due to the appearance of the core–hole potential in the final state of photoelectron emission.<sup>32)</sup>

In the case that there exist several chemical bonds, an XPS spectrum consists of chemical components corresponding to these states. Thus the XPS analysis requires decomposition of the spectrum into several curves. This task is not easy, however, because many free parameters are involved: the number of curves, and the parameters for the position, height, width, and symmetry of each curve. The method of quantitative analysis has not been fully established yet.<sup>8–24)</sup>

We previously reported<sup>33)</sup> the angle-resolved C 1s XPS (AR-XPS) analysis of a DLC film prepared by the ionized deposition (ID) method, which is denoted here as an ID-DLC film, using the Doniach–Šunjić (DŠ) function<sup>32)</sup> convoluted with a Gaussian function. The DŠ function is

usually used for the analyses of asymmetric XPS spectra of metals<sup>27)</sup> and semi-metallic graphite.<sup>28–31)</sup>

Recently, Takata *et al.* reported<sup>34)</sup> the recoil effect in the C 1s photoemission spectra of graphite. The recoil effect causes a peak shift to higher binding energy and asymmetric peak broadening. With a fixed geometrical setup for XPS measurements, the magnitudes of the energy shift and asymmetric broadening due to the recoil effect are essentially determined by the mass of the atom and the kinetic energy of emitted photoelectrons. In the present study, the recoil effect does not affect our analyses since we evaluate the change of chemical structure of DLC as a function of the electrical resistivity at fixed incident photon energy. We used the DŠ function in order to quantify the variance in the asymmetry as a function of electrical resistivity.

An important parameter of the DŠ function is the singularity index ( $\alpha$ ), which measures the asymmetry of a spectrum. When  $\alpha$  is zero, the DŠ function is reduced to the Lorentzian function, which is the symmetric function. The  $\alpha$  value is related to the electronic state at  $E_F$ : for example, that of graphite, a conductor, is a finite value;<sup>28–31)</sup> on the other hand, that of diamond, an insulator, is zero.<sup>35–38)</sup>

The C 1s spectrum of an ID-DLC film shifted to higher binding energy with increasing the takeoff angle of the photoelectrons measured from normal to surface. This result demonstrated that the ID-DLC film had two types of chemical components, surface and bulk components: the surface component was located at higher binding energy and the bulk at lower. DLC has two types of carbons, sp<sup>2</sup> and sp<sup>3</sup> carbons. Thus, it was expected that the ID-DLC film contained at least “ $2 \times 2 = 4$ ” unique chemical bonds. We concluded that the C 1s spectra of the ID-DLC film were decomposed into four chemical components. The assignments are as follows: in order of binding energy, bulk sp<sup>3</sup> carbon (283.7–283.8 eV), bulk sp<sup>2</sup> carbon (284.2–284.3 eV), surface sp<sup>2</sup> carbon (284.7–284.8 eV), and surface sp<sup>3</sup> carbon (285.3–285.4 eV).

\*E-mail address: stak@hiroshima-u.ac.jp

One of the interesting characteristics of DLC is that the electrical resistivity can be controlled by the preparation process.<sup>39)</sup> The electrical resistivity ranges from the value of a conductor (graphite-like) to that of an insulator (diamond-like). It has been concluded that the electrical resistivity of DLC increases as the amount of hydrogen increases.<sup>40,41)</sup> The  $\text{CH}_x$  species in DLC produce large free spaces in the structure and inhibit the conductive routes leading to high electrical resistivity.<sup>42-45)</sup> Thus the electrical resistivity of DLC has an important correlation with the chemical structure. In this study, we have analyzed the C 1s XPS spectra of DLC with different electrical resistivities to clarify their chemical structures.

## 2. Experimental Procedure

DLC films with different electrical resistivities were purchased from Kobe Steel. The films were prepared on 625- $\mu\text{m}$ -thick single-crystal Si(100) wafers ( $10 \times 10 \text{ mm}^2$ ) with a low electrical resistivity ( $0.1 \Omega \text{ cm}$ ) by the unbalanced magnetron sputtering (UBMS) method. The films are denoted here as UBMS-DLC films. The thickness of the films was 200 nm. The UBMS method is an improved magnetron sputtering method.<sup>41,46-51)</sup> The target was graphite fixed in the chamber. The ratio of  $\text{CH}_4/\text{Ar}$  gas in the plasma was varied to control the electrical resistivity of the UBMS-DLC films.<sup>39-41)</sup> The electrical resistivity was measured using the four-point probe method at room temperature and at a pressure of about  $1 \times 10^{-1}$  Torr.<sup>52,53)</sup> Table I shows the correlation between the  $\text{CH}_4/\text{Ar}$  gas ratio in the plasma and electrical resistivity of UBMS-DLC films.

The XPS measurements were conducted on a surface area of  $0.8 \times 2.0 \text{ mm}^2$  with an ULVAC-PHI PHI 1600 system. The system had an unmonochromated Al  $K\alpha$  (1486.3 eV) line with a voltage of 15 kV and a power of 400 W. All measurements were performed at room temperature and at a pressure below  $3.0 \times 10^{-9}$  Torr. The Shirley method was used to subtract the background lines.<sup>25,26,54)</sup> The energy resolution of the spectrometer was estimated from the spectrum of the Fermi edge of a Au plate analyzed by the Fermi-Dirac distribution function convoluted with a Gaussian function. The full-width at half maximum (FWHM) of the Gaussian function was 0.6 eV.

Before the XPS measurements, a few  $\mu\text{L}$  of an aqueous solution of Au nanocolloids with a diameter of 11 nm<sup>55)</sup> were dropped onto a small local surface area about  $2 \times 2 \text{ mm}^2$  of the target UBMS-DLC film using a syringe in air to calibrate the binding energy during the XPS analysis.<sup>33,53)</sup> The surface area covered with the droplet was then gradually dried *in vacuo* to become a stain of Au nanocolloids. The target C 1s spectrum was observed at a native surface area (an area without Au nanocolloids) of the UBMS-DLC film. The

observed binding energy at the peak position of the C 1s spectrum was calibrated by setting that of the Au  $4f_{7/2}$  spectrum of the Au nanocolloids at another area to  $84.0$  ( $83.98 \pm 0.02$ ) eV.<sup>56)</sup>

The inhomogeneous charging effect was not observed on the UBMS-DLC films with electrical resistivities listed in Table I.<sup>53)</sup> The Au  $4f_{7/2}$  spectrum of the Au nanocolloids dispersed on every film was almost same with that of a Au plate. Thus the calibration method using Au nanocolloids was applicable to the UBMS-DLC films.

## 3. Results and Discussion

Figure 1 shows the C 1s spectra of UBMS-DLC films with different electrical resistivities. The spectrum of a freshly-cleaved, highly-oriented pyrolytic graphite (HOPG) film, which is composed of  $\text{sp}^2$  carbon only, is also shown. The C 1s spectra of the UBMS-DLC films become more asymmetric with decreasing electrical resistivity.

Figure 2(a) shows the correlation between the FWHM of the C 1s spectra and the electrical resistivity of the UBMS-DLC films. Figure 2(b) shows the correlation between the

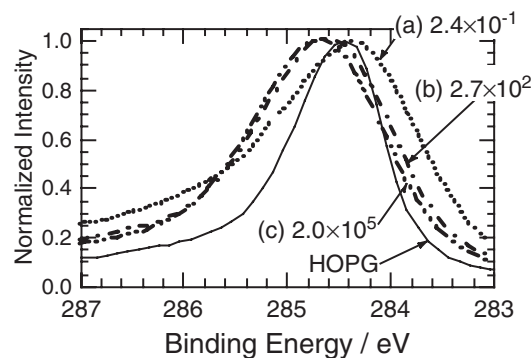


Fig. 1. C 1s XPS spectra of the UBMS-DLC films with electrical resistivities of (a)  $(2.4 \pm 0.1) \times 10^{-1}$ , (b)  $(2.7 \pm 2.0) \times 10^2$ , and (c)  $(2.0 \pm 1.4) \times 10^5 \Omega \text{ cm}$ . The spectrum of a freshly-cleaved HOPG film is also shown. Every spectrum is normalized by dividing the observed spectrum by its peak intensity (the normalized peak intensity is set 1.0).

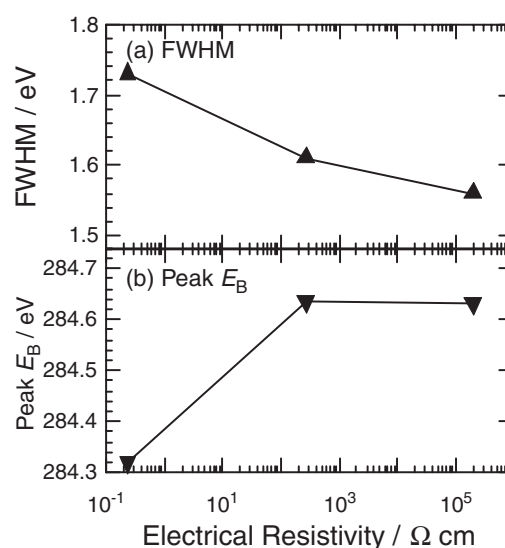


Fig. 2. Correlations between (a) the FWHM and (b) the binding energy at the peak positions (peak  $E_B$ ) of the C 1s spectra and the electrical resistivity of the UBMS-DLC films.

Table I. List of the correlations between the  $\text{CH}_4/\text{Ar}$  gas ratio in the plasma during the preparation by the UBMS method and electrical resistivity of UBMS-DLC films.

Sample	Ratio of $\text{CH}_4/\text{Ar}$ gas in the plasma	Electrical resistivity ( $\Omega \text{ cm}$ )
(a)	0/100	$(2.4 \pm 0.1) \times 10^{-1}$
(b)	6/100	$(2.7 \pm 2.0) \times 10^2$
(c)	12/100	$(2.0 \pm 1.4) \times 10^5$

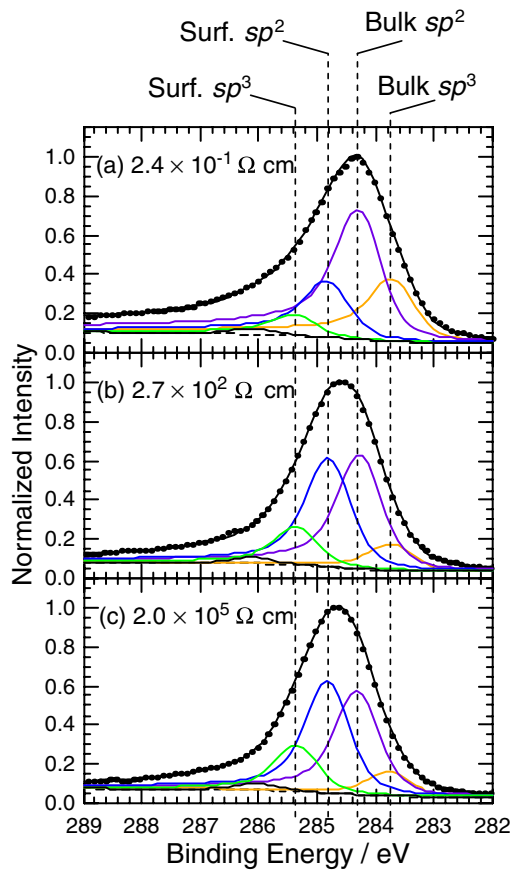


Fig. 3. (Color online) C 1s XPS spectra of the UBMS-DLC films with the fitting-curves of the chemical components represented by the DŠ function convoluted with a Gaussian function according to the AR-XPS analysis.<sup>33)</sup> Every spectrum is normalized by dividing the observed spectrum by its peak intensity (the normalized peak intensity is set 1.0). For simplicity of analysis, the singularity index and the FWHMs of the Lorentzian and the Gaussian functions are assumed to be common values for every curve ( $\alpha$  for the  $sp^2$  carbons :  $\alpha$  for the  $sp^3$  carbons = 5 : 5). The assignments are as follows: in order of binding energy, for the bulk  $sp^3$  carbon (283.7–283.8 eV), the bulk  $sp^2$  carbon (284.2–284.3 eV), the surface  $sp^2$  carbon (284.7–284.8 eV), and the surface  $sp^3$  carbon (285.3–285.4 eV).

binding energy at the peak positions of the C 1s spectra (peak  $E_B$ ) and the electrical resistivity. The dependence of these indices on the electrical resistivity gives information on variations of the chemical structures of the UBMS-DLC films.

Figure 3 shows the C 1s spectra of the UBMS-DLC films with the fitting-curves of the chemical components represented by the DŠ function convoluted with a Gaussian function according to the AR-XPS analysis.<sup>33)</sup> The fitting parameters for a peak are the binding energy ( $E_B$ ), the spectral intensity ( $I$ ), the FWHMs of the Lorentzian and Gaussian functions ( $\Gamma_L$  and  $\Gamma_G$ ), and the singularity index ( $\alpha$ ). For simplicity of analysis,  $\alpha$ ,  $\Gamma_L$ , and  $\Gamma_G$  are assumed to be common values for every curve. As a result, the total number of parameters was reduced to 10: four  $E_B$ 's, four  $I$ 's, one  $\Gamma_L$ , one  $\Gamma_G$ , and one  $\alpha$ . The assignments are follows: for bulk  $sp^3$  carbon (283.7–283.8 eV), bulk  $sp^2$  carbon (284.2–284.3 eV), surface  $sp^2$  carbon (284.7–284.8 eV), and surface  $sp^3$  carbon (285.3–285.4 eV).

Figure 4(a) shows the correlation between the singularity index and the electrical resistivity of the UBMS-DLC films obtained from the analysis in Fig. 3. The singularity index decreased with increasing electrical resistivity, which sug-

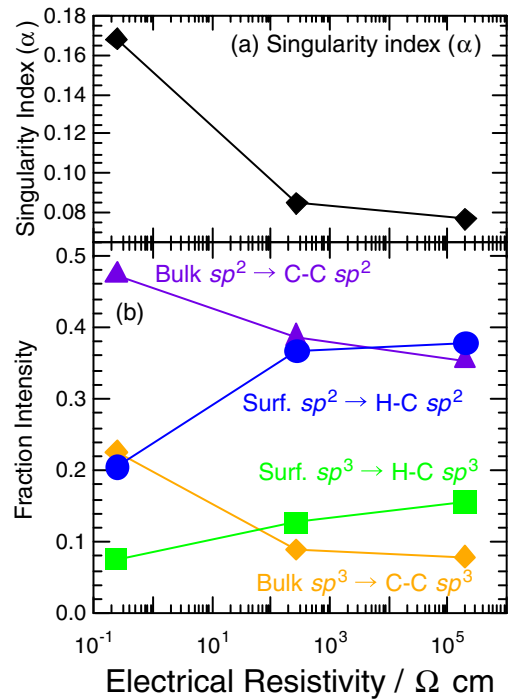


Fig. 4. (Color online) Correlations between (a) the singularity index and (b) the fraction intensities of the chemical components of the C 1s spectra and the electrical resistivity of the UBMS-DLC films obtained from the analysis in Fig. 3:  $\blacklozenge$  the bulk  $sp^3$  carbon,  $\blacktriangle$  the bulk  $sp^2$  carbon,  $\bullet$  the surface  $sp^2$  carbon, and  $\blacksquare$  the surface  $sp^3$  carbon. In the present analysis, these assignments should be regarded as follows: the  $sp^3$  carbon with carbon–carbon bonds (C–C  $sp^3$  carbon), the  $sp^2$  carbon with carbon–carbon bonds (C–C  $sp^2$  carbon), the  $sp^2$  carbon of hydrogen–carbon bonds (H–C  $sp^2$  carbon), and the  $sp^3$  carbon with hydrogen–carbon bonds (H–C  $sp^3$  carbon).

gests the electron–hole pair creation at  $E_F$  is reduced. Figure 4(b) shows the correlation between the fraction intensities of the chemical components and the electrical resistivity. These fraction intensities were obtained by assuming that the magnitudes of the singularity index  $\alpha$  for the  $sp^2$  carbon [ $\alpha(sp^2)$ ] is equal to  $\alpha$  for the  $sp^3$  carbon [ $\alpha(sp^3)$ ], namely,  $\alpha(sp^2) : \alpha(sp^3) = 5 : 5$ . We note that the fraction was almost constant for  $\alpha(sp^2) : \alpha(sp^3) = 5 : 5 - 10 : 0$ . The singularity index does not affect the quantitative analysis within this range. The surface components increase with electrical resistivity, but the bulk components show the opposite trend. Hydrogen-rich DLC shows high electrical resistivity<sup>39–41)</sup> because the hydrogen atoms are incorporated as  $CH_x$  species in DLC, produce large free spaces in the structure, and inhibit conductive routes leading to high electrical resistivity.<sup>42–45)</sup> It is reasonable to expect that the  $CH_x$  species are distributed homogeneously in these samples. Based on these analyses, the surface components are correlated with  $CH_x$  species, while the bulk components are not. Consequently, we regard the surface carbons as carbons with hydrogen–carbon (H–C) bonds and bulk carbons as carbons with carbon–carbon (C–C) bonds. The assignments are as follows: in order of binding energy,  $sp^3$  carbon with C–C bonds (C–C  $sp^3$  carbon, 283.7–283.8 eV),  $sp^2$  carbon with C–C bonds (C–C  $sp^2$  carbon, 284.2–284.3 eV),  $sp^2$  carbon with H–C bonds (H–C  $sp^2$  carbon, 284.7–284.8 eV), and  $sp^3$  carbon with H–C bonds (H–C  $sp^3$  carbon, 285.3–285.4 eV).



#### 4. Conclusions

We analyzed the C 1s XPS spectra of UBMS-DLC films with different electrical resistivities. The magnitude of the asymmetry of the spectra decrease with increasing electrical resistivity, which suggests the reduction of the electron-hole pair creation at  $E_F$ . The binding energy shifts of the C 1s spectra also depend on the electrical resistivity, indicating that the chemical structure of DLC depends on the electrical resistivity. The C 1s spectra are decomposed into four chemical components using the DS function convoluted with a Gaussian function according to the AR-XPS analysis.<sup>33)</sup> Considering that the electrical resistivity of DLC increases with the amount of hydrogen, the chemical components are correlated with hydrogen content. The assignments of the C 1s spectrum of DLC are as follows: in order of binding energy, C–C sp<sup>3</sup> carbon (283.7–283.8 eV), C–C sp<sup>2</sup> carbon (284.2–284.3 eV), H–C sp<sup>2</sup> carbon (284.7–284.8 eV), and H–C sp<sup>3</sup> carbon (285.3–285.4 eV).

#### Acknowledgements

The authors gratefully acknowledge Mr. Hiroshi Kiriara and Mr. Satoshi Hirota of Machinery and Engineering Company, Kobe Steel, Ltd., for preparing the UBMS-DLC films, and Mr. Akihiro Suga for preparing the aqueous solution containing Au nanocolloids.

- 1) J. Robertson: *Mater. Sci. Eng. R* **37** (2002) 129.
- 2) A. Grill: *Diamond Relat. Mater.* **8** (1999) 428.
- 3) A. Grill: *Diamond Relat. Mater.* **12** (2003) 166.
- 4) P. Koidl, Ch. Wild, B. Dischler, J. Wagner, and M. Ramsteiner: *Mater. Sci. Forum* **52–53** (1989) 41.
- 5) Y. Lifshitz: *Diamond Relat. Mater.* **5** (1996) 388.
- 6) Y. Lifshitz: *Diamond Relat. Mater.* **8** (1999) 1659.
- 7) Y. Lifshitz: *Diamond Relat. Mater.* **12** (2003) 130.
- 8) S. T. Jackson and R. G. Nuzzo: *Appl. Surf. Sci.* **90** (1995) 195.
- 9) J. Schäfer, J. Ristein, R. Graupner, L. Ley, U. Stephan, T. Frauenheim, V. S. Veerasamy, G. A. J. Amaratunga, M. Weiler, and H. Ehrhardt: *Phys. Rev. B* **53** (1996) 7762.
- 10) J. Díaz, G. Paolicelli, S. Ferrer, and F. Comin: *Phys. Rev. B* **54** (1996) 8064.
- 11) V. N. Apakina, A. L. Karuzskii, M. S. Kogan, A. V. Kvit, N. N. Melnik, Y. A. Mityagin, V. N. Murzin, A. A. Orlikovsky, A. V. Perestoromin, S. D. Tkachenko, and N. A. Volchkov: *Diamond Relat. Mater.* **6** (1997) 564.
- 12) S. Bhattacharyya, J. Hong, and G. Turban: *J. Appl. Phys.* **83** (1998) 3917.
- 13) S. Bhattacharyya, C. Cardinaud, and G. Turban: *J. Appl. Phys.* **83** (1998) 4491.
- 14) P. Mérel, M. Tabbal, M. Chaker, S. Moisa, and J. Margot: *Appl. Surf. Sci.* **136** (1998) 105.
- 15) P. Petrov, D. B. Dimitrov, D. Papadimitriou, G. Beshkov, V. Krastev, and C. Georgiev: *Appl. Surf. Sci.* **151** (1999) 233.
- 16) M. Ramm, M. Ata, K. W. Brzezinka, T. Gross, and W. Unger: *Thin Solid Films* **354** (1999) 106.
- 17) E. Riedo, F. Comin, J. Chevrier, F. Schmithusen, S. Decossas, and M. Sancrotti: *Surf. Coat. Technol.* **125** (2000) 124.
- 18) J. G. Hong, S. Lee, C. Cardinaud, and G. Turban: *J. Non-Cryst. Solids* **265** (2000) 125.
- 19) J. Díaz, S. Anders, X. Zhou, E. J. Moler, S. A. Kellar, and Z. Hussain: *Phys. Rev. B* **64** (2001) 125204.
- 20) R. Haerle, E. Riedo, A. Pasquarello, and A. Baldereschi: *Phys. Rev. B* **65** (2002) 045101.
- 21) B. Bouchet-Fabre, E. Marino, G. Lazar, K. Zellama, M. Clin, D. Ballutaud, F. Abel, and C. Godet: *Thin Solid Films* **482** (2005) 167.
- 22) N. Paik: *Surf. Coat. Technol.* **200** (2005) 2170.
- 23) S. S. Roy, R. McCann, P. Papakonstantinou, P. Maguire, and J. A. McLaughlin: *Thin Solid Films* **482** (2005) 145.
- 24) F. C. Tai, S. C. Lee, C. H. Wei, and S. L. Tyan: *Mater. Trans.* **47** (2006) 1847.
- 25) D. Briggs and M. P. Seah: *Practical Surface Analysis: Auger and X-Ray Photoelectron Spectroscopy* (John Wiley & Sons, Chichester, U.K., 1990) 2nd ed.
- 26) S. Hüfner: *Photoelectron Spectroscopy: Principle and Applications* (Springer-Verlag, Berlin, 2003) 3rd ed.
- 27) P. H. Citrin, G. K. Wertheim, and Y. Baer: *Phys. Rev. B* **27** (1983) 3160.
- 28) K. C. Prince, I. Ulrych, M. Peloi, B. Ressel, V. Chab, C. Crotti, and C. Comincioli: *Phys. Rev. B* **62** (2000) 6866.
- 29) T. Balasubramanian, J. N. Andersen, and L. Wallden: *Phys. Rev. B* **64** (2001) 205420.
- 30) R. A. P. Smith, C. W. Armstrong, G. C. Smith, and P. Weightman: *Phys. Rev. B* **66** (2002) 245409.
- 31) D.-Q. Yang and E. Sacher: *Langmuir* **22** (2006) 860.
- 32) S. Doniach and M. Šunjić: *J. Phys. C* **3** (1970) 285.
- 33) S. Takabayashi, K. Motomitsu, T. Takahagi, A. Terayama, K. Okamoto, and T. Nakatani: *J. Appl. Phys.* **101** (2007) 103542.
- 34) Y. Takata, Y. Kayanuma, M. Yabashi, K. Tamasaku, Y. Nishino, D. Miwa, Y. Harada, K. Horiba, S. Shin, S. Tanaka, E. Ikenaga, K. Kobayashi, Y. Senba, H. Ohashi, and T. Ishikawa: *Phys. Rev. B* **75** (2007) 233404.
- 35) J. F. Morar, F. J. Himpsel, G. Hollinger, J. L. Jordan, G. Hughes, and F. R. McFeely: *Phys. Rev. B* **33** (1986) 1340.
- 36) R. Graupner, F. Maier, J. Ristein, L. Ley, and C. Jung: *Phys. Rev. B* **57** (1998) 12397.
- 37) K. Bobrov, G. Comtet, G. Dujardin, L. Hellner, P. Bergonzo, and C. Mer: *Phys. Rev. B* **63** (2001) 165421.
- 38) K. Bobrov, A. Mayne, G. Comtet, G. Dujardin, L. Hellner, and A. Hoffman: *Phys. Rev. B* **68** (2003) 195416.
- 39) R. D. Mansano, M. Massi, L. S. Zambom, P. Verdonck, P. M. Nogueira, H. S. Maciel, and C. Otani: *Thin Solid Films* **373** (2000) 243.
- 40) M. Massi, H. S. Maciel, C. Otani, R. D. Mansano, and P. Verdonck: *J. Mater. Sci.: Mater. Electron.* **12** (2001) 343.
- 41) H. Ito, K. Yamamoto, and M. Matsuko: 6th Asian–European Int. Conf. Plasma Surface Engineering (AEPSE 2007), 2007, KN0700.
- 42) E. Findeisen, R. Feidenhansl, M. E. Vigild, K. N. Clausen, J. Bindslev Hansen, M. D. Bentzon, and J. P. Goff: *J. Appl. Phys.* **76** (1994) 4636.
- 43) C. Barholm-Hansen, M. D. Bentzon, M. E. Vigild, E. Findeisen, R. Feidenhansl, and J. Bindslev Hansen: *Surf. Coat. Technol.* **68** (1994) 702.
- 44) M. E. Vigild, E. Findeisen, R. Feidenhansl, C. Barholm-Hansen, M. D. Bentzon, and J. B. Hansen: *J. Appl. Phys.* **79** (1996) 4050.
- 45) E. Neyts, A. Bogaerts, and M. C. M. van de Sanden: *Appl. Phys. Lett.* **88** (2006) 141922.
- 46) B. Window and N. Savvides: *J. Vac. Sci. Technol. A* **4** (1986) 196.
- 47) B. Window and N. Savvides: *J. Vac. Sci. Technol. A* **4** (1986) 453.
- 48) N. Savvides and B. Window: *J. Vac. Sci. Technol. A* **4** (1986) 504.
- 49) B. Window and G. L. Harding: *J. Vac. Sci. Technol. A* **8** (1990) 1277.
- 50) S. C. Seo, D. C. Ingram, and H. H. Richardson: *J. Vac. Sci. Technol. A* **13** (1995) 2856.
- 51) X. T. Zeng: *J. Vac. Sci. Technol. A* **17** (1999) 1991.
- 52) L. J. van der Pauw: *Philips Tech. Rev.* **20** (1958) 220.
- 53) S. Takabayashi, K. Okamoto, K. Motomitsu, A. Terayama, T. Nakatani, H. Sakaue, H. Suzuki, and T. Takahagi: *Appl. Surf. Sci.* **254** (2008) 2666.
- 54) D. A. Shirley: *Phys. Rev. B* **5** (1972) 4709.
- 55) G. Tsutsui, S. J. Huang, H. Sakaue, S. Shingubara, and T. Takahagi: *Jpn. J. Appl. Phys.* **40** (2001) 346.
- 56) M. P. Seah: *Surf. Interface Anal.* **14** (1989) 488.